

https://dspace.org/

Investigation into the mechanism of strength and failure in squat coal pillars in South Africa

Mathey, Markus

2016-03-17
http://hdl.handle.net/10539/20114

Downloaded from a DSpace repository. https://dspace.org/

INVESTIGATION INTO THE MECHANISM OF STRENGTH AND FAILURE IN SQUAT COAL PILLARS IN SOUTH AFRICA

Markus Mathey

A thesis submitted to the Faculty of Engineering and the Built Environment, University of the Witwatersrand, Johannesburg, in fulfilment of the requirements for the degree of Doctor of Philosophy

Johannesburg, 2015

Declaration

I, Markus Mathey, declare that this thesis is my own unaided work. Where use has been made of work of others, it has been duly acknowledged. It is being submitted for the degree of Doctor of Philosophy in the University of Witwatersrand, Johannesburg. It has not been submitted before in any form for any other degree or examination in any other university.

_____

Markus Mathey

_____day of_____2015

Abstract

The mechanism of strength and failure in squat coal pillars with large width-to-height ratio has piqued the interest of researchers and mining operators for many years. In South Africa, the view has been adopted that pillars with width-to-height ratios greater than 5 have the ability to increase their peak load-bearing capacity exponentially and therefore obey a distinctly different law than the more slender pillars.

This view has not always been shared in the international mining community, for good reasons: a literature review of evidence and indications on squat pillar behaviour is not conclusive. A competing philosophy on strength and failure in squat pillars is that such structures did not exhibit a peak strength, but rather performed in a ductile or strain-hardening manner. If this holds true, they were able to increase their load-bearing capacity beyond the point of yield with increasing deformation.

Hence, the research presented in this thesis is designed to investigate the mechanism of strength and failure in squat coal pillars in greater detail.

A statistical survey of the mechanical properties of coal in South Africa was conducted with the intention to evaluate coalfield-, seam-, or site-specific patterns, which may demand individual treatment in the further analysis of pillar performance. Such differences are, however, not discernible from a laboratory specimen point-of-view. The average uniaxial compressive strength of coal seams is practically constant in South Africa and there are indications that this is also the case for individual mining sites. Only the triaxial compressive strength of coal specimens from different seams shows individual trends, but further statistical evidence is required to substantiate these. Nevertheless the survey yields important insights into the adverse influence of natural discontinuities on the strength of coal, which is observed to diminish in a sufficiently large triaxial confining environment. It is postulated that this confining environment can be generated in pillars with large width-to-height ratios, which ultimately means that the presence of natural discontinuities does not have a major influence on the strength of squat pillars.

A comparative laboratory study into the relationship between strength, failure, and the width-to-height ratios of model pillars of different materials reveals the following insight:

(1) The residual strength of model pillars after crushing increases progressively with increasing width-to-height ratio.

(2) The relationship between the peak pillar strength and the width-to-height ratio is bi-linear, whereas the second branch of strength increase is steeper than the first one. This behaviour is termed the squat effect.

(3) At sufficiently large width-to-height ratios, the peak strength trend ends in a brittle-ductile transition.

Bi-linearity is an entirely newly observed phenomenon and has been identified for hard and soft rock materials, as well as for a soft composite material, but notably not for coal.

The described characteristics (1 – 3) are qualitatively reproduced in a numerical modelling investigation, which yields the following insights as to the mechanism behind the trends:

(Ad 1) The rate of progressive strength increase in the residual domain is controlled by the residual material properties. The higher the residual material properties, the more rapid the strength increase, and the lower the critical width-to-height ratio for brittle-ductile transition in pillars.

(Ad 2) Bi-linearity in the peak strength trend is caused by a change of failure mechanism in pillars from a critical width-to-height ratio onwards.

In the first and slower ascending branch of the bi-linear relationship, typically up to a width-to-height ratio of 5, the pillar's maximum load-bearing capacity is reached when the first shear band develops in the pillar sidewall. The pillar cannot recover from this initial failure, and fractures soon propagate further into the core while the load-bearing capacity gradually decreases with further deformation.

In the second and faster ascending branch of the bi-linear relationship, pillars do re-cover from the first shear band in their extremities. The pillars then regain and increase their load-bearing capacity until core failure occurs.

The critical width-to-height ratio at which the squat effect occurs is dependent on the residual material properties. The higher the residual properties, the lower the critical width-to-height ratio. Also, the rate of strength increase in the second branch of bi-linearity depends significantly on the competence of the residual material properties.

(Ad 3) Brittle-ductile transition appears to be only a practical concept for the interpretation of the stress-strain behaviour of pillars. Every model pillar is seen to ultimately show a certain amount of strength drop at the point when its core fails, even if 50 % strain or more is required at very large width-to-height ratios. However, because such large strains are unlikely to occur for coal pillars in-situ, the concept of brittle ductile transition may remain valid for practical purposes.

The new insight into the outstanding importance of residual material properties for the performance of squat pillars stimulates the demand for further research, in particular for rock pillars, for which the characteristics (1 – 3) have been observed in physical tests.

Coal model pillars, however, evidently behave different from rock: All physical tests in the laboratory demonstrate unambiguously that the strength versus width-to-height relationship in coal follows one single, continuous trend from w/h= 1 up to 9 or 11. A squat effect is not discernible in this range for coal. This suggests that, at the current state of knowledge, coal pillar strength in South African mines is most suitably addressed by extrapolating established empirical strength equations into the squat range to at least w/h= 10. The extrapolation is further validated by experience made with squat coal pillars in mines in the United States.

Acknowledgements

This thesis was developed during my time as a full-time doctoral candidate at the School of Mining Engineering, University of the Witwatersrand, and has benefitted in many ways from contributions by colleagues, friends and professionals in the South African and international mining community.

I would like to thank my supervisor, Prof. Dr. Nielen Van der Merwe, Centennial Chair of Rock Engineering at the School, for the guidance and encouragement that I received from him during my research.

Likewise, my appreciation goes to the Head of School, Prof. Dr. Frederick Cawood, for the support and opportunities he offered me, and to all members and colleagues at the School who included me warmly.

My work and learning in rock mechanics has benefitted substantially from two friends and co-researchers, who shared their one hundred years of experiences in this field with me: Uli Vogler, formerly CSIR Division of Mining and Technology, from whom I learned the intricacies of laboratory rock testing; and Rudi Kersten, formerly Group rock mechanics engineer at Anglovaal Ltd., with whom I enjoyed many critical discussions around pillar mechanics, design and modelling practice. I thank both of them cordially for their support.

Further, I am indebted to Prof. Emer. Dr. Thomas Stacey, School of Mining Engineering and Dr. Jan Kuijpers, formerly CSIR Miningtek, for their valuable comments on individual aspects of my thesis. I thank Sandor Petho, Group rock engineer at Xstrata Coal, for supplying me generously with relevant information, test samples and geotechnical data from the coal mines.

My special thanks go to Dr. Carlos Carranza-Torres, Associate Professor at the Department of Civil Engineering**,** University of Minnesota, Duluth Campus, who hosted me for academic exchange on analytical and numerical pillar modelling at his university.

Further, my work with numerical models would not have been possible in this form without the support of the Itasca Consulting Group, which granted me a license of FLAC and a placement in the Itasca educational program. I would like to thank my Itasca mentor Dr. Richard Brummer, President of Itasca Consulting Canada, and Dr. Christine Detournay, Principal Engineer at Itasca head office in Minneapolis, for their attendance to my numerous questions.

I am deeply grateful to Sanisha C. Naidoo, for her love, patience and genuine interest in my work which encouraged me to reach that far. I am also indebted to her for the many hours she spent on proofreading this thesis.

Table of Contents

Declaration ii
Abstract iii
Acknowledgements v
Table of Contents vi
List of Figures ix
List of Tables xiv
List of Abbreviations xv

1 General introduction 16

2 Squat pillar terminology 19

PART I: ADVANCES IN SQUAT COAL PILLAR DESIGN AND REQUIREMENTS FOR FURTHER RESEARCH

3 Literature review and own contributions 22
3.1 South African and international strength formulae for slender and squat pillars 22
3.2 Evidence from in-situ pillar behaviour 28
3.3 Insights from laboratory testing 32
3.4 Contributions from analytical models 38
3.5 Contributions from numerical modelling 42

4 Discussion of advances in squat coal pillar strength and design 48

5 Research scope and objective 52

PART II: SURVEY OF THE MECHANICAL PROPERTIES OF INTACT COAL IN SOUTH AFRICA

6 Introduction to the properties survey 56

7 The mechanical coal properties database 58
7.1 Overview 58
7.2 Data validation 58

8 Results 64
8.1 The uniaxial compressive strength 64
8.2 Elastic moduli 69
8.3 The triaxial compressive strength 70
8.4 The indirect tensile strength 75
8.5 Correlations 77

9 Conclusions from the survey 84

PART III: LABORATORY INVESTIGATION INTO THE SHAPE EFFECT IN MODEL PILLARS WITH LARGE WIDTH-TO-HEIGHT RATIOS

10 Introduction to experimental investigations 87
10.1 Nature of the problem 87
10.2 Objective 88
10.3 Scope 89

11 Development of a composite material analogue for in-situ coal 91
11.1 Introduction to coal-crete 91
11.2 Testing programme, sample and specimen preparation 91
11.3 Mechanical characterisation of coal-crete 94
11.4 Conclusions on coal-crete 100

12 Experiment details 102
12.1 Experiment design 102
12.2 Testing materials and mechanical properties 102
12.3 Testing apparatus and specimen boundary conditions 105
12.4 Specimen preparation 107

13 Experimental results 109
13.1 Force-displacement curves and elastic specimen stiffness 109
13.2 Peak strength 120
13.3 Fracture patterns 124

14 Discussion of results 130
14.1 Fracture patterns 130
14.2 Shape and squat effects in the laboratory 130
14.3 Comparison of findings with in-situ coal pillar behaviour 136
14.4 Conclusion from laboratory study 139

PART IV: NUMERICAL MODELLING OF STRENGTH AND FAILURE IN SQUAT COAL PILLARS

15 Introduction to pillar modelling in FLAC 142

16 Survey of published numerical coal pillar models 144
16.1 Constitutive laws for coal pillars 144
16.2 Mechanical parameters for coal pillars 145
16.3 Mechanical parameters for coal-rock-interfaces 146

17 Conceptual modelling of shape effects in pillars 149
17.1 Model design 149
17.2 Observations on shape effects and failure patterns 151

17.3 Correlations between material properties and shape effects 159
17.4 Accounting for in-situ boundary conditions 162
17.5 Comparison with shape effects in physical specimens 168

18 On calibrated coal pillar models – in-situ compression tests revisited 173

PART V: CONCLUSIONS AND OUTLOOK

19 Research conclusions 180

20 Implications for squat coal pillar design 188

21 Indications for further research 191
21.1 Laboratory investigation into the brittle-ductile transition in coal 191
21.2 The strength of coal pillars after spalling 192
21.3 Monitoring of failure patterns in coal pillar sidewalls 194
21.4 Probe-hole drilling in coal pillars 194

22 References 196

List of Figures

Figure 1. Comparison of South African coal pillar strength formulae for an assumed pillar height of 3 m. 25

Figure 2. Shape effects in coal pillars as predicted by the Bieniawski formula for the United States and the combined Australian and South African formulae. 28

Figure 3. Frequency distribution of collapsed pillar width-to-height ratios. 29

Figure 4. Link between the safety factor and failure probability for coal pillars whose strength is calculated with the updated maximum likelihood strength equation. 30

Figure 5. Coal pillar strength after Maleki (1992). 31

Figure 6. Compression tests on laboratory sized specimens of coal in the squat region by different investigators. 34

Figure 7. Compression tests on laboratory sized specimens of hard rock in the squat region by different investigators. 36

Figure 8. Relationship between specimen width-to-height ratio and average load bearing capacity of crushed granite aggregates at various levels of compression, reproduced after Schümann and Cook (1967). 37

Figure 9. Limit equilibrium conditions around a pillar 'slice' in analytical models. 38

Figure 10. The residual strength of coal pillars for different internal friction angles ϕ according to the analytical model of Napier and Malan. 40

Figure 11. Comparison between the pillar strength for the Witbank coalfield predicted by the Barron and Pen (1992) analytical model and the South African squat pillar formula. 42

Figure 12. Strength and width-to-height for different geological environments, according to Gale (1999), overlain with current South African squat pillar strength and improvement opportunity. 44

Figure 13. Reduction of strength for pillars of 2 – 4 m height due to a set of 2 m distant joints inclined at an angle of 30˚. 45

Figure 14. Histogram of the axial strain at strength failure for UCS specimens (left) and QQ-plot (right) for a hypothesised lognormal distribution of the data. 61

Figure 15. Density histogram for UCS specimens (left) and QQ-plot (right) for a hypothesised lognormal distribution of UCS specimen density up to 2.1 g/cm^3. 62

Figure 16. Density histogram for all ITS specimens (left) and QQ-plot for a hypothesised lognormal distribution of the density up to 2.0 g/cm^3 (right). 62

Figure 17. Density histogram for all TCS specimens (left) and QQ-plot for a hypothesised lognormal distribution of the density up to 1.9 g/cm^3 (right). 62

Figure 18. UCS histogram for all 403 specimens (left) and QQ-plot for a hypothesised lognormal distribution of the UCS (right). 64

Figure 19. The influence of discontinuities on the strength of coal in uniaxial compression. 65

Figure 20. Seam-specific average UCS with accompanying standard deviations of coal in various coalfields in South Africa after removal of outliers in the dataset. The amount of tests evaluated per coal seam are given in the base of the columns. 68

Figure 21. UCS histogram (left) for 44 specimens sampled from 11 boreholes on a mine site in the Highveld coalfield and QQ-plot for a hypothesised lognormal distribution of the UCS in ranges between 14 – 33 MPa (right). 69

Figure 22. Histogram for the tangential elastic modulus measured on 322 coal specimens (left) and QQ-plot for a hypothesised lognormal distribution of the sample data (right). 69

Figure 23. Histogram for the tangential Poisson's Ratio measured on 322 coal specimens (left) and QQ-plot for a hypothesised normal distribution of the sample data (right). 70

Figure 24. Histogram of the strength of 41 coal specimens at 2.5 MPa confinement (left) and QQ-plot for a hypothesised normal distribution of the data (right). 71

Figure 25. Histogram of the strength of 44 coal specimens at 5 MPa confinement (left) and QQ-plot for a hypothesised normal distribution of the data (right). 71

Figure 26. Histogram of the strength of 47 coal specimens at 10 MPa confinement (left) and QQ-plot for a hypothesised normal distribution of the data (right). 71

Figure 27. Influence of confinement on the failure mode and average peak strength of coal specimens. 72

Figure 28. The average compressive strength of coal specimens from different seams at 0 MPa, 5 MPa and 10 MPa confinement. The number of tests evaluated for each confinement level are given at the base of the bars. 73

Figure 29. $\sigma_1 - \sigma_3$ plots of triaxial coal strength in different coal seams. 74

Figure 30. Histogram for the indirect tensile strength of South African coal determined on 186 coal specimens (left) and QQ-plot for a hypothesised lognormal distribution of the sample data (right). 76

Figure 31. Seam-specific average ITS with accompanying standard deviations of coal in various coalfields in South Africa. The number of tests evaluated per coal seam are given in the base of the columns. 77

Figure 32. Coal specimen density versus depth below surface. 78

Figure 33. UCS versus density of coal specimens. 79

Figure 34. UCS versus depth of all coal specimens. 80

Figure 35. UCS versus depth of coal specimens from the Witbank No. 2 seam (left) and Highveld No. 4 seam (right). 80

Figure 36. UCS versus tangential elastic modulus E_t for all coal specimens. 81

Figure 37. Average sample UCS versus average sample ITS of coal. 81

Figure 38. ITS versus depth of all coal specimens. 82

Figure 39. Normalized frequency distribution of average uniaxial compressive strength in 11 South African, 13 Indian and 36 U.S. coal seams. 83

Figure 40. Sieve analysis of coal debris used in the coal-crete development study. 92

Figure 41. Specimens for UCS tests with 15%, 30%, 50% and 67% coal content (L-R). 93

Figure 42. Stress-strain curves for coal-crete samples 5 – 9 without polymer binder. 94

Figure 43. Stress-strain curves for coal-crete samples 10 – 13 with polymer binder. 95

Figure 44. The uniaxial compressive strength of coal-crete. 97

Figure 45. Young's Modulus E versus UCS of coal-crete. 97

Figure 46. Relationship between ITS and UCS of coal-crete. 98

Figure 47. Mohr-Coulomb and Hoek-Brown curve fit for a coal-crete with 32.5 N cement and 67 % coal content. 99

Figure 48. Grain-size distribution for coal debris used in the coal-crete mixtures for 42 mm, 100 mm and 150 mm specimens. 104

Figure 49. Schematic drawing of the testing apparatus 105

Figure 50. The effect of indentation in the testing setup on the recorded force-displacement curve for specimens. 106

Figure 51. Mould for casting of 100 mm square specimens. 108

Figure 52. Examples of force-displacement curves for sandstone specimen and varying w/h-ratio. 110

Figure 53. Specimen stiffness over w/h-ratio for different tested materials. 111

Figure 54. Schematic illustration of end-effects and induced triaxial stress-state in compression tests on flat specimen. 111

Figure 55. Examples of calculated stress-strain curves for sandstone specimens of 42 mm diameter at different w/h-ratios. 112

Figure 56. Examples of calculated stress-strain curves for granite specimens of 42 mm diameter at different w/h-ratios. 113

Figure 57. Examples of calculated stress-strain curves for coal specimens of 42 mm diameter at different w/h-ratios. 113

Figure 58. Examples of calculated stress-strain curves for coal-crete specimens of 42 mm diameter at different w/h-ratios. 114

Figure 59. Examples of calculated stress-strain curves for coal-crete specimens of 100 mm square width at different w/h-ratios. 114

Figure 60. Examples of calculated stress-strain curves for coal-crete specimens of 150 m square width at different w/h-ratios. 115

Figure 61. Modulus ratios E_p/E_s for coal-crete specimen of 100 mm square width and varying w/h-ratios. The plotted values correspond very closely with those obtained for 150 mm square specimen. 118

Figure 62. Modulus ratios E_p/E_s for coal-crete specimen of 42 mm diameter and varying w/h-ratios. 118

Figure 63. Modulus ratios E_p/E_s for sandstone specimen of 42 mm diameter and varying w/h-ratios. 119

Figure 64. Modulus ratios E_p/E_s for coal specimen of 42 mm diameter and varying w/h-ratios. 120

Figure 65. Strength of coal-crete specimen of 100 mm width and various w/h-ratios. 121

Figure 66. Strength of coal-crete specimen of 150 mm width and various w/h-ratios. 122

Figure 67. Strength of sandstone specimen of 42 mm diameter and various w/h-ratios. 122

Figure 68. Strength of granite specimen of 42 mm diameter and various w/h-ratios. 123

Figure 69. Strength of coal specimen of 42 mm diameter and various w/h-ratios. 123

Figure 70. A coal-crete specimen of 100 mm square width and $w/h=$ 1 after failure. The fractured sidewalls have been removed to expose the hourglass shape and the shear failure through the centre of the specimen. 124

Figure 71. A coal-crete specimen of $w/h=$ 5 in top view after failure. 125

Figure 72. Coal-crete specimens of $w/h=$ 5 in side-view after failure. 125

Figure 73. Idealized cross-section of fracture patterns in specimens of $w/h=$ 2 – 6. 126

Figure 74. Coal-crete specimens of $w/h=$ 7 (left) and $w/h=$ 10 after compression. 127

Figure 75. Double-cone type shear failure on a sandstone specimen of $w/h=$ 1 and wedging observed on a sandstone specimen core of $w/h=$ 4. 128

Figure 76. A granite specimen of $w/h=$ 3 after failure in top view (left) and side view (right). 128

Figure 77. Sandstone specimens with various w/h-ratios after failure. 129

Figure 78. Coal specimens with various w/h-ratios after failure. 129

Figure 79. Correlation between the material cohesion (c) and the gradient of strength increase (m) over $1 \leq w/h \leq 4$. 132

Figure 80. Correlations between the gradient of strength increase m and the mechanical properties of the materials. 133

Figure 81. The strength of in-situ coal pillars in linear expression. 136

Figure 82. Strength of coal pillars normalized to the strength of a coal cube. 137

Figure 83. Post-beak behaviour of specimens in the laboratory and in-situ. 139

Figure 84. Normalized frequency distribution of coal-rock friction angles, re-analysed after specimen tests provided by York, Canbulat and Jack (2000). 147

Figure 85. Schematic illustration of constitutive material model (left) and boundary conditions used in the pillar model scenarios S1 – S3 (right). 150

Figure 86. Typical stress-strain behaviour for brittle FLAC pillar models in scenario S2. 151

Figure 87. FLAC-computed peak and residual pillar strength versus w/h-ratio for model pillars in scenario S1. 152

Figure 88. FLAC-computed peak and residual pillar strength versus w/h-ratio for model pillars in scenario S2. 152

Figure 89. FLAC-computed peak and residual pillar strength versus w/h-ratio for model pillars in scenario S3. 153

Figure 90. Evolution of failure in a pillar of $w/h=$ 3 with perfectly stiff and rigid interfaces with the surrounding strata, demonstrated as stepwise loss of cohesion (red zones) during pillar loading. 154

Figure 91. The effect of residual friction on the squat effect in FLAC model pillars. 157

Figure 92. Relationship of the exponential strength parameters a and b with ϕ_r in the FLAC models. 160

Figure 93. Rates of pillar strength increase m_1 and m_2 prior and subsequent to the squat effect as a function of the assigned residual friction in failed zones of the FLAC models. 161

Figure 94. Conceptual FLAC pillar model with in-situ boundary conditions. 163

Figure 95. Stress-strain behaviour, strength trends and failure pattern in FLAC model pillars with “fine” mesh, non-brittle constitutive law, in-situ boundary conditions and different w/h-ratios. 165

Figure 96. Stress-strain behaviour, strength trends and failure pattern in FLAC model pillars with “coarse” mesh, brittle constitutive law, in-situ boundary conditions and different w/h-ratios. 167

Figure 97. Trends in the residual strength of coal specimens of different w/h-ratio. 169

Figure 98. Yield and peak stresses observed in granite specimens (left) and numerical models (right). 171

Figure 99. Stress-strain behaviour of coal pillars in Van Heerden’s large-scale in-situ tests, reproduced from Van Heerden (1974). 174

Figure 100. Average yield, peak and residual stress and strains in coal pillars of different w/h-ratios tested by Van Heerden. 174

Figure 101. Extrapolated trends for peak and residual strength (top) and post-peak stiffness (below) in Van Heerden’s large-scale in-situ tests. 176

Figure 102. Extraction ratio in slender pillar layouts (w/h< 5) over time (left) and safety factors used in squat pillar layouts calculated after the latest maximum-likelihood updated pillar strength equation (right). 189

Figure 103. Extraction ratio versus mining depth for pillar design based on the updated empirical pillar strength equations. 190

Figure 104. Estimation of brittle-ductile transition in coal specimens through Mogi’s criterion in conjunction with extrapolated peak strength trends for South African coals (left) and from triaxial tests conducted by Kripakov (1981) (right). 192

Figure 105. Test specimen design for laboratory investigation into the strength of ‘hourglass’ shaped pillars. 193

List of Tables

Table 1. Observed sidewall fracturing in squat pillars in KwaZulu-Natal collieries. 30
Table 2. Uniaxial compressive strength characteristics for different coal seams. 66
Table 3. Mechanical parameters for *TCS* specimens from different coal seams. 75
Table 4. Coal-crete design mixtures with coal and binder proportions by weight. 92
Table 5. Mechanical properties of coal-crete. 101
Table 6. Mechanical properties of materials used in the investigation on shape-effects. 104
Table 7. Rock-steel loading platen contact friction angles φ published in literature. 106
Table 8. Overview of specimens prepared for each material at different *w*/*h*-ratios. 108
Table 9. Data for comparison between material properties and the shape effect. 132
Table 10. Mechanical properties assumed in Mohr-Coulomb pillar models. 145
Table 11. Mechanical properties assumed in different Hoek-Brown pillar models. 146
Table 12. Mechanical properties for coal-rock-interfaces assumed in different pillar models. ..147
Table 13. Material properties for FLAC model scenarios S1 – S3. 149

List of Abbreviations and Symbols

w	Pillar width
h	Pillar height
w/h	Pillar width-to-height ratio
H	Mining depth below surface
B	Mining bord width
SF	Safety factor
T	Specimen stiffness
E	Young's modulus
E_s	Specimen modulus
E_p	Post-peak modulus
ν	Poisson's Ratio
σ	Stress or strength
UCS	Uniaxial compressive strength
TCS	Triaxial compressive strength
ITS	Indirect (Brazilian) tensile strength
MLM	Maximum likelihood method
APS	Average pillar stress
c	Mohr-Coulomb cohesion
ϕ	Mohr-Coulomb angle of internal friction
β_0	Mohr-Coulomb gradient of strength increase in σ_1- σ_3 space
k	Triaxial strength factor
m	Gradient of strength increase over width-to-height ratio, or Parameter in Hoek-Brown failure criterion
s	Parameter in Hoek-Brown failure criterion
φ	Contact friction angle
μ	Coefficient of friction
ρ	Density
κ	Ratio of strength increase, m_1/m_2
$\mathrm{d}\varepsilon_p$	Plastic strain interval for parameter softening in FLAC

1 General introduction

Coal pillar design for underground roof support must operate at an optimal trade-off between economic benefit and safety. Both factors depend directly on each other: the smaller the pillars left behind in the working environment, the higher the deposit extraction but the less competent the structures are. Historically, this trade-off can be quantified by the average extraction rate in South Africa of around 65 %, with the remaining coal being sacrificed in the form of permanent pillars for the sake of mine stability and safety.

Optimizing the extraction rate for underground coal mines without compromising safety has therefore been of keen interest to researchers and mine operators. The question gained momentum through the coal mine disaster of Coalbrook in 1960, where thousands of coal pillars in the underground workings collapsed and 437 miners lost their lives.

The pioneering work of Salamon and Munro (1967) from the South African Chamber of Mines Research Organization (COMRO) was directed at developing a statistical method to distinguish collapsed and stable pillar layouts based on the pillar and panel layout geometry. This led to the world-renowned coal pillar strength equation and safety factor design approach named after the authors, which is still applied as state-of-the-art in many countries.

The developed technique was also sufficiently convenient to facilitate the update of knowledge around coal pillar strength in the different coalfields and seams of South Africa in the course of time. The idea that the best pillar strength design equation is one that distinguishes optimally between failed and stable cases was taken further by Van der Merwe (2003b) and resulted in the development of a reliability-based design approach for coal pillars.

Other pioneering work was conducted by Bieniawski (1968a) from the Council for Scientific and Industrial Research (CSIR), who was the first in South Africa to address the question of coal pillar strength by conducting underground large-scale compression tests on model coal pillars. This was subsequently followed by researchers Wagner (1974) and Van Heerden (1975) who conducted similar testing programmes at different sites in the country.

All this research created a wealth of information on in-situ coal pillar strength and failure — knowledge that was sourced from, and for, a South African coal mining environment which remained fairly unaltered in the second half of the 20th century. The depth of mining seldom exceeded 250 m, with mined seam thicknesses of average 3 m and typical pillar width-to-height ratios of 3 – 4.

It is therefore not surprising that comparatively little research has been directed at the prediction of coal pillar performance in deeper lying deposits, where squat pillars of larger width-to-height ratios will be required to support the overlying strata. Nevertheless, a

thorough understanding of squat pillar performance will be required, should the remaining deep coal deposits be extracted in future, for instance in the Waterberg or Ermelo coalfields of South Africa.

The current expectation of squat coal pillar strength in South Africa is such that some form of exponential strength increase should occur for pillars with width-to-height ratios greater than 5. This idea was advocated by Salamon (1982; Salamon and Wagner, 1985), and substantiated through laboratory tests and field observations by Madden (1990, 1991). If this holds true, then squat pillars must obey a distinctly different mechanism of strength and failure than pillars with smaller width-to-height ratios, for which only a linearly or regressively increasing strength versus width-to-height relationship is evident.

The question as to why a change in strength trends should occur, and what would cause the squat pillar strength trend to take an exponential form, remains largely unanswered so far. There is also a question as to how the current squat coal pillar formula, if valid, can be adopted to fit continuously with the new empirical strength equations for slender pillars (Van der Merwe and Mathey, 2013c).

Interestingly, the South African interpretation of squat pillar strength has not always been accepted in other mining countries of the world. For instance in the United States the understanding is such that for squat pillars there is no deviation from the strength trend that is known for slender pillars, only that brittle-ductile transition occurs eventually. The brittle-ductile transition means that at some point a pillar might be sufficiently squat to not exhibit a peak strength drop at failure, but rather is able to sustain or even increase a high load-bearing capacity with further deformation forced upon it.

The conflict between the two philosophies highlights the need for further research into the mechanisms of strength and failure in coal pillars with large width-to-height ratios. The investigation conducted in the present thesis outlines as follows:

In Part I, the international advances in the understanding of squat coal pillar strength and design are reviewed and discussed. Evidences from in-situ pillar behaviour, insights from laboratory testing and indications from numerical and analytical models are taken as a basis to identify the requirements for research in this thesis.

A statistical analysis of the basic mechanical properties of coal in South Africa, conducted in Part II, is aimed at establishing possible coalfield-, seam-, or site-specific requirements for squat pillar strength considerations.

Part III is designed as a laboratory study into the role of mechanical material properties for shape and possible squat effects in physical model pillars. A series of compression tests on selected coal, rock and coal-crete materials of slender and squat shape is conducted in order to evaluate the different strength, deformation and failure patterns.

A conceptual study of shape and possible squat effects in numerical model pillars is conducted in Part IV, with particular reference to the influence of residual mechanical

properties of crushed material. The phenomena associated with strength and failure observed on physical specimens in the laboratory are qualitatively reproduced, and allowance for in-situ boundary conditions is made in an attempt to bridge the gap between the laboratory and the underground mining environment.

The research findings from Parts I – IV are reconciled in the overall conclusions of Part V, where a unified understanding of squat pillar strength and failure is presented and implications for pillar design are discussed. Finally, indications for further research are given.

2 Squat pillar terminology

The use of the term *squat pillar* differs internationally and is discussed in this chapter for the purpose of clarity and use in this thesis.

Pillars of unmined ground are left behind in underground mines to ensure excavation stability on a regional or local scale. The terminology for the various kinds of pillars usually relates to their function and location in the mine.

For example, *barrier pillars* are designed to prevent the collapse of a mining panel from spreading towards adjacent excavations or to prevent water flow between different regions in the mine. A *bracket pillar* is a piece of unmined ground on either side of a fault or other major discontinuity in the rock mass, designed to prevent mining-induced stress changes that affect the stability of the discontinuity and the accompanying risk for excavation stability. A *shaft pillar* serves a similar function, namely to avoid adverse impacts of mining on the stability of the shaft and shaft-service infrastructures. Further, pillars inside a production panel, which serve as support for the immediate roof above them, are termed *in-panel pillars*. In contrast, those pillars which are intended for regional improvement of stresses and displacement around excavations are called *regional* or *stabilising pillars.*

The term *squat pillar* does not prescribe a certain location nor a function of the structure but merely describes the pillar shape, i.e. the width-to-height ratio. A squat pillar may therefore serve as in-panel roof support for production panels at great depth, as a safety pillar in geologically disturbed ground, or to ensure entry stability adjacent to longwall panels.

As the term implies, a squat pillar is one with a relatively large width-to-height ratio, i.e. $w>>h$ in general. However, the critical width-to-height ratio above which a pillar is considered to be a squat pillar is not agreed upon internationally.

In the United States, Mark (2000) suggested the following definition of coal pillars according to their width-to-height ratio by considering the mode of their collapse:

- Slender pillars ($w/h< 3.0$), which have little residual strength and which are prone to massive collapse when used over a large area;
- Intermediate pillars ($4\leq w/h\leq 8$), where ‘squeezes’ are the dominant failure mode in room-and-pillar mining, and where empirical strength formulae seem to be reasonably accurate, and;
- Squat pillars ($w/h> 10$), which can carry very large loads and are strain-hardening, and which are dominated by entry failure (roof, rib and floor) and by coal bumps.

In other words, according to Mark (2000) a squat pillar is one that does not have an ultimate compressive strength, because a strain-hardening pillar increases its load-bearing capacity with increasing deformation. Yet, the pillar can fail to provide its ground-control function because it allows excessive deformations to take place in the surrounding strata, which ultimately causes failure of the same.

Mark (2000) also noted that the strength of pillars of up to $w/h = 8$ appear to conform to empirical strength formulae. It can therefore be argued that no squat effects occurs in this width-to-height range, since all empirical coal pillar strength formulae describe pillar strength as a merely linearly or regressively increasing function of the pillar width-to-height ratio.

In South Africa, the development of knowledge around coal pillar behaviour was initially focussed only on the lower width-to-height ratio range (i.e. $w/h < 4$) because this was the only range where pillars were observed to collapse. The pioneering work of Salamon and Munro (1967), Bieniawski (1968a), Wagner (1974) and Van Heerden (1975) was fundamental to this knowledge and proved that (a) the peak strength of pillars in this interval increases only linearly or regressively and (b) the residual strength of pillars is relatively low. Yet, it was agreed amongst rock engineers that at some very large width-to-height ratio, presumably $w/h \geq 10$, the strength of a coal pillar would be such that it becomes practically indestructible.

Therefore it was suggested that the strength of pillars had to increase drastically from some critical width-to-height ratio onwards. This critical width-to-height ratio was assumed to be around $w/h = 5$, since no pillar collapse had been observed above this value. An individual pillar strength formula with exponential strength increase was suggested by Salamon (1982; Salamon and Wagner, 1985) and investigated by Madden (1990, 1991). The formula was termed the *squat pillar formula*, implying that all pillars beyond a width-to-height ratio of 5 were squat pillars.

The difference in the understanding of squat pillars in the U.S. and in South Africa are of major mechanical significance: while in the U.S. the *squat effect* is assumed to be strain-hardening behaviour (i.e. no ultimate strength exists) in pillars above a width-to-height ratio of 10, in South Africa it is assumed to be an exponential increase in the maximum load-bearing capacity beyond a critical width-to-height ratio of 5.

This discrepancy already sketches the scope of investigation in this thesis. Therefore a definition of squat pillars by a fixed width-to-height ratio or by a strength or failure mechanism does not appear to be meaningful at this stage.

The term *squat pillar* is preliminarily used in this thesis for all pillars with width-to-height ratios outside the range of which empirical evidences on strength and failure mechanisms are established in South Africa, i.e. $w/h > 4.4$. In the course of research, the term might be adapted according to new evidences for changes in strength and failure mechanisms in pillars above a critical width-to-height ratio. These changes, which can manifest either as a true deviation from previously experienced trends in peak-strength (i.e. linear or regressively increasing trends), or as a transition from strain-softening into strain-hardening behaviour, will then be termed accordingly as the *squat effect*.

PART I

Advances in squat coal pillar design and requirements for further research

3 Literature review and own contributions

The literature review is conducted with the aim of providing background to the current South African squat coal pillar strength formula and the performance of pillars designed accordingly. In the same context, the international strength equation for coal pillars with large width-to-height ratios and for pillar design at greater depth will be identified.

Published evidences on in-situ squat pillar behaviour from South African and international sources, as derived from statistics on stable and collapsed cases, field observations on pillar fracturing or stress measurements, will be compiled and discussed.

A review of laboratory tests on coal and rock specimens in the slender and squat shape range will provide insight into the trends in the strength versus width-to-height relationship and possible changes in the failure mode of specimens.

Numerical modelling has been used extensively in the past 20 years to evaluate the performance of the pillar system (coal pillar-interface-rock strata) in different geological conditions and findings will be reviewed in order to identify crucial factors influencing squat pillar design.

Analytical models and their applicability to squat coal pillar design will be included in the review for completeness.

3.1 South African and international strength formulae for slender and squat pillars

3.1.1 South African pillar strength formulae

The South African approach to squat pillar design must be seen in relation to established knowledge on pillar strength in the slender shape region of $w/h \leq 5$, which is therefore briefly summarized in the following.

The first pillar strength formula for South African coal was published by Salamon and Munro (1967). They based their research on a database of 27 collapsed and 98 stable pillar geometries and derived a statistical maximum likelihood pillar strength equation under the argument that collapsed pillars must have a predicted safety factor close to one and stable pillars should have safety factors larger than one. This resulted in the following formula,

$$\text{Strength} = 7.2\, w^{0.46}/h^{0.66} \tag{1}$$

where strength is in MPa units, w is the pillar square width [m] and h the pillar height [m]. The formula has remained the most frequently applied pillar strength equation in South Africa.

At around the same time of the investigation of Salamon and Munro, Bieniawski (1968a) conducted in-situ compression tests on large-scale specimens of coal at Witbank colliery

in order to determine the elastic deformation and peak-strength characteristics. His pillar strength formula,

$$\text{Strength} = 2.5 + 2\ w/h \tag{2}$$

took a linear expression and found subsequently widespread application in the United States. In the 1970s, researchers Wagner (1974) and Van Heerden (1975) followed the example of Bieniawski and conducted further in-situ compression tests on coal at Usutu and New Largo colliery, using some modifications in the testing setup. The resulting pillar strength equations are:

$$\text{Strength} = 7 + 4.0\ w/h \tag{3}$$

in the case of Wagner's tests at Usutu and

$$\text{Strength} = 10 + 4.2\ w/h \tag{4}$$

for Van Heerden's tests at New Largo.

The linearized versions of the site-specific pillar strength equations as summarized by Van Heerden (1975) are used here for the ease of comparison.

It is apparent that the site-specific strength of coal pillars varies significantly. The cube strength of coal at Witbank was found to be 4.5 MPa, while at New Largo it is more than three times as high with 14.2 MPa. The formula by Salamon and Munro (1967) for the average strength of failed coal pillars predicts a cube strength value of 7.2 MPa that lies in the lower middle field of the compression test results.

Over the years, the pioneering work of the aforementioned researchers has been further updated by different investigators, for instance by Madden (1991), who in his re-analysis of collapsed and stable cases only found smaller deviations from the Salamon and Munro (1967) formula.

Van der Merwe (2003b) introduced a new approach to the statistical evaluation of stable and collapsed coal pillars, subsequently termed the overlap reduction method (Van der Merwe and Mathey, 2013c), and defined pillar strength in "normal" coal areas as:

$$\text{Strength} = 3.5\ w/h \tag{5}$$

Furthermore, Van der Merwe (2003b) distinguished the Klip Rivier and Vaal Basin coalfields from the areas of "normal" coal in South Africa and grouped them as areas of "weak" coal, since a great number of pillars of very high safety factors failed there. In the latest 2011 statistical review of coal pillar strength in South Africa based on failed and stable cases, Van der Merwe and Mathey (2013c) utilized both the maximum likelihood and the overlap reduction technique in comparison. From a database of 86 failed and 334 stable cases, two alternative pillar strength equations were derived for coalfields of normal coal strength. For maximum likelihood estimation:

$$\text{Strength} = 6.61\ w^{0.5}/h^{0.7} \tag{6}$$

And for the overlap reduction technique:

$$\text{Strength} = 5.47\ w^{0.8}/h \tag{7}$$

Also, the Free State coalfield was added to the list of weak coal areas. Equations (1) to (4) as well as (6) and (7) are plotted in Figure 1 on page 25 for comparison. Extrapolations outside the empirical ranges are shown as dotted lines. A pillar height of 3 m was assumed for this plot, which is important to note, since the power-law of Equations (1), (6) and (7) introduce a volume-effect on the predicted pillar strength.

It should also be noted that a number of seam-specific pillar strength equations have been developed for South African coals (Salamon, Canbulat and Ryder, 2006), based on failed and collapsed cases and the maximum likelihood method as used initially by Salamon and Munro (1967).

All the above mentioned coal pillar strength formulae are only valid within the empirical range from which they were derived. In terms of pillar shape it means that only width-to-height ratios of less than 5 are considered.

Salamon (1982; Salamon and Wagner, 1985) recognised that his strength equation for the more slender square pillars of $w/h \leq 5$ should not be extrapolated beyond the range of statistical evidence. A separate equation for squat pillars with width-to-height ratios greater than 5 was therefore proposed.

The fundamental assumption was made that the strength of a squat coal pillar increases progressively with increasing width-to-height ratio, as opposed to the regressive strength increase determined for slender pillars. Salamon and Wagner (1985) stated that the reasoning behind the squat pillar formula was based on limit-equilibrium considerations for cohesionless granular ribsides, on further experimental work conducted on ribs consisting of granular material, and on compression tests conducted on cylindrical sandstone specimens.

The South African squat pillar formula was hence designed such that it connects to the established Salamon and Munro (1967) strength formula for normal coal pillars at a so called critical width-to-height ratio and to predict an exponential strength increase for increasing width-to-height ratios beyond this threshold.

The proposed ‘squat’ pillar strength equation takes the following form:

$$\text{Strength} = 7.2\ \frac{R_0^{0.5933}}{V^{0.0667}}\ \left\{\frac{0.5933}{\varepsilon}\ \left[\left(\frac{R}{R_o}\right)^{\varepsilon} - 1\right] + 1\right\} \tag{8}$$

R_0: Critical width-to-height ratio
R: Pillar width-to-height ratio
V: Pillar volume [m^3]
ε: rate of strength increase

The formula contains two parts: The first term standing outside the curly brackets is responsible for connecting the ‘squat’ to the ‘normal’ pillar strength equation. In fact, it can be shown that this term is identical with the Salamon and Munro formula when w/h is substituted for R_0 and w^2h for V. However, R_0 is not a variable but a fixed parameter which defines the threshold for the transition from a normal coal pillar to a squat pillar with

exponential strength increase. A critical width-to-height ratio of R_0= 5 was suggested based on the observation that no pillar with width-to-height ratio greater than R= 3.6 had been observed to collapse in South Africa.

The second part of the equation features the strength increase factor ε, for which a value of ε= 2.5 was proposed. A plot of this formula can be seen in Figure 1.

Madden (1990) reviewed the proposed parameters of the squat pillar formula based on field observations on fracturing of sidewalls of squat coal pillars, and on laboratory tests on sandstone specimens. He concluded that the proposed values for R_0 and ε can be regarded as conservative estimates, but was not able to determine more accurate parameters.

The production benefit which can result from the introduction of the squat pillar formula as compared to the Salamon and Munro formula will theoretically depend on the depth of the mining operation and the mined seam thickness, provided that the pillar safety factor and the bord width are constants in the mine design. The general trend is that the smaller the mining thickness and the greater the mining depth, the higher the production benefit will be.

Madden demonstrated that for a pillar of 3 m height, the production benefit may be as much as about 3 % at 200 m depth, 8 % at 300 m and about 12 % at 400 m depth. With pillars of only 1 m height the possible improvement in production at the same depth intervals will be approximately 7 %, 12 % and 18 % respectively. In all scenarios a safety factor of 2.0 and a bord width of 6 m was assumed. These results demonstrate the significant implication of the equation for the industry.

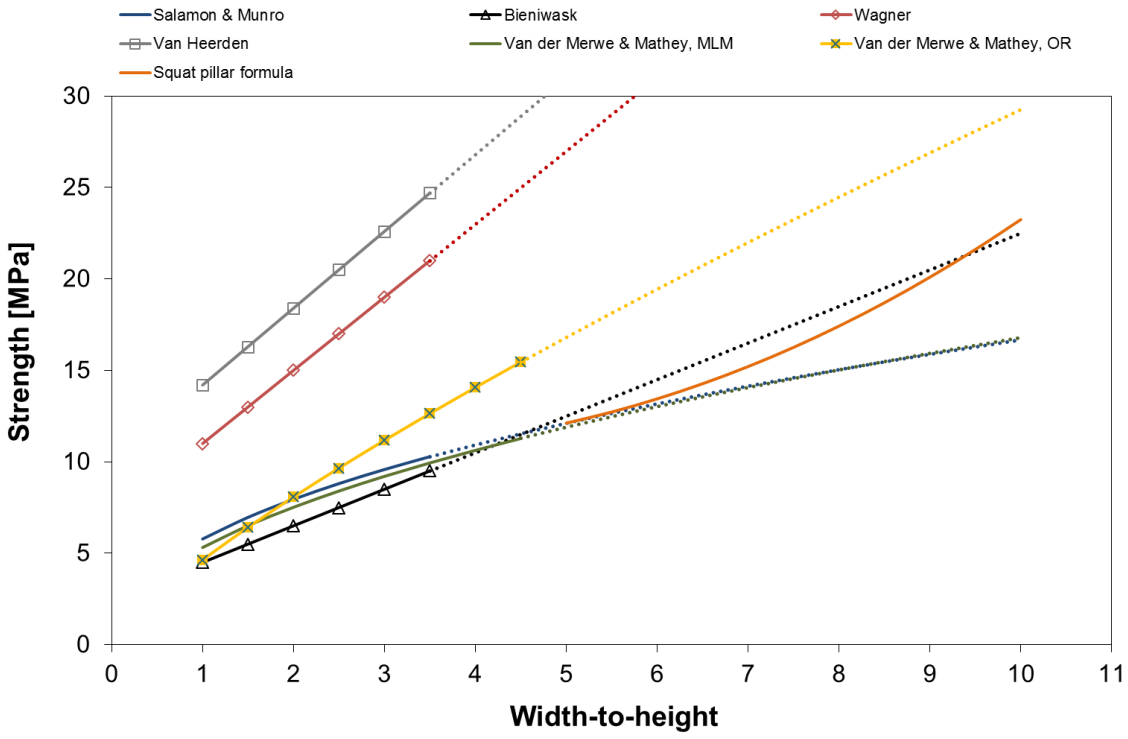


Figure 1. Comparison of South African coal pillar strength formulae for an assumed pillar height of 3 m.

3.1.2 International squat coal pillar formulae

The methodology developed in South Africa by Salamon and Munro (1967) to predict coal pillar strength based on a stochastic evaluation of stable and failed cases and the assumption of an exponential increase in strength for squat coal pillars have also been adopted in Australia.

Galvin and Hebblewhite (1995) published the first Australian coal pillar strength equation for pillar width-to-height ratios up to 5 based on maximum-likelihood estimation:

$$\text{Strength} = 7.4\ w^{0.46}/h^{0.66} \tag{9}$$

Their assumptions on the critical width-to-height ratio and the exponential strength increase factor for pillars in the squat range are essentially the same as in South Africa. The Australian squat coal pillar formula for pillar width-to-height ratios above 5 is given as:

$$\text{Strength} = \frac{19.24}{w^{0.133}h^{0.067}} \left\{0.237 \left[\left(\frac{w}{5h}\right)^{2.5} - 1\right] + 1\right\} \tag{10}$$

These strength equations were repeatedly reviewed in the years following their publication. In its latest review by Galvin et al. (1999), the Australian and South African databases on collapsed and stable cases were merged and analysed together. This resulted in the following pillar strength equations:

For $w/h \leq 5$:

$$\text{Strength} = 6.88\ w^{0.5}/h^{0.7} \tag{11}$$

And for $w/h > 5$:

$$\text{Strength} = \frac{19.05}{w^{0.133}h^{0.066}} \left\{0.253 \left[\left(\frac{w}{5h}\right)^{2.5} - 1\right] + 1\right\} \tag{12}$$

Equations (11) and (12) are plotted in Figure 2 on page 28.

In the United States the question of coal pillar strength was initially approached through laboratory testing of the size and shape effect in coal specimens from different coal seams and extrapolating the results to in-situ pillars, e.g. Greenwald (1939) and Gaddy (1956). Further tests were conducted by Meikle and Holland (1965) to investigate the influence of the interface friction between coal and strata on the strength of coal.

Different coal pillar strength equations emerged from these research efforts, the internationally best-known being the so called Holland and Gaddy (1957) coal pillar strength formula,

$$\text{Strength} = k\sqrt{w}/h \tag{13}$$

where k is a constant strength factor for each coal seam.

The laboratory derived equations presented the challenge that laboratory tests had to be extrapolated to in-situ coal pillar behaviour. This was overcome in South Africa by direct testing of large-scale coal specimens in-situ. The linear strength equation developed by Bieniawski (1992) found acceptance in the United States:

$$\text{Strength} = S_{cube}\ (0.64 + 0.36\frac{w}{h}) \tag{14}$$

Where S_{cube} is the representative cube strength for a coal seam. Bieniawski (1992) stated that the equation provided a good fit to in-situ observations on pillar strength up to a width-to-height ratio of 12. Above this value, it would provide a conservative estimate. The Bieniawski strength equation is plotted in Figure 2 on page 28 for Pittsburgh coal (S_{cube}= 6.4 MPa).

Equation (14) has been subsequently modified into the so-called Mark-Bieniawski equation (Mark and Chase, 1997), which can also account for pillars of rectangular shape with width w and length l:

$$\text{Strength} = S_{cube}\ [0.64\ (0.54 - 0.18\left(\frac{w^2}{hl}\right))] \tag{15}$$

Mark (2000) comments that the empirical strength formulae appear to be reasonably accurate for pillar width-to-height ratios up to 8. In this range, they are also used by other U.S. based researchers for calibration of numerical models (Esterhuizen, Mark and Murphy, 2010).

A unique approach to pillar design was presented by the India-based researchers Sheorey et al. (1987), in that their strength equation accounts for the influence of pre-excavation or virgin stress conditions on the load-bearing capacity of the pillar. The fundamental assumption made was that a pillar may be able to retain some of the original horizontal confinement existing in the coal prior to excavation, depending on its width-to-height ratio and its contact conditions to the surrounding strata. Therefore, with increasing depth, the pillar confinement and vertical load bearing capacity should increase. For average coal measures of India, the formula is given as

$$\text{Strength} = 0.27\sigma_c\, h^{-0.36} + \frac{H}{160}(\frac{w}{h}\text{-}1) \tag{16}$$

where σ_c is the strength of 25 mm cubic coal specimens, h is the pillar height [m], w the pillar width [m] and H the depth below surface [m]. The equation implies that the shape effect in pillars is linear. The fixed coefficients used in the equation were found by evaluation of failed against stable cases in Indian coal seams. It should be noted that a subsequent refinement of the equation was proposed by Sheorey (1992).

Despite the formula not being designed particularly for pillars with large width-to-height ratios, it nevertheless offers an intriguing solution to the challenge of pillar design at greater depth.

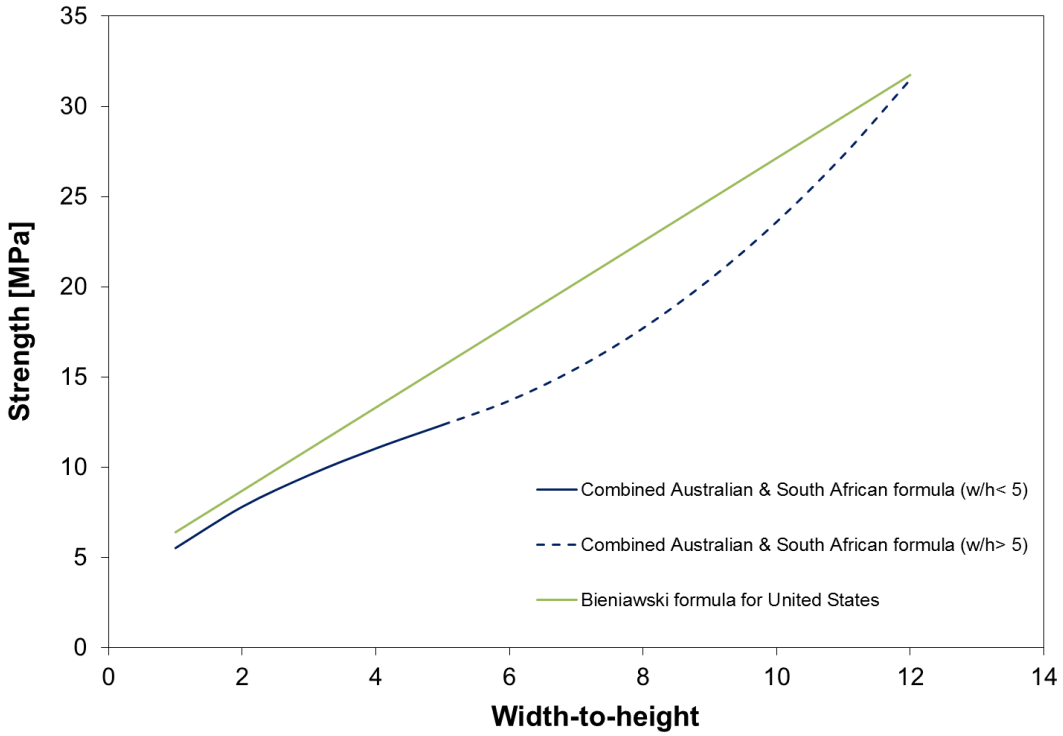


Figure 2. Shape effects in coal pillars as predicted by the Bieniawski formula for the United States and the combined Australian and South African formulae.

3.2 Evidence from in-situ pillar behaviour

The only means to establish confidence into the behaviour of underground pillars is through field observations. In the following sections, the most-recent update of the South African coal pillar databases on collapsed and stable cases is discussed with regards to the general squat pillar performance and seam- or site specific pillar behaviour.

Findings from in-situ pillar monitoring, e.g. stress measurements and fracture observations on local and international squat coal pillars are also included in the review.

3.2.1 Pillar collapses and stable cases

Since the first review of coal pillar performance in South Africa based on collapsed and stable cases by Salamon and Munro in the 1960s, the database has increased about threefold. In the latest update of the database in 2011 by Mathey (2011) a number of 86 failed and 334 stable cases across all South African coalfields was compiled.

The new cases of pillar failures did not change the overall characteristics of the database in a significant way. However, the maximum width-to-height ratio of collapsed pillars increased from the original 3.6 to 4.4, as can be seen in Figure 3.

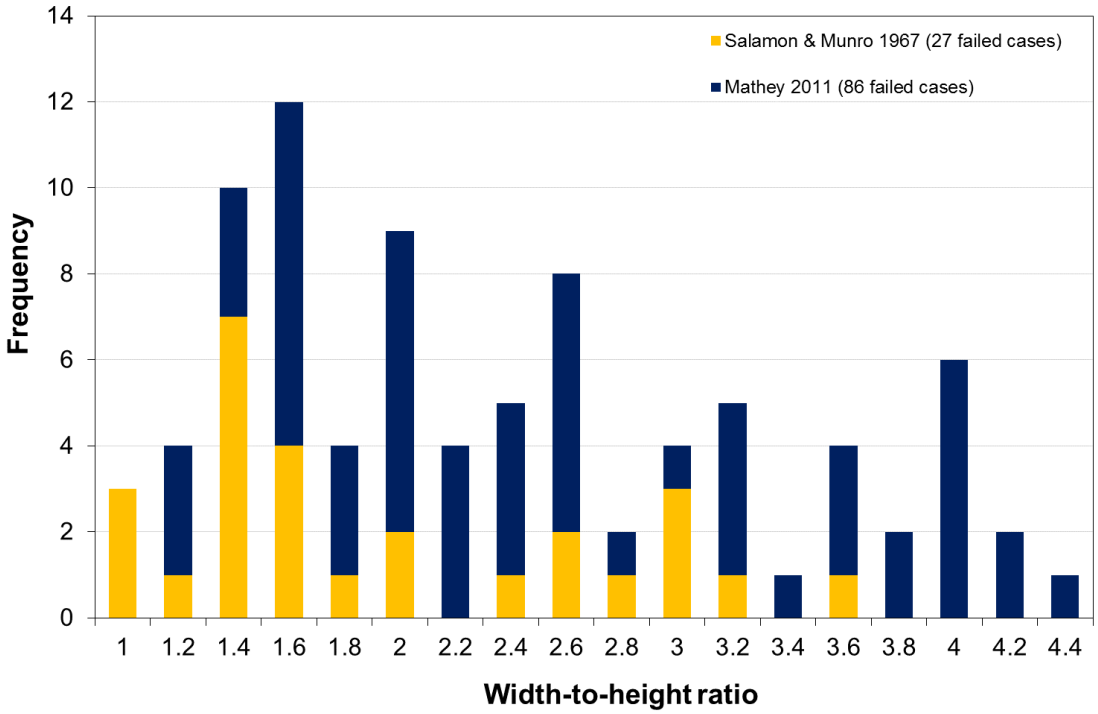


Figure 3. Frequency distribution of collapsed pillar width-to-height ratios.

The cases of pillar failures with $w/h>$ 3.6 come from mining operations in the Vaal Basin, Klip River and Free State coalfields, which are known to produce failures at higher safety factors and are therefore classified as areas of weak coal in South Africa.

Still, no pillar failure beyond the critical width-to-height ratio of 5 has been observed. Therefore Salamon's assumption on a squat effect occurring at $w/h=$ 5 remains unchallenged.

Based on the updated database of collapsed and stable cases, the probability of failure (PoF) has been determined (Van der Merwe and Mathey, 2013a). The PoF was based on a direct comparison between the number of observed pillar failures at a given safety factor to an observed and extrapolated number of stable cases of the same safety factor in all coalfields in South Africa. The link between the updated maximum likelihood pillar strength equation and the failure probability is plotted in Figure 4. For instance, it can be seen that the failure probability of a pillar with $SF=$ 1 is estimated to be less than 10 %.

The fact that mining panels are being found in stable conditions despite the calculated safety factor for the pillars being one or less may point again to the seam- and site-specific nature of coal pillar strength. The current strength equations (see Chapter 3.1.1) derived from failed cases only give the average strength of failed cases and may therefore be only a lower-strength estimate for coal in the country. This has also been found in the in-situ compression tests by Wagner and Van Heerden, who found significantly higher strength values than predicted by the statistical equations.

In the context of squat pillar design this means that a single strength equation which adequately approximates the strength of squat coal pillars in all seams and sites in the country is not likely to be found.

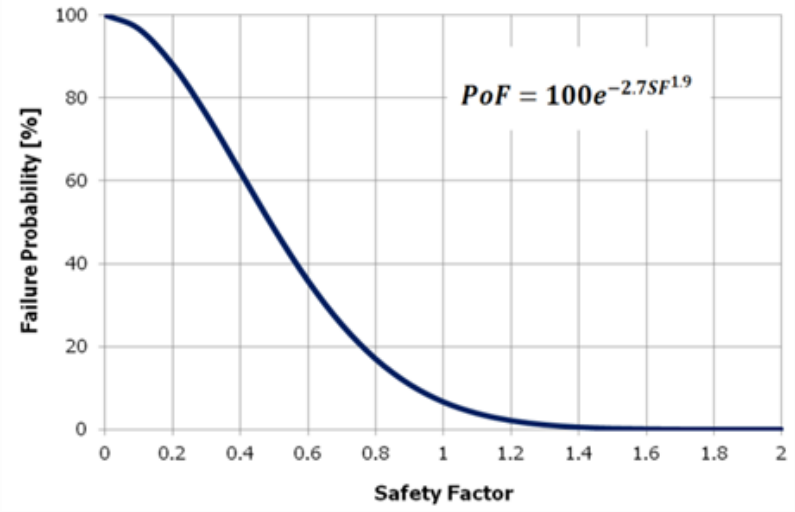


Figure 4. Link between the safety factor and failure probability for coal pillars whose strength is calculated with the updated maximum likelihood strength equation.

3.2.2 Field observations on squat pillar behaviour

In South Africa, confidence into the squat coal pillar formula was established by Madden (1990) through fracture monitoring on sidewalls of pillars and extensive field trials.

He inspected the sidewalls of squat pillars for the depth of fracturing at Piet Retief and Longridge collieries in KwaZulu-Natal. Table 1 summarizes his findings and presents the relevant pillar safety factors calculated according to the Salamon and Munro (S/M) and squat pillar formula (see column 'Squat' in Table 1).

Table 1. Observed sidewall fracturing in squat pillars in KwaZulu-Natal collieries.

#	Colliery	Mining dimensions				Safety factors		Fracturing	
		H [m]	w [m]	h [m]	w/h	S/M	Squat	Depth [m]	% of w
1	Longridge	155	15.3	2.5	6.2	1.86	1.92	2.6	34.0
2	Longridge	252	32.0	2.5	12.8	2.18	4.07	1.5	9.4
3	Piet Retief	550	28.0	2.0	14.0	1.04	2.19	1.9	13.6

Madden (1990) concluded that fracturing was restricted to the outer zones of the pillars and that the Salamon and Munro (1967) strength formula was very conservative when extrapolated to pillars at a depth of 550 m below surface. In further field trials at Hlobane and Piet Retief collieries the squat coal pillar formula was found to give stable pillar dimensions.

The predicted exponential increase in strength by the squat pillar formula suggests that pillars will become practically unfailable under the normal loads they are subjected to in regular mining practice, perhaps at width-to-height ratios of around 15.

This is challenged by findings from Maleki (1992) who reported that in the United States squat pillars with width-to-height ratios up to 15 have been observed to fail under load. In back-analysing the average peak vertical stresses on collapsed pillars from 7 coal seams and 8 collieries through means of empirical, numerical and stress-measurements analysis, he established strength versus width-to-height curves for coal pillars far into the squat pillar range.

In the analysis, he distinguished the confinement-controlled pillar collapses in competent geological environments from those where the failure mechanism appeared to be structurally controlled, i.e. failure was aided by persistent cleats and in-seam contact planes.

His pillar strength equations, modified to account for strength in MPa units, are reproduced in Figure 5. Maleki (1992) is the first author who proposes that coal pillars of even very squat dimensions do have a limited maximum strength, i.e. about 32 MPa or 26 MPa depending on geological conditions. He states that above these limits, stability problems may occur as a result of failures in roof, seam and floor. His strength equations therefore follow a regressive strength increase over width-to-height ratio, reaching an asymptotic value of between w/h= 10 – 15.

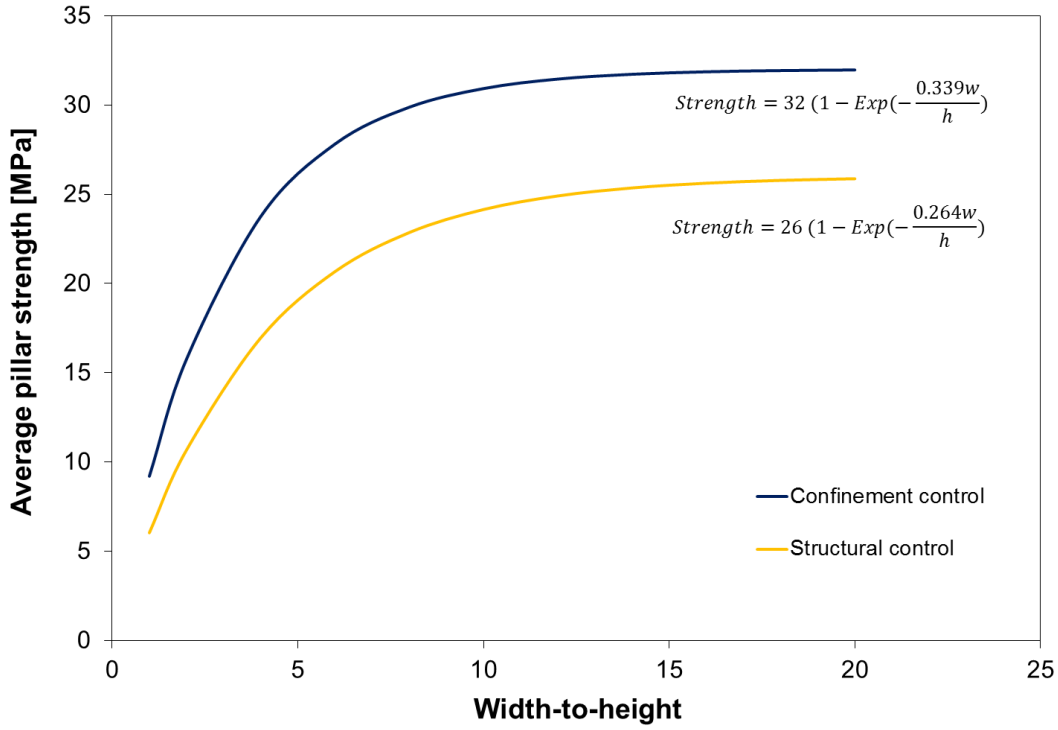


Figure 5. Coal pillar strength after Maleki (1992).

The influence of the geological environment on the strength of slender and squat coal pillars has also been noted in field observations by Australia-based researcher Gale (1999), who compared the pillar stress-measurement data with numerical models. His findings are discussed in Chapter 3.5.1.

3.3 Insights from laboratory testing

Laboratory testing cannot provide a quantitative assessment of in-situ pillar strength, due to the practical restrictions with regards to test specimen sizes, loading rates and boundary conditions. However, in comprehensive testing programs, the test parameters can be varied so as to give a qualitative estimate of what the expected in-situ pillar behaviour could be.

Typically, a pillar-oriented test design makes use of a range of specimen sizes and shapes. The specimens are tested in compression with a constant loading rate between hardened-steel loading platens. The ultimate load-bearing capacity of the specimens and the full stress-strain response are recorded and the alteration over different specimen shapes are compared. This provides useful insight into (a) the phenomena accompanying failure, e.g. fracture patterns or acoustic emissions, (b) trends in the yield, peak and residual strength, and (c) the mode of failure, e.g. brittle or ductile, of that particular material when shaped into different geometries.

In more complete investigations, the impact of boundary conditions can be investigated as well. The specimens are clamped between the loading-platens due to the friction acting along the specimen-steel-interface, which can impact the overall load-bearing capacity or deformational behaviour of the test specimens. Because this magnitude of friction is not necessarily the same as that experienced by the in-situ pillar sandwiched between the rock strata, it may be desirable to modify the contact friction angle in the test setup to extreme values, i.e. very low or zero friction and very high friction, so as to qualitatively assess the impact of the contact friction angle.

3.3.1 Shape effect in intact coal specimens

Such a series of compression tests on coal specimens with large width-to-height ratios has been conducted by Meikle and Holland (1965) in the Unites States. Three series of 20 specimens each were tested at width-to-height ratios of between approximately 4 – 8 by keeping the specimen height constant at 9.5 mm and varying the square width between 38 – 76 mm. The contact friction coefficient between coal and steel was kept natural, i.e. unaltered, in the first test series (μ= 0.3) and then reduced through lubrication for the following two series (μ= 0.15 and μ= 0.04 respectively).

The tests yielded the trends as shown in Figure 6 on page 34. The peak specimen strength reduces considerably with a reduction of the contact friction between the specimen and the steel platens. However the trends in all three test series take the form of a regressive increase in strength over specimen width-to-height ratio, irrespective of the contact friction. No squat effect is observed.

Khair (1994) conducted compression tests on coal specimens with a similar scope as Meikle and Holland (1965), ranging specimen width-to-height ratios between 4 – 8 and applying various boundary friction coefficients between μ= 0.04 – 0.51. The test results were generally similar to the findings of Meikle and Holland (1965), with the magnitude

of strength being reduced for all specimens of different shape for a lower contact friction. A regression analysis of the data fits a linear or regressively increasing trend in the strength over width-to-height relationship equally well. Again, a progressive increase in strength or brittle-ductile transition was not observed in the test series, even for those specimens tested with strong frictional contacts between the specimen and the platen ($\mu = 0.51$ or $\varphi = 27^{\circ}$).

A regressively increasing trend in the relationship between the compressive strength and the width-to-height ratio of specimens was also established by Kroeger, Roethe and Li (2004) in their laboratory tests on coal specimens from selected Illinois seams in the United States. Specimens of various square side length between 48 – 140 mm and width-to-height ratios up to 12.5 were considered in the investigation. Strain-hardening behaviour in specimens or an exponential increase in strength was *not* noted by the investigators. The equation for the shape effect as determined for the Murphysboro seam is presented within its empirical range in Figure 6 on page 34.

In South Africa, the shape effect in coal specimens has been studied intensively by Madden and Canbulat (1995) in the SIMRAC research project COL21. Twelve blocks of coal were sampled from 11 different collieries and over 900 specimens with varying sizes and shape were prepared. Strength magnitudes were found to vary significantly with changes in specimen size and origin. Size and shape effects up to $w/h = 8$ were analysed statistically, and it was found that the equation

$$\text{Strength} = k\, w^{0.139}/h^{0.449} \tag{17}$$

with k being a strength coefficient, w and h the specimen width and height in meter units respectively, provided an adequate fit to the data. The equation is plotted in Figure 6 on page 34 in its empirical width-to-height range, assuming the average strength factor for all collieries, $k = 15.83$ MPa, and a specimen width of 100 mm. Notably, the function describes a regressively increasing relationship between strength and width-to-height ratio. Neither an exponential increase in strength nor strain-hardening occurred in the tested specimens.

Das (1986) was the first investigator to present full compressive stress-strain curves for coal specimens modified in shape. He used specimens of coal from 5 different Indian seams, cut into constant cylindrical width of 54 mm and varying height, in order to obtain width-to-height ratios up to 13.5. He noted that all specimens with $w/h < 9$ failed in a brittle manner, i.e. exhibiting a significant loss in strength upon failure. Specimens of $w/h = 10 – 11$ and higher did not fail brittle but in a ductile, strain-hardening manner.

Das did not provide a regression analysis for the peak strength in the range of brittle specimen failure, but provided the full stress-strain curves. When the peak strength values for all specimens from the different seams are carefully read out from the diagrams and analysed together, the linear trend as shown in Figure 6 is suggested.

It should be noted that because of the generally non-linear character of the equations (i.e. the different exponents for w and h) plotted in Figure 6, the relationships are ambiguous. The strength plots in Figure 6 and in the following Figure 7 are for illustration of trends only.

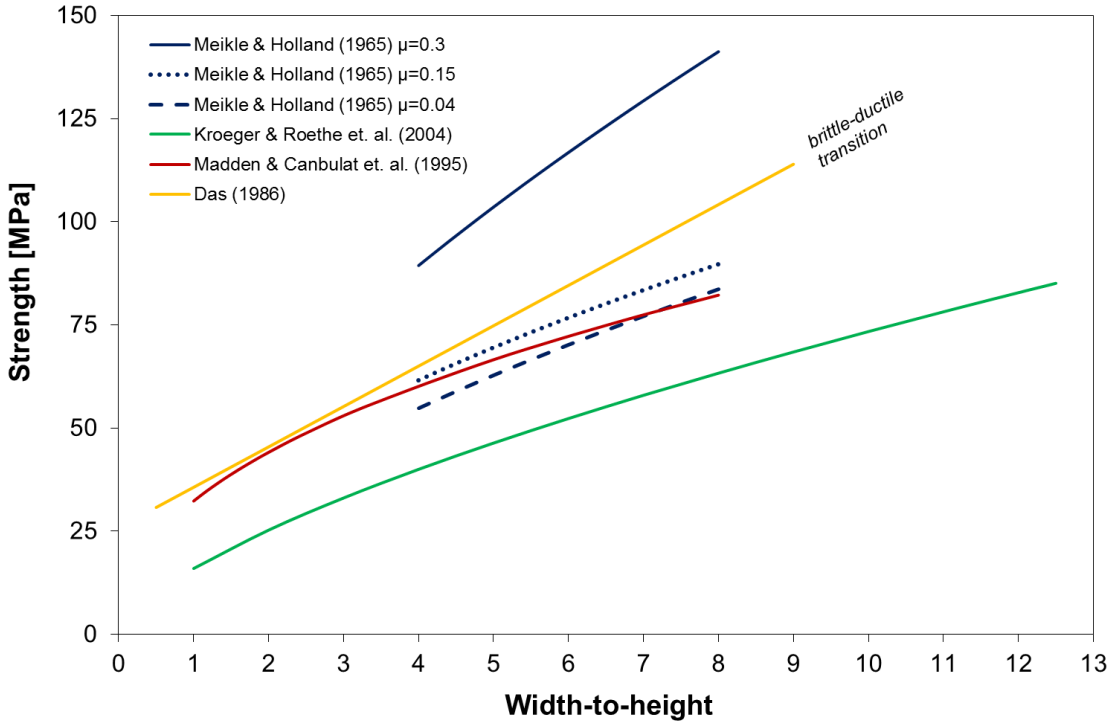


Figure 6. Compression tests on laboratory sized specimens of coal in the squat region by different investigators.

The review of compression tests on coal specimens has revealed so far that specimens in the suspected squat range of $w/h > 5$ do not show an exponential increase as assumed by the squat pillar formula. This appears to be irrespective of the contact friction angle between the specimen and the loading platens. A possible squat effect in coal could only be attributed to the occurrence of strain-hardening specimen behaviour, which is likely to occur at width-to-height ratios greater than 10.

3.3.2 Shape effect in intact rock specimens

Since coal itself is difficult to prepare in specimens, due to its friability and sensitivity to environmental changes, researchers have frequently made use of alternative modelling materials to investigate shape effects in pillars. Sandstone is commonly the preferred material for this purpose.

Cruise (1969) conducted compression tests on sandstone specimens of 12.7 mm height and varying square width, covering a width-to-height range between 1.8 – 6.6. The overall strength trend over width-to-height is clearly non-linear, i.e. upward curving and was found by Cruise to be best described by a polynomial curve, as shown in Figure 7 on page 36.

Bieniawski (1986) tested 145 sandstone specimens of 125 mm square width and varying width-to-height ratios up to 10. His analysis of the results suggested that a linear increase in specimen strength with width-to-height ratio occurs between w/h= 1 – 5. Thereafter, he observes a rapid increase in strength up to a w/h= 10, above which the specimens could not be broken in a 10 MN compression machine. It should be noted that no specimens between w/h= 5 – 10 were tested. Stress-strain curves for the specimens are not provided in the publication. The indicated trends by Bieniawski are reproduced in Figure 7 on page 36.

In his review of appropriate parameters for the squat coal pillar formula, Madden (1990) conducted a number of 222 compression tests on sandstone specimens of varying size between 24 – 100 mm and width-to-height ratios between 1 and 8. He established that the peak strength of specimens in all size categories increased linearly up to a w/h interval of 5 – 6. Thereafter, brittle-ductile transition occurred in the specimens. The average linear regression for all specimen sizes is plotted in Figure 7. Beyond this transitional interval, specimens did not exhibit an ultimate load bearing capacity but failed in strain-hardening (ductile) mode.

York et al. (1998) reported on compression tests on cylindrical Merensky Reef specimens with diameters ranging between 50 – 250 mm and shapes of w/h= 1, 3, 4 and 6. For all specimen diameters, a strong linear correlation was observed between the peak strength and the shape ratio of the specimens. No indication of a progressive strength increase above w/h= 5 could be found. Figure 7 plots the relationship between the strength and the w/h-ratio of 248 mm diameter Merensky Reef specimens.

For further background, some results of compression tests conducted by other researchers (Babcock, 1969; Sheorey and Singh, 1974; Baker-Duly, 1995) on hard rock specimens in the region of w/h< 5 are plotted in Figure 7 as well. All the data fits linear trends. Test setup of Babcock is unique in that the specimens were not directly tested between steel platens, but the specimen roof and floor where shaped continuously from the same rocks.

It is seen that linear relationships between strength and the specimen shape are well established for hard rocks and $w/h\leq$ 5. Madden's tests suggest that this trend also remains valid for slightly larger specimen width-to-height ratios, until the brittle-ductile transition occurs. However, Cruise and Bieniawski advocate a progressive increase in strength.

The results from Madden on sandstone generally compare to those from Das on coal, only with the difference that in coal the brittle-ductile transition occurs at much higher width-to-height ratios. The progressively increasing trends for specimen strength as found by Bieniawski and Cruise on sandstone, however, stand in contrast to the established regressive increase in coal specimen as shown by Meikle and Holland (1965), Madden and Canbulat (1995) and Kroeger, Roethe and Li (2004).

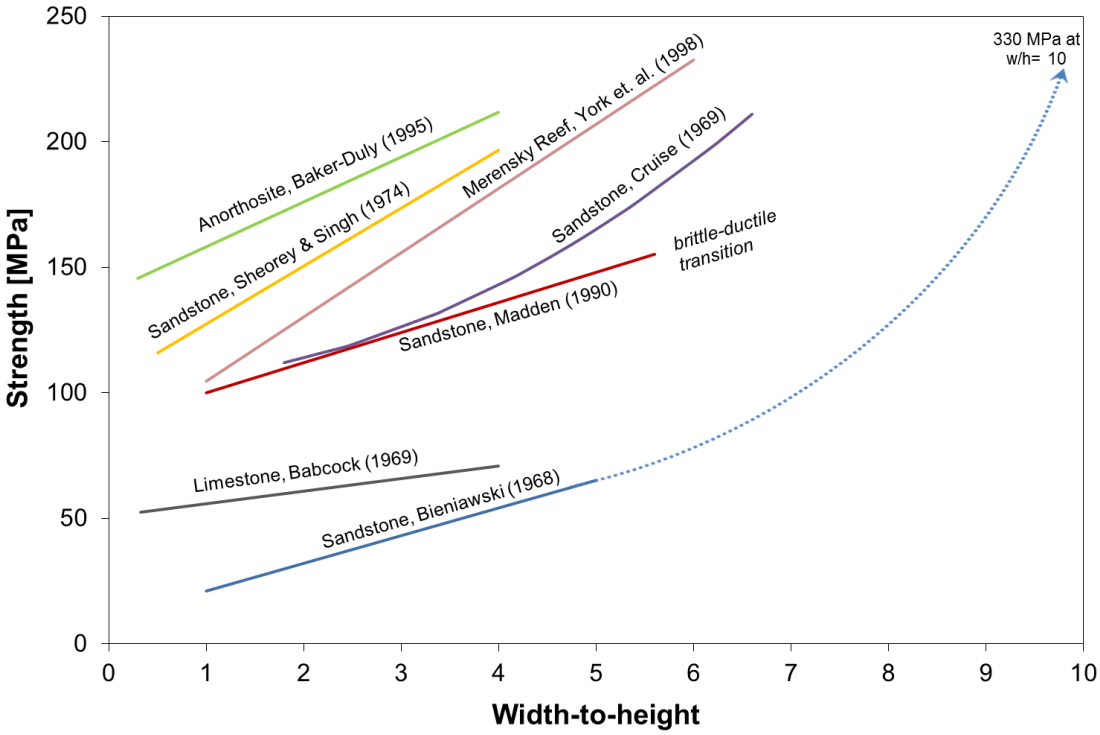


Figure 7. Compression tests on laboratory sized specimens of hard rock in the squat region by different investigators.

3.3.3 Shape effect in cohesionless, granular rock materials

Several researchers have reported on compression tests on cohesionless, granular rock piles in order to evaluate the performance of un-cemented backfill in mines. The performance of such granular rock fills in compression tests depends predominantly on the placement packing density or void ratio of the material and, in unconfined compression tests, on the width-to-height ratio of the specimen. Other influencing factors are the material's angle of internal friction, the magnitude of imposed loading rates and breakdown of material particles during loading.

A cohesionless granular material is different from intact cohesive material in its stress-strain relationship, because it experiences no major breakdown in load bearing capacity. Granular materials do not exhibit a peak load bearing capacity, but instead the stress-strain relationship follows a progressively upward curving trend.

A peak strength trend can therefore not be observed from width-to-height ratio tests on such granular materials. Nevertheless they can still provide a comparative insight into the influence of specimen shape on the capacity of a material as a resistant to loading.

In this context, Schümann and Cook (1967) tested granular piles of granite and quartzite with trapezoidal cross-section and various width-to-height ratios in the laboratory. The material was poured loosely into shape and loaded axially in compression. It was observed that the stiffness of laterally unconfined ribs increased significantly from an initial low $w/h=$ 4 up to approximately $w/h=$ 10. A further increase in shape was found to have

only a negligible influence on the strength and stiffness of the fill, as can be seen in the reproduction of the test analysis of Schümann and Cook (1967) in Figure 8.

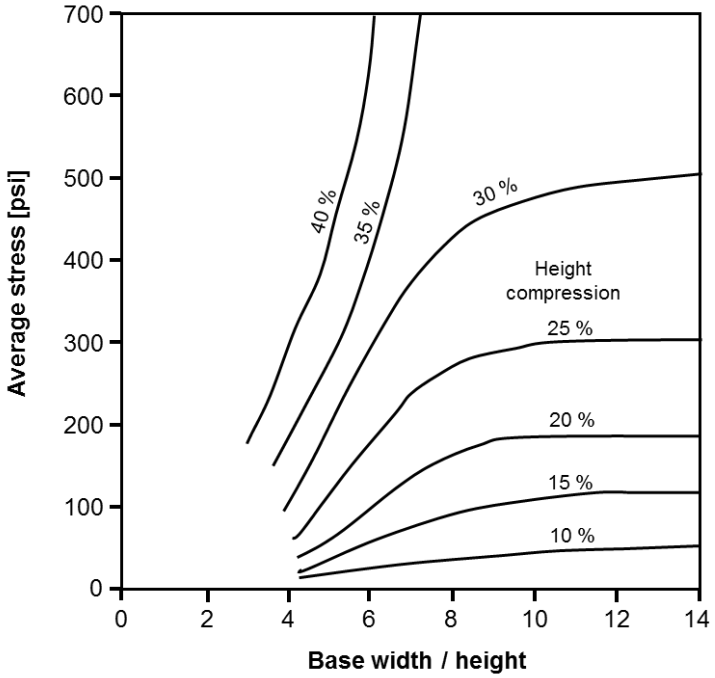


Figure 8. Relationship between specimen width-to-height ratio and average load bearing capacity of crushed granite aggregates at various levels of compression, reproduced after Schümann and Cook (1967).

In another test series, Schümann and Cook (1967) applied small lateral confinement to the toe of the samples and found that, despite the minimal strength of the constraint, lateral flow in the early stages was inhibited to the extent that the stiffness of narrow ribs was increased significantly. The conclusion was that “slight lateral constraint, which can be achieved in practice, increases the strength of narrow constrained ribs to the extent that for equal strength the width of a constrained rib can be reduced to a third of that of an unconstrained rib” (Schümann and Cook, 1967).

In other words, the experiments have shown that the shape effect in unconfined samples is one of *induced* lateral constraint. The larger the width-to-height ratio, the greater the induced triaxial stress state. The more confinement is induced in the material, the stiffer the material’s response to loading. The tests also demonstrate that a critical width-to-height ratio exists, at which optimal triaxial stress conditions are produced within the material.

These findings have been confirmed in a study conducted by Briggs (1988). He conducted various unconfined compression tests on crushed waste rock with various sample width-to-height ratios and with rectangular cross section. The tests showed an increase in stiffness with increasing width-to-height ratio up to approximately $w/h = 8$. For compression tests on de-slimed tailings, the critical value was again $w/h = 10$.

It is important to note that the critical width-to-height ratio appears to be fairly similar for a wide range of crushed rock aggregates investigated by the researchers (i.e. ranging from coarse crushed quartzite to fine de-slimed tailings).

3.4 Contributions from analytical models

Analytical pillar models attempt to predict a theoretical pillar stability and strength based on (a) basic mechanical properties for the pillar material, (b) its contact to the surrounding strata, (c) appropriate strength criteria for both the pillar material and interface and (d) an initial elastic vertical stress distribution across the pillar width. The analysis of pillar stability and strength follows the natural progress of failure, from the pillar sidewall into the core. Fundamental to all analytical pillars is therefore the assumption that any intact pillar must consist of at least two zones: An outer crushed or yielded zone, which is not capable of taking high loads but which provides constraint to the pillar core, and an intact pillar core, which is assumed to behave elastically. It is implicit in the differentiation of zones that the pillar exhibits non-uniform stress distributions across its width. Suitable model input parameters can be established by calibrating the model so that the predicted depth of yield is equal to the depth of failure observed in pillars in-situ.

Modelling starts by dividing a pillar of given size and shape into a number of thin slices, as shown in Figure 9. The forces acting on each slice are the vertical forces $\sigma_v(x)\mathrm{d}x$, the horizontal forces $\sigma_H(x)h$, $\sigma_H(x+\mathrm{d}x)h$ and the shear force along the pillar strata interface $\tau\mathrm{d}x$. It is postulated that all forces acting on both intact and failed slices must remain in equilibrium, so as to obtain a stable rib.

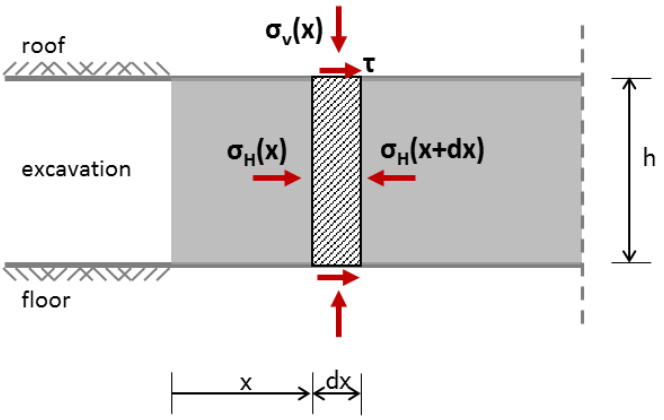


Figure 9. Limit equilibrium conditions around a pillar ‘slice’ in analytical models.

An initial elastic stress distribution is estimated across the pillar, usually obeying a hyperbolic or logarithmic function that simulates very high peak stresses at the pillar sidewalls and a rapid stress decrease towards the pillar centre. The integral value of this stress distribution is commonly equal to the estimated magnitude of tributary area load.

The strength of each slice is determined from an appropriate strength failure criterion. Slices close to the pillar sidewall have a comparatively low compressive strength, as only

little horizontal confinement exists there. Slices located more towards the pillar centre, however, are assumed to have a high triaxial strength due to high confinement in the core.

The stability of each slice is evaluated based on the comparison between the individual amount of stress that the slice is supposed to sustain and its inherent strength. Should a slice 'fail', i.e. the imposed stress exceeds the inherent strength, the pillar stress distribution is adjusted such that the failed slice only carries a residual stress and the peak stress is carried by the next intact slice in the pillar. Peak pillar strength is obtained after some amount of sidewall failure, however, the pillar core must remain intact. The pillar is finally deemed to have failed when all slices have failed and the pillar's residual load bearing capacity is calculated from the final stress distribution.

There are several different analytical pillar models published in literature (Wilson, 1981; Barron and Pen, 1992; Salamon, 1992; Napier and Malan, 2007) . The models differ in their assumptions on elastic stress distributions and build-up stress gradients across the yielded and the remaining intact slices, both vertically and horizontally in the pillar. The failure criteria and the complexity in which the pillar-strata interaction is simulated may differ as well.

To what extent these models have been used to evaluate the performance of squat pillars could not be determined from the literature review. Also, a calibration of appropriate material properties to be used in the models is not available. However, the models have assisted in predicting the theoretical influence of pillar width-to-height ratio on the residual and peak load-bearing capacity of the structures. A brief summary is provided in the following sub-sections.

3.4.1 Closed-form solutions for residual pillar strength

From limit equilibrium considerations described earlier (see Figure 9), Barron and Pen (1992) and Napier and Malan (2007) derived closed-form solutions for the distribution of stresses and the residual load-bearing capacity of crushed pillars.

The authors have shown that the vertical load bearing capacity in a crushed pillar rises exponentially with distance from the pillar sidewall. Also, it was shown that the residual load bearing capacity of a pillar increases exponentially with increasing width-to-height ratio. However, the derived closed-form solutions differ between the models of Barron and Pen (1992) and Napier and Malan (2007), which is likely to be due to a different choice of boundary conditions in the integration process of the differential limit equilibrium equations.

Napier and Malan's solution for the residual strength of pillars with varying width-to-height ratios (Du Plessis, Malan and Napier, 2011) is given by Equation (18),

$$\text{Strength}_{\text{resid.}} = \frac{Sh}{\mu kw}\left[e^{\frac{\mu mw}{h}} - 1\right] \tag{18}$$

where S is the residual unconfined compressive strength of rock, h is the pillar height, $\mu = \tan\phi$ the coefficient of friction of crushed rock, $k = (1+\sin\phi)/(1-\sin\phi)$ the triaxial strength factor, ϕ the angle of internal friction of crushed rock and w is the pillar width.

A demonstration of this equation for different values of ϕ is shown in Figure 10**.** One observes that the solutions are sensitive to the choice of an appropriate angle of internal friction ϕ of crushed coal.

The model also requires an estimate of the residual unconfined load-bearing capacity of the slice at the immediate pillar sidewall. Following suggestions by Salamon (1992), this value has been chosen to be $S = 0.1$ MPa for demonstration purpose. The pillar height is assumed to be $h = 3$ m.

Also plotted in Figure 10 is the updated MLM pillar peak strength formula as derived from collapsed coal pillar cases (see Chapter 3.1.1). Brittle-ductile transition is supposed to occur in pillars when the predicted residual pillar strength equals the estimated peak pillar strength. This point of intersection may therefore indicate the critical width-to-height ratio at which squat pillar behaviour begins.

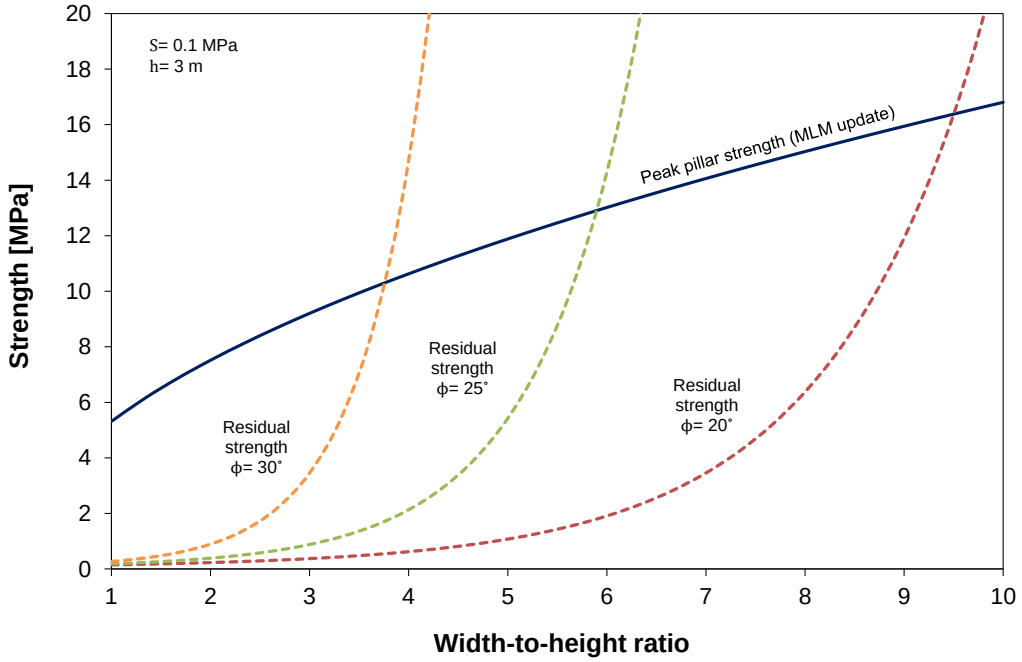


Figure 10. The residual strength of coal pillars for different internal friction angles ϕ according to the analytical model of Napier and Malan.

3.4.2 Indications for peak pillar strength

It has been shown experimentally by Wagner (1974) and analytically by Salamon (1992) that the peak load-bearing capacity of a pillar is only reached after some amount of failure has occurred along the pillar perimeter. How far failure can penetrate into the pillar before the structure has reached its load bearing capacity depends on the residual material strength properties, the mechanical properties of the pillar-strata interface and the stress decay distribution in the elastic portion of the pillar. Because of the complex relationship

between the contributing factors, no generally agreed closed-form solution for the relationship between peak pillar strength and the pillar width-to-height ratio has been developed so far.

However, some analytical models have been subjected to case studies. Some indications for the relationship between pillar width-to-height ratio and peak load-bearing capacity can be derived from these case studies.

The analytical model developed by Salamon (1992) was applied to a mining situation in a 2 m thick seam at 700 m depth below surface (Salamon et al., 2003). The pillars were assumed to have width-to-height ratios of w/h=3, 5 and 10. Incremental loading of pillars was simulated by stepwise enlarging the width of roadways surrounding the pillar and hence the tributary area load. In the specific environment, and with the assumed material properties, the pillar peak strength was determined to be 19.3 MPa (w/h= 3), 28.6 MPa (w/h= 5) and 33.6 MPa (w/h= 10) by the analytical model.

It is obvious from these numbers that Salamon's analytical solution for pillar strength does not predict a progressive increase in pillar strength over width-to-height ratio, but that rather a regressively increasing trend is indicated.

This also agrees with with the prediction of pillar strength based on the Barron and Pen (1992) analytical model. The authors estimated modelling parameters for coal based on the coal geology in the South African Witbank coalfields. The prediction for coal pillar strength based on their analytical model for square pillars is shown in Figure 11**,** where it can be seen that up to w/h= 12 there is a satisfying agreement with the magnitude of strength predicted by the South African squat pillar formula. However, it should be noted that the analytical solution on square pillar strength predicts a regressively increasing trend, and not an exponential trend as assumed in the established South African squat pillar formula (shown as 'Salamon formulae' in Figure 11).

One further and important observation has been made by Salamon et al. (2003) in their case study on coal pillar strength: For a pillar width-to-height ratio of 5 and higher the analytical solution predicted that the boundary between the yielding and elastic coal inside the pillar can become unstable and that the yielded pillar edges may disintegrate. They concluded that this event is likely to be sudden and therefore accompanied by some form of coal bump, which is potentially associated with severely adverse consequences for strata conditions.

This prediction coincides well with practical experiences made in the United States with pillars of intermediate and squat shape (see discussions in Chapter 2).

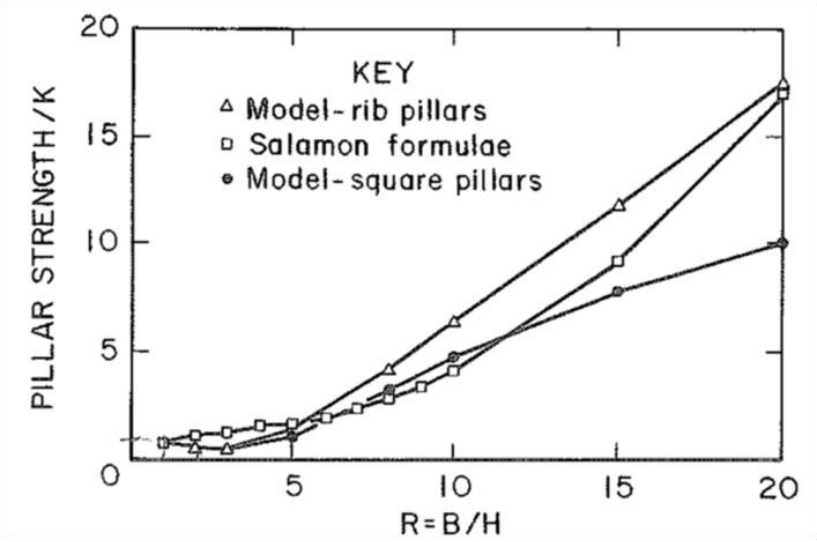


Figure 11. Comparison between the pillar strength for the Witbank coalfield predicted by the Barron and Pen (1992) analytical model and the South African squat pillar formula.

3.5 Contributions from numerical modelling

While empirical and analytical pillar design approaches can only consider the mechanics involved in a pillar system to a limited degree, numerical models are capable of considering it in greater complexity. The orientation and magnitude of the stress field as well and the material properties of pillars and the surrounding rock mass can be varied. Numerical models can also consider structural weaknesses within the pillar, such as bedding planes and joints. Non-linear computation codes can provide the opportunity to model the full loading behaviour of pillars, including the simulation of the post-failure strain-softening or strain-hardening.

Most of the published coal pillar models consider the mining environment essentially as a continuum with the only discontinuities being the interfaces between the coal pillar and the rock strata. Constitutive failure criteria for coal are usually based on Mohr-Coulomb or Hoek-Brown parameters. For a realistic assessment of the performance and possible failure progress in the pillar, however, it is important that the chosen strength parameters are allowed to evolve at the onset of failure. For instance, Mohr-Coulomb cohesion and friction are typically reduced in increments with further plastic strain to reach a residual level at some stage. This is called the Mohr-Coulomb strain-softening approach, but the same principle can be adopted for the equivalent Hoek-Brown parameters. If the pillar itself is considered to be the weakest link in the roof support system, the strata surrounding the pillar is usually modelled as an elastic medium. The interfaces between pillar and strata may obey a simple Mohr-Coulomb shear strength criterion.

3.5.1 Models to evaluate the performance of the pillar-strata system

Considerable efforts have been made by different investigators to evaluate the performance of individual components in the pillar system (strata-interfaces-seam):

Lu et al. (2008) conducted a comprehensive numerical study on the effects of coal-rock interface properties on the strength and stress-strain behaviour of slender and squat coal pillars. Mohr-Coulomb strain-softening parameters were assigned to the coal pillar, while the interface assumed a bi-linear Mohr-Coulomb behaviour: At low normal stresses, the interface was given only a frictional resistance to sliding. At higher normal stresses, the interface was then assumed to develop an effective cohesive strength that is due to the shear strength of asperities.

Four model pillars with width-to-height ratios between 3 and 10 were designed to investigate brittle-ductile transition in the structures dependant on the coal-rock interface properties. It was concluded that the critical width-to-height ratio, at which a pillar transits from strain-softening to strain-hardening failure, will depend on the shear strength of the pillar/rock interface. For weak interface conditions (e.g. cohesion in the range of 0.35 MPa) the amount of confinement induced in the pillar was insignificant, even if the w/h-ratio was as large as 10. The width-to-height threshold for brittle-ductile transition decreased with a higher interface cohesion: $w/h = 7$ for a cohesion of 1.03 MPa and $w/h = 5$ for 2.1 MPa.

The effect of interface friction between specimens and steel loading platens has also been investigated numerically for coal (York, Canbulat and Jack, 2000) and Merensky Reef samples (York et al., 1998). The models were calibrated to linear peak-strength equations as obtained from laboratory testing. By varying the contact friction angle in the numerical models, the occurrence of a squat effect was studied. The squat effect manifested as an abrupt peak-strength increase at a critical width-to-height ratio. It was found that the higher the interface friction angle, the lower the critical width-to-height ratio at which a squat effect occurs.

Su and Hasenfus (1999) used finite element codes to investigate various factors which are thought to have impact on the ultimate strength of coal pillars. Pillars modelled between strong roof and floor strata yielded similar results as predicted by the Bieniawski strength equation up to $w/h = 3$. The confinement generated in the pillar through the frictional resistance at the interfaces between the pillar and its surrounding strata was observed to accelerate pillar strength at a width-to-height ratio of 3. Thereafter, a more rapid, yet approximately linear strength increase up to $w/h = 7$ was observed. Finally, the slope of the strength versus width-to-height curve flattened again to assume a slope similar to the Bieniawski empirical formula (Su and Hasenfus, 1999).

The authors also found that rock partings in the coal seams will have a variable effect on the pillar strength: while a competent shale parting may reduce the effective height of a pillar and thus increase the pillar strength, a weak clay stone parting is likely to decrease pillar strength (Su and Hasenfus, 1999).

For pillars with squat dimensions they concluded that the seam strength itself would have a negligible impact on pillar strength. A more significant influence, however, was ascribed to the competency of the surrounding rock mass on the strength of the system: for instance, the authors predicted that weak floor rocks may decrease the ultimate pillar strength by as much as 50 %.

This latter conclusion is in accordance with findings made by Gale (1999), who states that the immediate strata surrounding a coal pillar is an equally important factor to the strength of the system as the coal itself. He postulates that “the strength of a pillar is determined by the magnitude of vertical stress that can be sustained within the strata-coal sequence forming and bounding it” (Gale, 1999).

If a pillar is being loaded due to underground mining and its tendency to expand into the adjacent voids is restricted by strong cohesive coal-rock interfaces, then additional lateral confinement can be built up, which allows the pillar to sustain high vertical stresses (Gale, 1999). Conversely in poor mining conditions with low shear strength along coal-rock interfaces lateral slip can occur totally unresisted and the pillar strength is limited to its unconfined value.

Gale (1999) assesses the performance of various pillar-interface-strata systems in a series of numerical models and his results are summarized in Figure 12. Also indicated in Figure 12 is the current South African squat pillar strength formula and the possible opportunity for improvement, assuming that most South African coal pillar design takes place in competent strata.

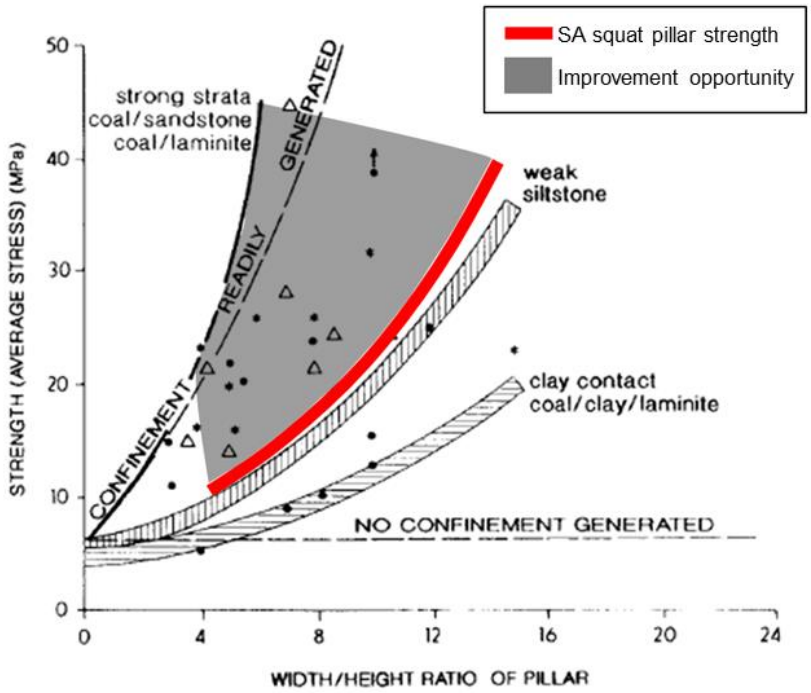


Figure 12. Strength and width-to-height for different geological environments, according to Gale (1999), overlain with current South African squat pillar strength and improvement opportunity.

The effect of jointing on coal pillar strength has been addressed by Esterhuizen (2000). The numerical models were set up in a way to account for varying frequency, orientation and shear strength of joints.

The models confirmed the expectation that the strength of pillars decreases with decreasing shear strength of joints and an increasing number of joints per meter. Pillars were also found to reach a minimum strength when the joints dip at an angle of 45 degree

towards the direction of loading, while the strength rises relative to this minimum with both an increasingly higher and lower dipping angle of the joints.

The most significant finding with regards to squat pillars, however, was that the weakening effect of jointing in pillars diminishes with increasing pillar width-to-height ratio.

Following the trends indicated by the computer models, Esterhuizen (2000) developed equations suitable for downgrading the strength of jointed coal pillars relative to non-jointed pillars according to the frequency, orientation and shear strength of joints:

$$\sigma_{pj} = \sigma_{pi} \exp(-0.017F) \tag{19}$$

In this equation σ_{pj} is the strength of jointed coal pillars, σ_{pi} is the strength of pillars without any joints and F is a function of the pillar height (h) and width-to-height ratio (w/h), the joint frequency per meter (J_f), the joint orientation (n) and the peak angle of friction (ϕ) of joints:

$$F = \frac{10\ (w/h)^{-0.5}\ (1- \exp(-0.23hJ_f)}{n\ \tan\phi} \tag{20}$$

The joint orientation factor n is a numerical value representing the influence of the angle of dip of joints on pillar strength and can be sourced from a table presented in the paper published by Esterhuizen (2000).

Figure 13 demonstrates the predicted percentage reduction in strength for jointed pillars with increasing width-to-height ratios for J_f= 0.5, ϕ= 30˚ and n= 0.3.

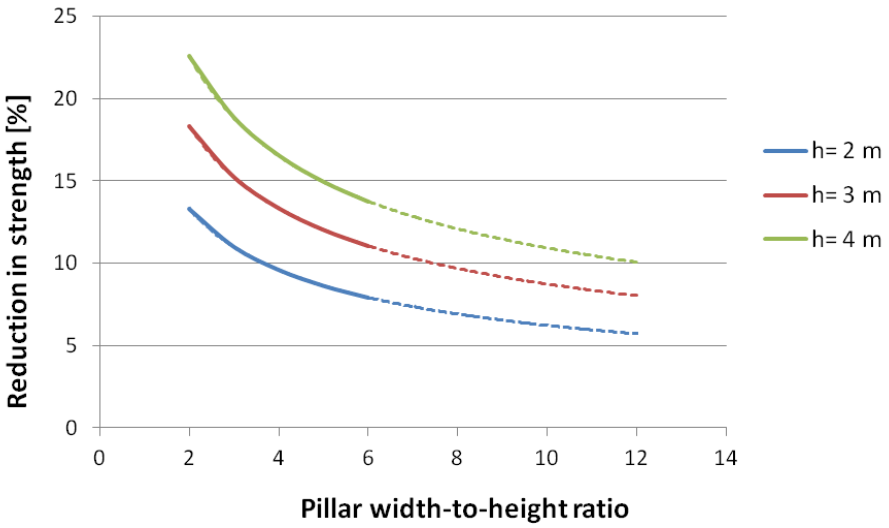


Figure 13. Reduction of strength for pillars of 2 – 4 m height due to a set of 2 m distant joints inclined at an angle of 30˚.

It should be noted that the equations are strictly speaking only valid for pillar width-to-height ratios of $2 \leq R \leq 6$. The extrapolation made in Figure 13 for $6 < R \leq 12$ is therefore indicated as a dash-dotted curve.

Figure 13 indicates that the weakening influence of joints on pillars in the squat range can be as low as about 10 %, presuming that the frequency of joints is relatively moderate. A higher frequency of, for example, three joints per meter is predicted to weaken the pillar by about 25 %. A loss of strength in this range can still be tolerated if the common approach to design pillars with a safety factor of 1.6 or higher is adopted.

3.5.2 Calibrated models to predict squat coal pillar behaviour

Calibration of the material and interface properties (and their evolution with plastic strain in the strain-softening approach) is usually conducted against an empirical peak strength criterion. The aim of such calibration is to match the model pillar peak strength at different width-to-height ratio with the predicted peak strength from empirical equations, e.g. Salamon and Munro (1967), Bieniawski (1968a), Wagner (1974) or Van Heerden (1975) equations or a combination of them. In-situ stress measurements, observations on sidewall fracturing, or full stress-strain curves for large-scale model pillars can serve as means of calibration as well.

Shen et al. (2010) report on a calibration procedure where the model pillar peak strength is matched against the combined South African and Australian coal pillar strength formula, Equation (11), in its empirical range. Extrapolating the model to larger width-to-height ratios beyond the empirical range of the strength equation predicted that brittle-ductile transition could occur in pillars at width-to-height ratios between $w/h = 5 – 6.7$.

Esterhuizen, Mark and Murphy (2010) presented a numerical coal pillar model that was calibrated to satisfy both the empirical coal pillar strength formula of Bieniawski (1992), Equation (14), and stress profiles measured in coal pillar ribs. The measured stress profiles also served in determining appropriate coal-rock interface properties. The resulting values of $\varphi = 25^{\circ}$ and $c = 0.1$ MPa were decided to be typical for coal-rock interfaces. The Hoek-Brown strength criterion was used for coal with the relevant parameters being allowed to soften from the onset of plastic strain.

The model pillar behaviour was compared to Bieniawski's peak strength criterion, Equation (14), in the range of $w/h = 3 – 8$ and the agreement was found to be satisfying. The predicted stress-strain response of the calibrated model pillars was such that a clear peak strength followed by strain-softening post-peak behaviour did only occur for width-to-height ratios of up to 6. At width-to-height ratios of 8 and higher, the model pillars had already transited into strain-hardening failure mode. This conclusion would be in line with the estimated point for brittle-ductile transition for coal pillars in Figure 10, for a residual angle of internal friction of $\phi = 25^{\circ}$.

Tesarik, Whyatt and Larson (2013) calibrated the material properties of their coal pillar model against the full stress-strain curves of a 1.4 m square specimen of coal with $w/h = 2.78$ as obtained by Van Heerden in his in-situ large-scale compression tests[1]. The

[1] It should be noted that in the publication from Tesarik, Whyatt and Larson (2013) the compression tests are incorrectly referred to as Bieniawski's compression tests.

constitutive model for coal followed a Hoek-Brown strain-softening approach, while the pillar roof was kept elastic and floor strength parameters were varied from elastic to Mohr-Coulomb plasticity with various strength properties inferred from in-situ floor heave monitoring.

The model was then extrapolated to greater width-to-height ratios of up to 16 to study the shape effect in pillar strength, depending on the different floor strength parameters. For both the competent elastic and inferred plastic floor conditions, it was found that the peak pillar strength developed in a regressively increasing manner over width-to-height, until the brittle-ductile transition occurred. The critical width-to-height ratio for brittle-ductile transition was found to be about 12 for pillar models with strong elastic roof and floor conditions, while models with a plastic floor transited into ductile behaviour only at approximately $w/h=$ 16.

It should be noted that Van Heerden's in-situ stress-strain curve for a pillar of $w/h=$ 2.78 was also used by Yavuz and Fowell (2001) to calibrate a coal pillar model in FLAC. However, they chose boundary conditions and grid sizes different from Tesarik, Whyatt and Larson (2013), so that the calibration yielded different elastic properties for coal. The constitutive law of coal in Yavuz and Fowell's case followed a Mohr-Coulomb strain softening approach, so that a further comparison to Tesarik, Whyatt and Larson's model is difficult. However, the magnitude of drop in strength properties (i.e. c and ϕ for Mohr-Coulomb, and m and s for the Hoek-Brown model) assumed in the post-peak stress-strain range is significantly lower in Yavuz and Fowell model, even though the calibrations for the residual pillar strength appear to be equally matched in both models.

From this it may be seen that calibration procedures are highly dependent on the individual model setup.

4 Discussion of advances in squat coal pillar strength and design

In South Africa the design of squat coal pillars is based on the assumption that an exponential increase in strength does occur for pillars with $w/h>$ 5 (Salamon, 1982; Salamon and Wagner, 1985; Madden, 1991). This suggestion has been adopted in Australia (Galvin and Hebblewhite, 1995) without further investigations, but in the U.S. the view on the shape effect is such that no meaningful deviation from empirical strength formula does occur until the pillar experiences brittle-ductile transition at some higher width-to-height ratio of approximately 8 (Mark, 2000) or 12 (Bieniawski, 1992). In India, the approach to pillar design at greater depth is very different, in that it is assumed that especially wide pillars can retain some of the pre-excavation confinement stresses and hence experience a strength increase with greater depth of mining (Sheorey, 1992).

Squat pillars in South Africa have not been observed to collapse so far (Van der Merwe and Mathey, 2013b). In-situ compression tests on large-scale squat coal specimens have only been conducted up to w/h-ratios of 3.4. Therefore, physical evidence of the strength magnitudes and shape effect related to squat coal pillars is not available in South Africa. Experiences in the U.S. with pillar failures involving cases of width-to-height greater than 5 suggest that coal pillars may fail in a brittle manner up to $w/h=$ 8 – 10 (Mark, 2000). At greater width-to-height ratios the pillar may fail in a strain-hardening manner.

Intensive international research has been directed at the form of strength increase over pillar width-to-height ratio (i.e. progressive, linear and regressive) in the squat range and into the failure mode (brittle or ductile) of coal pillars.

Based on the literature review, a progressive increase of peak pillar strength in the squat range, as suggested by the South African squat pillar formula, appears to be highly unlikely. Some laboratory tests on sandstone conducted by Cruise (1969) and Bieniawski (1986) showed that such a progressive trend may indeed exist for rocks. However, more comprehensive tests on sandstone performed by Madden (1990) rather suggest that the strength increase is linear up to approximately $w/h=$ 6 and that specimen failure thereafter is characterized by strain-hardening behaviour. Compression tests on Merensky Reef specimens (York et al., 1998) up to $w/h=$ 6 exhibited neither a progressively increasing trend in strength nor brittle-ductile transition in the empirical range. The compression tests on hard rock are therefore inconclusive.

Furthermore, coal appears to behave different from rock in laboratory tests: Investigations into shape effects consistently show that the strength of coal increases approximately linearly (Das, 1986; Khair, 1994) or regressively (Meikle and Holland, 1965; Madden and Canbulat, 1995; Kroeger, Roethe and Li, 2004). The brittle-ductile transition is only likely to occur at width-to-height ratios of about 10 or higher (Das, 1986), but has not always been encountered in the tests of different investigators. For instance Kroeger, Roethe and Li (2004) conducted tests on specimens with width-to-height ratios of up to 12.5 without noticing brittle-ductile transition.

It is important to note that extensive empirical tests on the influence of weak and strong interface friction coefficients between the coal specimens and loading platens (Meikle and Holland, 1965; Khair, 1994) did not produce a squat effect in coal specimens, neither in the form of a progressive increase in peak specimen strength beyond a critical width-to-height ratio, nor as brittle ductile-transition. This is opposed to numerical modelling results (York et al., 1998; York, Canbulat and Jack, 2000), which predicted a squat effect for coal and Merensky reef specimens in the form of an abrupt strength increase at a critical width-to-height ratio that depends on the interface friction.

The fact that some rocks do indeed exhibit a progressive strength increase or early brittle-ductile transition in laboratory shape tests, while coal consistently resists these effects even at high contact friction angles, raises the questions as to the mechanism behind the trends. It seems likely that the phenomenon may be attributable to basic mechanical or textural material properties, rather than boundary conditions. This deserves further investigation.

Theoretical considerations on pillar strength in analytical models from Barron and Pen (1992) and Napier and Malan (2007) have shown that the residual load-bearing capacity of a crushed pillar increases exponentially with increasing width-to-height ratio. This should eventually lead to the brittle-ductile transition in coal pillars, at the point where the residual strength equals the peak pillar strength. The critical width-to-height ratio for occurrence of brittle-ductile transition in pillars will therefore depend significantly on residual strength properties of coal.

Case studies (Barron and Pen, 1992; Salamon et al., 2003) in which the analytical models developed by Salamon (1992) and Barron and Pen (1992) were applied to predict the peak load-bearing capacity of coal pillars showed that the maximum pillar strength is unlikely to increase progressively. The limited information rather suggests that a regressively increasing trend exists between pillar strength and width-to-height ratio.

Numerical models which are calibrated to in-situ coal pillar behaviour agree that a progressive increase in the relationship between strength and width-to-height ratio cannot be expected for the squat pillar range. Shen et al. (2010) calibrated model pillars against the empirical peak strength criterion for the combined South African and Australian coal pillar database. The extrapolation of their models into the squat range predicted brittle-ductile transition in pillars between w/h= 5 – 6.7. Esterhuizen, Mark and Murphy (2010) calibrated models against Bieniawski's linear strength equation (Bieniawski, 1992) and stress-profiles in pillar ribs. They showed that brittle-ductile transition occurred in the numerical model pillars at around w/h= 8. Tesarik, Whyatt and Larson (2013) on the other hand calibrated models against one stress-strain curve as tested by Van Heerden and observed a regressive strength increase in coal pillars up to at least w/h= 12 or 16, depending on mine floor conditions, before brittle-ductile transition occurred.

The only conclusive results derived from these model studies with regards to the likely behaviour of squat coal pillars is that a progressive strength increase does not occur.

At least the qualitative influences of individual components in the pillar-strata-system on the overall strength of the structure are agreed upon:

Additional layers of rock inside the coal seam can weaken or strengthen the pillar-system, depending on the properties of the rock, as shown by Su and Hasenfus (1999). A weak roof or floor strata reduces pillar strength, as demonstrated by Gale (1999) and Tesarik, Whatt and Larson (2013).

Weak interfaces between the coal pillar and the surrounding strata move the critical width-to-height ratio for brittle-ductile transition further into the squat range (Lu et al., 2008) but can also weaken the overall magnitude of strength as observed in the laboratory investigation by Meikle and Holland (1965) and Khair (1994). Gale (1999) further concluded from modelling exercises and field observations that the rate of strength increase is seriously affected by the strength of the coal-rock interface and the amount of confinement that is induced in the pillar.

However, the actual strength of the coal seam appears to have a comparatively lower influence on the overall strength of a squat pillar system. This was concluded by various authors using numerical models, e.g. Su and Hasenfus (1999) and Gale (1999). Esterhuizen (2000) demonstrated in his analysis of jointing on coal pillar strength that the influence of joints diminishes for pillars with large width-to-height ratios.

So far one would have to conclude from the literature review that the predicted progressive strength increase in squat coal pillars by the South African formula is unlikely to exist. Physical evidence from compression tests on coal specimens, theoretical predictions in analytical models and predictions by calibrated numerical models do not support this theory. It is likely that the linear or regressively increasing trend between strength and shape as found for the more slender pillars of $w/h < 5$ is also valid in the squat range, until brittle-ductile transition occurs at some elevated width-to-height ratio. From the literature review it is suggested that the critical width-to-height ratio for brittle-ductile transition is around $w/h = 10$. This supports the American view on squat coal pillar strength as expressed by Mark (2000) and discussed in Chapter 2.

This conclusion contradicts Madden's in-situ observations on squat pillar sidewall fracturing (Madden, 1991), which suggested that the strength of the investigated pillars was considerably higher than predicted by the Salamon and Munro (1967) formula. It was therefore suggested by Madden that the South African squat pillar formula is likely to be a better strength estimate for very wide pillars.

There is however another possible explanation as to why the investigated pillars seemed so much more competent than that predicted by the Salamon and Munro (1967) formula:

The Salamon and Munro (1967) strength equation and its subsequent updates, e.g. the latest by Van der Merwe and Mathey (2013c), only give the average strength of failed coal pillars in South Africa, but not necessarily the average strength of all coal in the country. Therefore, it is likely that significant differences exist in the actual strength of coal pillars. This has been demonstrated effectively by the in-situ compression tests of

large-scale coal specimens in three different collieries by Bieniawski (1968a), Wagner (1974) and Van Heerden (1975). The cube strengths of coals at New Largo and Usutu collieries was double as strong as compared to Witbank colliery. Moreover, the Salamon and Munro formula predicts a pillar strength that is in the lower range of the results from the large-scale in-situ compression tests.

Furthermore it has been shown by Van der Merwe and Mathey (2013a) in their analysis of the failure probability of coal pillars that cases of stable pillars with a predicted safety factor of less than one exist. This points again to locally higher strength in coal pillars than assumed by the empirical strength equation.

The reason for the higher strength observed by Madden (1991) in pillars in KwaZulu-Natal may therefore be found in a higher site-specific strength of coal. The quest for an improved design of squat coal pillars in South African collieries is therewith open for further investigation.

5 Research scope and objective

It has been shown that the predictions for squat coal pillar strength vary between the different coal mining countries. The only agreement found in international literature is that an optimal squat coal pillar design must adopt to the seam-specific or site-specific conditions of mining. Furthermore it appears that the exponential increase in pillar strength, as predicted by the current South African squat pillar formula, is likely to be technically misleading, as most findings from laboratory tests and numerical modelling point to a linear or regressive strength increase with width-to-height ratio and that a squat effect only occurs in the form of brittle-ductile transition in pillars.

Direct physical evidence, in the form of failed squat pillar cases or large-scale in-situ compression tests on squat specimens would be the preferred method to establish confidence into the mechanical behaviour of these structures. However, in South Africa no squat pillar has been observed to collapse so far, and due to time and budget constraints, large-scale in-situ compression tests are beyond the scope of this investigation.

In absence of direct physical evidence, the research will have to utilize methods to deduce the most likely in-situ squat pillar behaviour through various techniques. As such the following will be considered in this study:

- a statistical review of coal mechanical properties in the different seams of South Africa;
- laboratory testing on coal and other rock specimens in the slender and squat shape range;
- numerical modelling of coal pillars with calibration against in-situ observations.

The findings from these studies will be translated into a most-likely in-situ squat coal pillar behaviour by sound engineering judgement.

The objective is to establish both the correct shape effect in squat coal pillars in terms of the trend in the strength over width-to-height relationship and to provide a practical solution for the mining industry to design coal pillars at greater depth. The following aspects are considered to be crucial for this investigation (for further background see Chapter 4):

Seam-specific coal strength

Previous research has shown that a single pillar strength formula which accurately approximates the strength of all coal pillars in the country does not exist (Salamon, Canbulat and Ryder, 2006; Van der Merwe and Mathey, 2013c). It is rather suggested that a coalfield, seam-, or even site-specific coal pillar strength must be considered. Broad approaches to identify coalfields of weak and normal coal strength have been successful already, but a further distinction between the individual seam strength in the coalfields is challenged by a lack of sufficient statistical evidence of collapsed pillars.

It is therefore imperative to investigate the different coal seam strength in South Africa. It is postulated that the components contributing to the strength of a coal pillar are (a) its

size and geometry (shape), (b) its direct geological environment, i.e. the surrounding strata and discontinuities in the pillar itself and (c) the intact material strength of the coal.

Aspect (a) has already been covered intensively by different investigators in South Africa and aspect (b) has been dealt with in terms of coal pillar jointing. Therefore, it falls within the scope of this thesis to approach the seam-specific coal strength from another angle: the angle of the intact material strength of different coal seams.

Laboratory tests on coal are usually treated with great caution by rock engineers, due to the variability of sampling procedures and the friability of the material, which possibly affects the test results adversely. However, the approach chosen here is to collect a comprehensive database of coal mechanical properties at different sites and seams from the various coal mining houses in South Africa and to evaluate the performance of coal on a statistical basis.

Shape effect in coal and rock specimens

The majority of literature reviewed for this thesis points to a regressive or linear strength increase over width-to-height ratio of squat coal specimens and pillars. A squat effect appears to be only likely to occur in terms of the brittle-ductile transition in specimens and pillars at very large width-to-height ratios, but not as an exponential strength increase as suggested by the current squat pillar formula.

Nevertheless, some important questions remained unanswered in the work conducted so far, in particular as to what causes the brittle-ductile transition to occur and at which width-to-height ratio it is likely to happen. The literature survey indicated that in coal specimens or pillars, the critical width-to-height ratio may vary between $w/h = 8 – 16$ and that this may depend on the frictional effects between the specimen/ pillar and the surrounding loading platens/rock strata.

Some other influencing factor is also apparent from the literature review, namely the influence of material type. Some researchers had indeed observed a progressively increasing specimen strength in granular sandstone, but at least one has described the shape effect in sandstone as linear until brittle-ductile transition occurred. Tests on Merensky Reef specimen also did not show brittle-ductile transition or a progressive increase in strength in the same width-to-height range. Furthermore, tests done on coal with various strong and weak frictional contact between the specimen and the loading platens showed that coal generally resists a squat effect in the form of a progressive increase in strength and that up to $w/h = 8$, the occurrence of brittle-ductile transition is highly unlikely. Therefore it is likely that the material texture and its basic mechanical properties are linked to the shape effect.

A key to the understanding of the mechanics involved in the shape effects and brittle-ductile transition in coal may therefore be found in a comparative assessment of different rock types tested in various shape configurations and compression.

In addition to laboratory testing on specimens, numerical modelling will have to be conducted in order to estimate the shape effect in full-size coal pillars. It is believed that the most accurate way to determine the shape effect in the squat range numerically is to calibrate models against the trends in stress-strain curves observed by Van Heerden (1975) in his in-situ tests. Finally, the findings from numerical modelling and laboratory testing will be compared and the most-likely squat coal pillar behaviour will be concluded based on engineering judgement.

PART II

Survey of the mechanical properties of intact coal in South Africa

6 Introduction to the properties survey

The strength and shape effect of coal pillars in South Africa is commonly judged based on the characteristics of pillar failures within the different coal fields and coal seam. Salamon and Munro (1967) were the first to determine an average coal pillar strength for South Africa based on statistical review of failed and unfailed pillar dimensions**.** With further pillar failures occurring in the course of time, their work has been updated by other investigators, e.g. Madden (1991), Van der Merwe (2003b), Salamon, Canbulat and Ryder (2006) and Van der Merwe and Mathey (2013c). This work has revealed that distinct differences exist between the pillar strength characteristics in different parts of the country.

Van der Merwe (2003b) showed that in some coalfields, namely the Vaal Basin and Klip Rivier, pillars frequently failed at very high safety factors, i.e. in excess of SF= 1.6, while this was not the case in any of the other coalfields. Hence, he distinguished coal pillar strength in 'weak' and 'normal' coal areas. Subsequently the Free State coalfield was added to the list of 'weak' coal areas (Van der Merwe and Mathey, 2013c).

An attempt to refine this broadly regional approach to pillar strength in the country was conducted by Salamon, Canbulat and Ryder (2006), who separated the occurrence of pillar failures by coal seams in order to derive statistical seam-specific strength formulae. The project concluded that except for the coal mining areas around Witbank, there would not be enough information on pillar collapses available to make reliable predictions.

The most recent statistical coal pillar strength review by Van der Merwe and Mathey (2013c) shed more light on coal pillar strength in the country. It was shown that even in the 'normal' coal areas, where the safety factors of failed pillars are closely scattered around SF= 1, the failure probability of such pillars is likely to be relatively small, i.e. 9 % for a pillar safety factor of one. This was demonstrated by comparing the amount of collapsed pillars with the statistically estimated number of pillars ever mined in the 'normal' coal areas at the same safety factor.

The implication of this finding is that the currently available coal pillar strength formulae do not represent the average coal pillar strength in the country (or in the relevant areas), but only the average strength of failed pillars. The average coal strength of all coal must be higher.

This conclusion is also supported by the in-situ large-scale compression tests on coal specimens conducted in South Africa. The three collieries at which the experiments were conducted, Witbank, Usutu and New Largo respectively, are situated within the identified coalfields of 'normal' coal strength. Yet, the experienced magnitude of coal strength varied significantly under very similar testing conditions, coal being more than double as strong at New Largo as compared to Witbank colliery. Also, the coal strength encountered at New Largo and Usutu is considerably stronger than predicted by the latest updated coal pillar strength formula for these areas.

Not only the magnitude of strength differed in these large-scale compression tests, but also the rate of strength increase over specimen width-to-height. The stronger the coal, the more rapidly the specimens appeared to increase their strength with increasing width-to-height ratio.

In summary, it is clear that coal strength can vary significantly in South Africa, even within regions which exhibit similar pillar failure characteristics. The difference may affect the magnitude of compressive strength of coal but also the shape effect in coal, and therefore also the behaviour of squat coal pillars.

For an improved site, seam and coalfield specific understanding of coal pillar strength it is therefore imperative to study the distribution of mechanical coal properties in the country.

As this task can only be conducted on laboratory-scale, it bears the limitation that a direct transfer of established parameters to the in-situ magnitude is not possible. However, it provides the opportunity to identify the relative distribution of strength parameters across the country, and therefore of localized weakness and strength differences, provided that a large amount of tests can be compiled for statistical interpretation.

The database must therefore be sourced from the wealth of information on mechanical coal tests that is available in the coal mining houses and through open source research programs.

7 The mechanical coal properties database

7.1 Overview

A database of mechanical coal properties in South Africa has been compiled from available information at Anglo Thermal Coal SA, Xstrata Coal SA and BHP Billiton Energy Coal SA. Further sources include the compression tests conducted under SIMRAC Project COL21A (Madden et al., 1993) and, to a smaller extent, compression tests on coal conducted by the author.

The information stored within the database comprise the uniaxial compressive strength, Young's Modulus and Poisson's Ratio, triaxial compressive strength and indirect tensile strength of coal specimens. An additional number of tests has also been conducted on a series of specimens modified in size and shape to investigate the related strength-reducing or strengthening effect in coal from different collieries.

The total amount of 1819 individual tests on coal in this database comes from 5 different coalfields and covers 13 different seams:

- Witbank Nos. 1, 2, 4 and 5 seams
- Highveld Nos. 2 and 4 seams
- Vereeniging-Sasolburg Nos. 2 A, 2 B seams and Top and Middle seams
- Ermelo E and C Lower seams
- Nongoma Main seam.

The database further splits into 491 tests in uniaxial compression, 198 triaxial compression, 186 indirect tensile tests and 944 tests on the shape effect in coal.

The focus of this investigation will be on the uniaxial compressive and triaxial compressive strength, elastic moduli and the indirect tensile strength only. Size and shape effects have already been covered in the SIMRAC Project COL21A report (Madden et al., 1993) and by Van der Merwe (2003a).

Around 80 % of all UCS tests specimens were prepared from 60 mm diameter borehole cores, the rest comes from 25 mm to 100 mm diameter cores drilled out of sample blocks. All of the indirect tensile strength specimens had diameters of 60 mm. Also, the vast majority (95 %) of triaxial compression tests were conducted on 60 mm specimens.

7.2 Data validation

Before the database can be analysed for the distribution of coal strength in the different coalfields and seams, the included information must be inspected for errors which may adversely impact on the consistency of the database. A verification method is proposed in the following paragraphs.

7.2.1 Verification method

It is to be expected that the observed mechanical parameters of coal are subjected to a certain amount of scatter. The scatter is a result of errors in the measurement and recording of parameters as well as of natural fluctuation in the composition of the examined coal specimens. Errors are to be rejected, while natural fluctuations are to be accepted.

For the analysis of the coal database it is therefore imperative to be able to detect errors. Different types of errors can be distinguished in this context:

- *Specimen preparation errors*, such as non-parallel and non-flat loading surfaces. Also for coal, the influence of time elapsed between in-situ sampling and testing in the laboratory and the related changes in specimen humidity plays a role. Since coal is very friable in handling, specimens may also be damaged in the coring, cutting and grinding process.
- *Testing errors,* such as significant changes in the specimen loading rates, incorrect positioning of specimens in the testing apparatus or unbalanced loading.
- *Measurement error*, as they can result from incorrect positioning of strain gauges or from using a non-calibrated testing machine. In the latter case, the error is systematic if it impacts all tests by the same magnitude and can therefore be corrected.
- *Recording error,* when the measured data is entered incorrectly into record files.
- *Confusion of material type* is an especially severe case of error, for instance when mudstone, shale or sandstone was mistaken for coal.

Even without these erroneous influences some scatter will remain in the data. It is postulated that this remaining scatter is due to random influences.

For instance, if a number of specimens from a single borehole in a single seam are analysed for compressive strength at that point, the error-free measurements will scatter randomly around the expected value due to random changes in the petrographic and micro-tectonic composition of the coal specimens. The frequency distribution of the measured strength values will therefore resemble a normal or lognormal distribution.

If samples are taken from the same seam but from different boreholes in close proximity, so that the overall composition of the coal has not changed significantly, it is to be expected that measurements which are free of error will again exhibit a normal or lognormal frequency distribution, characterized by a mean and a standard deviation.

It is possible that samples taken further/far apart from each other in a coal seam may not exhibit a single normal or lognormal distribution of their characteristics, because the nature of the coal seam would differ significantly over its vast extent. Also, a comparison of samples from different coal seams does not necessarily exhibit a single normal or lognormal distribution. However, in the absence of errors, a histogram over the entire range of the observed parameters should still indicate a number of independent normal or lognormal frequency distributions, representing the individual parameters of seams or areas within them.

Therefore, it is proposed that the database entries are validated by checking for normal or lognormal distributions amongst the observations. A normal or lognormal distribution would suggest random deviations in the sampled values, which are therefore to be accepted, while data points which deviate significantly from these distributions (outliers) will be regarded as errors and are rejected.

7.2.2 Specimen size and shape limitations

Further, it is of importance that only specimens of similar size and geometry are compared in the analysis, due to the known effects of specimen size and shape on specimen strength and deformational behaviour.

In the context of specimen size, it has already been said in Chapter 7.1 that the vast majority of specimens used for the determination of UCS, elastic moduli, TCS and ITS come from boreholes with 60 mm diameter. This is well above the ISRM recommended minimum specimen diameter of 50 mm for UCS tests and 54 mm for triaxial tests.

In the process of the analysis it has also been decided to include all test specimens between 42 mm and 100 mm diameter, as the test results of these specimens were consistent with the results obtained from 60 mm specimens. Only specimens with a diameter smaller than 42 mm differed in behaviour in that they showed a marked increase in strength, and were therefore excluded from the further comparative analysis.

The shape effect in coal specimens is not subject of investigation at this stage, because it has already received attention by other investigators, (Madden and Canbulat, 1995; Van der Merwe, 2003a). Of importance, however, is the shape of test specimens for UCS, elastic moduli, TCS, ITS. The ISRM suggested methods (Ulusay and Hudson, 2007) for tests on UCS is a minimum specimen length-to-diameter ratio of l/d= 2.0 in order to minimise the end-effects.

About 35 % of all UCS test specimens in the database exhibit l/d- ratios smaller than 2.0. In order to avoid an unnecessary discard of too great a number of tests, it was decided to include all specimens of a minimum l/d= 1.8 in the analysis. Thus the amount of discard was reduced significantly to 3 %. Again it was checked that the inclusion of specimens with l/d-ratios smaller than 2.0 did not have an adverse impact on the overall database characteristics.

About 60 % of triaxial test specimens in the database exhibit l/d-ratios below 2.0. In some cases the l/d-ratio was as low as one. However it could be observed that the expected end-effect was not pronounced for these specimens, probably due to the applied lateral confinement overshadowing the induced frictional confinement along the specimen/loading platen contacts. Since no deviating behaviour could be observed for these specimens, it was decided that no restrictions had to be made for the length-to-diameter ratio of triaxial test specimens.

The specimens for indirect tensile strength tests either agreed or deviated minimally from the ISRM suggested minimum l/d-ratio of 0.5 and were therefore all included in the analysis.

7.2.3 Data validation

Some of the possible errors sources listed in Chapter 7.2.1, in particular testing errors, cannot be identified in the database. Nevertheless errors in specimen preparation and load-deformation measurements should be distinguishable in the database. For instance, an incorrect specimen preparation may lead to unbalanced loading (point-loading) of specimens, which should consequently fail at comparatively small average axial deformations. By contrast, very large axial deformations could be obtained from malfunctioning strain gauges. Outliers in histograms on axial strain at failure or the elastic modulus give an indication in this regards.

Figure 14 plots a histogram for the average axial strain at failure observed for 373 UCS specimens or 92.6 % of all available UCS specimens (left). The values appear to follow a lognormal distribution in ranges between 1 – 16 mStr. Three outliers are detected and rejected from further investigations.

The hypothesised lognormal distribution of the data is verified in the QQ-plot (right). In the QQ-plot, the observed quantiles of the standardized sample distribution is plotted against the quantiles of the standardized normal distribution. The sample values have been converted to their logarithmic values to check the assumption of a lognormal distribution in the data. An ideal lognormal distribution follows the straight line indicated in the QQ-plot. It can be seen that the logarithmic sample data follow this line favourably. Only very few outliers occur at the right extremity of the distribution. It is therefore assumed that the sample is lognormally distributed in ranges between 1 – 16 mStr.

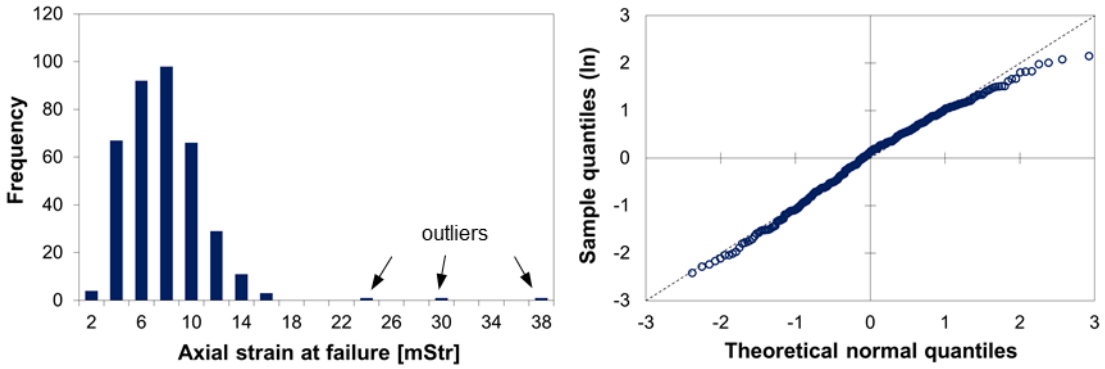


Figure 14. Histogram of the axial strain at strength failure for UCS specimens (left) and QQ-plot (right) for a hypothesised lognormal distribution of the data.

Further, it can be assessed whether the database includes errors which could have been introduced by confusing other materials, such as sandstone, mudstone or shale with coal. The materials can be distinguished from coal by their density. Coal has the lowest density of the aforementioned materials, the expected value being around 1.5 g/cm^3.

Sandstone, on the other hand, has the highest density of typically 2.6 g/cm^3. The density of mudstone and shale are scattered between these extremes, but commonly in excess of 2.0 g/cm^3. Figure 15 to Figure 17 plot density histograms for the UCS, TCS and ITS specimens respectively in the database.

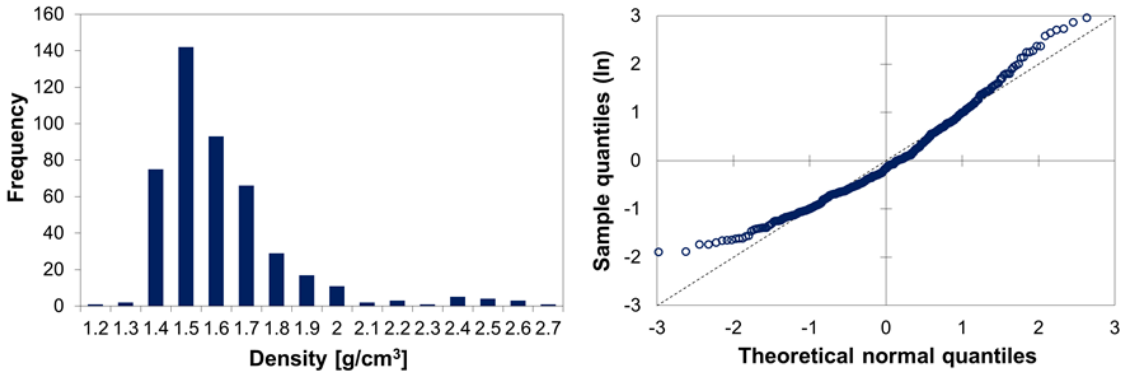


Figure 15. Density histogram for UCS specimens (left) and QQ-plot (right) for a hypothesised lognormal distribution of UCS specimen density up to 2.1 g/cm^3.

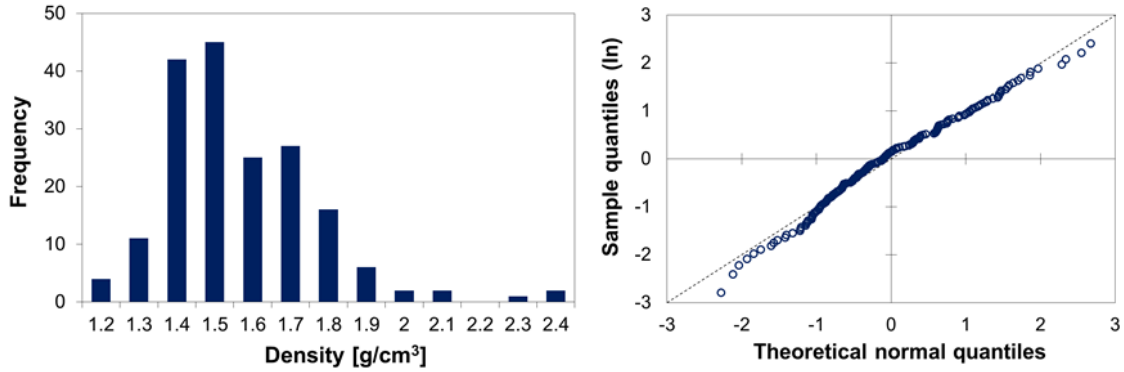


Figure 16. Density histogram for all ITS specimens (left) and QQ-plot for a hypothesised lognormal distribution of the density up to 2.0 g/cm^3 (right).

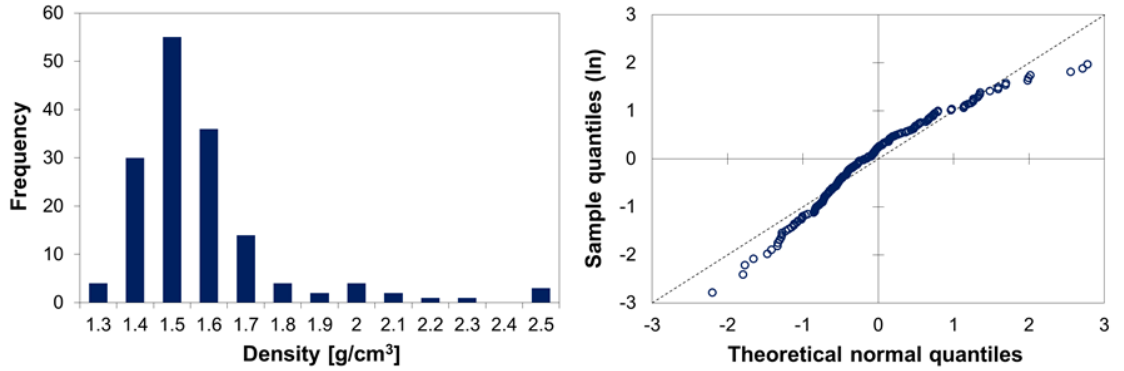


Figure 17. Density histogram for all TCS specimens (left) and QQ-plot for a hypothesised lognormal distribution of the density up to 1.9 g/cm^3 (right).

From the histograms it appears that the density could be lognormally distributed in intervals: in the case of UCS up to a value of about 2.1 g/cm^3, in the case of ITS up to 2.0 g/cm^3

and in the case of TCS about 1.9 g/cm^3. However, a satisfying lognormal fit in the specified ranges can only be observed in the QQ-plot for the ITS specimens. Some significant deviations from the straight-line are observed for the UCS and TCS specimens, indicating that there might be some errors in the dataset.

Above the specified upper limits the data appears to be even more erroneous, with the density being in the range of rock materials. It was confirmed that this data did not come from a single borehole or single mine so that an influence of regional coal anomalies could be excluded. Also, the uniaxial compressive strength of these outliers was in average 70 MPa, with some tests indicating strength as high as 106 MPa. These are typical values for sandstones and the relevant data points have therefore been discarded from further analysis

In absence of a conclusive, error-free density distribution for all datasets, it is decided that only specimens with a density less than 2.1 g/cm^3 are used for further analysis. This preliminarily cut-off value is applied consistently for UCS, TCS and ITS specimens and does not discard an unreasonably large number of tests. Also, the impact of the few possible outliers remains relatively small. For instance, it will be seen later in Chapter 8.5 that UCS specimens with densities between 1.9 and 2.1 g/cm^3 do indeed have strength values very close to the database average and are therefore not outliers. It is therefore decided that a further reduction of the upper density limit for inclusion of specimens in the analysis is not required.

The average density of the remaining UCS, TCS and ITS specimens is 1.54 g/cm^3, 1.50 g/cm^3, 1.50 g/cm^3 respectively.

8 Results

In the following sections, the validated database of mechanical coal properties is analysed in terms of central tendencies and spread in the uniaxial and triaxial compressive strength as well as the indirect tensile strength of coal. Possible correlations between the mechanical parameters are investigated as well.

It should be noted that the arithmetic mean is used as the measure of central tendencies in the samples, irrespective of the symmetry of the sample distribution. The implication is that for asymmetric (e.g. lognormal) distributions, the arithmetic mean may overestimate the central tendency in the samples and hence the central tendency of the population. This will have to be taken into account when conclusions are being drawn on the population of mechanical coal characteristics and the related practical implications.

Nevertheless, the arithmetic mean is used to describe all samples for the purpose of consistency and to facilitate a comparison with internationally published average coal strength data. The standard deviation of the samples, given as the measure of spread, are therefore also calculated based on the arithmetic mean.

8.1 The uniaxial compressive strength

A number of 403 tests on the uniaxial compressive strength are evaluated for the overall coal strength of South African seams. Amongst them, 350 tests provided complete information for a distinction of strength characteristics in 13 different seams and 6 different coalfields.

Figure 18 plots the histogram for the uniaxial compressive strength in all coalfields and seams. It is suggested that the data approximately exhibits a lognormal distribution (left), which may also be supported by the QQ-plot (right). Pronounced deviations from the ideal diagonal line only occur at the left and right extremity of the data. The arithmetic mean strength of all UCS tests on coal is 22.943 MPa, with a standard deviation of 9.523 MPa.

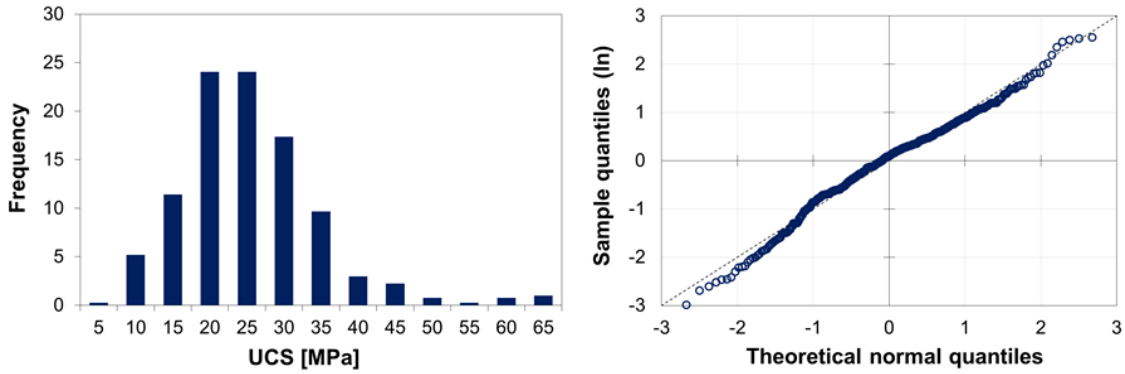


Figure 18. UCS histogram for all 403 specimens (left) and QQ-plot for a hypothesised lognormal distribution of the UCS (right).

Strength values above 50 MPa do not appear to obey the lognormal distribution of coal strength and were investigated for regional, i.e. seam or coalfield specific patterns. However, the origin of these specimens is dispersed across the country and their values stand in contrast to test results for other specimens derived from the same sample or borehole. It could therefore be that the deviational behaviour was caused by some rock, e.g. shale or sandstone intrusions in the coal specimens.

For a number of 284 tests, information on the failure mode in the specimens were reported by the test agencies and are available for analysis. Based on the reported figures, it is concluded that the peak uniaxial compressive strength of 92.3 % of all UCS specimens was influenced by failure on one or more discontinuities in the specimens. The remaining 7.7 % of specimens failed in shear-sliding mode through intact material or even exhibited complete double-cone developments during the tests.

Figure 19 plots the normalized frequency distributions of the strength of specimens failed through loss of intact material strength and through influence of discontinuities. Apparently, the influence of discontinuities in specimens manifests not only as a reduction of the average strength of specimens but also as a wider scatter of individual strength values. The specimens whose failure was reportedly not influenced by discontinuities are on average 27.8 % stronger and are scattered more closely.

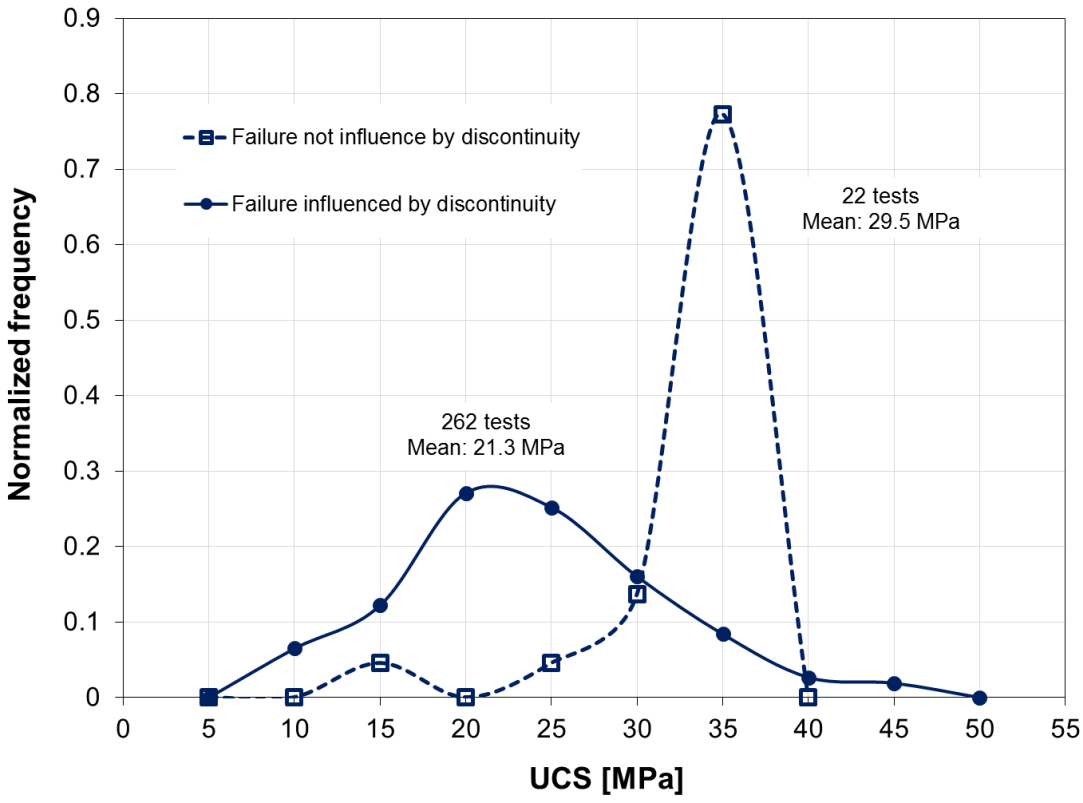


Figure 19. The influence of discontinuities on the strength of coal in uniaxial compression.

It should be noted that the presence of discontinuities also appears to be the predominant contributor to the skewness of the overall UCS sample histogram (Figure 18).

The absence of regional or systematic patterns in the histogram for all coal across the country in Figure 18 suggests that the distribution of unconfined compressive strength in the different seams and coalfields is relatively consistent.

To investigate regional coal strength further, the database is then split according to coal seams. An overview of the number of tests available per seam and the determined strength characteristics is given in Table 2**.**

It should be noted that only very little data was available for the Main seam in Nongoma coalfield and for coal in the Waterberg coalfield and therefore the table may not be representative of the entire sample. Some of the data collected under Witbank Nos. 2, 4 and 5 seams and Vereeniging-Sasolburg (V-S) Top and Middle seams had originally been subdivided in the database as No. 5 A, No. 2 L, Top seam Upper, Middle seam Lower etc., referring to local splits in the mother seam. The data has been unified here under the name of the mother seam since not enough data was available for statistical treatment of the subdivisions.

Table 2. Uniaxial compressive strength characteristics for different coal seams.

Coalfield	Seam	No. of tests	UCS, ave. [MPa]	UCS, SD [MPa]	UCS, min [MPa]	UCS, max [MPa]
Witbank	No. 1	7	19.29	8.34	11.65	35.95
Witbank	No. 2	82	23.95	10.58	7.13	63.20
Witbank	No. 4	61	20.10	6.28	8.49	36.37
Witbank	No. 5	26	22.38	5.57	9.65	34.60
Witbank	Unknown	23	25.08	10.53	10.87	56.02
Highveld	No. 2	13	24.32	8.48	9.78	40.07
Highveld	No. 4	69	24.20	8.16	9.31	61.10
Highveld	Unknown	11	15.35	9.52	3.10	32.41
V-S	Top	19	22.36	6.92	8.76	34.07
V-S	Middle	22	19.92	7.82	6.86	37.44
V-S	No. 2 A	8	31.10	24.33	11.30	62.00
V-S	No. 2 B	13	25.86	6.66	16.72	37.54
V-S	Unknown	7	24.27	7.71	11.25	31.85
Ermelo	C Lower	21	22.32	9.69	6.07	44.68
Ermelo	E	5	22.41	12.27	14.58	43.06
Nongoma	Main	4	32.73	6.92	8.76	34.07
Waterberg	Unknown	2	26.59	7.71	11.25	31.85

In Table 2 it is also important to observe that for two seams, namely the Witbank No. 2 and Highveld No. 4 seams, the observed maximum strength exceeds the 3σ (three times the standard deviation) interval of the entire population. This again points to possible outliers in the data and the reason behind this could possibly be rock intrusions in the coal.

The maximum strength observed for No. 2 A seam coal from the Vereeniging-Sasolburg coalfield exhibits a similar value compared to the suspected outliers in the Witbank No. 2 and Highveld No. 4 seams. All 8 specimens tested from this seam come from one sample block, of which 5 specimens had an average strength of 14 MPa only, while three specimens were in excess of 60 MPa. Clearly some significant heterogeneity must have been encountered in the coal sample and the tests cannot be taken as representative for the seam.

Whether or not the discussed outliers are to be discarded from the coal database depends on personal and not statistical judgement. While it is likely that the relevant specimens consisted predominantly of non-coal components (and should therefore be rejected as not representative for coal), it is nevertheless sometimes the case that this type of coal-rock mixture is the very element out of which underground pillars consist and therefore should remain included.

In the interest of having a more accurate view on what is likely to be pure coal strength, Figure 20 summarizes the average strength and standard deviation of coal in the different seams after discard of the outliers. Also included in the figure are tests from coalfields to which no seam could be related (labelled as ‘N/A’ in the plot). The results for the sample of Vereeniging-Sasolburg No. 2 A seam coal are excluded from the plot due to the significant heterogeneity encountered, as explained above.

Figure 20 confirms the assumption made earlier that the average uniaxial compressive coal strength is relatively consistent throughout the seams in the country.

The average strength values for the individual coal seams scatter within the interval of 19.29 (No. 1 seam) to 25.86 MPa (No. 2 B seam). The seam specific standard deviations are generally large, in the range of 25 to 55 % of the seam-specific mean value.

The average uniaxial compressive strength across all seams calculates to 22.23 MPa with a standard deviation of 7.65 or 34.2 % of the mean. Further, the average seam-specific values scatter at a maximum of 15 % around the population mean and therefore all lie within the standard deviation of the entire population.

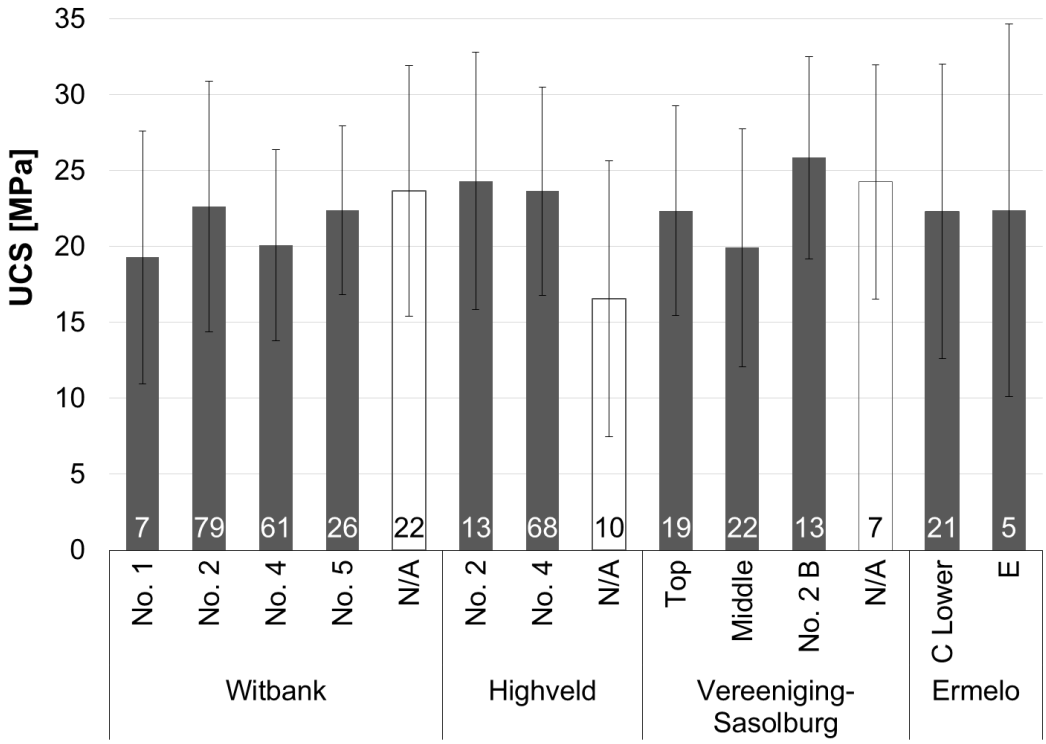


Figure 20. Seam-specific average UCS with accompanying standard deviations of coal in various coalfields in South Africa after removal of outliers in the dataset. The amount of tests evaluated per coal seam are given in the base of the columns.

Because of the relatively small difference in the average strength of coal from different regions and seams in South Africa, a further subdivision of the coalfields by mines is not required.

However, it is worth noticing that the distribution of intact coal strength is also random, i.e. non-systematic, for individual collieries. For example, Figure 21 (left) plots the frequency distribution of strength of 44 UCS specimens, sampled from 11 boreholes across one mine site in the Highveld coalfields.

It can be seen in Figure 21 (right) that in the interval 16 – 33 MPa the coal strength is lognormally distributed. Only 6 outliers above and below this interval do not conform to this distribution. The average uniaxial compressive strength in this example is 23.57 MPa with a standard deviation of 6.55 MPa.

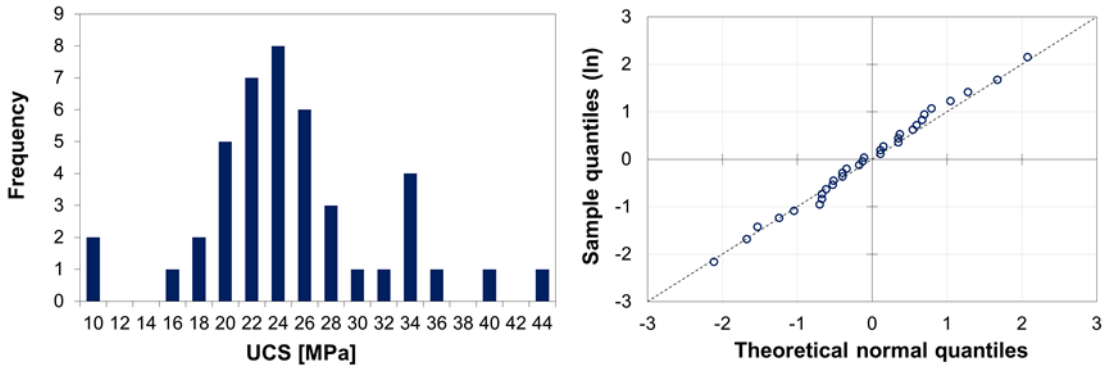


Figure 21. UCS histogram (left) for 44 specimens sampled from 11 boreholes on a mine site in the Highveld coalfield and QQ-plot for a hypothesised lognormal distribution of the UCS in ranges between 14 – 33 MPa (right).

8.2 Elastic moduli

A total number of 322 tests provides results on the elastic deformation characteristics: Young's Modulus (E) and Poisson's Ratio (ν) of coal. The values are determined as both the tangential and secant moduli at 50 % of the peak stress stored in the database. The following examination makes use of only the tangential Young's modulus E_t and Poisson's Ratio ν_t at 50 % stress level.

Figure 22 gives a histogram for the distribution of E_t across 5 different coalfields and 11 different seams. The histogram suggests a lognormal distribution of the data, which is found to be confirmed in the QQ-plot of the lognormal sample quantiles against the theoretical normal quantiles.

The average elastic modulus of coal specimens equates to 4.45 GPa with a standard deviation of 2.04 GPa.

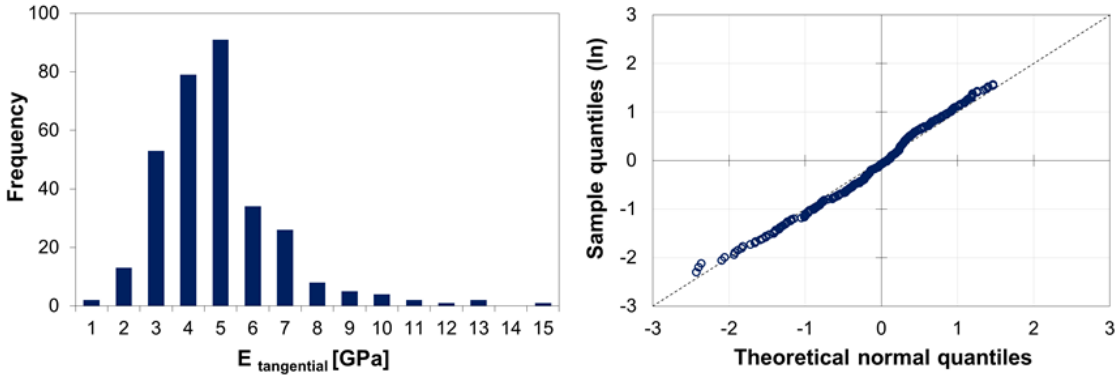


Figure 22. Histogram for the tangential elastic modulus measured on 322 coal specimens (left) and QQ-plot for a hypothesised lognormal distribution of the sample data (right).

Figure 23 displays the histogram of the Poisson's Ratio of the same coal specimens, for which the elastic modulus has been evaluated. It should be noted here that some values in excess of 0.5 have been recorded, which are obviously erroneous and have to be

discarded. Also it should be noted that the distribution can best be approximated by a normal distribution. This is also shown in the QQ-plot, where the normal sample quantiles are plotted against the theoretical normal quantiles.

The average Poisson's Ratio for the 290 specimens with ν_t= 0.5 is 0.306 with a standard deviation of 0.147.

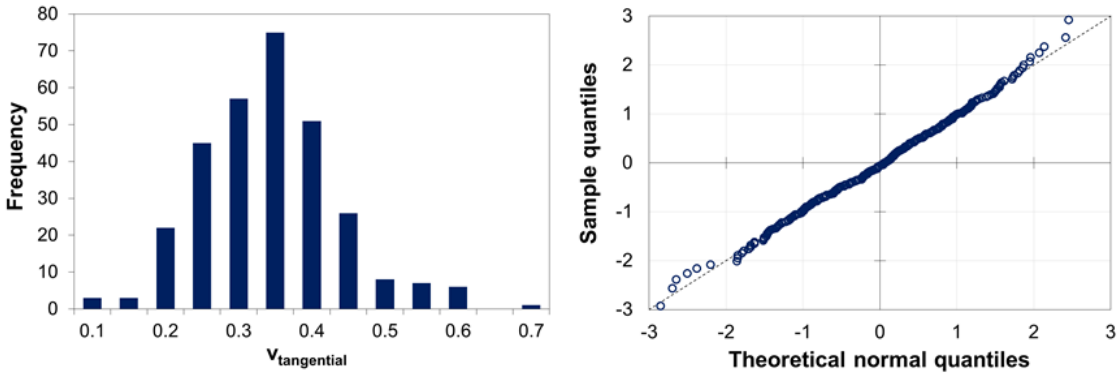


Figure 23. Histogram for the tangential Poisson's Ratio measured on 322 coal specimens (left) and QQ-plot for a hypothesised normal distribution of the sample data (right).

8.3 The triaxial compressive strength

A total of 198 coal specimens were tested in triaxial compression at confinement levels between 1.5 – 20 MPa. The tests cover 8 different coal seams and 4 coalfields. Two-thirds of all tests were performed at 2.5 MPa, 5 MPa and 10 MPa confinement levels and provide the basis for the following analysis of triaxial strength of coal in different seams of South Africa.

Frequency distributions of the specimen strength at 2.5 MPa, 5 MPa and 10 MPa confinement are presented in Figure 24 to Figure 26**.** It is hypothesized that the data is normally distributed, which can be seen to be confirmed in the related QQ-plots.

A lognormal distribution, as found for the UCS, may satisfactorily describe the data set but data in both the upper and lower extremes are more accurately described by a normal distribution.

Information on the strength failure patterns are available for 186 triaxial compressive strength specimens. It has been shown previously that for the vast majority, i.e. 92 % of unconfined test specimens, strength failure is influenced by one or more discontinuities in the coal.

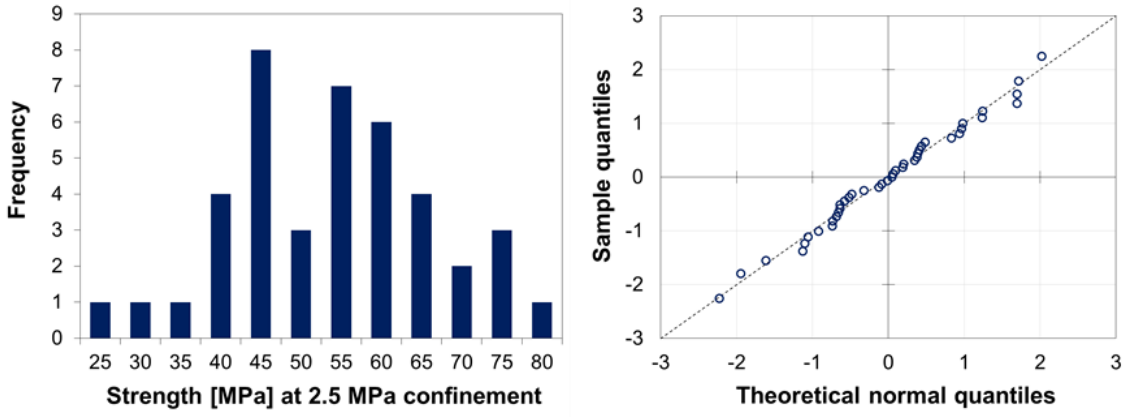


Figure 24. Histogram of the strength of 41 coal specimens at 2.5 MPa confinement (left) and QQ-plot for a hypothesised normal distribution of the data (right).

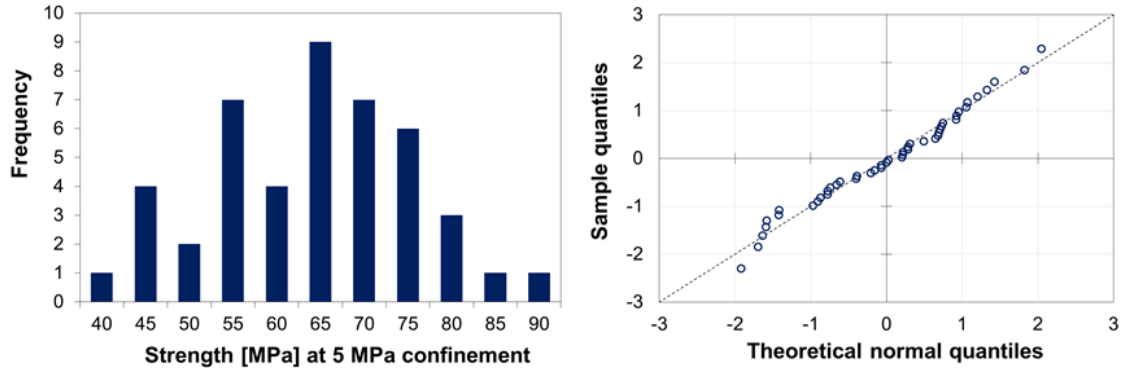


Figure 25. Histogram of the strength of 44 coal specimens at 5 MPa confinement (left) and QQ-plot for a hypothesised normal distribution of the data (right).

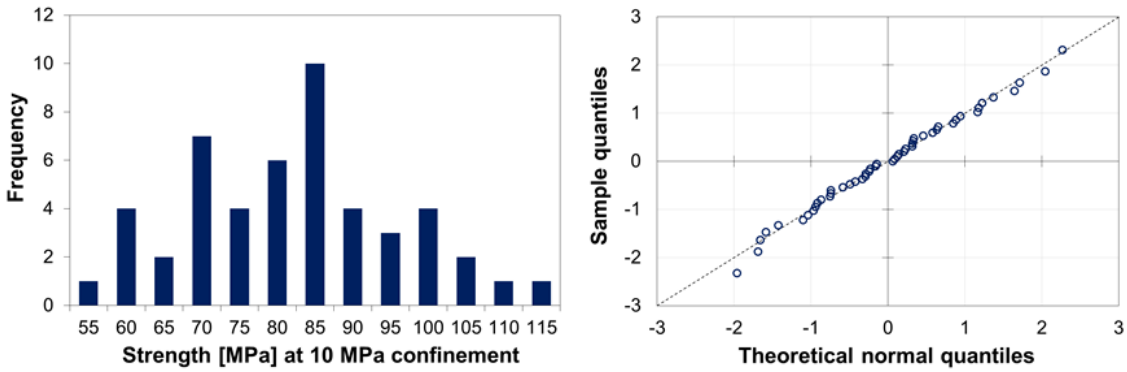


Figure 26. Histogram of the strength of 47 coal specimens at 10 MPa confinement (left) and QQ-plot for a hypothesised normal distribution of the data (right).

The influence of discontinuities is seen to be substantially reduced for specimens tested at lateral confinement, as shown in Figure 27. Only about 25 % of all specimens fail on discontinuities at relatively low confinement levels of 2.5 MPa, with the remaining specimens failing by shear sliding through intact material. This ratio is further seen to remain fairly constant for higher lateral confinement levels up to 20 MPa, i.e. an increased lateral

constraint does not further decrease the relative number of specimen failures on discontinuities. The average ratio of these specimen failures to the overall number of triaxially tested specimens in the range of 1.5 – 20 MPa is 27 %.

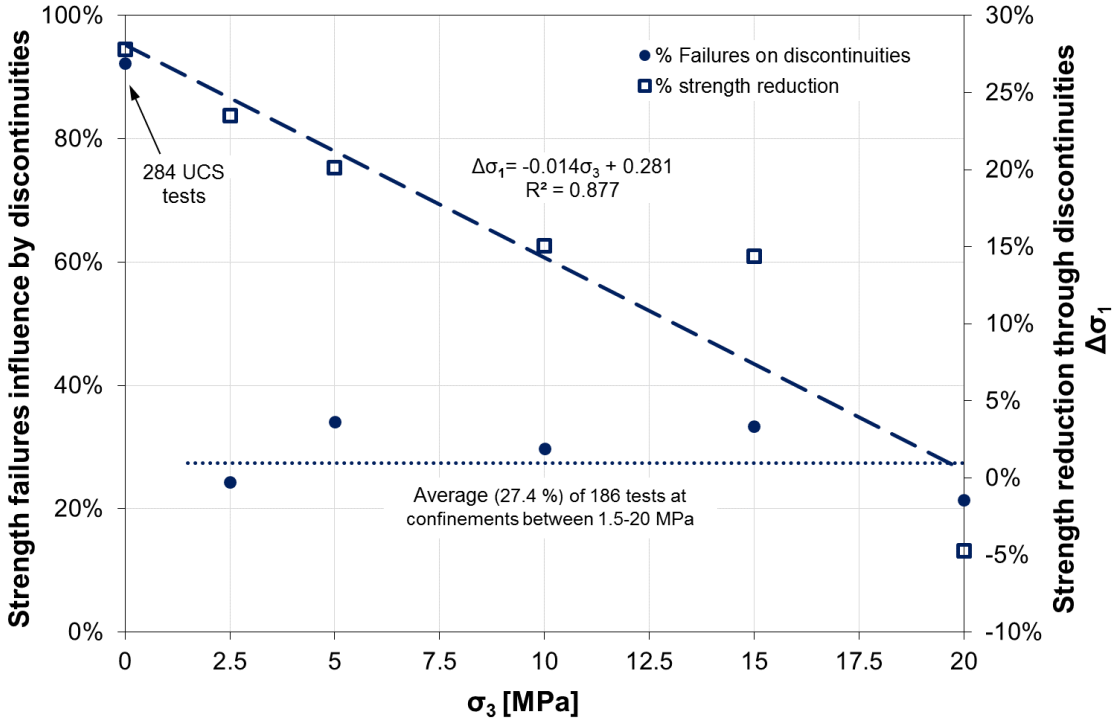


Figure 27. Influence of confinement on the failure mode and average peak strength of coal specimens.

For each confinement level, the average strength of specimens which failed in shear of intact material and the average strength of specimens that failed on discontinuities are compared in Figure 27. The differences in peak strength $\Delta\sigma_1$, for the two groups of specimen failures reduces linearly in a confinement range between 0 – 10 MPa. At higher confinement levels, i.e. 15 MPa and 20 MPa, $\Delta\sigma_1$ shows a larger scatter around the predicted linear trend. The reason for this may be that only very few numbers of tests (i.e. three and 4 at confinements of 20 MPa and 15 MPa respectively) are available for the calculation of the average failure strength of specimens influenced by discontinuities.

Nevertheless, the observations made over the entire range of 0 – 20 MPa confinement levels are reliable enough to assume a linearly decreasing influence of discontinuities on specimen peak strength (see correlation in Figure 27). The weakening influence of discontinuities is predicted to become practically zero at a confinement of around 20 MPa.

For further analysis of possible seam-specific trends, the samples of all triaxial tests conducted at 5 MPa and 10 MPa confinement are split into seam-specific groupings and average strength is determined for the different coal seams. The results are presented in Figure 28**,** together with the average uniaxial compressive strength of the seams.

The average uniaxial compressive strength has previously been shown to be relatively consistent throughout the coal seams (Chapter 8.1), so that the comparison of strength increase with confinement in between the seams is based on a fairly even level.

Notably it can be observed that coal from some seams can pick up in strength quicker than others after increase in confinement. In particular the Witbank No. 5 and Highveld No. 4 seams exceed all other seams in strength already after a moderate confinement increase to 5 MPa. After a further increase to 10 MPa confinement, the Witbank No. 2 seam catches up with these aforementioned seams at strength levels between 83 – 94 MPa and exceeds the somewhat weaker group of Witbank No. 4, Vereeniging-Sasolburg Middle and Top seams and the Ermelo C Lower seam, which range at around 70 – 75 MPa.

This trend indicates that the coal in the different seams may have different cohesion and internal friction properties. This is to be examined further.

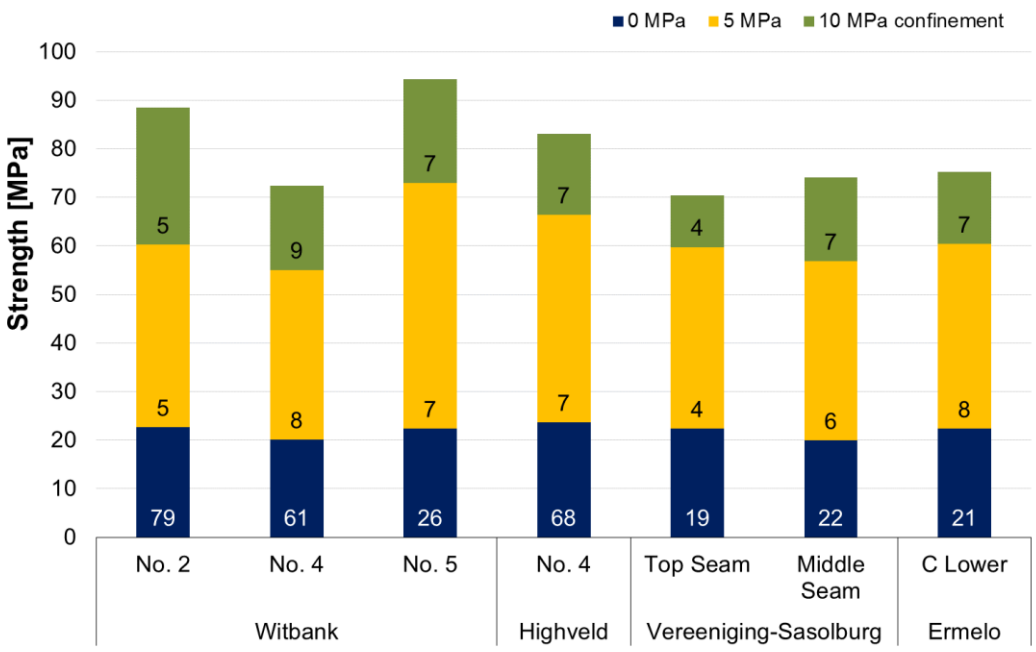


Figure 28. The average compressive strength of coal specimens from different seams at 0 MPa, 5 MPa and 10 MPa confinement. The number of tests evaluated for each confinement level are given at the base of the bars.

Figure 29 provides $\sigma_1 - \sigma_3$ plots for the entirety of triaxial tests conducted in the Witbank Nos. 2, 4 and 5 seam, the Highveld No. 4 seam, Vereeniging-Sasolburg Top and Middle seams and the Ermelo C Lower seam. A linear curve is fitted to the seam-specific data, providing the average gradient of strength increase β_0 over confinement and the intercept with the y-axis, which is the estimated intact compressive strength σ_c at 0 MPa confinement.

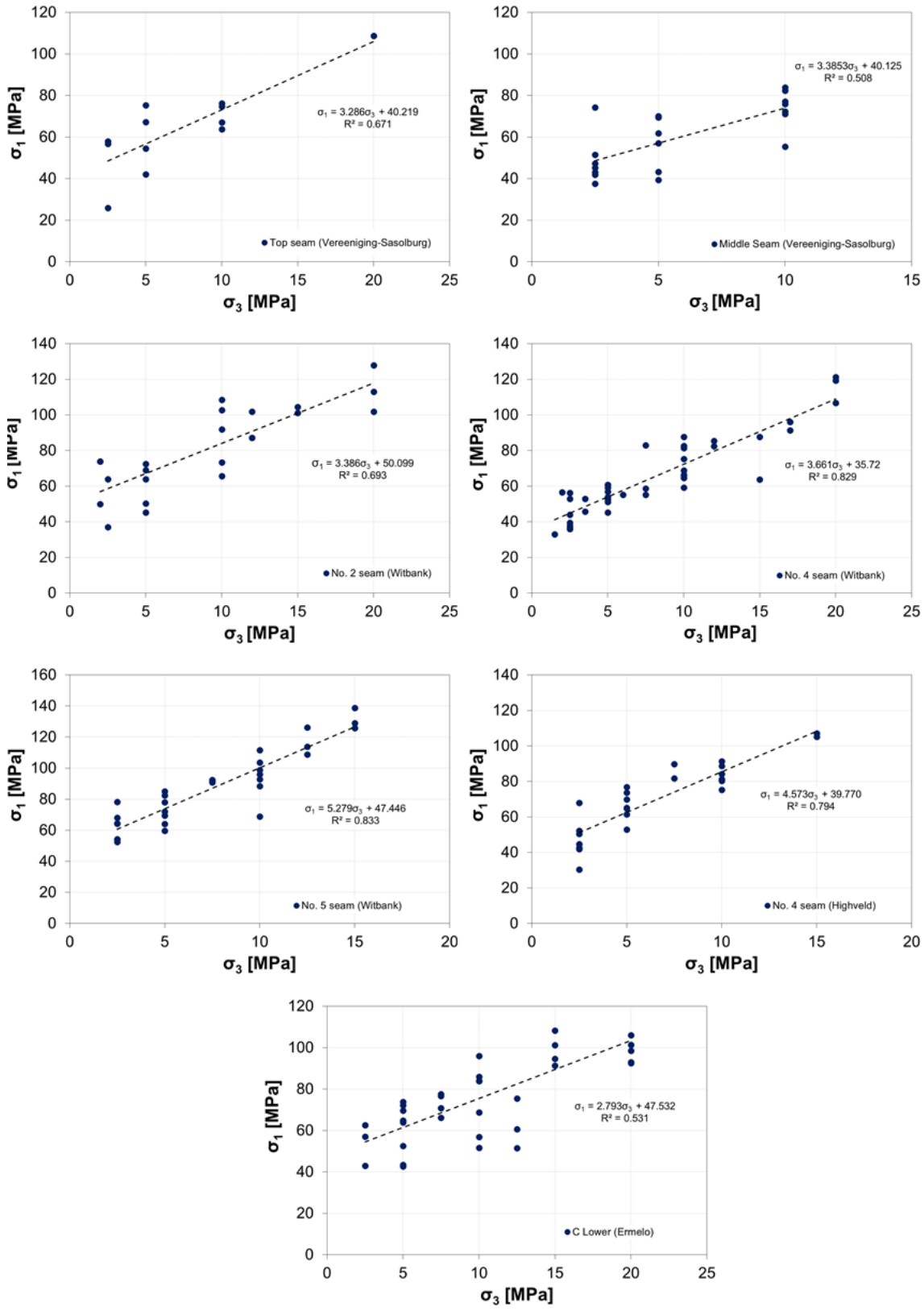


Figure 29. $\sigma_1 - \sigma_3$ plots of triaxial coal strength in different coal seams.

The Top and Middle seams in the Vereeniging-Sasolburg coalfield exhibit very similar triaxial strength behaviour in terms of both β_0 and σ_c. The gradient β_0 in the Witbank Nos. 2 and 4 seams is also very similar to the ones observed in the Vereeniging-Sasolburg

coalfield. However, a difference in σ_c is apparent, with the No. 2 seam being the strongest one of the 4 aforementioned seams and the Witbank No. 4 seam being the weakest.

The Witbank No. 5 and Highveld No. 4 seams have higher gradients of strength increase in the group of analysed seams, i.e. 54 % and 33 % higher than the average of the 4 aforementioned seams. The strength σ_c lies within the range observed for the 4 seams.

Another individual in terms of β_0 is the Ermelo C Lower seam, which has the lowest strength increase gradient of all investigated seams.

Another point of interest is that the predicted unconfined strength by the equations in Figure 29 is in all cases substantially higher than the average UCS tested for the same seams. The explanation for this phenomenon lies in the cleating and discontinuities present within the coal specimens: the unconfined uniaxial strength of coal specimens is unavoidably affected by these discontinuities. The measured strength is therefore not necessarily the intact strength of coal. However, with lateral confining stresses being applied to the specimens the detrimental impact of discontinuities is gradually reduced. Some researchers, e.g. Medhurst and Brown (1998), therefore suggest that the intact and unconfined strength of coal could better be determined by loading specimens under low confining pressures and extrapolate a more appropriate unconfined strength.

A set of Mohr-Coulomb and Hoek-Brown parameters for different coal seams has been calculated from the $\sigma_1 - \sigma_3$ plots and is listed in Table 3**.** The distribution of Mohr-Coulomb cohesion c and the angle of internal friction ϕ in the different coalfields follow the same trends as described for σ_c and β_0 above. The parameters σ_{ci} and m_i in the Hoek-Brown notation of triaxial strength are the equivalents of Mohr-Coulomb cohesion and angle of internal friction.

Table 3. Mechanical parameters for TCS specimens from different coal seams.

Coalfield	Seam	Mohr-Coulomb				Hoek-Brown	
		c	ϕ	σ_c	β_0	σ_{ci}	m_i
		[MPa]	[°]	[MPa]		[MPa]	-
Witbank	No. 2	13.61	32.96	3.39	50.10	46.47	7.56
Witbank	No. 4	9.33	34.81	3.66	35.72	29.15	11.53
Witbank	No. 5	10.33	42.96	5.28	47.45	39.92	16.82
Highveld	No. 4	9.30	39.88	4.57	39.77	31.26	15.62
V-S	Top	11.09	32.23	3.29	40.22	36.50	7.60
V-S	Middle	10.90	32.95	3.39	40.13	38.05	6.89
Ermelo	C Lower	14.22	28.21	2.79	47.53	44.23	4.48

8.4 The indirect tensile strength

The indirect tensile strength (also Brazilian tensile strength) for coal has been determined on a number of 186 specimens from 4 coalfields, 10 collieries and 10 different seams.

The samples exhibit a lognormal frequency distribution as shown in Figure 30**.** Only tensile strength values below 0.5 MPa are not well represented by the lognormal distribution.

The average indirect tensile strength of the sample is 1.60 MPa with a standard deviation of 0.72 MPa.

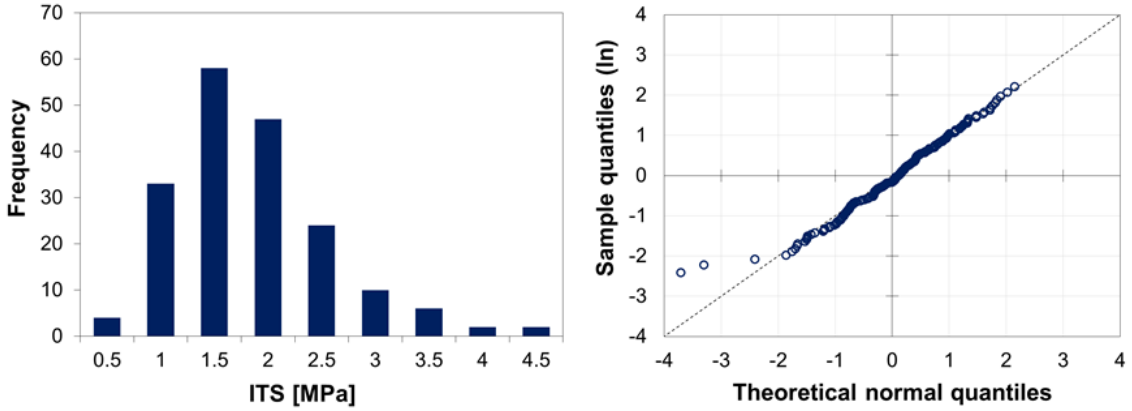


Figure 30. Histogram for the indirect tensile strength of South African coal determined on 186 coal specimens (left) and QQ-plot for a hypothesised lognormal distribution of the sample data (right).

The indirect tensile strength of coal was further investigated by grouping the database according to individual coalfields and seams. Figure 31 plots the results. The seam-specific indirect tensile strength ranges from 1.05 MPa (Top seam) to 1.89 MPa (No. 5 seam). The individual deviation from the overall sample average of 1.59 MPa is therefore significantly larger than previously observed for the characteristics of the uniaxial compressive strength in the different seams.

The reason for this phenomenon could be that coal specimens for UCS testing are generally loaded perpendicular to the bedding plane of the coal, hence the determined load bearing capacity is easier to compare. Indirect tensile test specimens, however, are cut from a borehole core and loaded parallel to the bedding plane and the outcome of the test is affected by the anisotropy in this plane. Results may vary according to the orientation of the specimen in the testing machine.

In summary, the indirect tensile strength tested appears to be less uniformly distributed across the coal seams in the country. However, it is not clear whether the scatter is attributable to real differences in the coal or to unavoidable shortcomings of ITS laboratory testing. It should be noticed that only very few tests are available for most of the coal seams, in particular the No. 2 (Highveld), Top and C Lower seams. The latter two coal seams exhibit a very high standard deviation. It is therefore unlikely that the presented indirect tensile strength averages are representative of the actual seam-specific values.

A further sub-grouping of coal seams by collieries is not meaningful because of the limited data available.

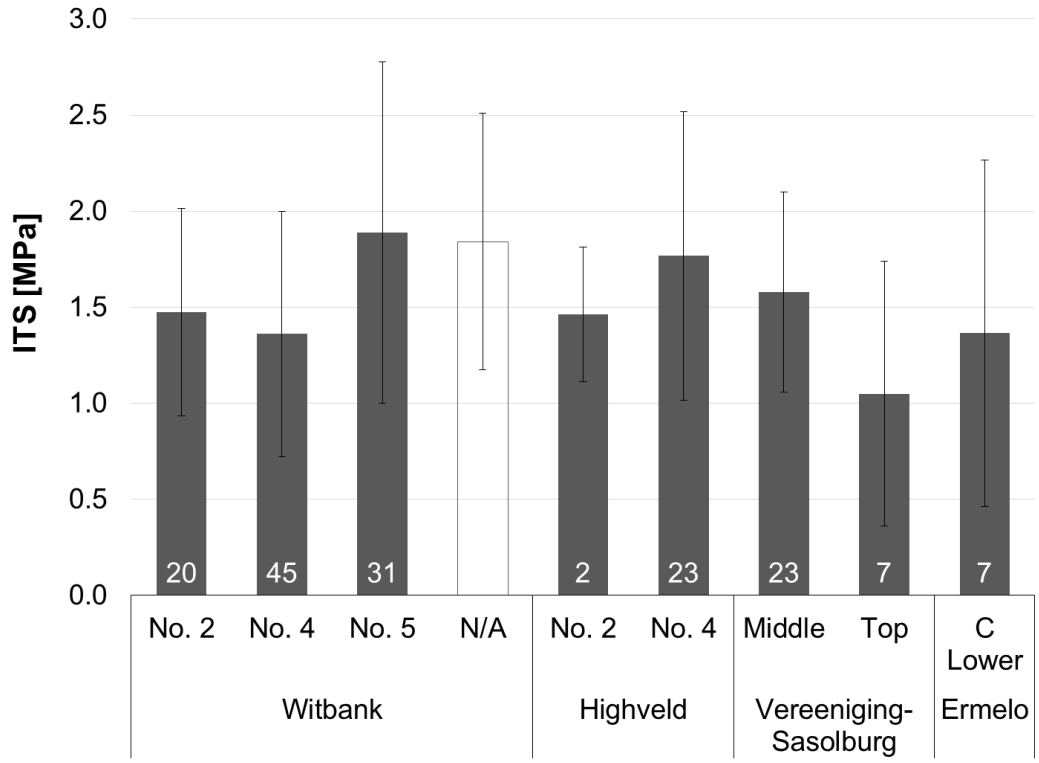


Figure 31. Seam-specific average *ITS* with accompanying standard deviations of coal in various coalfields in South Africa. The number of tests evaluated per coal seam are given in the base of the columns.

8.5 Correlations

Correlations between material properties are of interest because they allow reasonable estimation of rock behaviour when only limited test data is available.

Some fundamental links between material properties are already established for rock materials, for instance the correlation between the uniaxial compressive strength and the tensile strength or between the uniaxial compressive strength and the elastic modulus. Other correlations are of particular interest in the context of squat pillar design, particularly the correlation of material properties with the depth of the seam.

Depth-dependent rock specimen behaviour, for instance, was advocated by Watson (2010) in his review of rock behaviour of the Bushveld Merensky reef. He investigated 11 anorthosite specimens sampled from boreholes in depth between 600 – 1100 m below surface. Strength and elastic modulus tended to decrease with increasing depth, while the Poisson's Ratio increased. Even more significantly, he observed that specimens below 1000 m depth exhibited non-linear elastic deformation behaviour, as opposed to the linear elasticity of specimens at shallower depth.

Watson (2010) related the phenomena to the closing and sliding of micro-cracks in the rock. He theorised that a critical stress-drop threshold is required for the opening and development of micro-cracks in first case. The stress-drop being caused by excavation

of the rock from its environment. This in return will only occur in specimens at greater depth, i.e. greater in-situ virgin stresses.

In terms of coal one observed that most specimen deformation behaviour is non-linearly elastic, irrespective of the depth of sampling. This is due to the unavoidable presence of cleats, fissures, pores and other micro-cracks in coal, which upon loading first close and then slide. The elastic part of the stress-strain curve is therefore generally upward curving at first, i.e. the specimen stiffness increases gradually. This is also manifested by the fact that at 50 % peak-stress level, the tangent modulus of coal is generally larger than the secant modulus.

8.5.1 Coal density versus sampling depth

The majority of specimens analysed in this study come from a depth of less than 120 m below surface and exhibit a large scatter in density, as previously discussed in Chapter 7.2.3. However, some data is also available for a depth of 430 m below surface. Figure 32 plots the distribution of measured coal density versus depth.

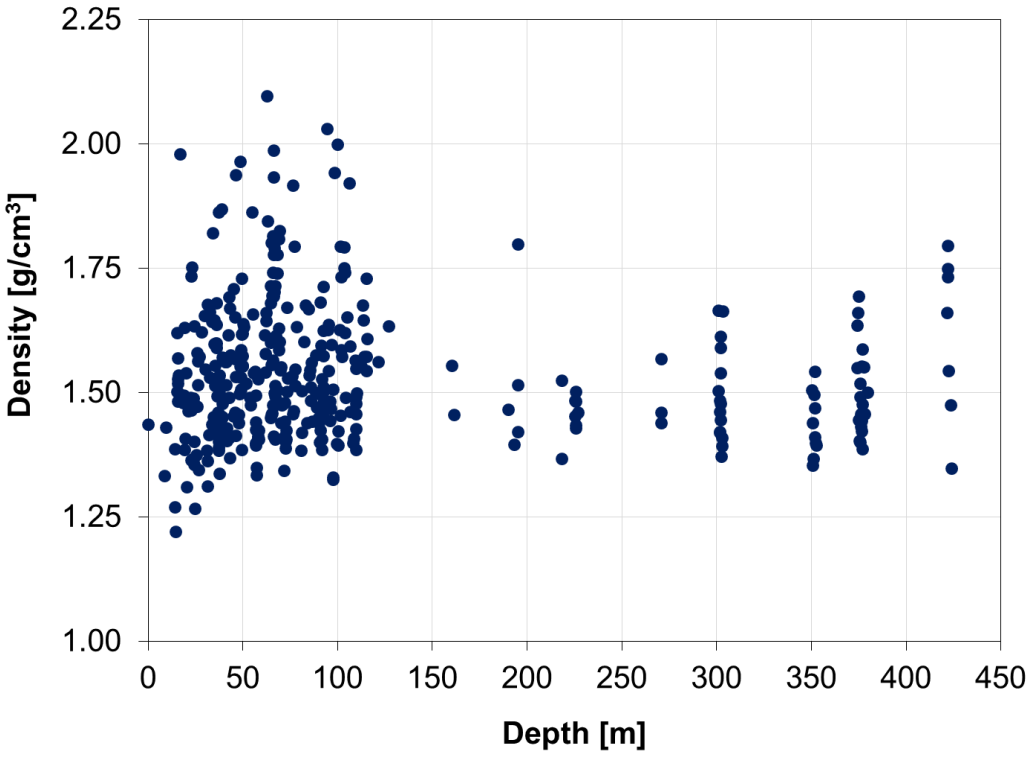


Figure 32. Coal specimen density versus depth below surface.

One observes no trends between the two parameters. The density of coal scatters in all depth fairly consistently around the overall mean value of 1.5 g/cm3. Therefore no trend exists between the two parameters. However, the density plotted is measured on de-stressed specimens and the in-situ density of coal is likely to increase under the increasing pressures at greater depth.

8.5.2 *UCS* versus density, depth, *E* and *ITS*

The uniaxial compressive strength of coal is investigated for its relationship to the depth of sampling and elastic modulus as measured on the same specimens**.** It is also of interest to evaluate how the uniaxial compressive strength relates to the indirect tensile strength of coal. Since both characteristics cannot be determined on the same specimen, the comparison must be done on the basis of average *UCS* and *ITS* for specimens from the same borehole/sample and seam.

The relationship between the specimen density and the *UCS* is plotted in Figure 33. So far it has been assumed that the higher the specimen density, the higher the chance that the coal may contain portions of rock, or that in worst case the entire specimen was not of coal but of rock material. If this is true, then the higher densities should also correspond to higher *UCS* values. This, however, is not found to be the case. Various specimens at around 2.0 g/cm^3 density, for instance, are seen to have *UCS* values well in the range which has been identified for coal in South Africa. In general, no correlation between the specimen density and the *UCS* in the database can be observed.

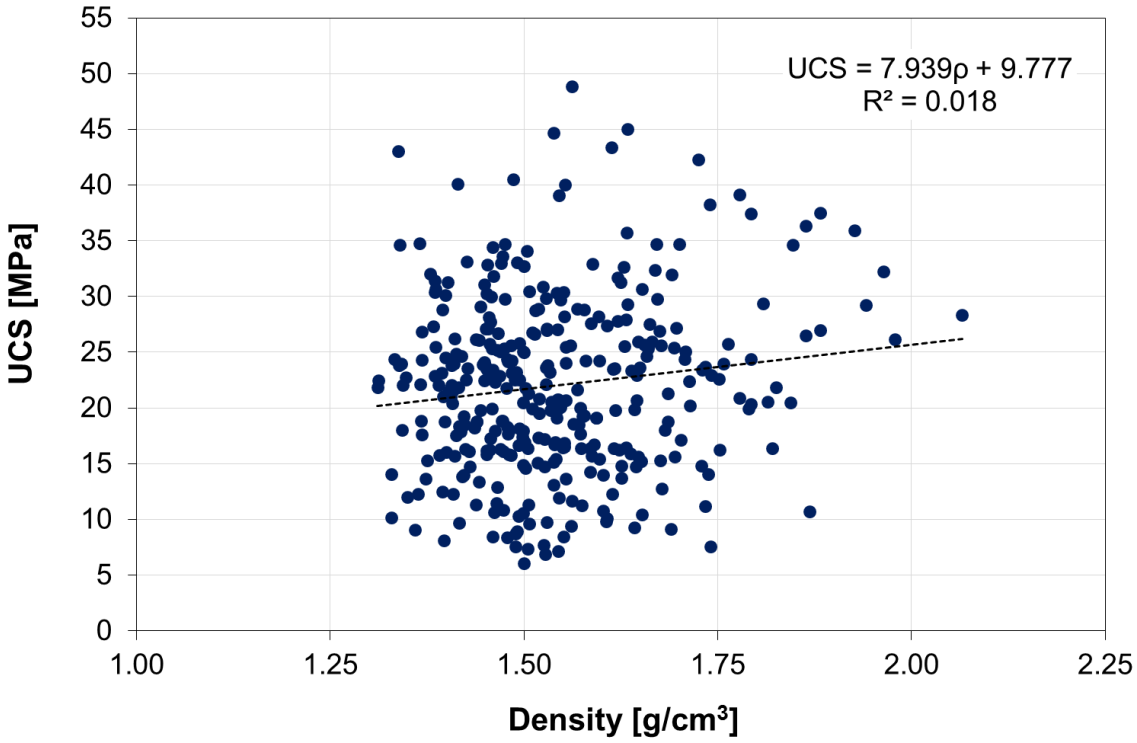


Figure 33. *UCS* versus density of coal specimens.

The relationship between the *UCS* of all specimens in the database and the corresponding depth below surface is plotted in

Figure 34. It is observed that the *UCS* of coal does not correlate with the depth of the seam. It appears that both the magnitude of *UCS* and its scatter remains relatively consistent across the entire depth of sampling. This can also be confirmed based on an individual seam analysis. For example, Figure 35 displays the relationship between coal

specimen strength and depth of sampling for the Witbank No. 2 and the Highveld No. 4 seam.

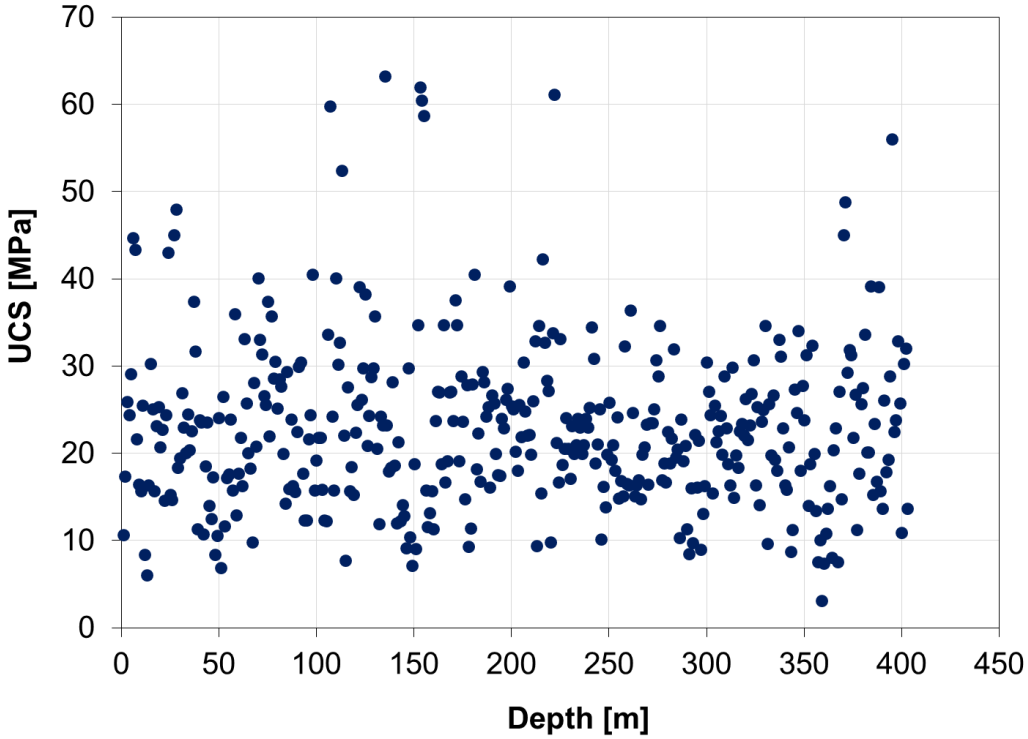


Figure 34. UCS versus depth of all coal specimens.

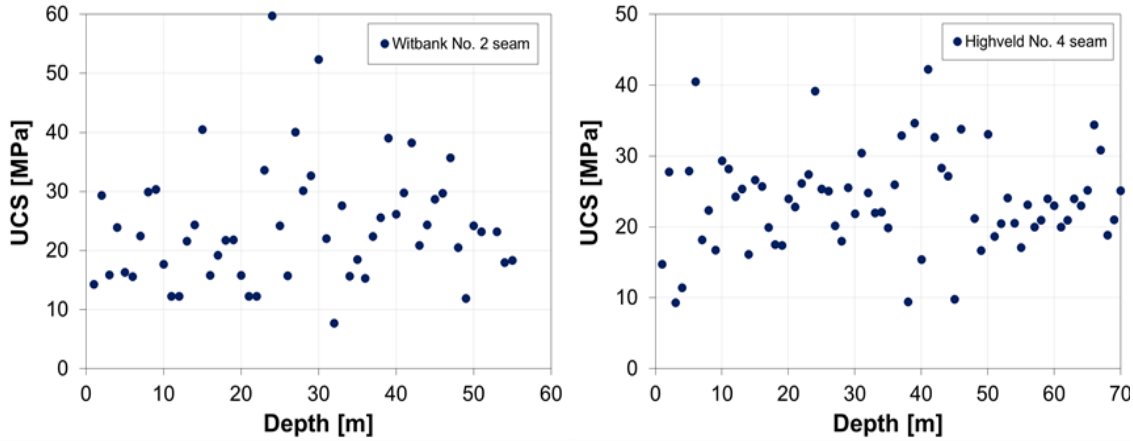


Figure 35. UCS versus depth of coal specimens from the Witbank No. 2 seam (left) and Highveld No. 4 seam (right).

The relationship between the specimen UCS and elastic tangent modulus E_t is presented in Figure 36. The scatter is relatively large for both individual parameters. It can also be seen that no correlation exists. Also, a sub-division of the data set according to seams and collieries did not result in improvement of the correlation between the two parameters.

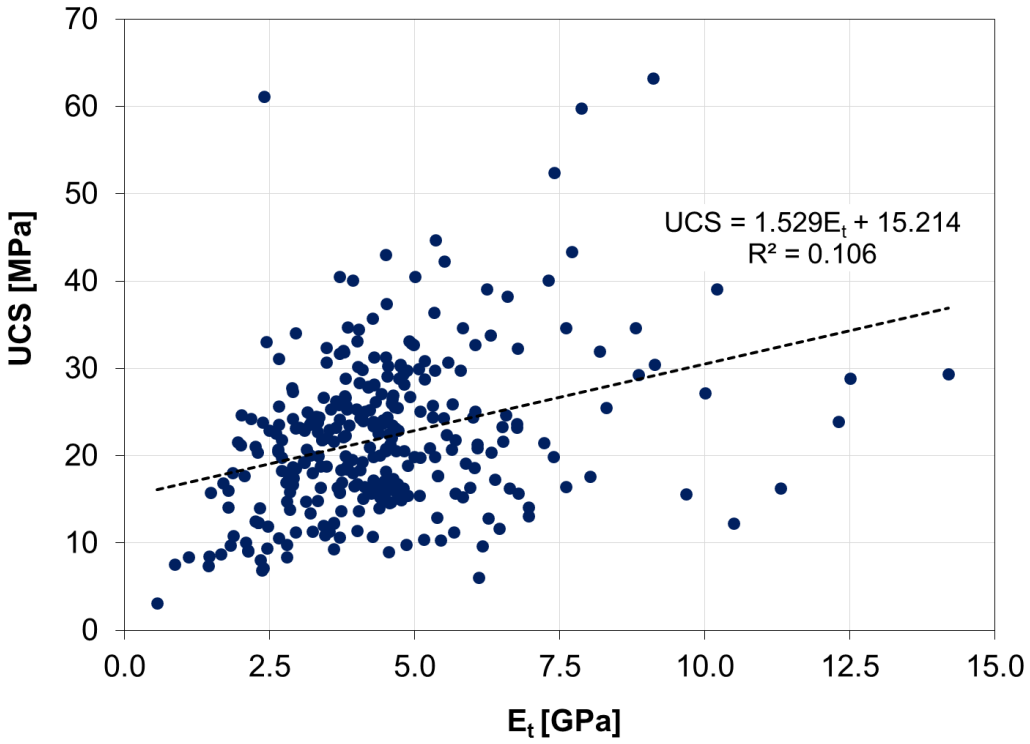


Figure 36. UCS versus tangential elastic modulus E_t for all coal specimens.

The uniaxial compressive strength and the indirect tensile strength, as compared on a borehole-average or sample-average level, is presented in Figure 37. A correlation between the two parameters cannot be identified.

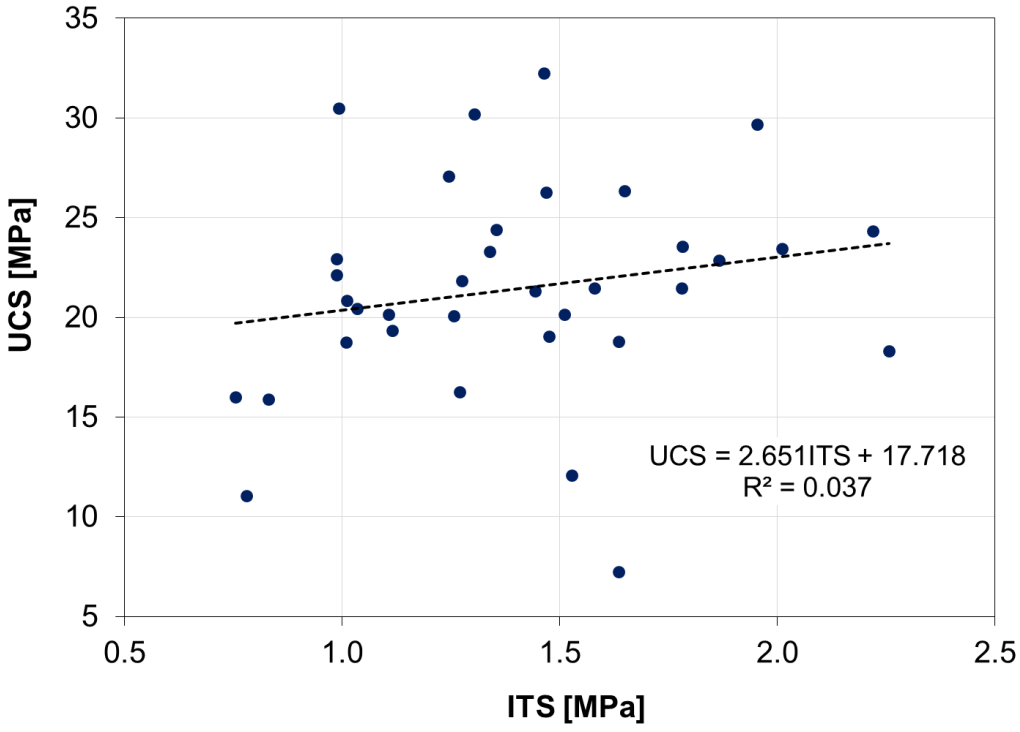


Figure 37. Average sample UCS versus average sample ITS of coal.

8.5.3 ITS versus sampling depth

The relationship between the indirect tensile strength and the depth of sampling below surface is plotted in Figure 38. No correlation exists between the two parameters. Instead it appears that the magnitude of ITS and its scatter remain relatively consistent throughout the entire depth of sampling.

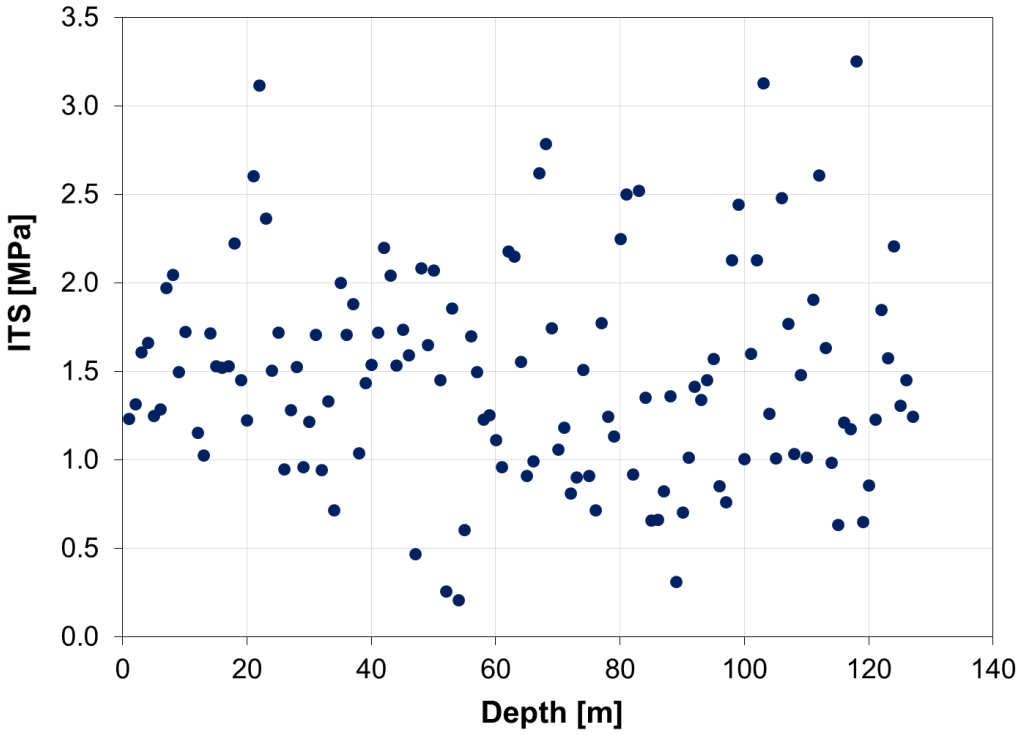


Figure 38. ITS versus depth of all coal specimens.

8.5.4 Comparison with international coal strength

In order to assess the compressive strength characteristics of South African coal in an international context, the findings of this research are evaluated against available data from the United States, and India.

The compressive strength of coal in India is presented by Ghose and Chakraborti (1986) and was derived by sampling each one block of coal from 13 different coal seams and testing of the uniaxial compressive strength on 50 mm diameter cores and $w/h=$ 2. The U.S. data, published by Mark and Barton (1996), was compiled by the authors from a literature survey on published coal strength tests. It includes tests with an average $w/h=$ 1 and covers 54 coal seams. Only 36 coal seams for which at least 10 specimens were tested have been selected for the following comparative analysis.

Because of the shape restriction to $w/h=$ 1 the magnitude of coal strength in the U.S. may not be directly comparable with the Indian and South African strength magnitudes. Nevertheless it is of interest how the coal strength varies between the different seams.

Figure 39 plots the normalized frequency distribution of average specimen strength from coal seams in South Africa, India and the United States. The laboratory strength of South African coal seams is again seen to cluster very closely around the average value of 22.3 MPa (here calculated from the individual average seam strength and not from individual specimens). The strength of coal from seams in India and the U.S., however, show a relatively large scatter of between 12.5 – 42.5 MPa in India and between 10 – 47.5 MPa in the United States. The average laboratory tested coal seam strength is again very close to the South African value, i.e. 23.5 MPa in the case of India and 22.1 MPa for the analysed U.S. coal seams.

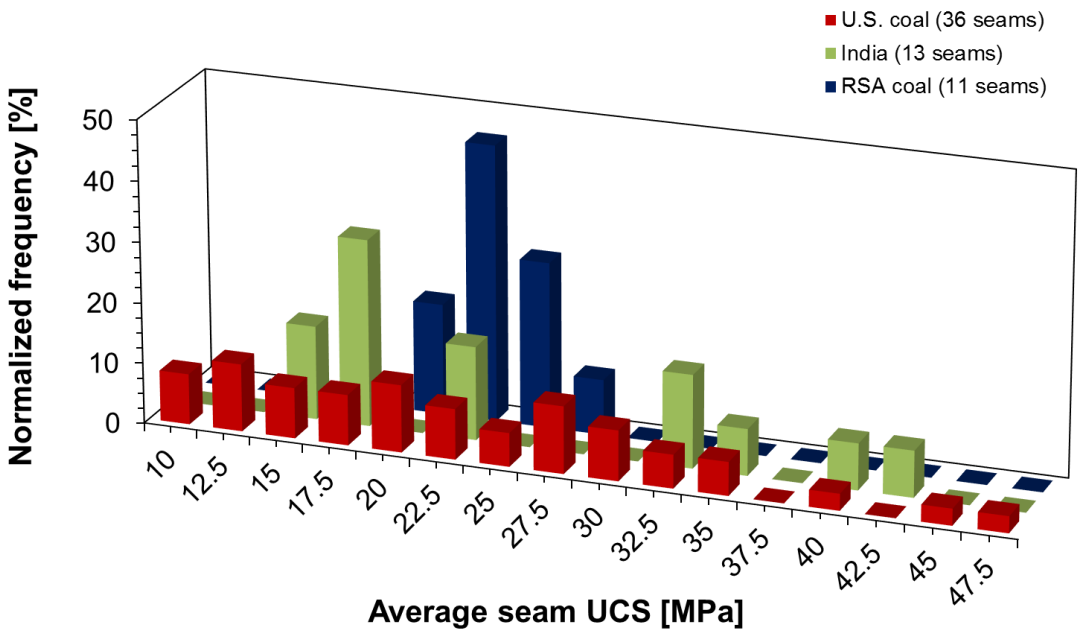


Figure 39. Normalized frequency distribution of average uniaxial compressive strength in 11 South African, 13 Indian and 36 U.S. coal seams.

9 Conclusions from the survey

The survey of the mechanical material properties of coal set out to clarify if regional or site-specific trends in the compressive or tensile strength and deformation behaviour of coal exists in South Africa.

The overall consistency of the available database was found to be favourable for analysis of possible regional patterns. The data was shown to follow lognormal or normal distributions with only few outliers. This may indicate that despite the relatively small number of tests available, the samples did indeed realistically approximate the distribution of intact coal strength in the country.

All major coal seams in which current mining activities are taking place are represented in the analysis. Of particular interest is the finding that the average uniaxial compressive strength of intact coal is relatively evenly distributed throughout the country, varying in the different seams by only about 15 % around the overall mean strength of 22.23 MPa.

However, distinct differences were observed for the triaxial strength behaviour of coal specimens. The samples from Witbank No. 5 and Highveld No. 4 seam exhibited a significantly more rapid increase in strength with increasing confinement, as compared to the relatively consistent group of Witbank Nos. 2 and No. 4 seams and the Vereeniging-Sasolburg Top and Middle seams. Notably, the sample from Ermelo C Lower seam exhibited the lowest strength increase gradients.

From a fundamental perspective, this should have a direct impact on pillar performance in the different seams. However, this can only be hypothesized at this stage. The number of triaxial tests available is relatively small and may not be statistically significant. Furthermore, the laboratory specimen behaviour may not be representative for in-situ coal.

The indirect tensile strength of specimens was found to be on average 1.6 MPa or 7 % of the average uniaxial compressive strength of coal. The samples from different seams showed a larger variation around that mean value and it must be acknowledged that for three of the 8 seams analysed, the amount of data available was insufficient.

A review of possible correlations between physical or mechanical coal properties was conducted with the outcome that the density, UCS and ITS of coal specimens is independent of the depth of the seam below surface. The mean value of these parameters appear to remain unchanged at depth intervals of between 5 and 420 m.

Further, a correlation between the uniaxial compressive strength with either the elastic modulus or the indirect tensile strength of coal could not be established.

Of particular interest is the fact that mechanical properties such as UCS, E and ITS are most suitably represented by lognormal distributions, while the TCS of coal at different confining levels is normally distributed. There is enough evidence to conclude that the differences arise from the influence of natural discontinuities in the coal specimens. While the adverse influence of discontinuities on strength was pronounced in 90 % of all UCS specimens, only 27 % of all TCS specimens appeared to be affected by pre-existing

discontinuity in their load-bearing capacity. It was shown that very small confining pressures of 2 MPa can already minimise the chance for failure occurring on pre-existent discontinuities. This in return suggests that the unconfined compressive strength of *intact* coal free from discontinuities can be more suitably addressed from triaxial strength tests at low confining pressures than from direct unconfined testing. This is in line with suggestions made by Medhurst and Brown (1998) in their experimental study of the strength of coal in Australia.

It was observed that the adverse influence of discontinuities on strength specimen strength vanishes at large confining pressures of 20 MPa. This has an important implication for coal pillar strength, as it suggests that if a pillar can generate this level of confinement in its core, then the weakening effect of discontinuities should diminish. Interestingly, the numerical study of Esterhuizen (1998) on the influence of discontinuities on coal pillar strength has predicted that the influence of jointing on coal pillar strength reduces for squat pillars with significantly confined cores.

PART III

Laboratory investigation into the shape effect in model pillars with large width-to-height ratios

10 Introduction to experimental investigations

10.1 Nature of the problem

Expressions such as ‘squat pillar’ or ‘squat effect’ are used in South Africa to distinguish the behaviour of pillars of a certain shape above a critical width-to-height ratio from the behaviour of pillars below this critical aspect ratio. A squat pillar is believed to be one where the pillar edges provide sufficient confinement to the pillar core to strengthen it substantially.

From the experience of practicing rock engineers it has been suggested that a pillar of $w/h = 10$ cannot fail, in the sense that it does not shed load or collapse abruptly. This is in contrast to the behaviour of the more frequently employed pillars of $w/h = 2 – 4$, which indeed have been observed to collapse.

The conclusion was thus that somehow in between pillar shapes of $w/h = 4$ and 10, the pillar strength must increase drastically. Salamon (1982; Salamon and Wagner, 1985) proposed a formula for the strength of these squat pillars that takes an exponential form, Equation (8). The mechanism behind this expected exponential strength increase remained somewhat unclear, since the exact reasoning that led Salamon to the conclusion of an exponential strength trend was never published.

The question was addressed experimentally by Madden (1990), using sandstone specimens. In his tests he first observed a linear increase in specimen strength between $w/h = 1 – 6$ and then the brittle-ductile transition in specimens with higher aspect ratios. Notably, Madden did not observe an increase in peak strength values for specimens with $w/h > 6$, since the peak strength concept does not apply to specimens beyond the brittle-ductile transition. Instead, they increase their load-bearing capacity with ongoing deformation beyond elasticity.

Therefore, a definition of the squat effect as an exponential increase in peak strength is technically misleading, from the point of view of excavation integrity.

In turn, to define the squat effect by the occurrence of brittle-ductile transition in specimens or pillars only might be equally inappropriate. This is because other investigators have indeed observed a non-linear, progressive increase in specimen peak strength with increasing width-to-height ratio, e.g. Cruise (1969).

What adds to the confusion is that so far evidence of squat coal pillar behaviour was sought from tests on sandstone specimens, whose material properties are very different from coal. Yet, it was shown in the literature review that not even sandstone exhibits consistent behaviour. Coal in particular does not show any squat effects at all (see Chapter 3.3).

In the light of this fact, it appears to be highly necessary to investigate the basic mechanical properties of rock and coal materials and their relationship to the shape effect, before any suggestions for in-situ coal pillars can be made from a laboratory point of view.

In conclusion, the important questions on the design of pillars outside the well-experienced 'slender' width-to-height range of $1 \leq w/h \leq 4$ still remain unanswered:

- Is there a difference in behaviour for pillars above and below a critical width-to-height ratio? And if yes:
- What are the phenomena accompanying this change?
- Under which conditions does the change occur?
- What are the mechanisms behind this effect?
- How can it be quantified?

The laboratory investigation is intended to give answers to these questions.

10.2 Objective

The objective of the experimental study is to investigate possible links between the basic mechanical properties of rocks and coal and the shape effect in rock, in particular a possible squat effect, when tested in uniaxial compression.

Of interest in this context are especially the triaxial rock properties, Mohr-Coulomb cohesion and angle of internal friction. Since it has been argued by numerous investigators that the shape effect in rock or coal is principally related to the build-up of triaxial confinement in the specimen/ pillar, it stands to reason that cohesion or internal friction will play an important role. Other material properties, such as the material strength (as tested under standard UCS conditions or as cube strength) and the elastic properties are to be investigated in this context as well.

In order to establish whether a squat effect occurs and what the nature of this effect is, the compression tests with load-deformation measurements were conducted over both the slender and the squat width-to-height region, i.e. $1 \leq w/h \leq 10$ or higher.

It was also the objective of the testing programme to observe how fracture patterns evolve in specimens and how different fracture patterns may relate to different failure mechanisms, i.e. brittle or ductile. The observed fracture patterns of laboratory specimens may assist in extrapolating the expected behaviour of in-situ pillar behaviour.

It has been suggested by various investigators that the mechanical boundary conditions can play an important role in tests on the shape effect in rock. This deserves some comments:

The effect of mechanical boundary conditions, i.e. the external angle of friction φ at the specimen/loading platen interface, has been studied comprehensively by Meikle and Holland (1965) and Khair (1994) in compression tests on coal.

Meikle and Holland (1965) varied the boundary conditions in their tests from a glue-bonded specimen-platen contact over a natural friction-controlled contact to a lubricated, friction-minimised contact condition. Specimens were prepared for width-to-height ratios between $4 \leq w/h \leq 8$. The outcome was that the magnitude of strength observed in the three different test series was markedly influenced by the boundary condition. It was the highest for the glue-bonded interface and the lowest for the lubricated boundary conditions. Notably, however, the trends for strength increase over width-to-height took the form of a regressive increase in all three cases, irrespectively of the specimen contact condition. No squat effect was observed.

Khair (1994), in testing several hundred specimens, observed similar trends in the width-to-height ratio range between 4 – 8, with the specimen strength decreasing the lower the interface friction was. Notably, a very high contact friction angle of $\varphi = 27^{\circ}$ did not produce a progressive increase in strength or brittle-ductile transition in specimens. For all contact friction angles under investigation, the shape effect manifested as a linear or regressive increase in specimen peak-strength only.

It was therefore not the objective of the laboratory study to further investigate the effect of boundary conditions. Instead, it is suggested that the influence of boundary conditions can be suitably addressed by calibrated numerical models. All tests were therefore carried out under the same boundary conditions in terms of the applied loading rates and natural (i.e. unlubricated and unglued) contacts between specimens and steel loading platens.

10.3 Scope

Since the parametric laboratory investigation is ultimately intended to assist in the evaluation of in-situ squat coal pillars, it is required that the selected test materials have mechanical properties similar to the range of parameters that can be expected for in-situ coal.

From the large-scale in-situ test conducted by Bieniawski (1968a), Wagner (1974) and Van Heerden (1975), the following parametric range was obtained: elastic modulus around $E = 4$ GPa, Poisson's Ratio around $\nu = 0.25$, Strength at $w/h = 1$ varying between 4.5 – 14.2 MPa. Oravecz (1973) conducted long-time deformation measurements on full-size pillars, prior, during and after extraction of two panels and found a significantly lower range of elastic modulus, i.e. 0.83 and 0.34 GPa respectively.

It is therefore clear that predominantly soft materials are to be used in the testing program, such as a soft sandstone and coal itself. For comparative purpose it is also of interest to test a rock material far outside this 'soft' range, e.g. a granite, and to observe if differences in the shape or squat effect would occur.

Also it was thought to be advantageous if a composite material, similar to a concrete, could be designed to mechanical specifications as the above listed for in-situ coal. The

benefits of such a mechanical analogous material are particularly practical: the ingredients for a composite material are easier to obtain than intact coal samples of sufficient size. Also, a composite material can be easily reproduced in number and size according to requirements and it can be cast into moulds of specified shape, therefore reducing time consuming specimen preparation steps such as cutting and grinding.

The laboratory study therefore commences with an investigation into the development of a composite material analogue for in-situ coal, called coal-crete.

From this material, specimens of 100 mm and 150 mm square width and various width-to-height ratios up to $w/h=$ 15 were prepared, in order to facilitate the observation of fracture patterns after failure.

Further specimens for width-to-height testing were prepared from a soft sandstone and coal, as well as from a strong granite. Since the investigation is not concerned with size effects in the material, the specimen sizes were kept relatively small, of 42 mm diameter. This had the advantage that a larger number of specimens could be prepared and tested, which in turn may improve the consistency of observed patterns and trends.

The specimens were tested in uniaxial compression between hardened steel loading platens. The full force-displacement response from the elastic range to the residual strength phase was recorded. The results are interpreted based on the calculated stress-strain behaviour and peak specimen strength and observed fracture patterns over the entire width-to-height range.

The shape investigation was preceded by a series of standard compression tests in uniaxial loading with strain-gauges and under triaxial conditions, so as to characterize the basic mechanical properties of the materials.

The results were finally discussed in the context of 1) what the squat effect in rock and coal is, 2) how the shape effect and in particular the squat effect is linked to the basic mechanical properties of rock, 3) the relevance of the findings for in-situ pillar behaviour.

11 Development of a composite material analogue for in-situ coal

11.1 Introduction to coal-crete

The testing of coal in the laboratory is frequently accompanied by great difficulty in that coal can be very friable when subjected to drilling, cutting and grinding. Coal is even sensitive to more subtle irritations such as those resulting from a change in temperature and humidity.

It was therefore attempted to develop a model material which behaves both mechanically similar to coal and which satisfies the requirement of convenient machinability. It may also be desirable to alter and predict the mechanical properties of such a material according to needs.

Such a material can be created artificially. In the following sections the development and mechanical characterisation of a composite material called coal-crete is described. Coal-crete is generated from coal fragments and a binder, which in the simplest case consists of cement and water only. Further ingredients can be added to the mixture, such as sand, fly ash or polymers for instance, to alter its mechanical properties.

11.2 Testing programme, sample and specimen preparation

Even though some American researchers published results of laboratory experiments with coal-crete (Rose and Howell, 1979; Dolinar, 1993) around the 1980s, only little insight was provided into the mechanical behaviour of this material, especially when different ingredients and mixing proportions were used. Therefore it was accepted that any first experimental design undertaken within the present study is some kind of a shot in the dark. The series of experiments was hence designed to develop from simplicity to complexity:

First, a ‘baseline’ mixture had to be established, i.e. a simple design with a small number of ingredients where only one parameter was allowed to be varied. The baseline mixtures in the present investigation is a coal-crete consisting of coal fragments with 15 %, 30 %, 50 % and 67 % proportion by weight, while the binder is a mix of general purpose cement (32.5 N strength class) and water in a ratio of w/c= 0.5.

Based on the characteristics of the ‘baseline’ mix, an interval of interest was selected for the coal-to-binder ratio and the binder material was refined for the subsequent tests. Binder materials tested in this exercise included cement of 52.5 N strength class, fly ash and sand. Finally Tunnel Guard, a mixture of sand, cement and a polymer is applied in different proportions as a binder material to the coal fragments. An overview of all sample mixtures, their ingredients and proportions is given in Table 4.

Table 4. Coal-crete design mixtures with coal and binder proportions by weight.

	Coal-crete mixture (with relative binder proportions)	Coal content	Binder contents Sand	Cement	Ash	Polymer	Water
		[%]	[%]	[%]	[%]	[%]	[%]
1	32.5 N cement*	15.0	-	56.7	-	-	28.3
2	32.5 N cement*	30.0	-	46.7	-	-	23.3
3	32.5 N cement*	50.0	-	33.3	-	-	16.7
4	32.5 N cement*	67.0	-	22.0	-	-	11.0
5	52.5 N cement	50.0	-	33.3	-	-	16.7
6	52.5 N cement	65.0	-	23.3	-	-	11.7
7	52.5 N cem. + sand (52.9/47.1)	30.0	30.0	26.7	-	-	13.3
8	52.5 N cem./ fly ash (60/40)	60.0	-	16.0	10.7	-	13.3
9	52.5 N cem./ fly ash (80/20)	60.0	-	21.3	5.3	-	13.3
10	Sand/cem./polymer (20/40/40)	70.0	6.0	12.0	-	12.0	-
11	Sand/cem./polymer (20/40/40)	60.0	8.0	16.0	-	16.0	-
12	Sand/cem./polymer (40/30/30)	60.0	16.0	12.0	-	12.0	-
13	Sand/cem./polymer (60/23.5/16.5)	50.0	30.0	11.8	-	8.3	-

* Baseline mixture

The coal debris were obtained from three seams at New Vaal colliery and processed in a jaw breaker to finer particle size. A representative grain-size analysis is plotted in Figure 40. It should be noted that the crushed coal fragments are very irregular in shape and their maximum dimension can be significantly larger than the minimum dimension required to pass through the sieves.

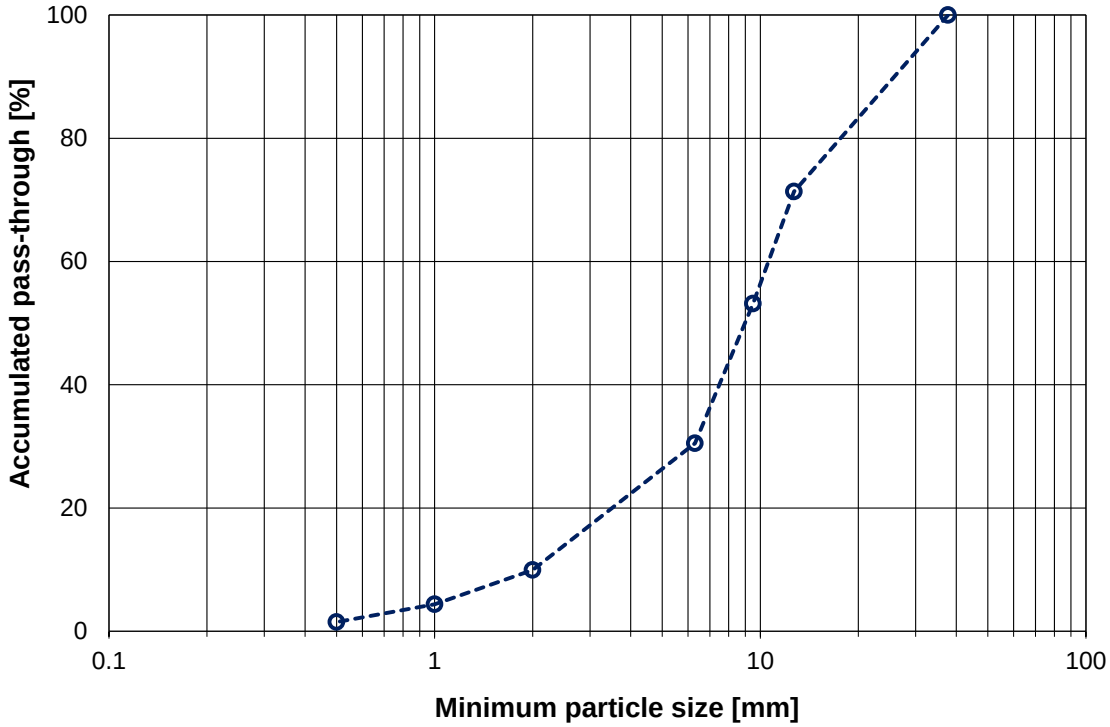


Figure 40. Sieve analysis of coal debris used in the coal-crete development study.

Each coal-crete sample mixture was prepared by hand and cast into a cubic mould of 200 mm edge length. The viscosity of the fresh mixtures was found to vary depending on the coal content. For low coal contents, i.e. up to 30 %, the mixture remains liquid like water. With an addition of an equal amount of fine sand the mixture turns into slurry. At coal contents around 50 – 65 % the mixture is more comparable to a medium-dry soil and needed to be stamped into the moulds. The reduced amount of binder and filling liquid also implied that more air pockets were present in these mixtures. A level of 65 – 70 % coal content appeared to be the practical limit for a coal-crete mix based on cement. Above this threshold there is not enough binder liquid to create a strong bond between the coal grains. There are indications, however, that the upper limit for the coal-content can be increased by using a polymer as binder.

After casting, a time of 24 hours was allowed for the samples to set to initial stiffness. The material was then removed from the moulds and cured in water for 28 days.

A total number of 220 specimens were prepared for a full mechanical characterisation of the material through a set of uniaxial and triaxial compressive strength and indirect tensile tests. A smaller number of UCS tests were also performed with strain gauges to obtain indications on the elastic properties of the mixtures.

All specimens were cored from the samples with a 42 mm diamond drill bit and cut to length in order to obtain length-to-diameter ratios of 2.5 for UCS specimens, 2.0 for TCS and 0.5 for indirect tensile strength tests. Contact surfaces for compressive strength tests were ground flat according to ISRM specifications (Ulusay and Hudson, 2007). Some examples of the coal-crete specimens are shown in Figure 41.

Specimens which were designed with high coal contents (≥ 50 %) and simple cement as binder proved to be friable in the preparation process. The machinability was significantly improved when low coal contents were used or when fly ash, sand or a polymer was added to the high coal content mixtures.



Figure 41. Specimens for UCS tests with 15%, 30%, 50% and 67% coal content (L-R).

11.3 Mechanical characterisation of coal-crete

11.3.1 Stress-strain behaviour

A number of 2 – 4 specimens from each sample mixture were prepared with strain gauges in order to obtain indications on the deformation behaviour of coal-crete.

For the initial tests on the 'baseline' coal-crete mix an Amsler 2000 kN compression testing machine was used. On discovery of the low strength levels of these mixtures, generally in the range of 6 – 25 MPa (see Chapter 11.3.2), the subsequent tests could be performed with a 100 kN MTS Criterion testing machine, with improved test control and data acquisition facilities. The loading of the specimen was velocity-controlled with 0.5 mm/min.

Due to the superior relative stiffness of this testing machine the coal-crete specimen did not fail violently at peak stress but disintegrated only very slowly with further increasing axial deformation.

During the tests the coal-crete proved to be a very soft material, taking large axial and radial strains in the order of 4 – 8 mStr or mm/m at low stress levels up to 23 MPa. Some examples of stress-strain curves up to peak strength failure for the non-polymer samples are plotted in Figure 42 and for the polymer samples in Figure 43.

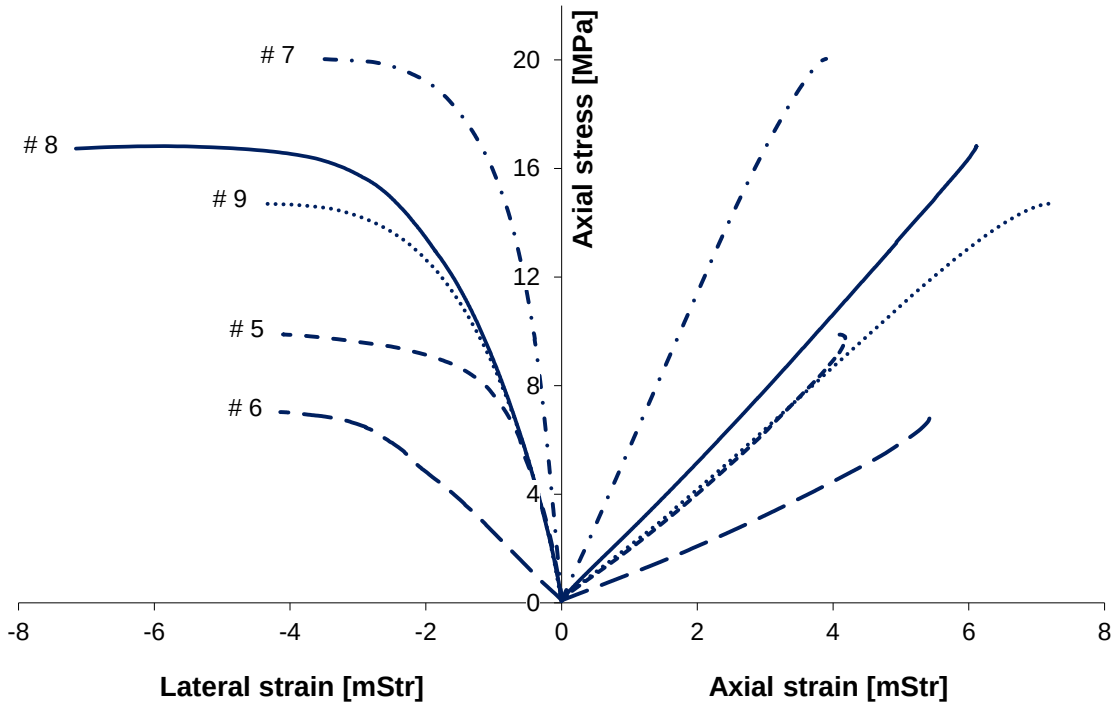


Figure 42. Stress-strain curves for coal-crete samples 5 – 9 without polymer binder.

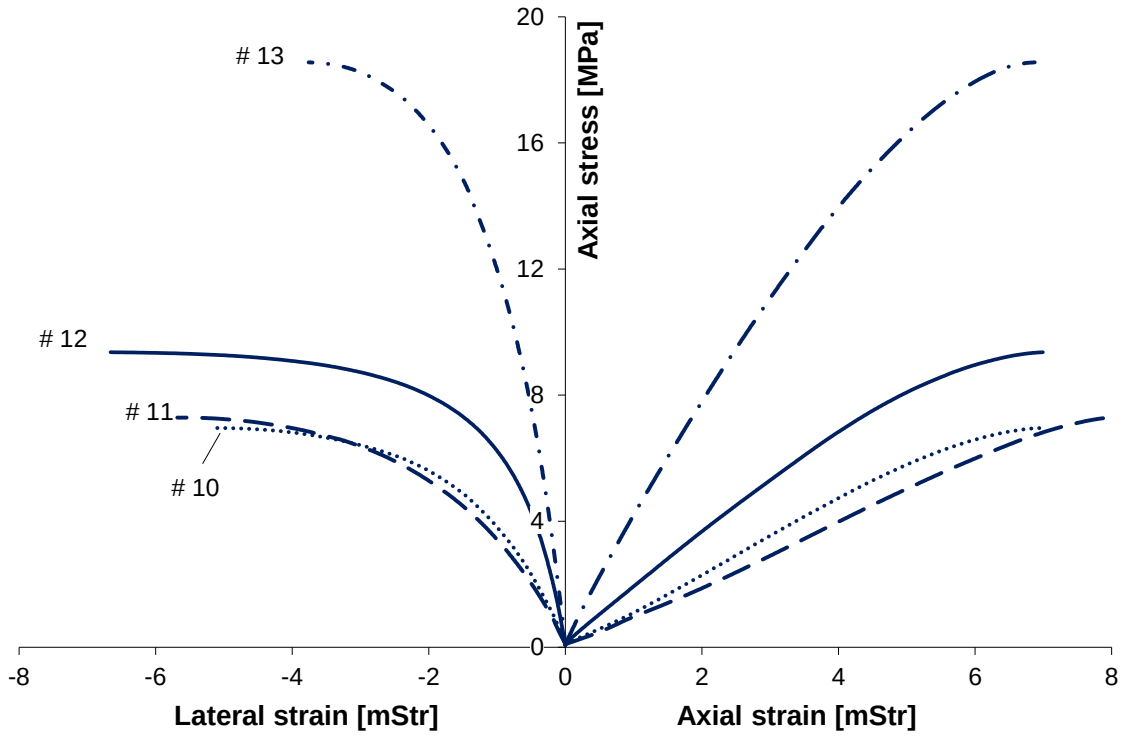


Figure 43. Stress-strain curves for coal-crete samples 10 – 13 with polymer binder.

For the non-polymer specimens, there is no significant deviation from linearity in the axial stress-strain relationship until shortly before peak strength failure. Some specimens with a high coal content of greater than 60 % show a slightly upward curving trend, e.g. # 5 and # 6 in Figure 42, which results from the closing of pores in the specimens during loading. The range of about 4 – 8 mStr at peak strength failure agrees favourably with the axial strain at failure observed for real coal specimens (see Figure 14, Chapter 7.2.3). A significant difference to real coal specimens, however, is observed for the lateral strain at failure: the range of lateral strain obtained for the coal-crete specimens is again about 4 – 8 mStr, while values measured on coal specimens are typically lower than 4 mStr. The large lateral strain values observed for the coal-crete signify a relatively large and stable volumetric expansion of the specimens.

The range of axial and lateral strains observed for the polymer specimens is the same as for the non-polymer coal-cretes, with typical values being closer towards the upper limit. However, the stress-strain relationship deviates clearly from linearity at stresses higher than 70 % of the peak load-bearing capacity. Failure in these specimens is not abrupt, but always characterized by a very slow development of a shear plane and further slow degradation in the post-failure range.

The Young's Modulus ranges between E= 0.9 – 5.7 GPa with an average sample coefficient of error of only 12 %. Notably, the average Young's Modulus of South African coal specimens is about 4.5 GPa (Figure 22, Chapter 8.2) and therefore lies within the range covered by coal-crete. For the baseline mixture it is further observed that E decreases

significantly with increasing coal content. The stiffness of specimens with high coal contents can be increased substantially with changes in the binder mixture–optimal improvements are observed from the addition of fly ash to coal-crete.

The Poisson's Ratios of the different mixtures, which is also determined at 50 % stress level, generally ranges between ν= 0.22 – 0.33 with an average sample coefficient of variation of 26 %. It therefore lies well in the range of South Africa coal specimens, which average at about ν= 0.3 (Figure 23, Chapter 8.2). Despite the larger scatter of the data, there is some indication that the Poisson's Ratio increases with increasing coal content in the mixtures.

11.3.2 Uniaxial compressive strength

Figure 44 shows the results for the uniaxial compressive strength (UCS) for all coal-crete mixtures. An overview is also provided in Table 5 at the end of Chapter 11.

All coal-crete mixtures vary in strength between 6 – 23 MPa, with average sample coefficient of variations being only 10 %. The strength of the baseline coal-crete mixtures decreases regressively with increasing coal content between 15 – 67 %. An influence of the cement strength class on the UCS of coal-crete is not clearly discernible, as the 52.5 N cement mixtures of 50 % and 65 % coal content do not differ significantly from their 'baseline' counterparts.

The addition of sand and fly ash to the binder matrix of the coal-crete improves the UCS remarkably: The addition of 30 % sand (by weight) to a simple cement coal-crete at 30 % coal content results in about 30% increase in strength of the material. The influence of fly ash on the UCS of the coal-crete is significant, even when small amounts are added to cement in a cement/ash ratio of 80/20 and 60/40. At 60 % coal content, the strength of the coal-crete improved drastically, by 80 % and 120 % respectively.

The Tunnel Guard binder mixture of sand, cement and polymer also yields some strength improvement as compared to the baseline coal-crete. However, the change is not as pronounced as for the fly ash mixtures. Only four samples of coal-crete with three different Tunnel Guard binder proportions were tested, and trends between the proportions of sand/cement/polymer and the rate of strength increase cannot be established in the study.

Statistical relationships between the UCS and the Young's modulus of the mixtures are well developed, as demonstrated separately for the cement (only), fly ash and polymer mixtures in Figure 45. The Modulus Ratio E/UCS (Deere and Miller, 1966) is generally low, ranging from about 210 for the fly ash mixtures over 247 for the polymers to 282 for the cement-only mixtures.

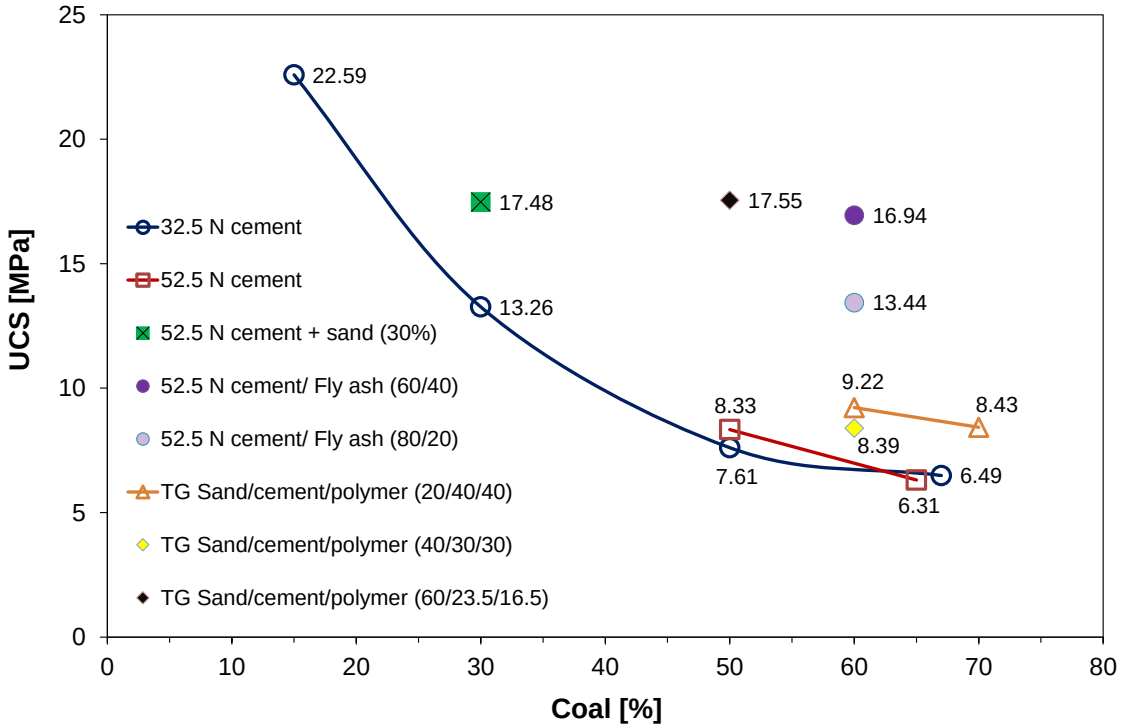


Figure 44. The uniaxial compressive strength of coal-crete.

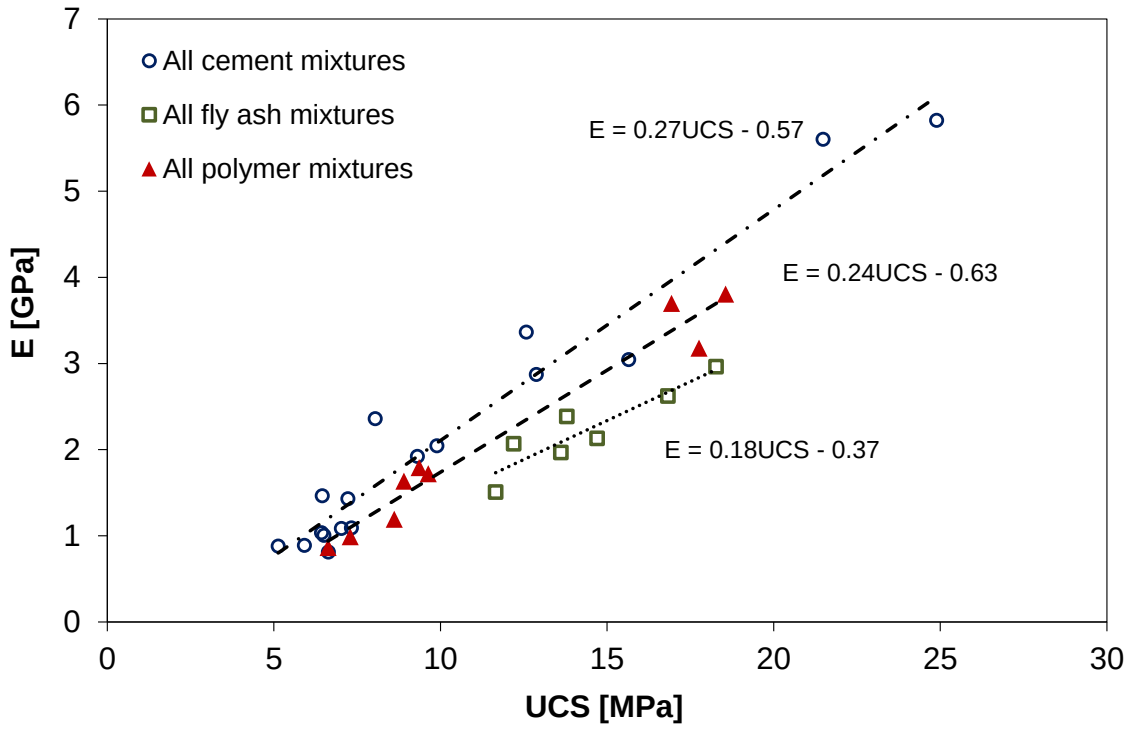


Figure 45. Young's Modulus E versus UCS of coal-crete.

11.3.3 Indirect tensile strength

The indirect tensile strength (ITS) of the coal-crete was tested on an average number of 7 specimens per sample mix. Again, the obtained results are very favourable in terms

of consistency, with sample averages falling into a range of 0.5 – 1.9 MPa across all mixtures with an average coefficient of variation per sample mix of 17 %. A full overview of the individual tensile strength of the sample mixtures is given in Table 5 at the end of Chapter 11. For comparison, the *ITS* of South African coal is in average 1.6 MPa (see Figure 30, Chapter 8.4)

The strength-reducing influence of an increasing coal-content, as well as the strength increasing influence of sand, fly ash and polymer (which was initially observed for the *UCS* data) can also be observed here.

A comparison between the average sample ITS and UCS values for the few available mixtures (Figure 46) indicates that an approximately linear relationship between these two parameters may exist within the group of all cement, sand and fly ash mixtures (samples # 1 - 9). However, the 4 polymer mixtures (samples # 10 - 13) have a markedly different ratio of *ITS*-to-*UCS*. A linear regression analysis of the few data points would suggest that the polymer mixtures could have some *ITS* at zero *UCS*, which is clearly contradictory. The functional relationship provided in Figure 8 is therefore purely descriptive and it is suggested that further tests are to be conducted on polymer coal-cretes to improve the understanding of the relationship.

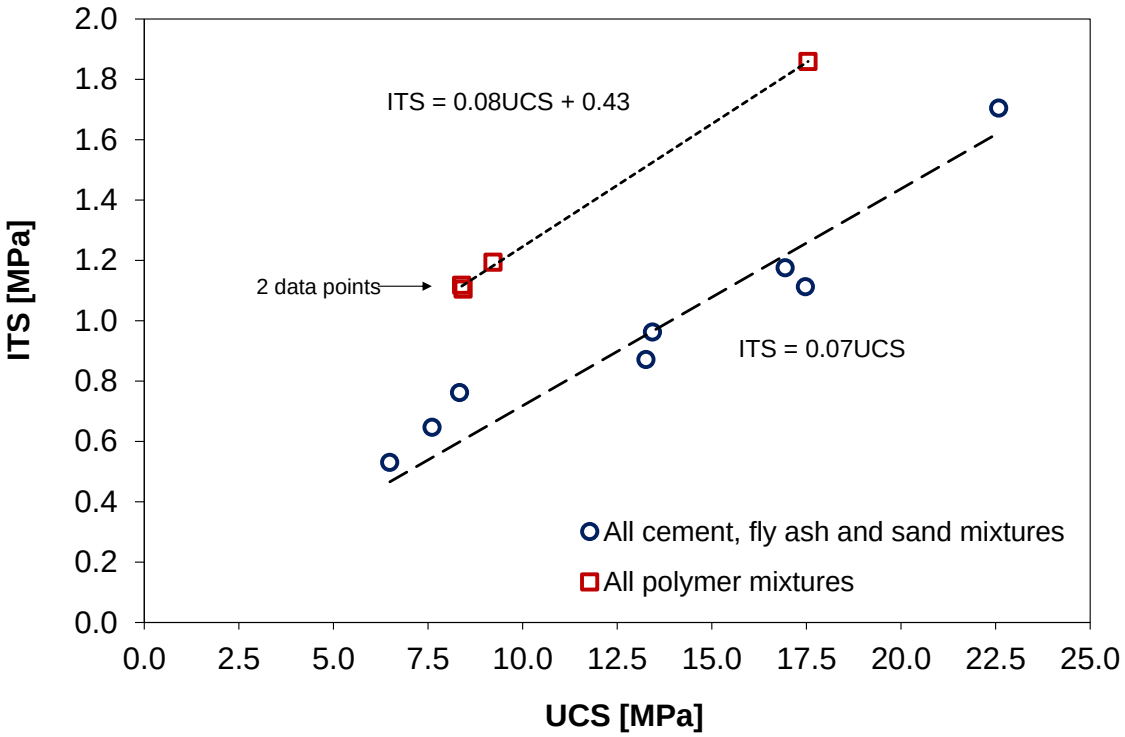


Figure 46. Relationship between *ITS* and *UCS* of coal-crete.

11.3.4 The triaxial compressive strength

Triaxial strength tests were performed for confinement levels ranging from 2.5 to 15 MPa. The most conclusive and reliable insight into the triaxial behaviour of coal-crete comes

from tests on the ‘baseline’ mixtures, where a number of 8 or 9 specimens of each sample were available. The subsequent tests on coal-crete with sand, fly ash and polymer could only give roughly indicative results from the 2 – 4 specimens available.

Hoek-Brown and Mohr-Coulomb parameters were fitted to the triaxial strength data for description of the material behaviour and are listed in Table 5 at the end of Chapter 11.

A comparison between the coal-crete and coal specimens based on Mohr-Coulomb properties reveals that that cohesion is weaker developed in coal-crete, ranging between 2 – 10 MPa, whereas typical values for South African coals (see Table 3, Chapter 8.3) are around 9 – 14 MPa. There is however a closer agreement in the angle of internal friction, which varies between 25 – 38˚ for the different coal-crete mixtures, and 28 – 43˚ for South African coals.

An example of the Mohr-Coulomb and Hoek-Brown curve fit is shown in Figure 47. Both curves appear to be equally suitable for predicting the triaxial strength behaviour at the investigated confinement levels. However, the Hoek-Brown criterion appears to give a more likely estimate of the triaxial strength for coal-crete at small confinement values of lower than 2.5 MPa.

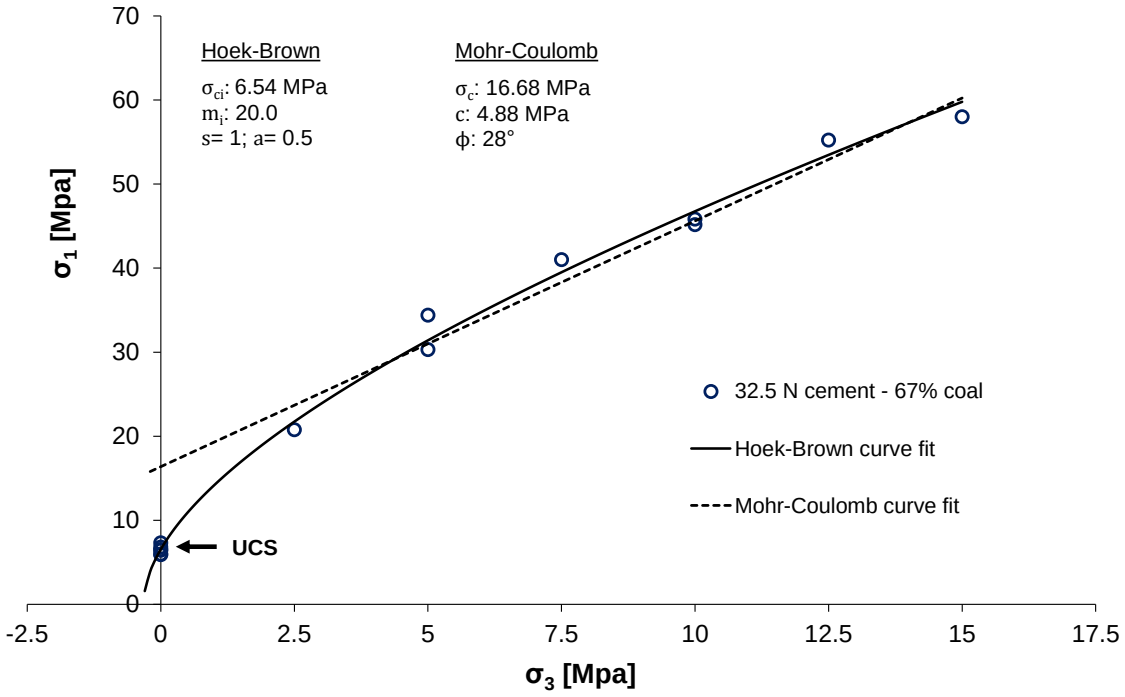


Figure 47. Mohr-Coulomb and Hoek-Brown curve fit for a coal-crete with 32.5 N cement and 67 % coal content.

The tests performed on 8 specimens of each ‘baseline’ mix show consistently that the Mohr-Coulomb cohesion reduces and the angle of internal friction increases with increasing coal content in the coal-crete. Since the latter parameter expresses the rate of strength increase with increasing confinement in a material, the same trend should be

observed for the m_i-value of the Hoek-Brown criterion. This is confirmed for all but one of the samples.

The derived Hoek-Brown parameters were investigated for their suitability to predict the tensile strength of the coal-crete mixtures. A good relationship between the tested and predicted tensile strength was found for those coal-crete mixtures in which Hoek-Brown parameters could be accurately determined based on a sufficiently large number of specimens (8 – 9). When involving all other coal-crete mixtures in the correlation analysis (for which only a few number of tests were conducted and only indicative strength parameters were found), the relationship becomes somewhat weaker.

11.4 Conclusions on coal-crete

The developed coal-cretes are soft materials. The range of mechanical properties encountered are: UCS= 6 – 23 MPa; ITS= 0.5 – 1.9 MPa; E= 0.92 – 5.72 GPa; ν= 0.22 – 0.33; c= 2.5 – 9.5 MPa, ϕ= 25 – 38°. Within these intervals the material strength and Young's Modulus decreases with increasing coal content. For the UCS and ITS, this trend is particularly regressive, i.e. strength variations at high coal contents (50 – 65 %) are less than at low coal contents (15 – 30 %). The lowest strength is always obtained for coal-cretes with simple cement and water as binder. The addition of fine sand, poly-mer, and in particular fly ash, to the binder matrix increases the strength significantly. The maximum coal content that can be mixed into the coal-crete appears to be about 65 – 70 % by weight for the types of binder used in this study.

The material's mechanical resemblance with coal is generally satisfying, as pointed out in the different sections on the mechanical properties. The coal-cretes with mechanical properties that are closest to average South African coal are mixtures with fly ash or fine sand in the binder matrix, e.g. samples # 7, # 8 and # 9. These materials may therefore make practical and reliable substitutes for coal in mechanical laboratory studies. They are practical because they can be readily mixed from crushed coal according to a customized design recipe and machined or cast into moulds with ease to obtained specimens of any required size and geometry. They are reliable because the variability of mechanical properties in samples is very moderate when mixed carefully, and because of the strong correlations between UCS, ITS, E that can be expected.

Because of the coal-cretes' mechanical similarity with coal it can also be of use as coal mine backfill. This option is particularly attractive when cheap power station refuse coal and fly ash are available in sufficiently large quantities to constitute the largest proportion in the backfill. It has been shown in this study that coal-cretes with large coal contents and large proportions of fly ash produce a strong material. The disadvantage of coal-cretes with high coal contents is only that the mixture cannot be pumped properly, as it resembles a medium-dry soil in the fresh state, and may therefore not be suitable for mechanized backfilling.

Table 5. Mechanical properties of coal-crete.

Sample #	Coal-crete mixture (with relative binder proportions)	Coal content [%]	Density [g/cm³]	No. of tests	Elastic properties E [GPa]	CoV [%]	ν -	CoV [%]
1	32.5 N cement*	15	1.61	2	5.71	2.72	0.22	9.81
2	32.5 N cement*	30	1.55	3	3.09	8.06	0.24	47.57
3	32.5 N cement*	50	1.56	3	1.91	23.37	0.26	58.07
4	32.5 N cement*	67	1.49	4	1.04	4.14	0.28	40.56
5	52.5 N cement	50	1.66	2	1.74	25.03	0.26	33.11
6	52.5 N cement	65	1.60	4	0.92	12.82	0.33	23.3
7	52.5 N cem. + sand (52.9/47.1)	30	1.88	3	4.98	19.4	0.24	21.76
8	52.5 N cem./ fly ash (60/40)	60	1.52	3	2.66	15.13	0.24	20.42
9	52.5 N cem./ fly ash (80/20)	60	1.49	4	1.92	14.7	0.23	33.1
10	Sand/cem./polymer (20/40/40)	70	1.39	3	1.45	2.39	0.32	10.93
11	Sand/cem./polymer (20/40/40)	60	1.47	3	1.72	4.64	0.22	2.65
12	Sand/cem./polymer (40/30/30)	60	1.44	3	1.01	16.33	0.25	18.91
13	Sand/cem./polymer (60/23.5/16.5)	50	1.55	3	3.56	9.42	0.27	12.98

* Baseline mixture

Sample #	Coal content [%]	Unixial compression tests No. of tests	Strength [MPa]	CoV [%]	Indirect tensile strength No. of tests	Strength [MPa]	CoV [%]	Triaxial compression tests No. of tests	Hoek-Brown m_i	σ_{ci}	Mohr-Coulomb σ_{c0} [MPa]	c [MPa]	ϕ [°]
1	15	6	22.59	1.33	6	1.70	24.50	8	6.74	23.09	29.66	9.30	24.97
2	30	6	13.26	11.32	6	0.87	28.46	9	10.64	13.37	22.92	7.03	25.99
3	50	6	7.61	13.59	5	0.65	19.57	8	22.61	7.90	24.01	7.20	26.99
4	67	6	6.49	8.16	6	0.53	26.06	8	20.01	6.54	16.68	4.88	28.09
5	50	7	8.33	19.23	7	0.76	9.41	9	24.48	8.26	18.06	4.66	33.22
6	65	7	6.31	9.81	-	-	-	4	29.12	6.37	24.95	7.69	25.74
7	30	4	17.48	10.80	4	1.11	11.34	4	21.35	17.46	26.90	6.18	37.31
8	60	6	16.94	12.56	8	1.17	18.68	2	16.39	16.90	31.76	7.38	36.92
9	60	6	13.44	9.39	8	0.96	12.17	2	18.03	13.04	22.23	5.58	34.20
10	70	5	8.43	9.89	8	1.10	16.51	2	9.11	8.43	12.39	3.75	26.60
11	60	5	9.22	7.21	8	1.19	10.36	3	10.40	9.27	13.71	3.99	28.30
12	60	5	8.39	16.76	7	1.12	20.79	2	14.87	8.34	10.93	2.73	34.41
13	50	5	17.55	4.64	8	1.86	8.41	3	5.77	17.45	16.88	4.77	29.56

12 Experiment details

The following chapters provide the experimental details for the laboratory investigation into the ‘squat effect’ in rocks.

12.1 Experiment design

The experiment is designed to test specimens of coal, sandstone, granite and coal-crete in uniaxial compression and under variation of the specimen shape, i.e. with different width-to-height ratios. The width-to-height range between w/h= 1 – 15 will be tested.

The difference in the specimen shape is accounted for by keeping the specimen width constant and adjusting only the height of the specimen. A constant specimen width has the advantage that the boundary conditions at the specimen-steel contact stay practically unchanged in all tests, except for very slight variations that may come with the preparation of specimen surfaces. The effect of size on specimen strength will not be considered.

The selected specimen sizes for coal, sandstone, granite and coal-crete is 42 mm and these will be prepared from drill cores. In addition to the 42 mm tests on coal-crete, larger specimens of the same material with a 100 mm and 150 mm square width will be prepared in order to facilitate the observations of fracture patterns after the test is completed.

The compressive tests will be performed between hardened-steel loading platens and a constant loading rate for coal and rock of 0.25 mm/min. Since coal-crete has proved to take very large deformations before failure, the loading rate will be kept at a higher level of 0.5 mm/min for these specimens. All tests will be conducted long enough for the residual strength phase of the specimen to be approached.

During the compression tests, the full force-displacement response will be recorded. This is to identify the development in peak specimen strength over changes in width-to-height, and to observe how the post-peak behaviour of the specimens is affected by the modifications of the specimen shape. The latter phenomenon will be useful for interpreting the specimen failure mode, i.e. brittle or ductile. Finally, the fracture patterns in specimens of different width-to-height ratios will be investigated.

12.2 Testing materials and mechanical properties

The materials used in this experimental study comprise of coal, sandstone, granite and coal-crete. The origin, petrographic description for rocks and mechanical properties of the samples are provided in the following sub-sections. Also, the boundary conditions at the interface between the test specimens and steel loading platens will be characterized.

12.2.1 Description of material samples

12.2.1.1 Coal

Coal was obtained from the No. 4 seam underground operations at South Witbank Colliery in the Witbank coalfields. A larger block of coal had detached from the sidewall of a pillar as a result of natural jointing. From that block, a sample measuring sizes of approximately 100 x 50 x 20 cm was separated and protected against moisture changes by bitumen-seal and bubble wrap.

12.2.1.2 Sandstone

The selected sandstone sample is of even and fine-grained texture, consisting of evenly disseminated quartz and ferruginous minerals which caused a yellowish discolouration. There are no indications of structural deformations. The sample was obtained from a quarry as a rectangular block of approximately 30 x 20 x 15 cm edge length.

12.2.1.3 Granite

The Quarz-Feldspar-Biotite Granite is medium-to-fine grained, homogenous and pinkish in colour. The sample exhibits a weakly developed cleavage plane, along which biotite is distributed. The granite was obtained from a quarry as a block of 20 x 20 x 20 cm edge length.

12.2.1.4 Coal-crete

Three different mixtures of coal-crete were designed for specimens of 42 mm diameter, 100 mm and 150 mm square width.

The mixture for the 42 mm specimens was designed from 60 % coal debris and 40 % binder, of which the latter consisted of 33.3 % water, 40 % 32.5 N cement and 26.7 % fly ash (all proportions by weight).

The mixtures for 100 mm and 150 mm specimens consisted of 50 % coal debris and 50 % binder, whereas the latter was again a mixture of 33.3 % water, 40 % 32.5 N cement and 26.7 % fly ash.

The practical reason for the reduction of the coal content in the 100 and 150 mm mixtures was that only a limited amount of coal-debris was available and it was considered to be more important for the success of the testing program to have a greater amount of lower coal content specimens prepared than a smaller number of high coal content specimens.

The grain sizes of the coal debris were adjusted for the different specimen sizes, the smallest grain size being used for the 42 mm specimens and the largest size for 150 mm specimens. The grain-size distributions of coal debris used for the different specimen sizes are shown in Figure 48.

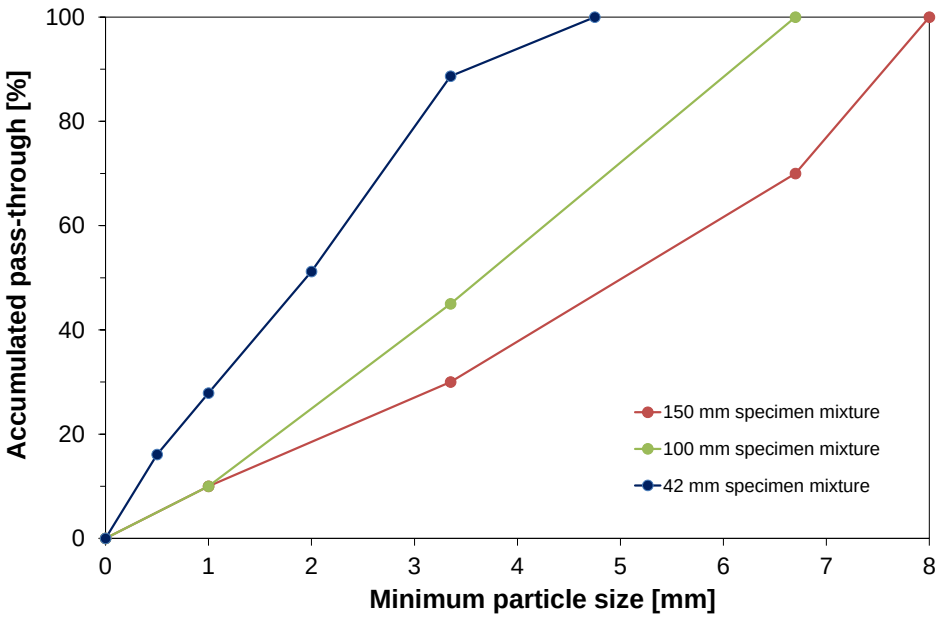


Figure 48. Grain-size distribution for coal debris used in the coal-crete mixtures for 42 mm, 100 mm and 150 mm specimens.

12.2.2 Mechanical properties

A series of standard uniaxial compression tests with strain-gauges and triaxial compression tests were carried out on the selected materials in order to establish their elastic deformation properties and strength characteristics. The material density (ρ), unconfined compressive strength (UCS), elastic modulus (E), Poisson's Ratio (ν), cohesion (c) and angle of internal friction (ϕ) are summarized in Table 6**.** The properties of the coal-crete mixtures were tested two days after the mixtures had cured in water for 28 days.

Table 6. Mechanical properties of materials used in the investigation on shape-effects.

Material	ρ [g/cm^3]	UCS [MPa]	E [GPa]	ν -	c [MPa]	ϕ [°]
Coal-crete (42 mm)	1.58	8.1	1.62	0.31	3.11	35.80
Coal-crete (100 mm)	1.45	4.6	0.64	0.23	0.62	54.54
Coal-crete (150 mm)	1.43	4.2	0.85	0.27	0.79	47.66
Coal (No. 4 seam)	1.51	19.4	-	-	5.29	41.38
Sandstone	2.10	27.2	7.33	0.49	8.19	42.19
Granite	2.63	193.3	63.37	0.29	33.56	50.89

12.3 Testing apparatus and specimen boundary conditions

An MTS Rock Mechanics and Concrete Testing System (Model 815), as schematically shown in Figure 49**,** is utilized for the laboratory testing programme[2]. Compressive loading is applied to the test specimens through upward movement of a hydraulic-driven actuator with 2600 kN load capacity positioned at the bottom of the machine.

The rock and coal specimens are uniaxially confined within the machine through direct contact at top and bottom with hardened-steel loading platens. A pair of circular 54 mm diameter loading platens with 50 mm thickness is used for all 42 mm specimens. The bottom platen is designed as a spherical seat to allow for self-alignment to the specimen contact surface.

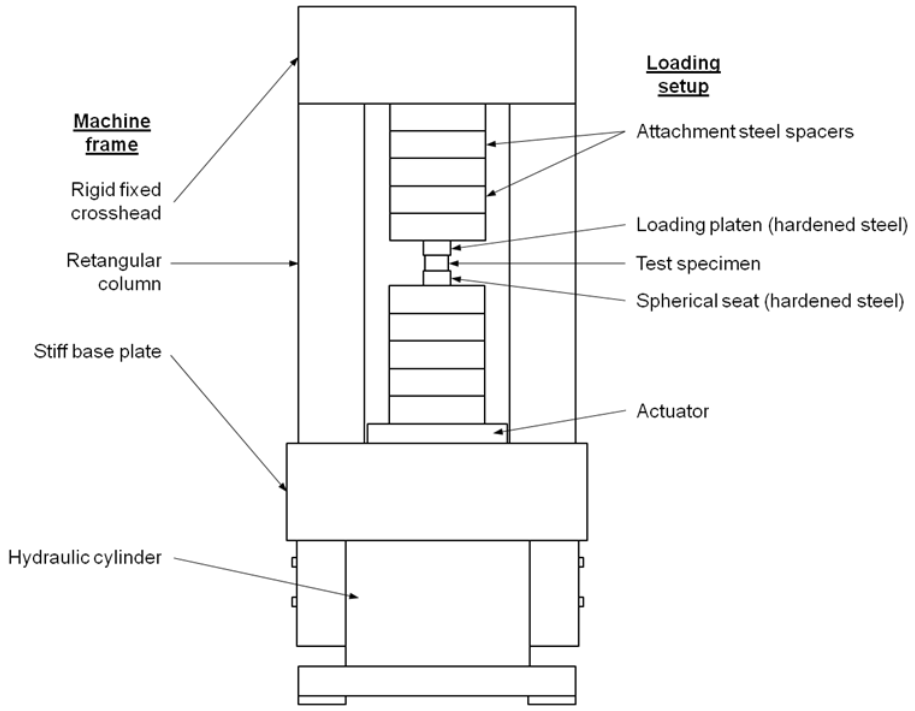


Figure 49. Schematic drawing of the testing apparatus

The typical frictional contact conditions of coal or rock specimens with hardened steel loading platens (both prepared to flatness according to ISRM specifications) is determined based on three indicative shear box tests for each rock type. The results are as follows: coal-steel $\varphi = 21.2^{\circ}$ ($\mu = 0.389$), sandstone-steel $\varphi = 20.0^{\circ}$ ($\mu = 0.364$), granite-steel $\varphi = 13.7^{\circ}$ ($\mu = 0.244$). These values compare well to findings from other researchers in similar tests, as shown in Table 7.

Table 7

[2] This is except for the 42 mm coal-crete specimens, which were tested in an MTS Criterion tester with 100 kN loading capacity.

Table 7. Rock-steel loading platen contact friction angles φ published in literature.

Investigator(s)	Material	No. of tests	φ [°]
York, Canbulat and Jack (2000)	Coal	3	15.0
Meikle and Holland (1965)	Coal	20	16.7
Khair (1994)	Coal	5	19.8
York et al. (1998)	Merensky Reef	3	13.7
Madden (1990)	Sandstone	-	19.3

The coal-crete specimens of 100 mm and 150 mm square width are tested between square loading platens of 260 mm edge length and without spherical adjustment. The absence of spherical self-alignment was not considered a problem, since the coal-crete specimens were prepared to accurate flatness and parallelism in moulds. Furthermore, the material was known to take very large strains before failure, so that minor irregularities in the load-contact surface would be compensated during the elastic compression phase.

A number of mild steel spacers are rigidly attached to the machine actuator and crosshead to allow positioning of the specimen-platen combination in the centre of the machine frame.

It was anticipated that the forces induced on the specimens during compression were ultimately in excess of the measuring capacity of an available 100 kN load cell, and for this reason it was decided to not make use of this equipment. Also, direct strain measurements on the specimens were impractical due to small specimen size and very flat geometries.

Therefore, the loads applied to the specimen contact surfaces during compression had to be determined from the oil pressures measured in the hydraulic unit of the actuator. Similarly, specimen deformation and strains had to be related to the displacement of the actuator, which were recorded during the tests through a built-in LVDT.

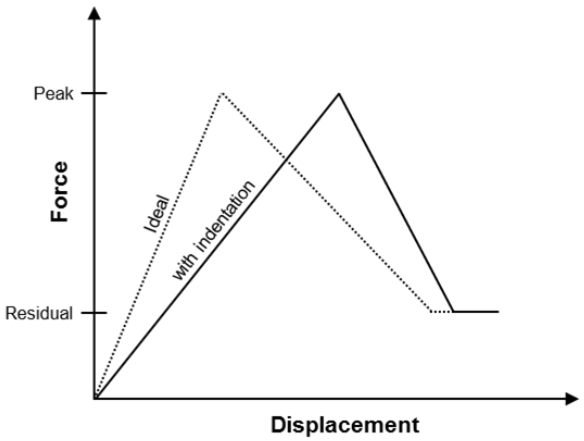


Figure 50. The effect of indentation in the testing setup on the recorded force-displacement curve for specimens.

This method of determining the specimen deformation bears some complication, since the specimen must be expected to indent into the steel spacers and loading platens during compression, and consequently the measured displacement at the actuator is only partially transferred onto the specimen. For a given specimen, the magnitude of indentation is proportional to the stress level acting on the specimen, as shown in Figure 50.

A correction factor for the predicted displacement of the specimen would be required, if the exact magnitudes of induced strain in the specimen was of importance for the test evaluation.

However, due to the fact that the same magnitude of error will occur in both the pre-peak and post-peak slope of the force-displacement or stress-strain curve, the ratio of the two slopes will stay unaffected by the indentation. This will give a correct understanding of the relative development of the post-peak behaviour over width-to-height for the different materials. The determination of correction factors is therefore not required.

12.4 Specimen preparation

The obtained samples of sandstone, granite and coal were prepared to cylindrical specimens of 42 mm diameter using a diamond core drill. The cores were cut to various length with a diamond saw in order to accommodate for a range of width-to-height ratios, as listed in Table 8. The load-contact surfaces of the specimens were ground flat to ISRM specifications (Ulusay and Hudson, 2007) with a barrel wheel grinder.

It was initially intended to preserve the natural moisture level in the coal as well as possible. On obtaining the sample at the mine, the block was sealed with bituminous paint and bubble-wrap. Coring of the specimens commenced immediately on arrival in the laboratory. It was attempted to core specimens without cooling liquid, but dry-coring proved to be practically not feasible. Since coring then had to be accomplished with water lubrication, the natural moisturer content of the coal could not be maintained.

In additional to the coal and rock materials, three further series of 42 mm cylindrical specimens, as well as 100 mm and 150 mm square coal-crete specimen were prepared to various width-to-height ratios (Table 8).

For the 42 mm specimens, a block of 20 x 20 x 20 cm coal-crete was cast and cured in water for 28 days. Thereafter, the material was removed from the water, and 42 mm cylindrical specimens of various width-to-height ratios were cored, cut and ground flat, following the same procedure as outlined above for the rock specimens. Testing commenced and was completed on day 30 after casting.

The square coal-crete specimens of 100 mm and 150 mm width were prepared by casting them into moulds (Figure 51). The 100 mm moulds were designed in order to accommodate specimens of w/h-ratios up to 10 and the 150 mm moulds to produce specimens of w/h-ratios up to 15 (Table 8). Further, the moulds were designed such that the load-

contact surfaces of the cast specimens were parallel and flat, so that no subsequent treatment was required.

The mixtures were allowed to set to initial stiffness in the moulds for 24 hours, at time they were then removed from the moulds and cured in water basins for 28 days. Thereafter, the specimens were removed from the water and excess material was trimmed off by means of a diamond saw, when required.

For practical reasons not related to the testing program, the testing of the 100 mm and 150 mm square specimens could only commence in the laboratories 14 days after the specimens were removed from the water. Nevertheless, the tests on the specimens were timed with the day of casting such that every specimen had the same age on the day of testing.

Table 8. Overview of specimens prepared for each material at different w/h-ratios.

Material	Size	Width-to-height ratio																Total
	[mm]	0.75	1	2	3	4	5	6	7	8	9	10	11	12	13	14	15	
		Number of specimens																309
Coal	42	-	8	8	7	8		8	5	7	2	2	1	-	-	-	-	61
Sandstone	42	-	5	7	8	10	11	11	-	5	4	-	1	4	2	-	-	68
Granite	42	-	5	6	5	3	10	6	-	4	-	-	-	-	-	-	-	39
Coal-crete	42	5	5	5	10	10	10	8	2	-	3	-	-	-	-	-	-	58
Coal-crete	100	-	5	5	5	5	5	13	5	3	-	5	-	-	-	-	-	51
Coal-crete	150	-	-	3	3	5	5	4	-	4	1	3	1	1	-	-	2	32



Figure 51. Mould for casting of 100 mm square specimens.

13 Experimental results

The following sections provide the experimental results from the compression tests on specimens of coal, coal-crete, sandstone and granite, which were conducted as outlined in Chapter 12.4.

To begin with, the load-deformation response of the specimens during the tests will be discussed. Thus the influence of specimen shape on the elastic pre-peak and the non-elastic post-peak behaviour of the materials will be identified. Of particular importance in this context is the question of a transition from brittle to ductile failure which occurs within specimens at some width-to-height ratios.

Further, the evolution of peak specimen strength will be analysed for those specimens which have failed in a brittle manner. Lastly, the observed fracture patterns in both brittle and ductile specimens will be discussed.

13.1 Force-displacement curves and elastic specimen stiffness

The force displacement response to compression of specimens with varying width-to-height ratios will be discussed in the following section.

An example of typical force-displacement curves as recorded by the actuator of the testing machine is shown in Figure 52 for a set of sandstone specimens.

It is observed that the slope of the force-displacement curve in the elastic deformation range, termed the stiffness T of the test specimens in kN/mm, increases with increasing width-to-height ratio. This is expected, since one can derive from the fundamental relationship,

$$T = E\,\frac{A}{l} \tag{21}$$

where E is the Young's Modulus of the material, A the specimen's base area and l the specimen length or height, that the stiffness must increase with decreasing specimen length or height.

For specimens which exhibit brittle behaviour, T is calculated as the average slope in the interval of 30 – 70 % of the peak stress. For specimens which do not exhibit a peak stress but ductile behaviour, i.e. $w/h \geq 6$ in the case for sandstone, T is calculated in the interval of 30 – 70 % of the force at maximum curvature of the stress-strain curve.

The phenomenon of increasing stiffness with increasing w/h-ratio is not limited to sandstone specimens only but can be observed for all other tested materials as well. A regression analysis of the calculated specimen stiffness T over width-to-height range of $1 \leq w/h \leq 8$ for the different materials yields the results shown in Figure 53.

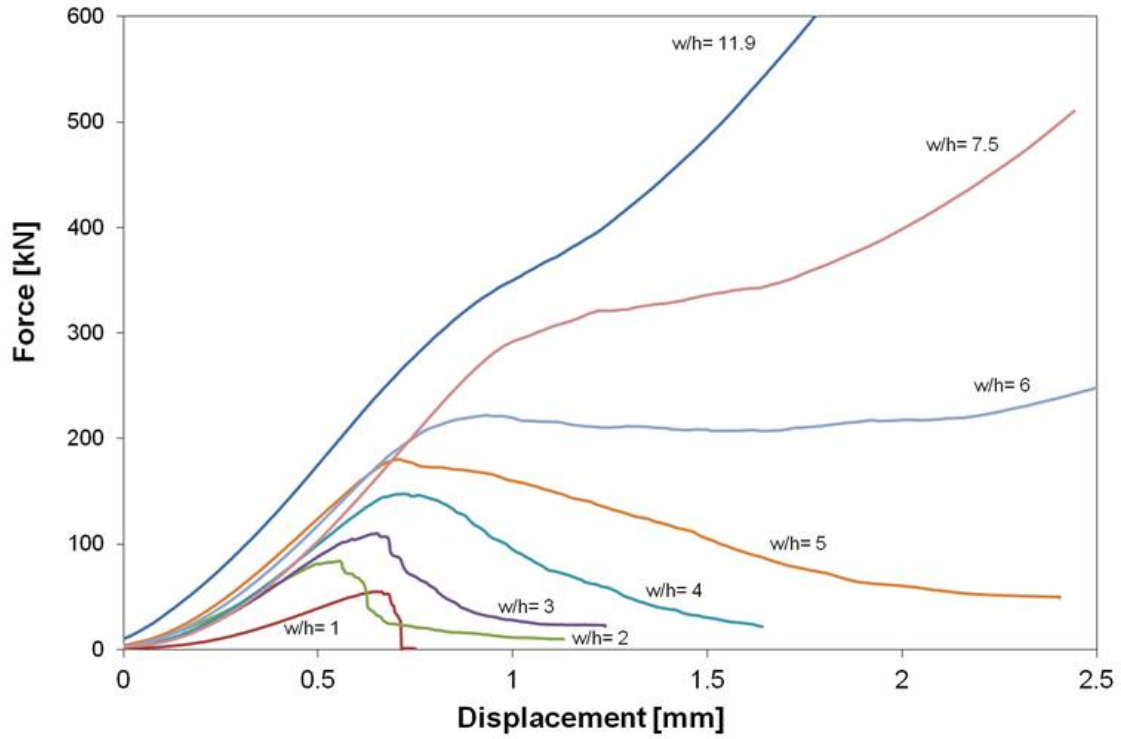


Figure 52. Examples of force-displacement curves for sandstone specimen and varying w/h-ratio.

The correlation coefficients for the shown curves are generally in excess of $R^2 = 0.93$. The 150 mm coal-crete specimens are the only ones for which results are more scattered and yield a lower but still good correlation of $R^2 = 0.77$.

The stiffness of specimens of $w/h > 8$ are excluded from the regression, because of too great inconsistency. The general tendency, however, is that the stiffness values of these specimens are lower than those that would be predicted by the regression curves. Also, it should be noted that the 42 mm coal-crete specimens were tested in a different compression machine than the rest of the materials.

Coal-crete, sandstone and granite exhibit a relatively similar gradient of stiffness increase over width-to-height. It is interesting to observe that in this context, coal exhibits a distinctly different behaviour and a higher rate of stiffness increase, even though tested with the same size, shape and boundary conditions as coal-crete, sandstone and granite. The derived equations as plotted in
Figure 53 all fit the generic form,

$$T = f(w/h) = a\left(\frac{w}{h}\right)^{b} \tag{22}$$

where a and b are constants for the material and the specific boundary conditions with $a > 0$ and $0 < b \leq 1$.

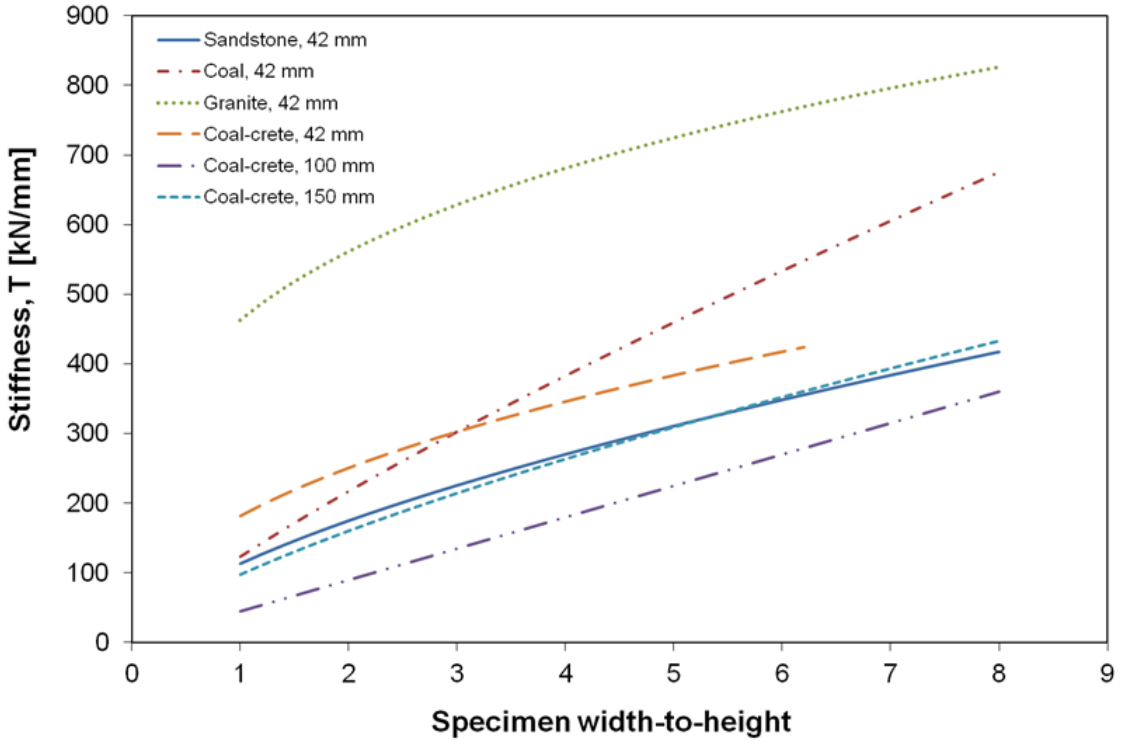


Figure 53. Specimen stiffness over w/h-ratio for different tested materials.

The term stiffness, in this context, should not be confused with the Young's modulus of the material. Here it describes the capacity of a specimen *of specific shape and in its specific boundary conditions* to resist deformation in response to the applied force. The boundary conditions in this series of compressive tests are such that lateral confinement is induced into the specimens through the frictional contacts with the steel loading platens. The influence of this end-effect is schematically shown in Figure 54**.**

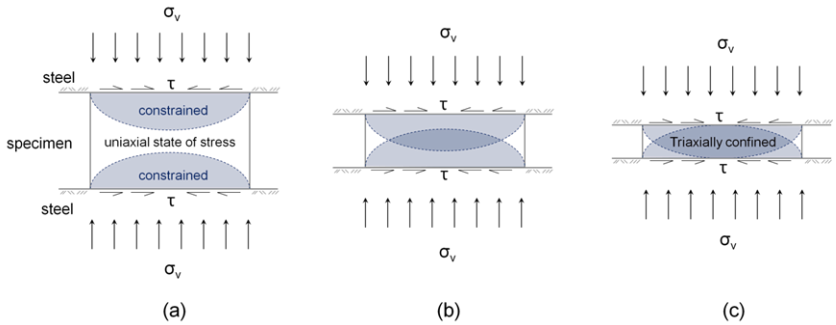


Figure 54. Schematic illustration of end-effects and induced triaxial stress-state in compression tests on flat specimen.

At a sufficiently small specimen width-to-height ratio, the specimen centre is effectively free from end constraints and a uniaxial state of stress exists (a). With the same specimen base area and increase flatness of the specimens, (b) and (c), a triaxial state of stress is produced within the specimen due to the overlap of end constraint. The triaxial stress state will be best developed for a specimen with a very large w/h-ratio.

The model explains why the observed specimen stiffness should not to be confused with the Young's modulus of the material: the Young's modulus is the stiffness of a material which is allowed to expand freely in lateral direction upon axial loading, and clearly this does not apply to the model pillar specimens in this study. The model also explains why an increasing specimen stiffness is observed for increasing width-to-height ratios: similarly to direct triaxial compression tests, the induced triaxial state of stress in the model pillars increases the resistance of the same to vertical deformation and hence its stiffness.

13.1.1 Stress-strain curves and elastic specimen moduli

It is common in rock mechanics to express the stiffness of rock structures as a modulus in GPa units, as the ratio of stress over strain. This convention will be followed further.

Stress-strain curves for the tested specimens can be calculated from the force-displacement measurements over the height and base area of the specimens. Examples of stress-strain curves for the different materials tested are shown in Figure 55 to Figure 60.

Note that although the stiffness is seen to increase with increasing width-to-height ratio, the calculated elastic specimen modulus E_s decreases. A more detailed explanation of this phenomenon is given in the following sub-section.

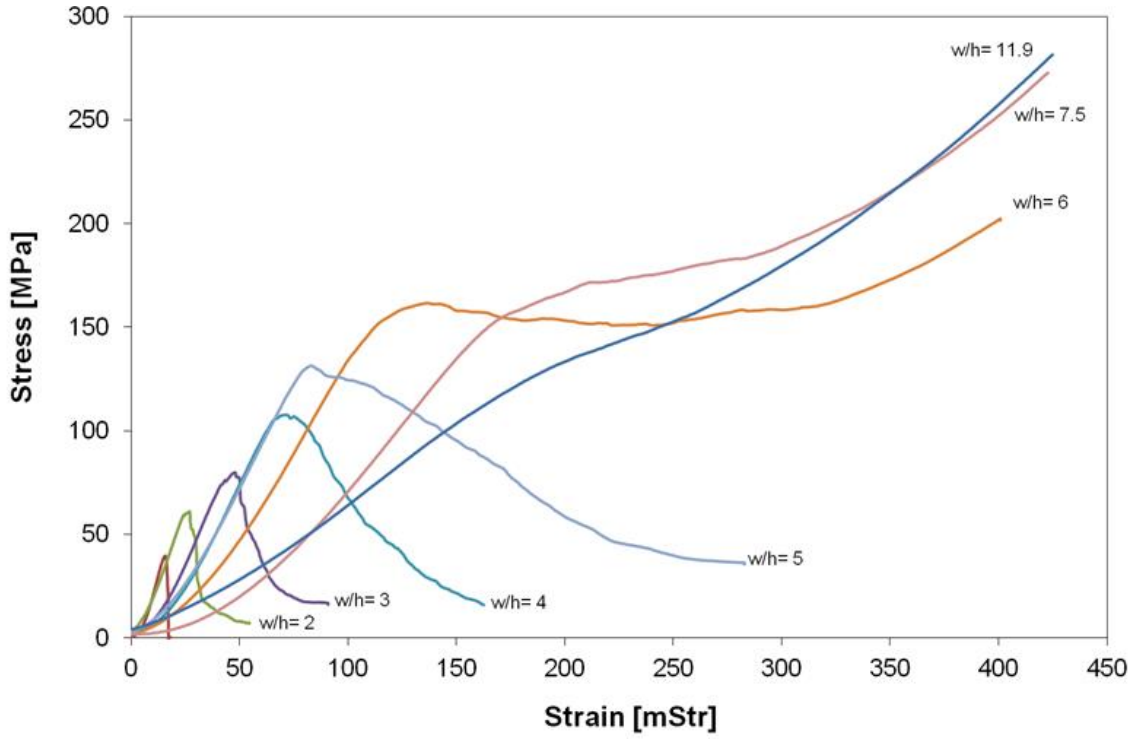


Figure 55. Examples of calculated stress-strain curves for sandstone specimens of 42 mm diameter at different w/h-ratios.

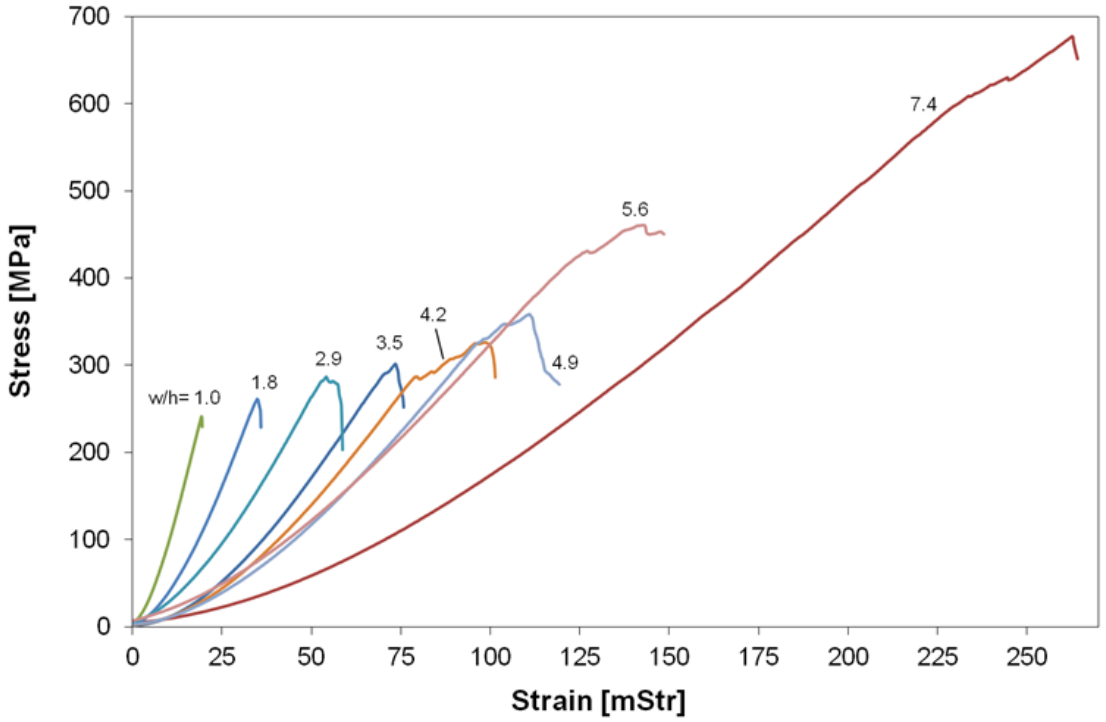


Figure 56. Examples of calculated stress-strain curves for granite specimens of 42 mm diameter at different w/h-ratios.

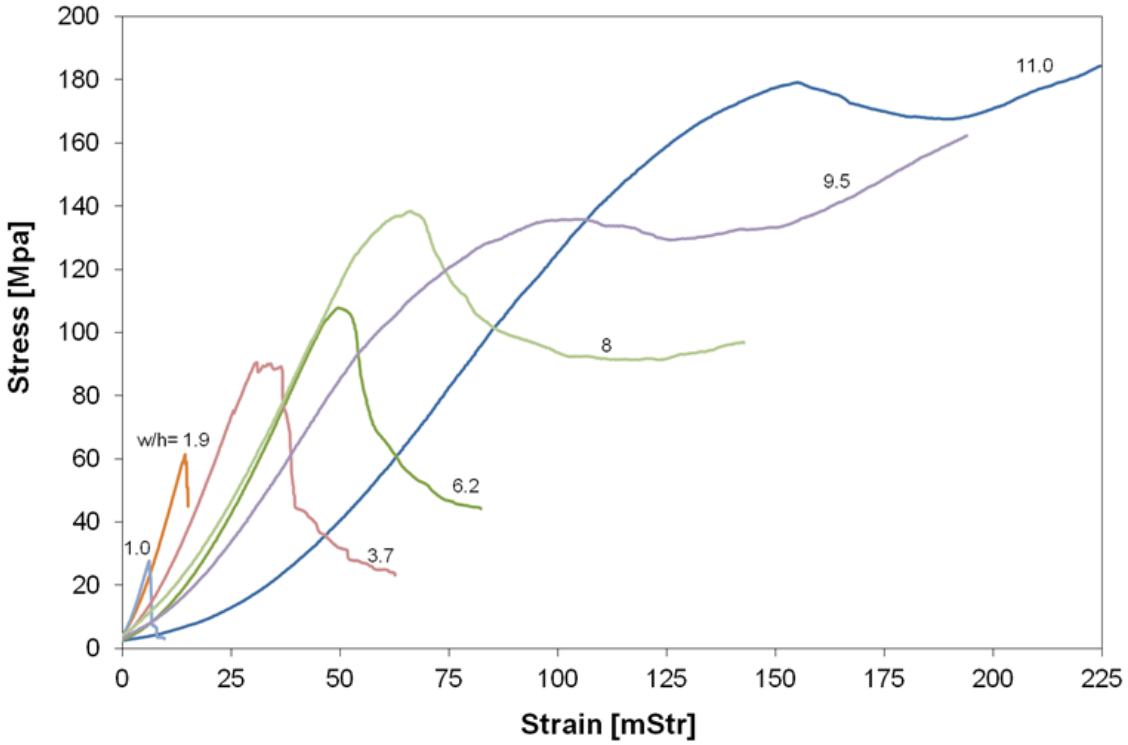


Figure 57. Examples of calculated stress-strain curves for coal specimens of 42 mm diameter at different w/h-ratios.

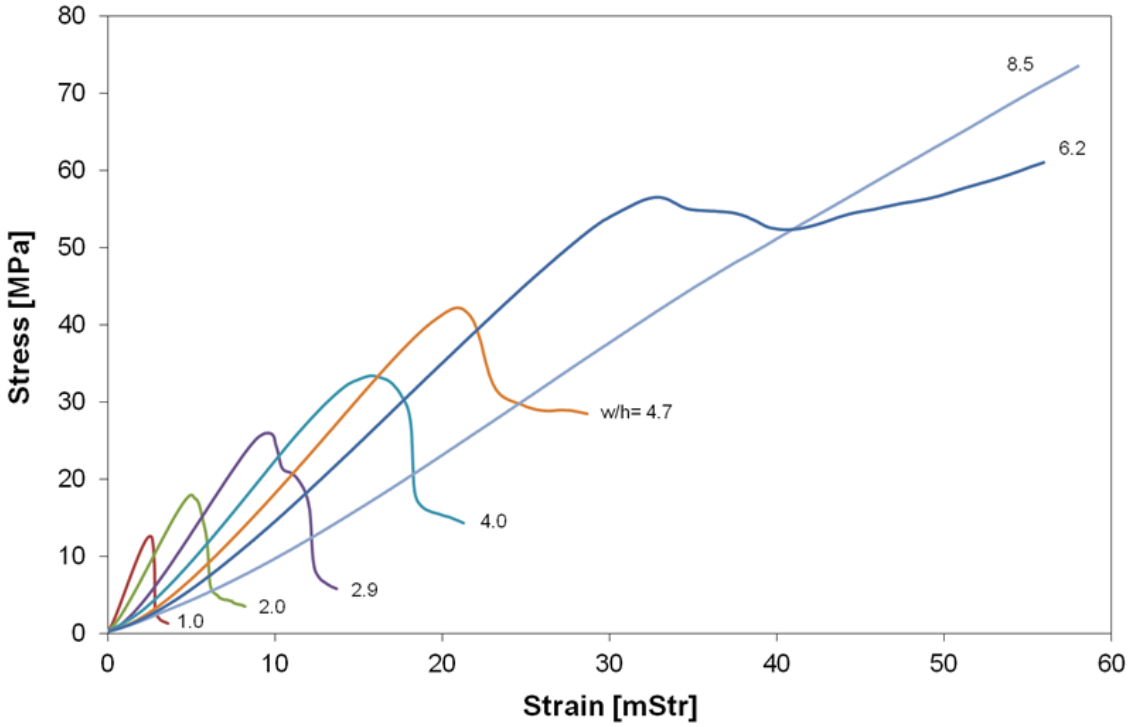


Figure 58. Examples of calculated stress-strain curves for coal-crete specimens of 42 mm diameter at different w/h-ratios.

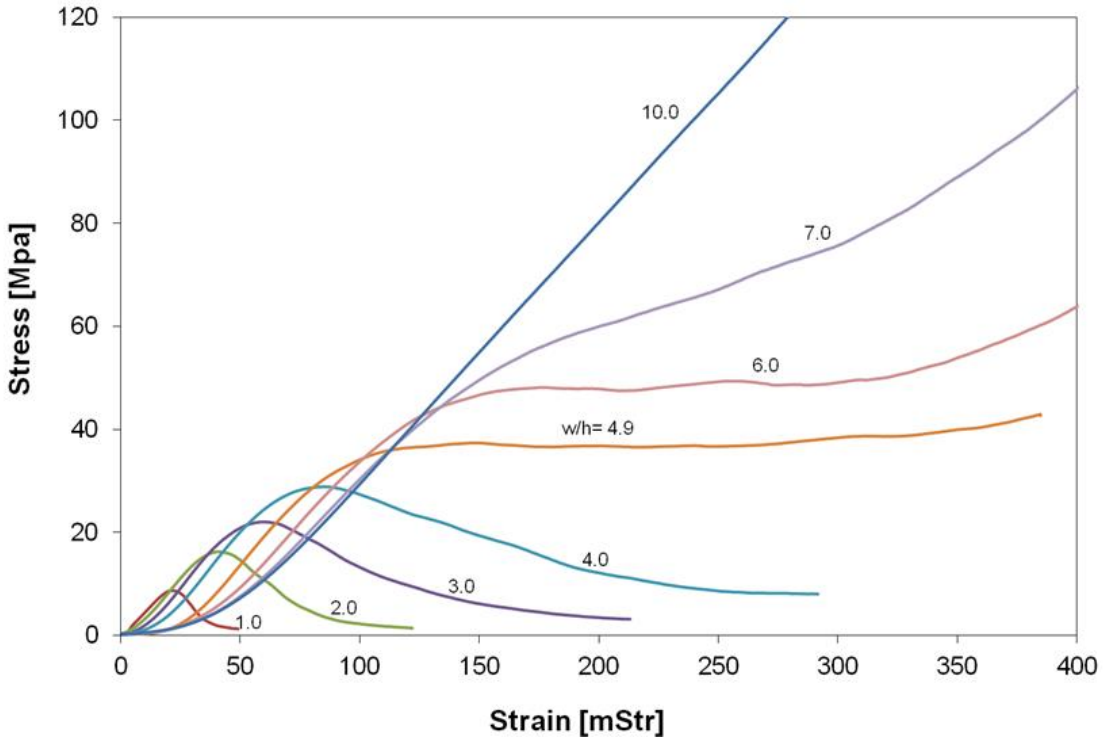


Figure 59. Examples of calculated stress-strain curves for coal-crete specimens of 100 mm square width at different w/h-ratios.

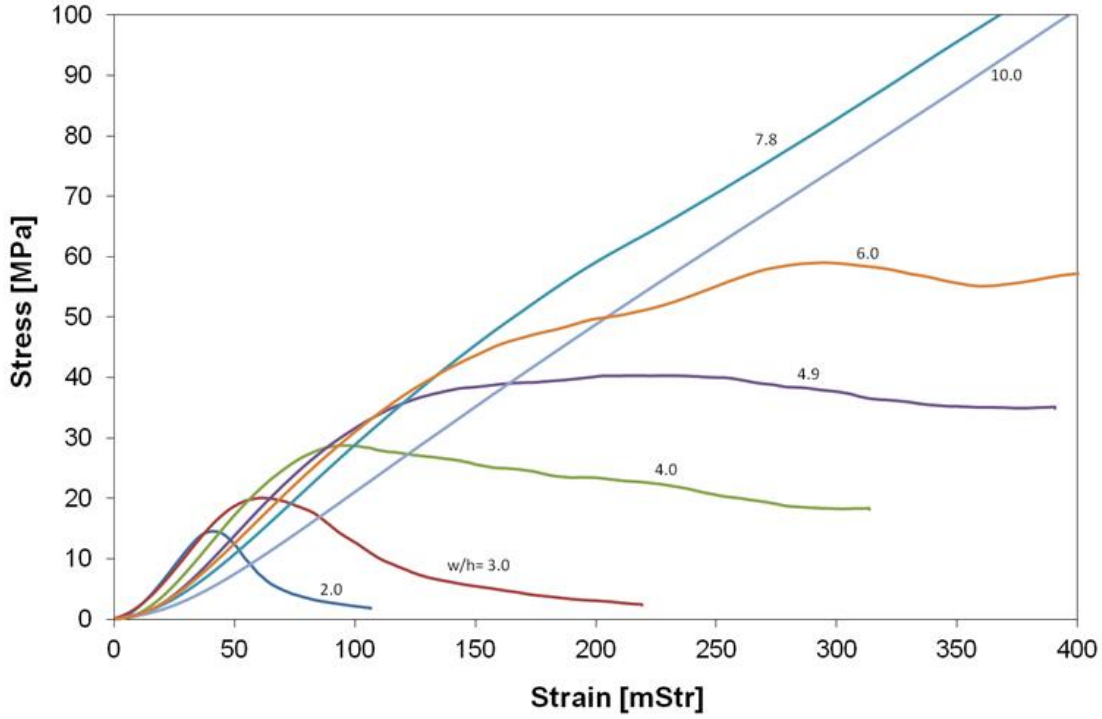


Figure 60. Examples of calculated stress-strain curves for coal-crete specimens of 150 m square width at different w/h-ratios.

13.1.2 Pre-peak behaviour

Notably, the calculated elastic specimen modulus E_s (again not to be confused with the Young's Modulus) has been seen to decrease with increasing specimen width-to-height ratio. The same phenomenon has previously been observed by Das (1986) in his laboratory investigation on the shape effect in coal specimens and attributed to increasing platen indentation occurring with higher specimen width-to-height ratios.

Another approach is followed here. In the previous section it was shown that the specimen stiffness T is either a regressively or linear increasing function of the specimen width-to-height ratio, which can be written in its generic form:

$$T = \mathrm{f}(R) = aR^b \tag{23}$$

where R is a substitute for the ratio of w/h, and a and b being constants ($a > 0$ and $0 < b \leq 1$). The calculated specimen modulus E_s relates to the stiffness T by the functional relationship

$$E_s = T\frac{h}{A} \tag{24}$$

where h is the specimen height and A is the area of the load contact surfaces. In a test series with varying w/h-ratios, the specimen height can also be expressed as a function of the width-to-height ratio R,

$$h = \mathrm{f}(R) = h_0 R^{-1} \tag{25}$$

with h_0 being the height of a specimen with R= 1 in mm. Therefore, the calculated elastic specimen modulus E_s can be expressed as a function of the specimen's width-to-height ratio,

$$E_s = \mathrm{f}(R) = \frac{a h_0}{A} R^{b-1} \tag{26}$$

Because 0< b≤ 1, this function is exponentially decreasing for values of R> 0 and b≠ 1, but gives a constant value for all R> 0 and b< 1.

In other words, the build-up of specimen stiffness T with increasing width-to-height ratio is not proportional to the reduction of the specimen height in the same range. Since the specimen height decreases more rapidly over width-to-height than the specimen stiffness increases in the same range, the net effect is that the calculated specimen modulus E_s decreases with increasing width-to-height ratio.

13.1.3 Post-peak behaviour

The specimens prepared from coal-crete, sandstone and coal exhibit a distinct post-peak stress-strain behaviour and residual strength. Failure in granite, however, was generally violent and resulted in an explosive disruption of the specimens, so that no post-peak behaviour could be recorded.

For coal-crete, sandstone and coal, the negative slope of the stress-strain curves after failure reduces gradually with increasing width-to-height ratio to first become horizontal (or near-horizontal). Finally, after significant further deformation of the specimen, an upward trend was observed. This phenomenon is called the brittle-ductile transition in specimens.

Transitional behaviour occurs within small intervals of width-to-height ratios, namely:

- for coal-crete: 4.9≤ w/h≤ 6.3
- for sandstone: 6.1≤ w/h≤ 7.5
- for coal: 9.5≤ w/h≤ 11.0

The interval given for coal-crete is the minimum and maximum values of transitional intervals observed on circular 42 mm, square 100 mm and 150 mm specimens. The upper limit of the interval given for coal may well be higher, but no specimen with w/h> 11 was tested for this material.

Specimens with width-to-height ratios above the specified transition interval show pure ductile behaviour, i.e. the post-failure slope of the stress-strain curve remains always positive (E_p> 0). This was not observed for coal for since no specimen has been tested in this range. A differentiation between the region of ductile flow and the initial elastic deformation based on stress-strain curves can only be made after observation of pronounced curvature in the stress-strain relationship. This method of distinction is, in the case of weakly pronounced curvature, somewhat arbitrary, yet unavoidable.

Notably, the ductile part of the stress-strain curve can exhibit two gradients. The curves of a sandstone specimen of w/h= 7.5 in Figure 55 and a coal-crete specimen of w/h= 7 in Figure 59 illustrate this phenomenon. For distinction and later use, the first slope following the elastic slope will be termed E_{p1} (therefore E_{p1}= E_p in the case of brittle failure), while the second and generally faster upward trending slope is termed E_{p2}.

In Chapter 12.3 it has been explained that the exact magnitudes of gradients along measured force-displacement curve, and therefore also for the calculated stress-strain curves, are distorted to some extent by specimen indentation into the testing setup under load. Since the same distortion applies to the pre- and post-peak slopes, the actual ratio of the two moduli stays unaffected.

The specimen modulus ratio E_p/E_s is therefore used for further evaluation of the specimen stress-strain behaviour. A negative ratio indicates brittle failure in the specimens, i.e. the specimens exhibited a peak strength followed by a lower residual strength. A positive ratio indicates ductile behaviour. At a ratio equal to zero, pure transitional behaviour was observed. It should also be understood that specimens that have a negative modulus ratio very close to zero were generally able to transit into ductile behaviour after some further deformation. Examples for such behaviour can be seen for instance in the case of coal in the stress-strain curves of specimens at w/h= 9.5 – 11, as shown in Figure 57.

Figure 61 to Figure 64 plot the specimen modulus ratios for coal-crete, sandstone and coal. It should be noted that there is a natural upper limit of E_p/E_s= 1 to the data, since the magnitude of ductile slope cannot exceed the elastic, intact stress-strain slope of the specimen. Any data point above that limit would therefore indicate an invalid influence by the testing machine stiffness on the measurement result.

For coal-crete specimens, the upper limit of E_{p1}/E_s= 1 is only reached at about w/h= 10. The post-peak slope E_{p1} of sandstone specimens does not reach the upper limit within the investigated width-to-height range. Coal, as a special case, maintains a negative value for E_{p1}/E_s over the entire empirical test range (1≤ w/h≤ 11), i.e. distinct global or local maximum exists in each stress-strain curve. Only the two specimens tested at w/h= 9.5 and w/h= 11 transit after a short, initial negative post-peak modulus E_{p1} again into an upward trending stress-strain behaviour (E_{p2}> 0).

The scatter of the obtained modulus ratios at same specimen width-to-height is favourably small for coal-crete and sandstone. Yet, comparable trends between the two materials cannot be established. While the modulus ratio appears to develop linearly in intervals between 2≤ w/h≤ 8 for coal-crete, the trend in sandstone specimens appears to follow a logarithmic pattern. The modulus ratios for coal are highly scattered and do not allow a meaningful trend quantification. In all cases, however, there is a well-established trend for E_p/E_s to increase with increasing w/h-ratio.

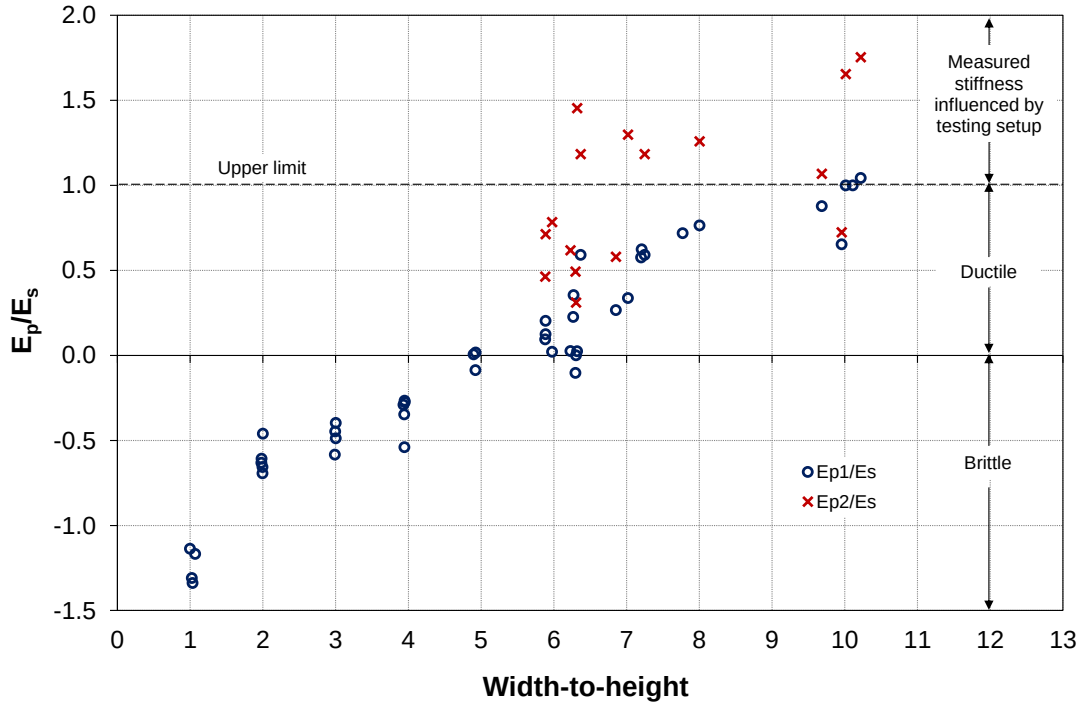


Figure 61. Modulus ratios E_p/E_s for coal-crete specimen of 100 mm square width and varying w/h-ratios. The plotted values correspond very closely with those obtained for 150 mm square specimen.

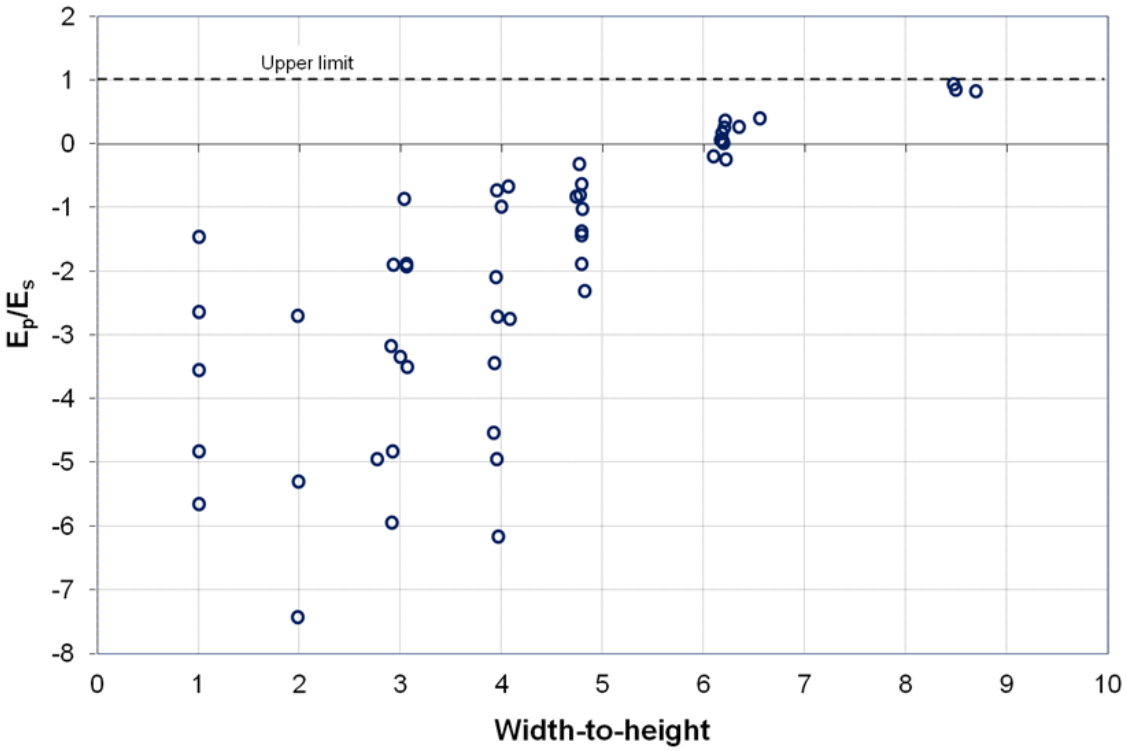


Figure 62. Modulus ratios E_p/E_s for coal-crete specimen of 42 mm diameter and varying w/h-ratios.

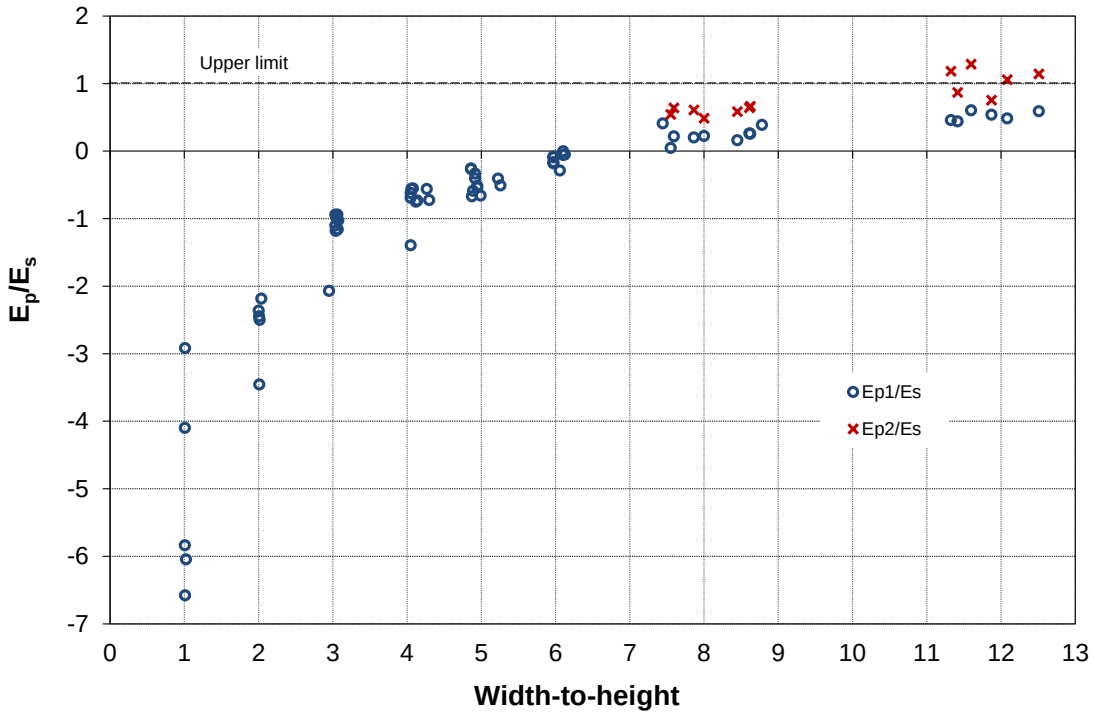


Figure 63. Modulus ratios E_p/E_s for sandstone specimen of 42 mm diameter and varying w/h-ratios.

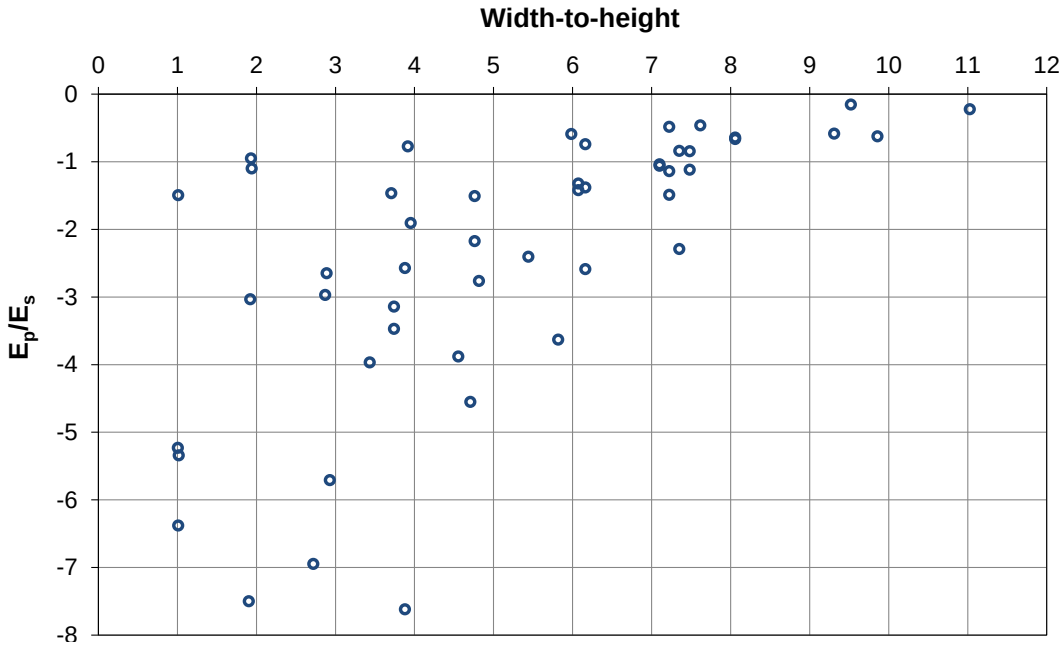


Figure 64. Modulus ratios E_p/E_s for coal specimen of 42 mm diameter and varying w/h-ratios.

13.2 Peak strength

A peak strength value could only be obtained for specimens that failed in a brittle manner, i.e. for specimens which displayed a distinct local maximum in their stress-strain behaviour. Specimens which underwent the brittle-ductile transition, i.e. having an initial post-peak slope of $E_{p1}= 0$ (or, for practical purpose, near zero), maintain a relatively consistent level of load-bearing capacity for a very long range of deformation (i.e. at least equal to the elastic deformation range or more), before they eventually continue to increase their strength with further deformation. This level is taken as a practical cap for the load-bearing capacity of these specimens and included in the trend analysis of peak specimen strength as well.

Figure 65 to Figure 69 plot the strength versus width-to-height relationship for the tests conducted on coal-crete, sandstone, granite and coal. Transitional specimens, even though equally involved in the regression analysis, are highlighted as separate symbols. Also shown in the plot are the values of uniaxial compressive strength (42 mm diameter specimen, $w/h= 0.4$). They were, however, excluded from the regression analysis.

Coal-crete, sandstone and granite all have a maximum load-bearing capacity which follows a progressively increasing trend over the full brittle and transitional width-to-height range. Best-curve-fits for the entire empirical range are second-order-polynomials with high correlation coefficients ($R^2> 0.9$). Exponential curve fits also achieve high statistical correlation coefficients, but represent the empirical data less appropriately. An exponential fit is a better choice only in the case of the 150 mm coal-crete specimens (Figure 66).

Upon a more incremental inspection of the data, one finds that the strength of coal-crete, sandstone and granite specimens first follows a linear trend up to $w/h = 4$. The strength of specimens tested at $w/h = 5$ already lie distinctly higher than the values which would have been predicted by these linear trends. This deviation increases in magnitude with further increasing width-to-height ratio. Clearly, there is a larger scatter in the data in this second interval compared to the first one. Nevertheless, it is suggested that the strength in the second width-to-height ratio interval ($w/h \geq 5$) can be expressed as a linearly increasing trend as well. The net effect is therefore a bi-linear trend of the data over its full empirical range. All regression trends and corresponding equations are provided in the figures.

Notably, the experiments with coal did not produce the phenomena described for coal-crete, sandstone and granite. Coal does not increase its strength progressively but only regressively with increasing width-to-height ratio. The best-curve-fit obeys a power-law over the entire data range, as indicated in Figure 69, with a lower correlation coefficient than those found for trends in the other tested materials. This is owed to a larger scatter in the actual tested strength values. Due to this relatively large scatter, a more detailed, incremental analysis of the data does not appear meaningful.

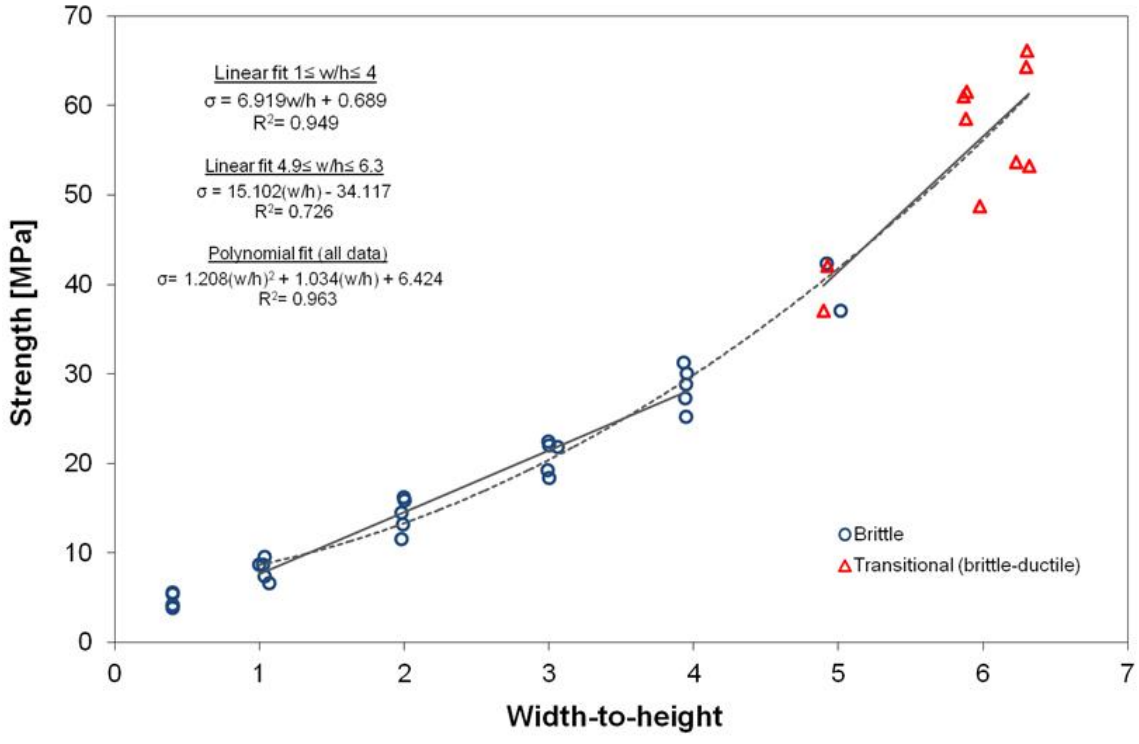


Figure 65. Strength of coal-crete specimen of 100 mm width and various w/h-ratios.

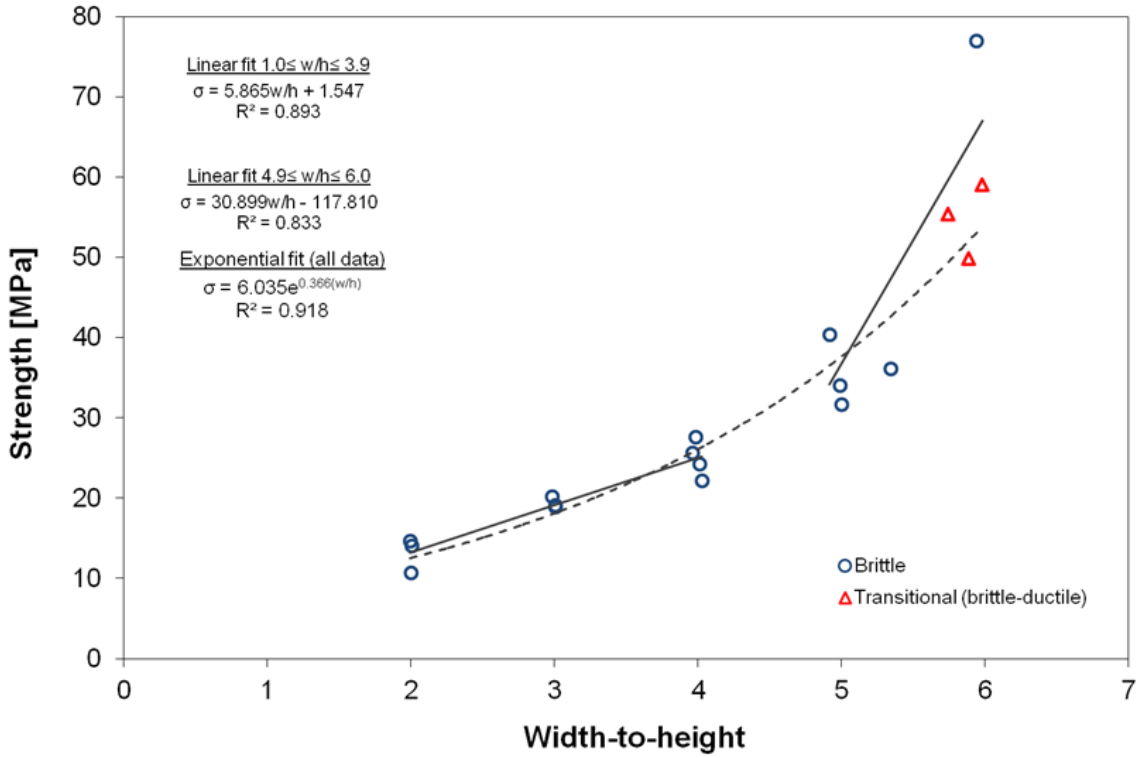


Figure 66. Strength of coal-crete specimen of 150 mm width and various w/h-ratios.

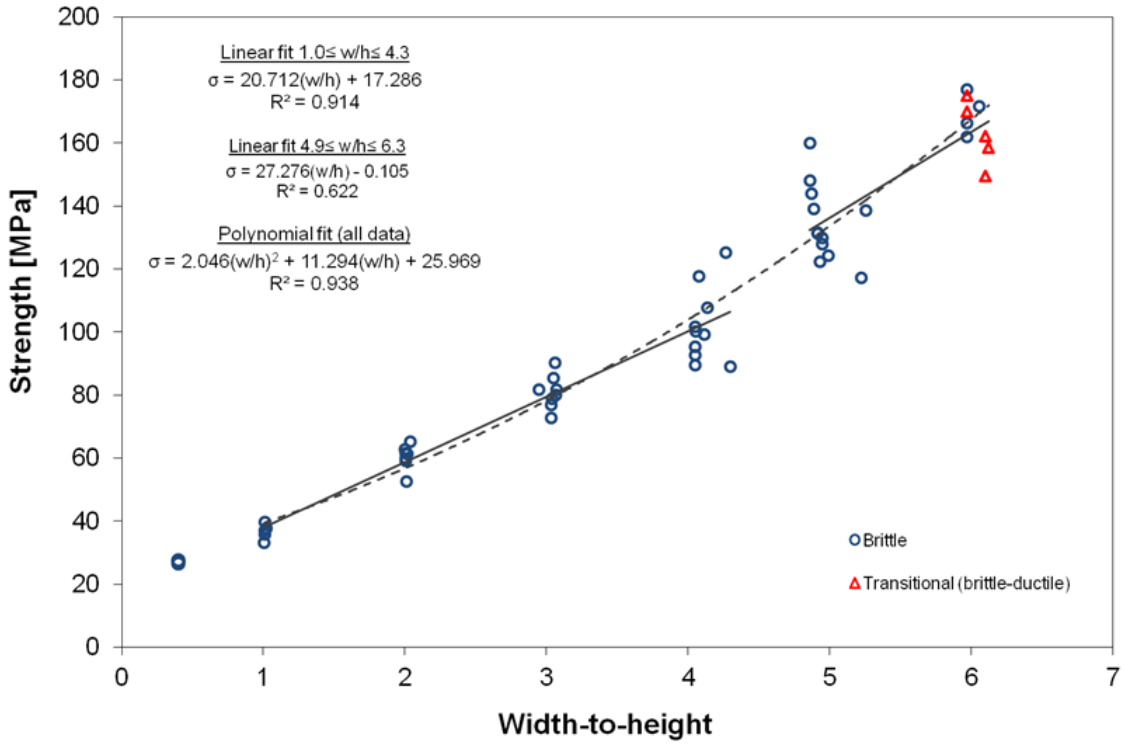


Figure 67. Strength of sandstone specimen of 42 mm diameter and various w/h-ratios.

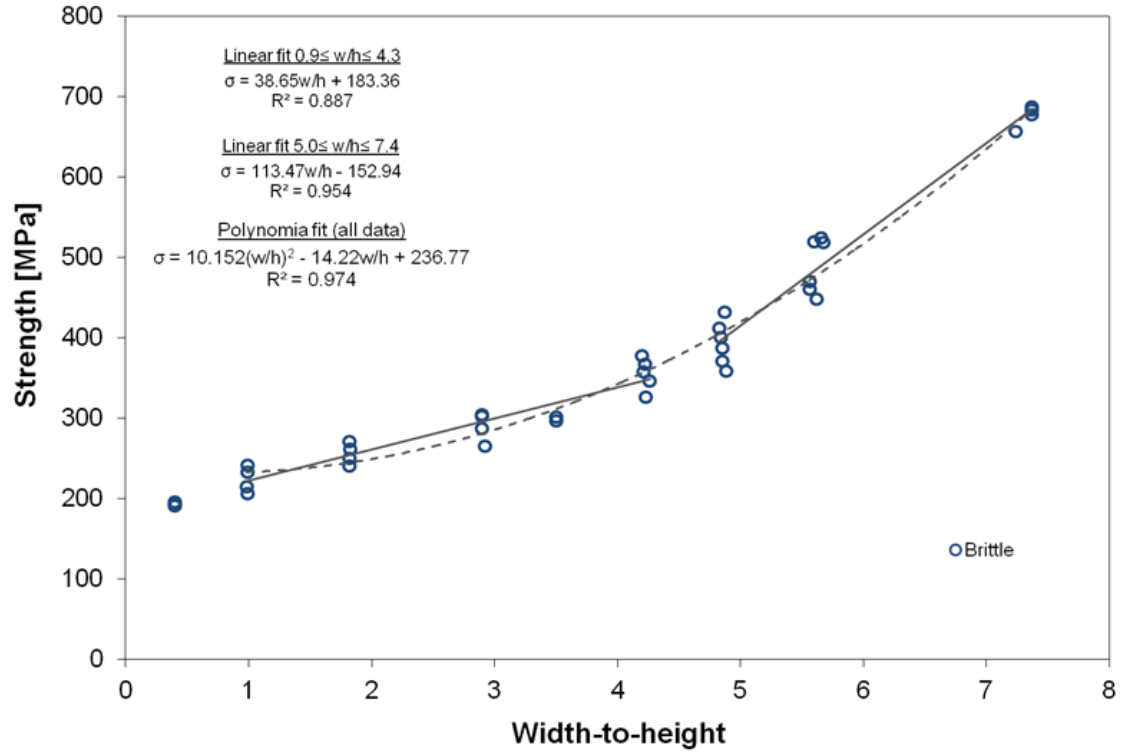


Figure 68. Strength of granite specimen of 42 mm diameter and various w/h-ratios.

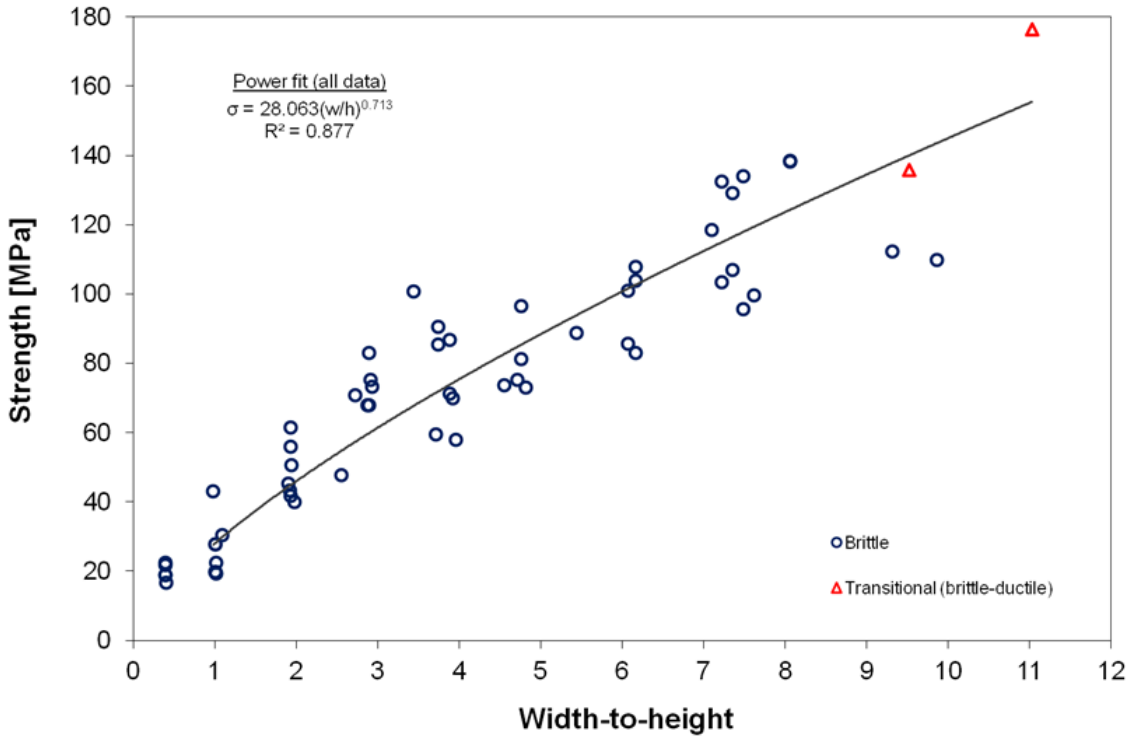


Figure 69. Strength of coal specimen of 42 mm diameter and various w/h-ratios.

13.3 Fracture patterns

13.3.1 Coal-crete

Specimens of w/h= 1 – 2 are observed to fail in the typical double-cone fashion: before the peak load-bearing capacity of these specimens is reached, the sidewalls fracture in a curved pattern to form the specimen into an hourglass shape. The sidewall material does usually not spall off during the tests but can be removed by hand without effort after the tests have been accomplished. Upon removal of the sidewalls, the actual failure mechanism becomes obvious, namely a distinct shear plane crossing the specimen diagonally through its centre (Figure 70).

The failure patterns in specimens with aspect ratios of w/h= 3 – 6 are more complex. For specimens of lower aspect ratios in this interval, brittle failure is observed. The specimens with larger aspect ratios in the interval around w/h= 6 display brittle-ductile transition.

For these specimens one notices (in top view) a series of near-linear markings parallel to the four sidewalls, as highlighted in Figure 71. No markings are observed in the specimen centre. The higher the width-to-height ratio in the given range, the closer the markings are located towards that centre.



Figure 70. A coal-crete specimen of 100 mm square width and w/h= 1 after failure. The fractured sidewalls have been removed to expose the hourglass shape and the shear failure through the centre of the specimen.

On the first glimpse these lines appear to be only discolouration, perhaps due to the occurrence of strain. Upon closer inspection, however, they manifest as outcrops of fractures that run all the way through the specimen. Open cracks of approximately 1 – 2 mm width run diagonally from the outside corners of the specimen towards its centre. These cracks can only be observed to form in the residual strength phase of the specimen, long after the peak strength had been reached and excessive non-elastic deformation was taking place.

When the specimens are separated into single elements along the above mentioned fracture outcrop lines, one observes that the fracture surfaces are highly smeared, indicating that a significant amount of shearing must have taken place (Figure 71).

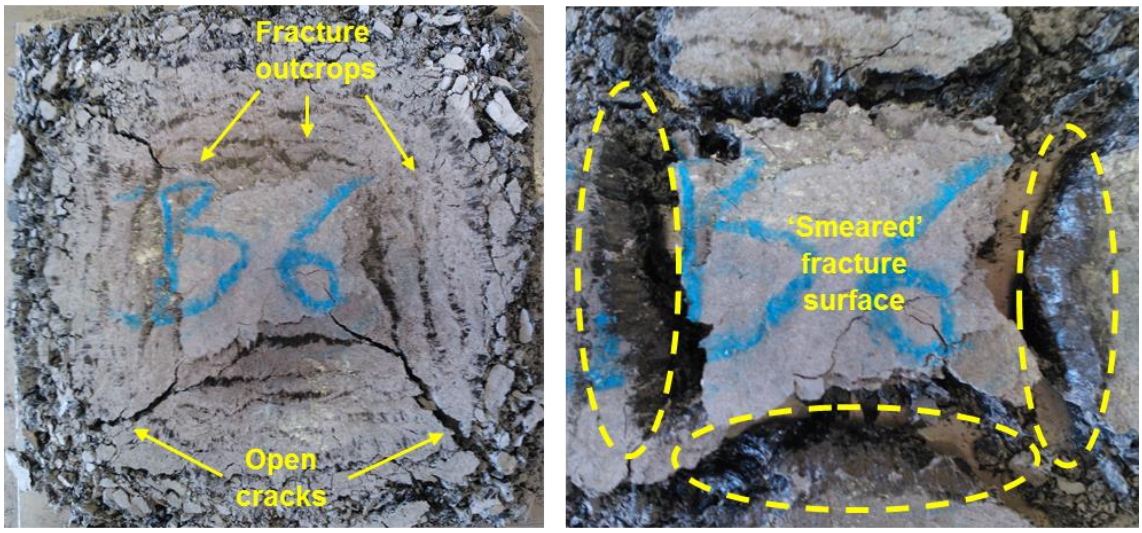


Figure 71. A coal-crete specimen of w/h= 5 in top view after failure.

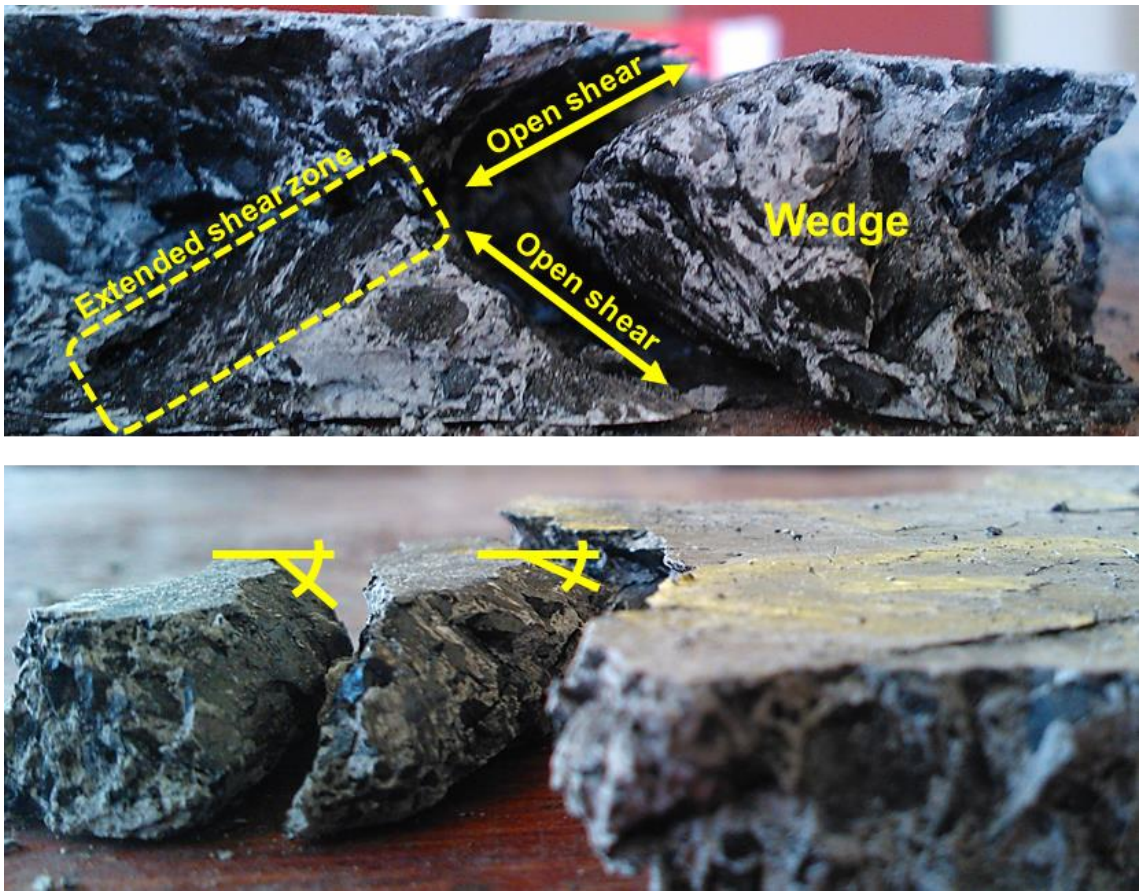


Figure 72. Coal-crete specimens of w/h= 5 in side-view after failure.

Of particular interest are the pathways of these shear-fractures through the specimens. Dissecting the specimens along the fracture outcrops yield a series of separate wedges whose curved sides, which are formed through the fractures, are pointing towards the specimen centre (Figure 72, top). Notably, the angle of fracturing becomes increasingly flatter, the more close the fracture outcrops are located towards the specimen centre (Figure 72, bottom).

For clarity, the observed patterns are reproduced in the idealized cross-sectional drawing in Figure 73. Points A, B, C are examples of observed fracture outcrops on the top surface of the specimen. The fractures run from the top side to the bottom side of the specimen in a more or less linear way (dashed lines), but with opposing directions, hence crossing each other. As a result, the specimen is divided into a number of wedges. Under vertical compression, those wedges towards the specimen centre are confined and only the wedges towards the free, unconfined side of the specimen can move. This is likely to be the reason why the wedge-type failure, as previously shown in Figure 72, can be observed.

Of great importance appears to be the fact that the fracture angles α are observed to become increasingly flatter the closer the fractures are located towards the specimen centre, as this may be an indirect manifestation of stress regimes in the specimen under vertical compression.

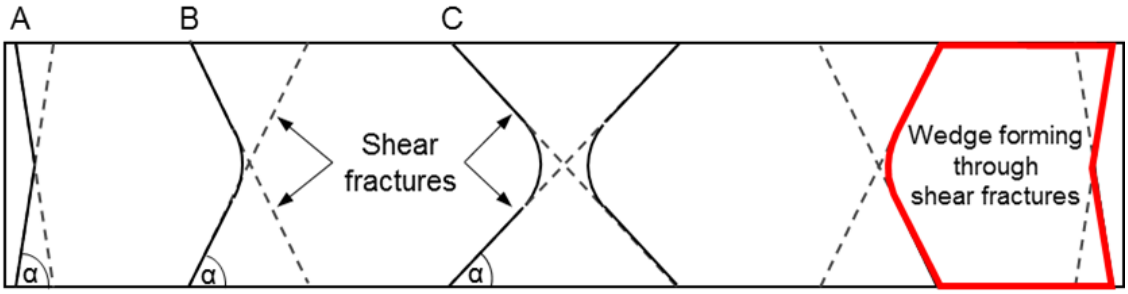


Figure 73. Idealized cross-section of fracture patterns in specimens of w/h= 2 – 6.

The phenomena of fracture outcrops and open cracks from the specimen corners can still be observed on specimens of w/h= 7 and 8 (Figure 74, left). This is the range where the specimen behaviour is purely ductile, i.e. the slope of the stress-strain curve is always positive, even though it displays different gradients along the line.

However, it is observed that the position of the cracks withdraw from the centre of the specimen the higher the width-to-height ratio, consequently leaving a larger area in the specimen centre unaffected. This behaviour is therefore opposite to the trend observed for the range of w/h= 3 – 6, where the location of the cracks moved closer towards the centre with increasing width-to-height ratio.

Specimens of w/h= 10 show ductile behaviour without any significant alterations in the slope of the stress-strain curve. It is observed that fracturing in these specimens is minimised and only located in the immediate vicinity of the specimens sidewalls (Figure 74, right)



Figure 74. Coal-crete specimens of w/h= 7 (left) and w/h= 10 after compression.

13.3.2 Rock and coal

The rock and coal specimens were too small for accurate observations on fracture patterns and were too friable after failure to be examined closer. Nevertheless, the fracture mechanism appear to be the same as observed for coal-crete. Figure 75 gives an example of double-cone shear failure of a sandstone specimen of w/h= 1 and the phenomenon of wedging as seen on a specimen of w/h= 4, for instance.

Notably, wedging was also observed on coal specimens, but could not be captured on camera due to the lack of visual contrast of the material.

In contrast, granite does not follow this pattern. On these specimens the fractures are only slightly inclined off the vertical, causing the specimens to fail in a multitude of sharp-edged slabs, as shown in Figure 76. Notably, the specimens of $w/h\geq$ 3 do not disintegrate explosively, despite the fact that failure is violent and accompanied by loud noises. Instead, the fractured pieces keep together and the specimen retains roughly its shape. This is probably due to the high lateral confinement induced in these specimen through the rock/platen contacts.

A similar behaviour is also observed on sandstone and coal specimens, Figure 77 and Figure 78. In particular, on the sandstone specimens it can be seen that in the lower range of width-to-height ratios (w/h= 4) fracturing leads to the disintegration of the specimen. For specimens with the higher aspect ratios, the core does not lose its shape, even though it is fractured and had failed. With increasingly higher aspect ratios, larger parts of the specimens do not lose shape (see w/h= 5 – 11 in Figure 77). This is believed to

be the result of the high triaxial stresses imposed on these flat specimens which pressed the specimen together in a horizontal direction.



Figure 75. Double-cone type shear failure on a sandstone specimen of $w/h=$ 1 and wedging observed on a sandstone specimen core of $w/h=$ 4.



Figure 76. A granite specimen of $w/h=$ 3 after failure in top view (left) and side view (right).



Figure 77. Sandstone specimens with various w/h-ratios after failure.



Figure 78. Coal specimens with various w/h-ratios after failure.

14 Discussion of results

14.1 Fracture patterns

It has been shown in Chapter 13.3.1 that the coal-crete specimens fail in a series of inclined shear fractures, resulting in the formation of a number of wedges. This failure type could also be observed on some sandstone and coal specimens, Chapter 13.3.2.

Of particular interest is the observation that the fracture angle α within the specimens becomes increasingly flatter the closer the fractures are located to the specimen centre. This has been demonstrated previously in Figure 72 and Figure 73.

The phenomenon bears a striking similarity to specimens which are tested in triaxial compression, where the angle of shear failure is generally observed to become increasingly flatter (measured towards the plane of loading) the higher the applied confining stress is.

When this stress-dependency of the shear fracture angle is translated back to the coal-crete specimens tested in uniaxial compression, one comes to the conclusion that the inclined fracture angles express different states of induced triaxial stress conditions inside the specimens: close to the specimen sidewalls the angle of fracturing is very steep, indicating a low triaxial or even uniaxial stress state. The fracture angle is then seen to become increasingly flatter towards the specimen core, where the induced triaxial stresses are the highest.

It was mentioned before in Chapter 13.3.2 that wedging was also observed on the small 42 mm coal and sandstone specimens. However, a closer examination of the angle of wedging was not possible due to the small scale of the specimens.

14.2 Shape and squat effects in the laboratory

The shape effect is expressed in the laboratory tests as an increase in specimen strength with increasing width-to-height ratio. It has been shown in Chapter 13.2 that over the entire empirical range of brittle and transitional failure of the coal-crete, sandstone and granite specimens, the strength versus width-to-height relationship appears to follow an upward trending law, statistically represented by a second-order polynomial curve. This behaviour has also been observed previously by Cruise (1969) in his tests on sandstone specimens over the same width-to-height ratio interval.

A second approach to the representation of the data was to assume incremental linear trends in the empirical range. This has the advantage that the indicated trends can be more easily compared with shape investigations conducted by other authors. It was noted in this incremental analysis of the data that a first linear trend can be fitted satisfactorily to width-to-height intervals of between $w/h = 1 - 4$. Thereafter, the strength values of specimens with greater width-to-height ratios increasingly deviated from this trend.

Therefore a second and faster increasing linear trend was suggested for specimens of $w/h \geq 5$.

However, coal has been observed to behave very differently from the above mentioned materials, in that it shows only a regressively increasing trend in strength over width-to-height and a very late brittle-ductile transition at around $w/h = 9.5 – 11$.

These phenomena agree with findings of other researchers on coal: Meikle and Holland (1965) in their tests on the effect of coal-loading platen contact friction on specimen strength only found regressively increasing strength trends in the interval of $w/h = 4 – 8$, and did not report on brittle-ductile transition or a rapid specimen strengthening beyond a critical w/h-ratio. Khair (1994) reported linear trends for the strength of coal specimens tested between $w/h = 4 – 8$, irrespective of relatively high coal-steel contact friction angles. Madden et al. (1995) also suggested a regressive specimen strength increase up to $w/h = 8$ and Kroeger, Roethe and Li (2004) did not experience the brittle-ductile transition of specimens up to a squat width-to-height ratio of $w/h = 12.5$.The only researcher who did observe brittle-ductile transition in coal was Das (1986), who encountered this phenomenon in a specimen shape interval of $w/h = 9 – 11$.

14.2.1 Strength of materials up to $w/h = 4$

The majority of the numerous published research reports on the shape effect in rocks addressed specimen shapes in the first interval of $1 \leq w/h \leq 4$. There is overall agreement that the shape effect takes the form of a linear strength increase in this interval.

This gives opportunity to analyse the characteristics of the linear trends in different rock materials and the related mechanical properties. A linear function can be characterized by its intercept, n, with the ordinate axis and the slope of the line, m. In the context of shape tests on specimens, these values represent the strength of a material with infinitely small width-to-height ratio and the gradient of strength increase over specimen width-to-height ratio respectively.

In addition to the tests conducted within this experimental study, further data was sourced from published research (Stavropoulou, 1982; Ozbay, 1987; Madden, 1990; Madden and Canbulat, 1995; York, Canbulat and Jack, 2000). A linear trend in intervals of $1 \leq w/h \leq 4$ was also fitted to the No. 4 seam coal tested in the laboratory investigation. The data is summarized in Table 9.

The essential results of a correlation analysis between the characteristic of the linear shape effect and the basic material properties are presented in Figure 79 and Figure 80. Of particular interest is the gradient of strength increase over width-to-height, m, and its correlation with the mechanical properties of the materials.

Notably, a very strong correlation is found between the gradient of strength increase and the cohesion of the material, Figure 79: the higher the material cohesion, the more rapid the increase in strength over width-to-height. This trend is so pronounced that it suggests

a fundamental mechanical relationship between the two parameters, i.e. that the strength failure in rock specimens of w/h= 1 – 4 is predominantly controlled by a loss of cohesion.

Table 9. Data for comparison between material properties and the shape effect.

Investigator(s)	Material	UCS [MPa]	E [GPa]	ν	c [MPa]	ϕ [°]	w/h	Linear strength n	Linear strength m
Madden (1990)/ Stavropoulus (1982)	Sandstone	80.8	22.0	0.3	6.1	48.9	1 - 6	88.0	10.0
York et al. (2000)	Coal	29.4	-	-	2.5	39.7	1 - 4	34.1	14.3
Ozbay (1987)	Norite	290.0	100.0	0.2	45.0	52.0	1 - 3	383.0	48.8
Ozbay (1987)	Sandstone	85.0	27.6	0.3	-	-	1 - 3	110.0	14.3
Mathey	Anorthosite	186.0	-	-	26.9	58.6	1 - 5	143.6	31.8
Mathey	Pyroxenite	153.5	-	-	37.1	41.6	1 - 5	127.1	34.6
Mathey	Sandstone	27.2	7.3	0.5	8.2	42.2	1 - 5	17.3	20.7
Mathey	Granite	193.3	63.4	0.3	33.6	50.9	1 - 4	183.4	38.7
Mathey	Coal-crete	8.1	1.6	0.3	2.5	37.5	1 - 4	4.5	7.0
Mathey	Coal-crete	4.6	0.6	0.2	0.6	54.5	1 - 4	0.7	6.9
Mathey	Coal-crete	4.2	0.9	0.3	0.8	47.7	1 - 4	1.2	6.0
Mathey	Coal	19.4	-	-	5.3	41.4	1 - 4	16.9	15.4

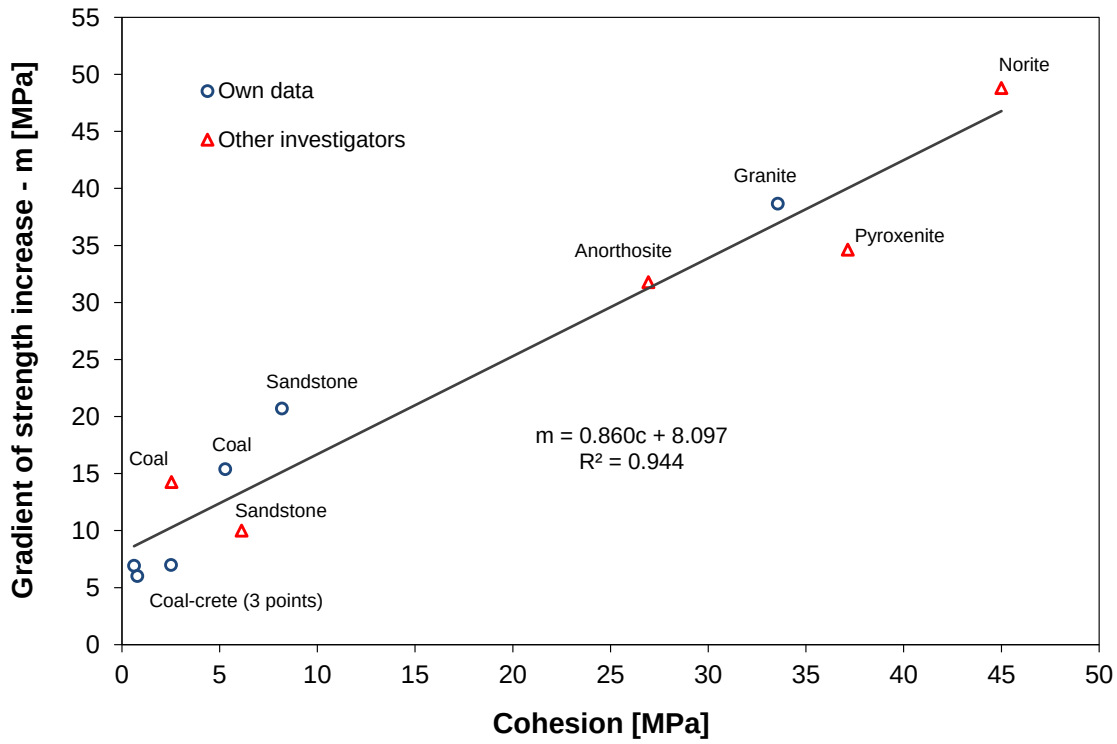


Figure 79. Correlation between the material cohesion (c) and the gradient of strength increase (m) over 1≤ w/h≤ 4.

In this context it is also worth noticing the angle of internal friction ϕ appears to have no influence on the shape effect in rock at all, as can be seen in Figure 80. Further, good correlations with the gradient of strength increase m have been found for the uniaxial compressive strength and the elastic modulus E of the materials.

The correlations between the gradient of strength increase m and cohesion c, uniaxial compressive strength UCS and elastic modulus E suggest that the three latter named parameters are interrelated as well. Indeed very high correlation coefficients are observed for the combinations of c and E (R^2= 0.967), E and UCS (R^2= 0.997) and UCS and c (R^2= 0.915). Notably, a somewhat weaker correlation (R^2= 0.782) is also found between the two parameters ϕ and ν, both of which do not correlate with m.

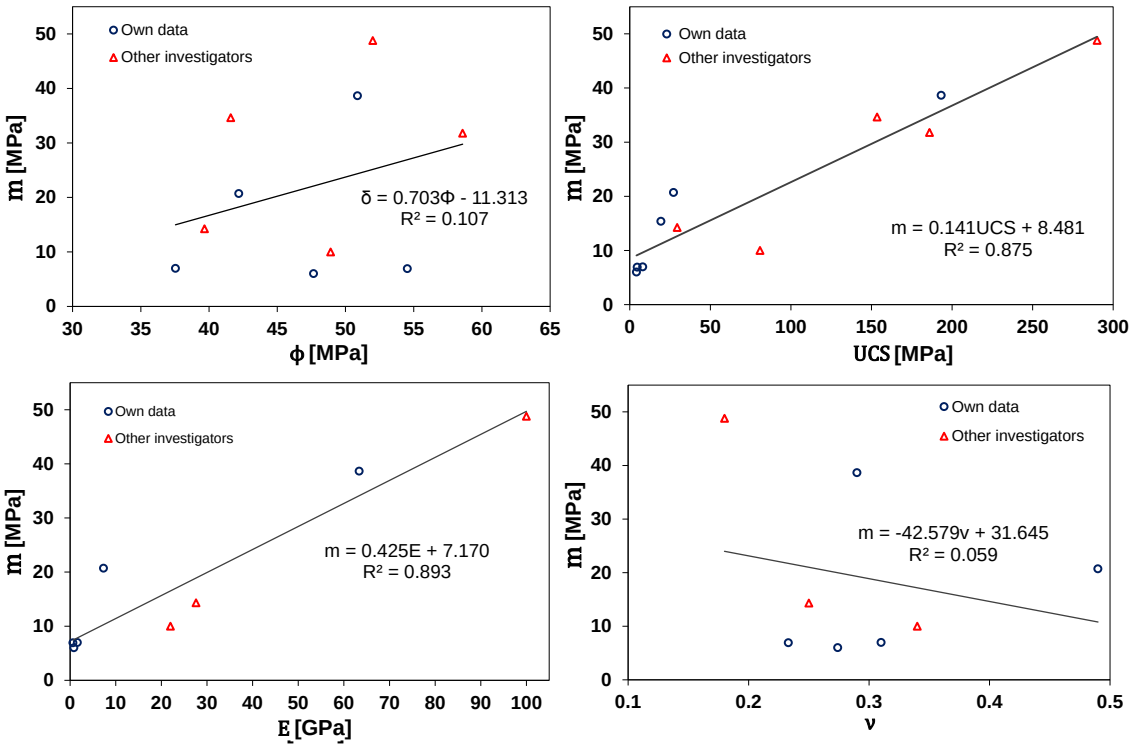


Figure 80. Correlations between the gradient of strength increase m and the mechanical properties of the materials.

Despite the generally high correlation coefficients observed in this analysis, it has to be kept in mind that only a relatively small number of tests (a maximum of 11) could be analysed for the relationships between the basic mechanical rock properties and their role in the shape effect of rock.

It must be kept in mind that an enlargement of the database can result in a reduction of correlation coefficients between the parameters. This, for instance, can be shown for the relationship between the UCS and the rate of strength increase m: upon increase of the database to 21 observations between the two parameters (the additional data was sourced from Babcock (1969), Baker-Duly (1995), Sheorey and Singh (1974) and Ozbay (1987)), the correlation coefficient already drops by 12 % to R^2= 0.745.

This observation warns against generalisation of the indicated trends in the above mentioned figures**:** the statistical correlations, especially in their isolated forms between two parameters, do not necessarily explain in part or in full the actual cause behind observed strengthening effects in rock.

14.2.2 The squat effect

After the width-to-height range of $w/h = 1 - 4$, in which the shape effect can be identified as a linear increase in strength of specimens, there appears a marked change in the strength over width-to-height relationship.

This change manifests as a more rapid increase in specimen strength than previously experienced for lower width-to-height ratios. This phenomenon is interpreted here as the so-called *squat effect* and occurs in granite, sandstone and coal-crete.

A first conclusion can be drawn as to the nature of the squat effect, namely that its occurrence is independent from the brittle-ductile transition. This is so because the change in strength increase appears for granite, sandstone and coal-crete, even though only the latter two materials experience brittle-ductile transition at higher width-to-height ratios.

The squat effect has not been observed to occur in coal specimens. On the contrary, the indicated trend for coal is such that the strength gradient decreases with higher width-to-height ratios. Consequently the question must be answered as to what the mechanism behind the squat effect is, and why it is not occurring on coal.

A clue to the mechanism of the squat effect might be found in the very fact that it does not occur with coal, despite the intact mechanical strength properties of coal being within the range covered by the parameters for coal-crete, sandstone and granite. This suggests that intact mechanical material properties do not directly or predominantly relate to the squat effect.

Another clue can be deduced from the following observation: it has been suggested in the previous chapter that the brittle strength of specimens in the lower width-to-height region is controlled to a significant extent, although perhaps not entirely, by the material cohesion and the loss thereof. On the upper end of the brittle range the brittle-ductile transition occurs in specimens (this phenomenon will be discussed in detail in the following Chapter). The mechanism of this brittle-ductile transition is likely to be friction-controlled sliding of particles along a pronounced fracture network within the specimen.

That is, even though the specimen has experienced a significant loss of cohesion at some point, the specimen can still bear the load due to the frictional resistance along the fracture network in the specimens. This is at least suggested by the observation that the relevant specimens are highly fractured when they undergo the transition.

What this observation implies is that a gradual transition must take place, from a predominantly cohesion-controlled strength at low width-to-height ratio to a significantly friction-dependent strength at very high width-to-height ratios. Notably, the latter mentioned friction is not to be confused with the angle of internal friction of the specimen, but is the effective friction acting on a complex network of fractures.

In the granite specimens, which did not undergo the brittle-ductile transition, one observes the transition from predominantly cohesion-controlled strength to friction-controlled strength markedly at width-to-height ratios of 4.2. In Figure 56 one observes that

specimens of this critical and higher aspect ratios begin to yield long before the peak strength is reached. The stress-strain curves exhibit a series of abrupt, yet small strength drops on their path towards the peak, which is interpreted here as a partial loss-of cohesion. The fact that these specimens can still increase in strength must then be a combination of residual cohesion and the build-up of friction in between the fractured particles.

If the above reasoning is valid, then the squat effect in rocks may be more accurately defined as the transition from predominantly cohesion-controlled strength to predominantly friction-dependent strength.

14.2.3 The brittle-ductile transition

The shape effect eventually results in the brittle-ductile transition of specimens of coal-crete, sandstone and coal. Granite did not reach the transition within the empirical range. For the granular materials of this study (coal-crete and sandstone) the transition appears consistently around $w/h = 6$. In this context, Madden's tests on stronger sandstone specimens with larger dimensions (Madden, 1990) also showed brittle-ductile transition at approximately the same aspect ratio.

The brittle-ductile transition in coal has only been observed for two specimens of the test series, at $w/h = 9.5$ and 11. Notably, the laboratory investigation by Das (1986) into the shape effect of coal from 5 seams in India has identified the same width-to-height range for brittle-ductile transition in coal.

The difference in the behaviour of coal on the one hand, and coal-crete and sandstone on the other hand, is significant. It indicates that the intact mechanical properties of rock do not determine at which width-to-height ratio the brittle-ductile transition occurs, since the tested coal in this experiment exhibits properties that fall in between those of coal-crete and sandstone.

In Chapter 13.3 it has been shown that specimens which undergo the brittle-ductile transition exhibit the same type of fracture patterns as the specimens in the lower width-to-height range which fail in a brittle manner. It is therefore very likely that the cause behind the ductility is specimen cataclasis: the specimen has lost a great portion of its cohesion and disintegrated into a complex network of macro and micro fractures, and the applied compressive forces are sustained by frictional sliding of the debris.

An essential parameter to the mechanism of brittle-ductile transition is therefore the effective friction that can build up on these fracture networks. The fact that in coal specimens the brittle-ductile transition only occurs at much higher width-to-height ratios, as compared to the rock and composite materials in this study, might then point to the fact that the build-up of residual friction in coal is a slower process than in coal-crete and sandstone.

The difference might be explained by the texture of the materials: while coal-crete and sandstone have a granular fabric, so that the particles can interlock more readily after shearing, the texture of the coal specimens is very smooth and the fracture surfaces are

slippery. The knowledge of how internal fractures are forming is important in orde to answer the question as to whether the brittle-ductile transition in coal pillars occurs or not.

14.3 Comparison of findings with in-situ coal pillar behaviour

14.3.1 The shape effect

The laboratory findings cannot be used to predict in-situ coal pillar behaviour directly, due to the difference in material, size and boundary conditions. However, it is clear that striking parallels can be observed between some of the aspects discussed under Chapter 14.2 and the large-scale in-situ tests that have been conducted by other investigators.

The shape effect for in-situ coal is relatively well explored through the work conducted by Bieniawski (1968a), Wagner (1974) and Van Heerden (1975), the statistical examination of pillar collapses by Salamon and Munro (1967) and, in the most recent review, by Van der Merwe and Mathey (2013c). To facilitate the comparison with the laboratory observation, the empirical in-situ pillar strength equations are presented in their linear form (Van Heerden, 1975) in Figure 81.

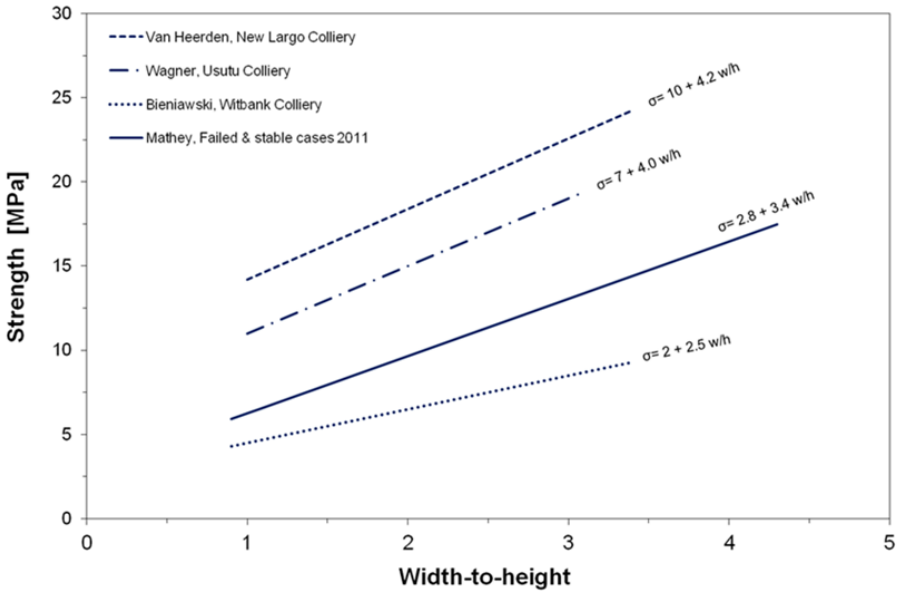


Figure 81. The strength of in-situ coal pillars in linear expression.

It was shown in the laboratory that the higher the compressive strength of the material, the greater the gradient of strength increase over width-to-height is (Figure 80).

The same correlation can be shown for in-situ coal. The values of cohesion and uniaxial compressive strength are unknown for coal mass, but for comparative purpose, the coal mass cube strength can be used as a measure here. The argument is that the higher the cube strength of coal, the more rapid the increase of coal pillar strength over width-to-height.

Figure 82 plots the strength of coal pillars, σ, normalized to the site-specific strength of a cube of coal of critical size, σ_{cube}, as tested by Bieniawski, Wagner and Van Heerden in their in-situ large scale-compression tests. Also included in the plot are the updated coal pillar collapses as reported by Van der Merwe and Mathey (2013b) for areas of normal coal in South Africa. The strength of the collapsed cases is calculated from the updated maximum likelihood strength equation (Van der Merwe and Mathey, 2013c).

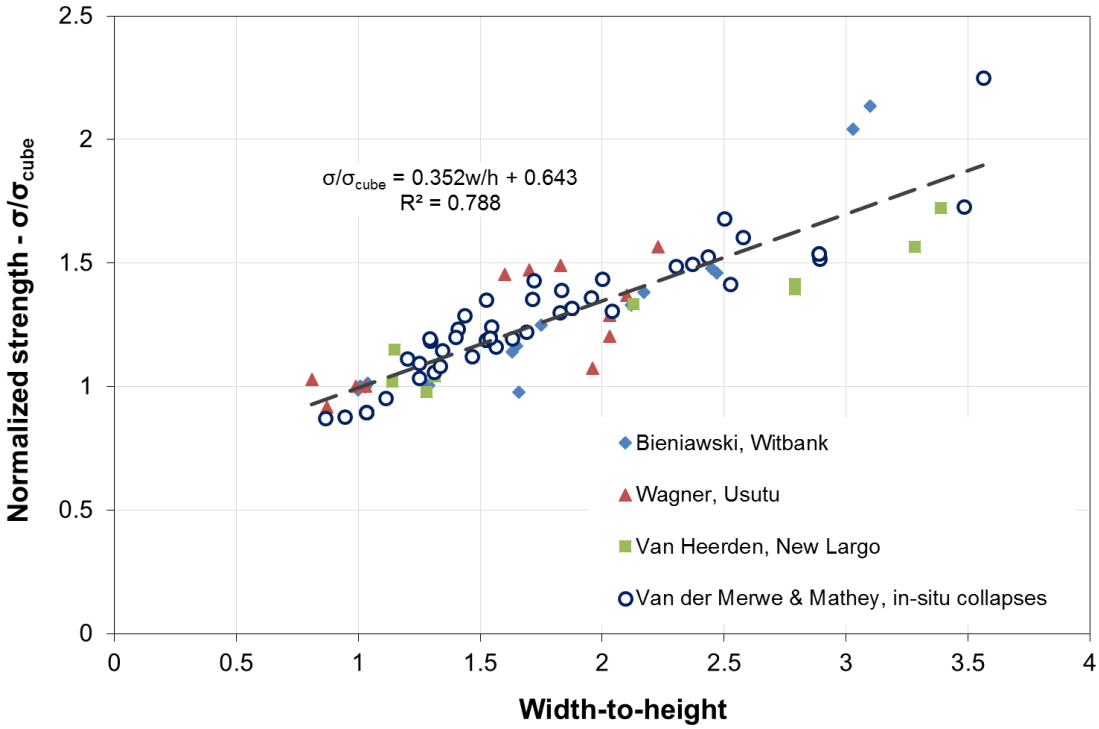


Figure 82. Strength of coal pillars normalized to the strength of a coal cube.

A linear regression analysis of the combined dataset demonstrates that the strengthening effect of pillar shape is related to the compressive cube strength of coal. The higher the cube strength of coal, the more rapid the increase in strength over width-to-height. This correlation has also been shown previously by Bieniawski (1992) based on a smaller set of data. The linear regression equation in Figure 82 is

$$\sigma = \sigma_{cube} \left(0.352 \frac{w}{h} + 0.643\right). \tag{27}$$

This equation can be used for coal pillar design purposes in the empirical range of its derivation and allows for a seam- or site-specific adoption, if the relevant average critical coal cube strength is known.

The boundary conditions which were applied to the test pillars and the in-situ collapses were highly variable, ranging from displacement-controlled and stiff loading to stress-controlled and soft loading, as analysed in detail by York and Canbulat (1998). Boundary conditions are often declared as prime contributors to the shape effect in pillars.

Further, it was shown that a statistical correlation exists between the elastic modulus of a rock and the rate of strength increase over width-to-height (Figure 80). Even though

there is not enough data available for in-situ coal to confirm this correlation, it is nevertheless interesting to note that Van Heerden and Wagner both report on very similar strength gradients (4.2 and 4.0 MPa respectively) and the same average elastic modulus of coal E= 4 GPa in their tests.

The cohesion of a material was also shown to correlate strongly with the strength gradient (as well as with the UCS and the elastic modulus). Unfortunately, the in-situ cohesion of coal has never been determined empirically. However, presuming that the correlation is also valid for in-situ materials, one could conclude from the coal strength equations presented in Figure 81 that the cohesion of in-situ coal might be very low, i.e. in the range of less than 5 MPa (corresponding to relatively low strength gradients). It should be noted in this context that the gradients in the strength equations derived from compression tests in three different collieries average to the same gradient observed from the statistical analysis by Mathey (2011) of 98 collapsed and 340 stable pillars in South Africa, i.e. m= 3.4. This may indicate that the three compression tests on coal conducted in different collieries represent the characteristics of coal in the country satisfactorily.

14.3.2 The post-peak behaviour

The post-peak behaviour of specimens in the present laboratory study and of the large-scale in-situ specimens tested by Van Heerden and Wagner is shown in Figure 83. Coalcrete of 100 mm and 150 mm size exhibited a very consistent post-peak behaviour over width-to-height and therefore the dataset has been unified in this plot.

The in-situ post-peak behaviour of 1.4 m square coal specimens is observed to be markedly different from the 42 mm coal specimens tested in this laboratory investigation, whose values lie on the right hand side of the sandstone specimens. There is also no pattern in the data that links the magnitudes of post-peak slopes to the corresponding mechanical properties of the materials: the in-situ coal, whose mechanical properties (strength, elastic modulus, cohesion) lie in-between the corresponding values for coalcrete and sandstone, has the lowest ratios E_p/E in the entire dataset.

This finding does not support the suggestion by Ozbay (1987) that a rock with greater elastic modulus results in a greater post- failure modulus.

The laboratory based post-peak slopes of specimens is therefore unlikely to assist in the evaluation of in-situ pillar behaviour.

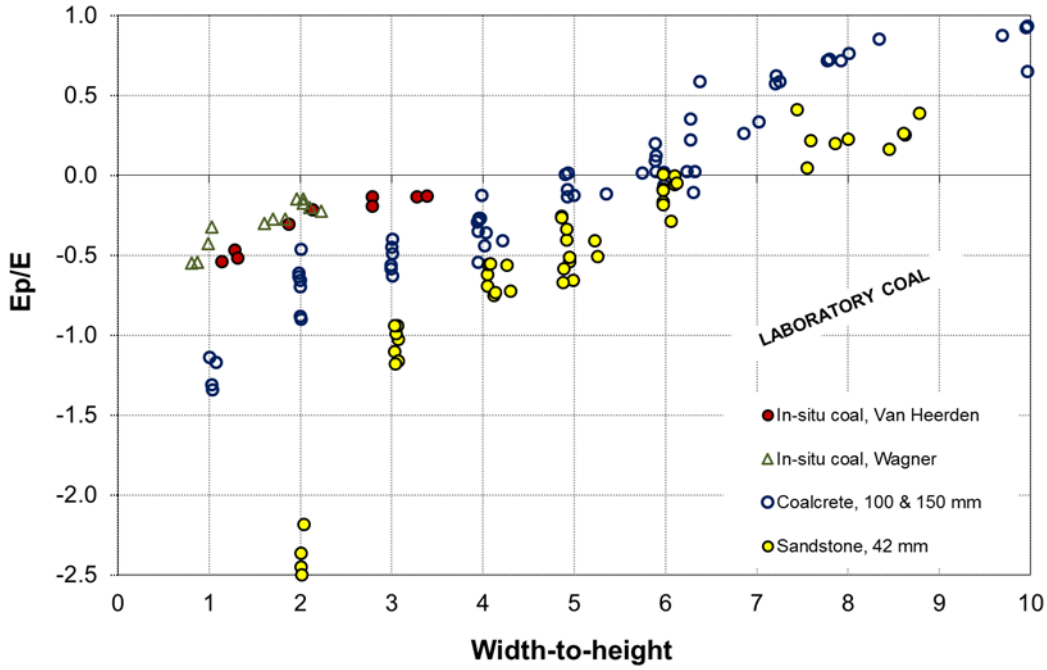


Figure 83. Post-beak behaviour of specimens in the laboratory and in-situ.

14.4 Conclusion from laboratory study

In the introduction to the investigation, Chapter 10.1, questions were raised as to the existence and the nature of a possible squat effect in specimens. The experiment therefore set out to investigate the shape effect in different rocks and materials to evaluate their behaviour when formed into very flat width-to-height ratios.

The question of whether a squat effect exists at all has been confirmed: coal-crete, sandstone and granite showed a marked increase in strength above a width-to-height ratio of 4. It was also explained that the squat effect is not identical to the occurrence of brittle-ductile transition in the materials. In the tests, the squat effect manifested as a true increase of the brittle strength of rocks. The trend in strength above width-to-height ratios of 4 could only be observed over a longer interval for granite, where it is interpreted as a linear behaviour. For coal-crete and sandstone however, the brittle-ductile transition occurred at width-to-height ratios very soon after the squat effect was noticed.

The mechanism behind the squat effect could only be hypothesised. An important indication was the finding that that strength and failure of specimens in the lower end of the width-to-height range was predominantly cohesion-controlled. This was deduced from the fact that the rate at which the shape effect impacted the strength increase in this range for different materials showed a very strong correlation with the material cohesion.

In the upper range of width-to-height ratios, the shape effect finally resulted in the brittle-ductile transition of specimens, as observed for sandstone, coal-crete and coal. By analysis of the excessive fracturing in the transitional specimens it was concluded that the strength for these specimens was predominantly friction controlled. A similar observation

was also made for granite, whose peak strength in width-to-height ratios above 4.2 appeared to depend on how readily a gradual loss of cohesion could be compensated with the build-up of friction.

The mechanism behind the squat effect was therefore preliminarily defined as the transition from predominantly cohesion-controlled to predominantly friction-controlled strength in specimens.

The friction that is meant here is the effective friction developing on the fracture network in specimens under compression. Since the fracture network is complex in nature, the effective friction acting on it cannot be quantified or predicted and hence the question on how the squat effect can be quantified remains unanswered so far.

The question remains unanswered as to why the coal tested in the experimental programme did not conform to the squat effect as observed in the above described rock and composite materials. The trend for the strength of coal was found to be only regressively increasing over the full width-to-height range of up to $w/h=$ 11, without showing any signs of a squat effect. Also, the brittle-ductile transition occurred very late on these specimens as compared to coal-crete or sandstone. It was suggested that the texture of coal and the roughness of developing fracture surfaces is not comparable to the texture and residual friction being built-up in the granular materials.

Due to the discrepancy of the test results between coal and the other test materials, it cannot be readily assumed that coal pillars will show a squat effect at all. The question that will have to be answered in this context is whether in-situ coal behaves like the coal-crete and rocks that were tested in the experimental study, or like the actual coal specimens.

It was hoped that indications to that question would be found by comparing the mechanical material properties of the materials with the shape effect in specimens and pillars. Some striking similarities were found, especially in terms of the link between the gradient of strength increase and the compressive strength, elastic modulus and cohesion of the material. However, the post-failure behaviour of in-situ coal pillars and specimens was shown to follow patterns which did not correlate with the basic material properties.

Further insight into the expected in-situ pillar behaviour will be deduced from the numerical modelling exercise in the following chapters.

PART IV

Numerical modelling of strength and failure in squat coal pillars

15 Introduction to pillar modelling in FLAC

In Chapter 13.2 it was reported that coal specimens with large width-to-height ratios tested in compression exhibited neither a squat effect, nor a marked brittle-ductile transition in the range of $w/h=$ 10. Coal-crete, sandstone and granite specimens however, showed a squat effect at about $w/h=$ 4 and, in the case of the first two named materials, also showed the brittle-ductile transition.

It has been reasoned in Chapter 14.2 that this difference in behaviour must be controlled by parameters other than external boundary conditions or internal, intact material properties. This was concluded because coal exhibited the most competent platen-specimen interface in terms of friction, and because the coal's intact material properties, c and ϕ, were shown to lie in between those of the materials which were able to perform a squat effect and the brittle-ductile transition.

Therefore it was suggested that the behaviour must be controlled, or at least significantly influenced by the residual material properties after fracturing.

This hypothesis is further tested by means of numerical modelling. The two-dimensional explicit finite difference code FLAC (Itasca Consulting Group, Minneapolis, U.S) for engineering mechanics computations, is used for this exercise.

The particular advantage of FLAC is its built-in Mohr-Coulomb strain-softening constitutive material law, which has the capacity to simulate brittle failure processes in coal and rocks.

A typical FLAC coal pillar model requires the following input parameters: density; elastic modulus and Poisson's Ratio, or alternatively, bulk and shear modulus; peak and residual material cohesion and friction and the related plastic strain that is allowed to take place during the transition from peak to residual strength; dilation angle of the material; tensile strength.

The complexity of input parameters increases when a failure criterion for the surrounding rock strata is used (the same catalogue of input parameters as for the coal may apply) and when a mechanical interface in the pillar-strata system is specified. The minimum requirements for the latter are: shear and normal stiffness, peak cohesion and friction. Residual interface properties may be specified as well.

Any given combination of the listed model input parameters influences the output of the model. In addition the model results will be controlled by the selected mesh density, shape, and the boundary conditions (rate of compressive loading, lines of symmetry, configurations of the pillar-strata system).

It is beyond the scope of this research to investigate all likely combinations of all these input parameters. Therefore, some limitations will be given to this study:

- Failure will only be allowed to occur in the coal pillar, i.e. the surrounding strata always remains elastic. The issue of pillars punching into the strata will not be addressed;
- The coal pillar will be simulated as a brittle material, i.e. the plastic strains for the transition between peak and residual material strength will be taken as practically zero for most of the modelling exercise;
- The study aims at identifying the sensitivity of pillar shape effects towards residual material properties. Hence some input parameters will be taken as constants, such as the elastic modulus, Poisson's Ratio and tensile strength of coal. Others, such as the angle of dilation, will be ignored. Those parameters will not be subjected to a sensitivity study.

In order to further limit the possible range of input parameters, a review of published coal pillar models is conducted so as to identify a typical range of coal properties and interface properties.

Shape and possible squat effects in the simulated coal pillars will first be analysed under very simplified boundary conditions. Here, the pillars are simply taken as rectangular blocks which are either entirely free to expand laterally, or rigidly confined along their top or bottom boundaries.

The scope of this first exercise is solely to study shape effects and their dependence on material properties under idealised boundary conditions, with particular focus on the influence of residual strength properties on the overall pillar performance. Once the basic mechanisms contributing to the relevant phenomena are established, the models will be extended to represent the more realistic boundary conditions, as they apply in-situ.

Subsequent to the conceptual modelling exercise, some considerations on calibrated coal pillar models and their extrapolation into the squat shape range will be presented.

16 Survey of published numerical coal pillar models

A literature survey of typical input parameters for numerical coal pillar models is conducted in the following section. The use of constitutive laws, model calibration procedures and the derived mechanical properties for the pillar-strata-system by different authors (Iannacchione, 1990; Müller, 1991; Vervoort, 1992; Duncan Fama, Trueman and Craig, 1995; Gale, 1999; York, Canbulat and Jack, 2000; Mohan, Sheorey and Kushwaha, 2001; Yavuz and Fowell, 2001; Ozbay and Rozgonyi, 2003; Roberts, Ryder and Van der Merwe, 2005; Lu et al., 2008; Gadde, 2009; Jaiswal and Shrivastva, 2009; Oraee, Hosseini and Gholinejad, 2009; Esterhuizen, Mark and Murphy, 2010; Wang et al., 2011) are briefly discussed.

16.1 Constitutive laws for coal pillars

Typical failure criteria for coal used by the different authors in pillar modelling are Mohr-Coulomb and Hoek-Brown failure criteria. The general argument for the Hoek-Brown failure criterion is that it is able to mimic the regressive increase of rock strength in triaxial compression tests, which should be particularly pronounced at high confining stresses. The Hoek-Brown criterion also has the advantage that extensive experience is available on how laboratory-determined intact material properties can be downgraded through rock mass ratings to arrive at suitable rock mass strength properties.

The use of the linear Mohr-Coulomb criterion however, may be justified by the fact that a regressively increasing triaxial strength trend is not discernible for coal. Particularly for confining pressures less than 35 MPa, the triaxial strength of coal exhibits a linear trend (see Chapter 8.3 and Hobbs (1964)). It is expected that this range of confinement will not be excessively exceeded in modelled coal pillars and therefore the use of the Mohr-Coulomb criterion is reasonable.

Either the Hoek-Brown or the Mohr-Coulomb failure criteria have to be implemented as a strain-softening constitutive law in FLAC. In the generic elastic-perfectly plastic notion of the two failure criteria, failed zones in the model would compensate excess stresses beyond their load-bearing capacity by deforming perfectly plastically. However, no breakdown of strength would occur in these plastic elements.

The strain-softening modification of the failure criteria is therefore necessary to simulate the breakdown of strength in failed elements. This is achieved by specifying the deterioration of peak material properties after failure with further increasing plastic strain, until a residual and constant level is reached. The brittleness of failed elements is controlled by the plastic strain increment over which failure is allowed to evolve.

This strain-softening constitutive function is readily available in FLAC for the Mohr-Coulomb failure criterion, which is another practical reason why this failure criterion might be the one of choice. From the literature review it appears that the Mohr-Coulomb strain-

softening approach is more popular amongst researchers as compared to the Hoek-Brown strain-softening model (see Chapter 16.2).

16.2 Mechanical parameters for coal pillars

Mechanical parameters for coal pillars in numerical models are usually determined by calibrating the models against empirical peak strength criteria, e.g. the equations from Salamon and Munro (1967), Bieniawski (1992), Wagner (1974), Van Heerden (1975) and others. Some researchers also made use of stress-measurements and sidewall fracturing observations to calibrate their models. The model input parameters may therefore differ according to which calibration procedure has been used. A summary of the input parameters for Mohr-Coulomb and Hoek-Brown models is provided in Table 10 and Table 11.

The elastic properties, Young's Modulus and Poisson's Ratio, are observed to vary widely between E= 0.36 – 4.0 GPa and ν= 0.2 – 0.34 respectively. Typically encountered values in large-scale tests for coal in South Africa are E= 4 GPa and ν= 0.25. The coal density which has been specified by a few researchers is found to be lower than the typical value of South African coal of ρ= 1.5 t/m^3. The Mohr-Coulomb strain-softening parameters used in numerical models for coal are summarized in Table 10.

Table 10. Mechanical properties assumed in Mohr-Coulomb pillar models.

Investigator(s)	Code, Constitutive law	Coal seam properties							Calibration
		ρ	E	ν	c	φ	δ	σ_t	
		[t/m^3]	[GPa]	[-]	[MPa]	[°]	[°]	[MPa]	
Lu et al. (2008)	FLAC 3D, MC SS	1.3	0.36	0.34	1.62 (i) 0.4 (r)	35 (i) 35 (r)	-	0.15	-
Mueller (1990)	FLAC 2D, MC SS	-	0.5-1 (i) 0.5-1 (r)	0.3 (i) 0.3-0.4 (r)	0.6-10 (i) 0-1 (r)	15-35 (i) 5-30 (r)	0-15	0-2	Laboratory data and in-situ experience
Oraee et al. (2009)	FLAC 2D, MC SS	1.4	4.00	0.30	0.8 (i) - (r)	30 (i) - (r)	0	0.9	Empirical pillar strength formulae
Ozbay et al. (2003)	FLAC 3D, MC SS	1.3	3.00	0.25	2.2 (i) - (r)	30 (i) 30 (r)	-	-	Empirical pillar strength formulae
Vervoort (1992)	FLAC 2D, MC	-	3.00	0.20	1.5-4 (i)	27	-	1.5- 4	Pillar stress and sidewall fracturing measurements
Wang (2011)	FLAC 3D, MC SS	-	1.10	0.30	1.02 (i) 0.102 (r)	36 (i) 30 (r)	6.0	0.04	Combined empirical South African and Australian strength formula
Yavuz et al. (2001)	FLAC 2D, MC SS	-	4.50	0.30	1.44 (i) 0.35 (r)	27 (i) 23 (r)	-	0.7	Van Heerden in-situ stress-strain curve
Roberts et al. (2005)	Elfen, CWFH	-	3.50	0.30	2.84 (i) 0.05 (r)	20 (i) 40 (p) 30 (r)	-	-	Wagner stress-strain curves for w/h= 1 and 2

MC SS – Mohr-Coulomb strain-softening; CWFH – Cohesion weakening friction hardening; (i) – intact; (r) - residual; (-) – not specified

The typical range for the intact angle of internal friction of coal is ϕ_i= 30 – 35˚. Residual values are often taken as equal to the intact values, i.e. no breakdown of friction after failure is specified. In some cases where friction is assumed to reduce in the post-failure state, the drop is observed to be only about 5˚.

The values used for intact cohesion are more dispersed and no more than c_i= 4 MPa. Unlike the frictional material strength, cohesion is always assumed to drop, and more drastically to very low levels of no more than c_r= 0.5 MPa.

The plastic strains over which this drop from intact to residual properties takes place is always different in the model scenarios used by the different researchers and is not listed.

Apparently, the angle of dilation δ of coal is not always specified in published studies, but maximum values of 15° have been observed. The tensile strength of coal is typically below σ_t= 1 MPa.

The Hoek-Brown strain-softening parameters for coal pillar models are summarized in Table 11. One observes that the 'a'- parameter is sometimes modified from the standard 0.5 to 0.65 in order to obtain a different curvature of the triaxial strength trend for coal. The m-value, whose function in the Hoek-Brown failure criterion can be likened to the angle of internal friction in the Mohr-Coulomb criterion, is relatively consistent for intact coal pillars with m= 1.47. Residual m-values differ but it is noteworthy that they are typically assumed to be significantly lower than the intact values. The s-parameter (which is the counterpart to cohesion in the Mohr-Coulomb model) can vary by magnitudes, which may be due to the different numerical codes used in the modelling exercise.

Table 11. Mechanical properties assumed in different Hoek-Brown pillar models.

Investigator(s)	Code, Constitutive law	Coal seam properties						Calibration
		ρ	E	ν	HB coal mass			
		[kg/m^3]	[GPa]	[-]	a	m	s	
Duncan Fama et al. (1995)	3D FEM, HB SS	-	2.50	0.24	0.5	2.83 (i) - (r)	0.0004 (i) - (r)	Empirical pillar strength formulae
Esterhuizen et al. (2010)	FLAC 3D, HB SS	-	3.00	0.25	0.7	1.47 (i) 1.0 (r)	0.07 (i) 0.001 (r)	Bieniawski formula and stress-measurements in coal ribs
Jaiswal et al. (2009)	3D FEM, HBSS	-	2.00	N/A	0.5	1.47 (i) 0.125 (r)	0.01 (i) 10E-6 (r)	Stable and failed cases in India
Tesarik et al. (2013)	FLAC 3D, HB SS	-	3.79	0.25	0.7	1.47 (i) 0.36 (r)	0.07 (i) 0.001 (r)	Van Heerden stress-strain curve of specimen w/h= 2.78

HB SS – Hoek-Brown strain-softening; (i) – intact; (r) - residual; (-) – not specified

16.3 Mechanical parameters for coal-rock-interfaces

Coal-rock-interfaces are consistently modelled by different investigators using the Mohr-Coulomb criterion in its original elastic-perfect plastic form. Only one researcher assumed that the interface to obeys a strain-softening law (Mueller, 1990). The interface properties found in literature are summarized in Table 12.

Table 12. Mechanical properties for coal-rock-interfaces assumed in different pillar models.

Investigator(s)	Code, Constitutive law	Interface properties		
		φ [°]	c [MPa]	σ_t [MPa]
Duncan Fama et. al. (1995)	3D FEM, MC	16	0.012	-
Esterhuizen et. al. (2010)	FLAC3D, MC	25	0.1	0
Lu et al. (2008)	FLAC 3D, MC	20	0.35-2.07	-
Mueller (1990)	FLAC 2D, MC SS	5-25 (i) 3-20 (r)	0-5 (i) 0-0.5 (r)	0-2
Ozbay et. al. (2003)	FLAC 3D, MC	20	0.5	-
Wang et al. (2011)	FLAC 3D, MC	20	0.5	-

MC – Mohr-Coulomb; MC SS – Mohr-Coulomb strain-softening; (i) – intact; (r) – residual; (-) – not specified

Typical values of interface friction used in FLAC codes range between φ= 20 – 25° and the interface cohesion is generally less than c= 0.5 MPa with only one exception. A tensile strength is generally not specified or set to zero.

The assumed values for the friction angle on coal-rock interfaces are further substantiated by empirical shear tests on specimens reported by York, Canbulat and Jack (2000). The authors had obtained a number of borehole samples for testing the contact friction angle between various combinations of coal and sedimentary rock types, i.e. sandstone, carbonaceous sandstone, laminated sandstone, shale, carbonaceous shale, mudstone, calcite and coal. The tests were conducted on both open and intact interface contact conditions.

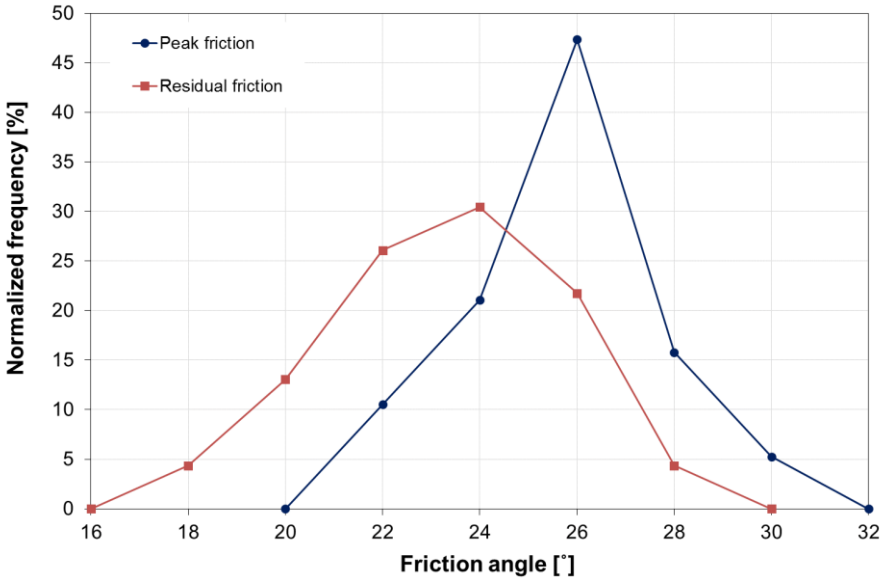


Figure 84. Normalized frequency distribution of coal-rock friction angles, re-analysed after specimen tests provided by York, Canbulat and Jack (2000).

The data provided by York, Canbulat and Jack (2000) was reviewed and two outliers[3] were removed from the database. The remaining data set of 23 tests on various combinations of coal and rock yielded the frequency distribution as shown in Figure 84. The average peak friction angle is found to be φ_p= 24.8˚ and the average residual friction angle to be φ_r= 22.4˚. The standard deviation is 2.3˚ for both the observed peak and residual friction angles.

Esterhuizen (1998) reported on laboratory shear tests on coal specimens with either natural discontinuities or saw-cut surfaces. He obtained values for peak friction of $\varphi_p \approx$ 22˚ and residual friction ranging between φ_r= 19 – 29˚.

[3] A very high residual friction angle of 34˚ between sandstone and granite was discarded because they were not representative for coal measures. Likewise, a very low peak friction angle of 11 ˚ between mudstone and carbonaceous shale was identified as not representative for coal-rock contacts as well.

17 Conceptual modelling of shape effects in pillars

In the following sections, the influences of material properties on shape and possible squat effects in pillars of different width-to-height ratios are investigated. The study focusses in particular on the influence of residual friction in failed material on the model performance.

17.1 Model design

Three scenarios (S1 – S3) are developed, in which two-dimensional pillars of varying width-to-height ratios between 1 and 10 are loaded in vertical compression. The material is assumed to behave in a brittle manner with instantaneous cohesion drop at the onset of plasticity. Friction is either allowed to remain constant prior and subsequent to failure (S1, S3) or is also instantaneously dropped to a residual level at onset of plasticity (S2). The instantaneous drop of material properties from intact to residual values is simulated with the FLAC strain-softening model, where the drop is defined to occur over a plastic strain interval of dε_p= 0.001.

The intact Mohr-Coulomb **material properties** (c_i, ϕ_i) and residual properties (c_r, ϕ_r) used in the three scenarios, together with the elastic properties (E, ν) and the material's tensile strength σ_t are listed in Table 13.

Table 13. Material properties for FLAC model scenarios S1 – S3.

Scenario	c_i [MPa]	c_r [MPa]	ϕ_i [°]	ϕ_r [°]	E [GPa]	ν	σ_t [MPa]
S1	4	0.1	30	30	4	0.25	0.5
S2	4	0.1	30	20	4	0.25	0.5
S3	4	0.1	20	20	4	0.25	0.5

Based on those three scenarios, a comparative assessment of the role of intact and residual properties on the shape effect in pillars can be made. Available for comparison are: one pair of models with the same intact properties but different residual properties (S1, S2), one pair of models with different intact but same residual properties (S2, S3) and one pair of models with the same intact and residual properties but different magnitudes (S1, S3).

The **pillar geometry** involves two lines of symmetry, i.e. along the vertical and horizontal centre lines. Hence only a quarter of the pillar needs to be simulated in FLAC, as shown in Figure 85. This has the advantage that for the same computation times, a higher resolution of the problem can be achieved. The quarter-pillars are modelled with 30 square zones in the vertical direction and a varying number of zones in horizontal direction, depending on the width-to-height ratio requirements. It was found that the used mesh was sufficiently dense to allow strain-localisation and distinct shear planes to develop.

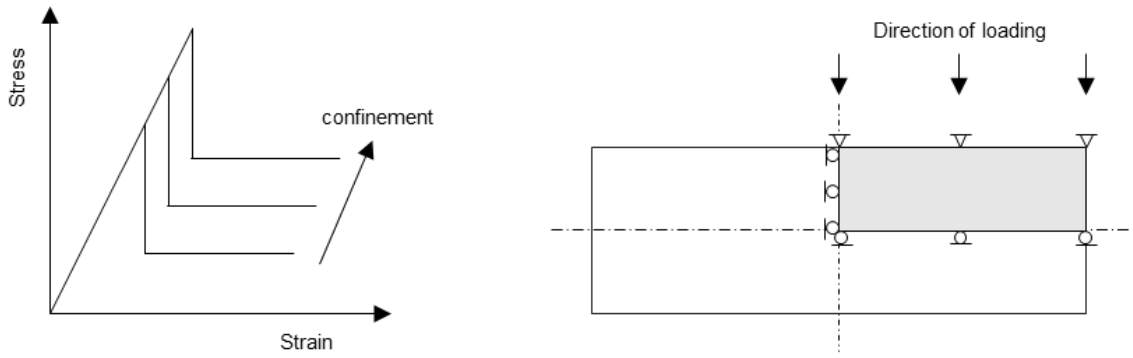


Figure 85. Schematic illustration of constitutive material model (left) and boundary conditions used in the pillar model scenarios S1 – S3 (right).

Failure patterns similar to those observed in laboratory specimens could be generated. The **boundary conditions** are such that the same rate of velocity-controlled loading is applied to the top side of all models. The supposed contacts between the pillar and the rock strata environment, which are not explicitly modelled, are simulated either as being perfectly lubricated or perfectly rigid (the latter case is demonstrated in Figure 85).

The perfectly lubricated boundary condition implies that there is no resistance of any kind to the lateral expansion of the pillar boundaries. Hence it is an exaggeration of the boundary condition of an in-situ coal pillar sandwiched between weak layers of clay.

The perfectly rigid case of boundary condition means that no lateral displacement is allowed at any grid point along the immediate pillar boundary. This may refer to underground environments where the coal pillar is sandwiched between very strong sandstone layers, and which has competent cohesive and frictional interfaces. In such an environment, lateral shear will eventually take place in the weakest element of the pillar-strata system, which is the coal itself. Thus the system can develop its own interface.

During loading of the pillars, the typical pillar stress-strain response is monitored by recording the average pillar stress (APS) across the pillar top surface and the average strain along the vertical symmetry line by means of a FISH (the built-in programming language of FLAC) function. From these stress-strain curves, the peak APS and the residual APS after failure are observed.

The stress-strain behaviour of a pillar will be evaluated over a fixed range of vertical strain. Brittle pillars in scenario S1, for instance, require about 20 mStr to reach the final residual stress state. Brittle pillars in scenarios S2 and S3 reaches their residual stage at not more than 15 mStr. This is important information for the evaluation of the brittle-ductile transition in pillars, since pillars of larger w/h-ratios, which deform in a ductile manner in the range up to 15 or 20 mStr, have been observed to ultimately exhibit a sudden strength drop. However, this drop occurs only at a much later stage, at strain values of about 5 times higher than the previous brittle pillars of lower width-to-height. These pillars will be judged as being ductile, for all practical purposes. Figure 86 shows such behaviour for model pillars in scenario S2.

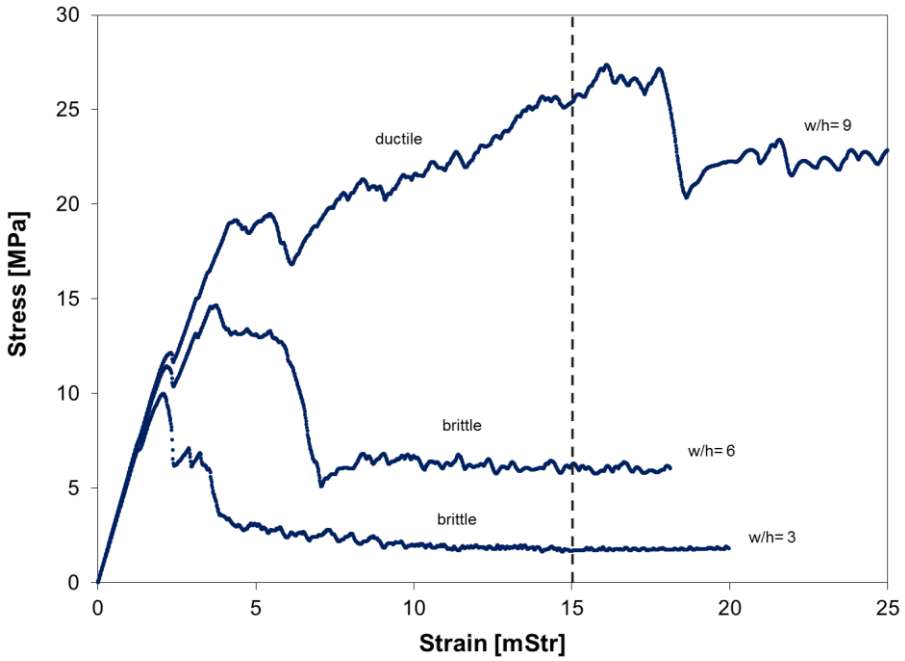


Figure 86. Typical stress-strain behaviour for brittle FLAC pillar models in scenario S2.

17.2 Observations on shape effects and failure patterns

The results of the peak and residual pillar strength produced by the three scenarios S1 – S3, under rigid and lubricated boundary conditions is shown in Figure 87 to Figure 89 and will be discussed in the following paragraphs.

For **unconfined**, fully lubricated contact conditions between the simulated pillar and the strata, FLAC computes constant peak and residual pillar strength values over the entire range of pillar width-to-height ratios up to 10 (Figure 87 to Figure 89). Consequently, there is no shape effect. It can be shown that the FLAC solutions are the same as the theoretical material strength from the Mohr-Coulomb failure criterion,

$$\sigma_1 = \sigma_c + k\sigma_3 \tag{28}$$

$$\sigma_c = 2\, c\, \sqrt{k} \tag{29}$$

$$k = (1 + \sin\phi)/(1 - \sin\phi) \tag{30}$$

where the equation for σ_1 returns the peak or residual load bearing capacity, depending on whether peak or residual cohesion and friction properties c and ϕ and the peak or residual horizontal confinement σ_3 is being used. In the pillar model with lubricated interfaces, the generated lateral confinement is $\sigma_3 = 0$. Hence, the pillar strength equals the unconfined compressive strength of the material σ_c for all width-to-height ratios. The peak and residual pillar strength values for the three scenarios with **fully rigid** contact conditions are plotted in Figure 87 to Figure 89.

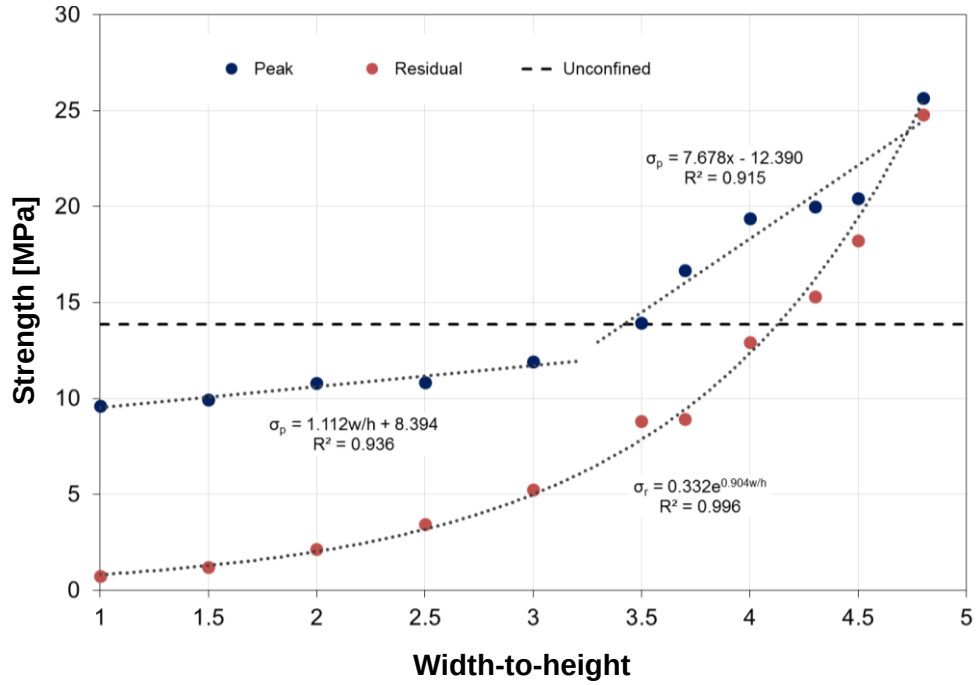


Figure 87. FLAC-computed peak and residual pillar strength versus w/h-ratio for model pillars in scenario S1.

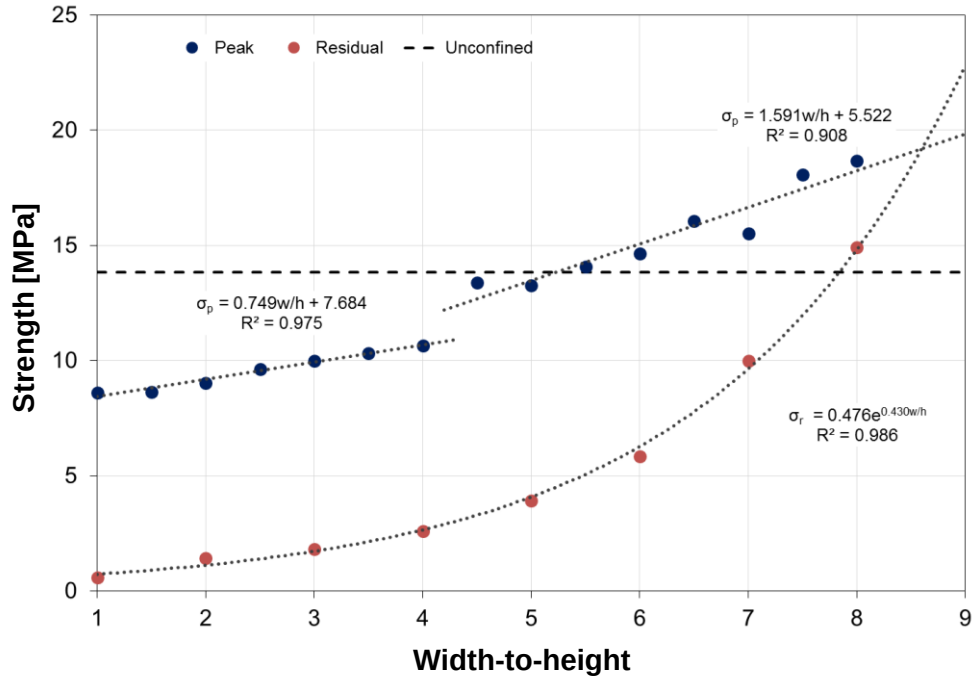


Figure 88. FLAC-computed peak and residual pillar strength versus w/h-ratio for model pillars in scenario S2.

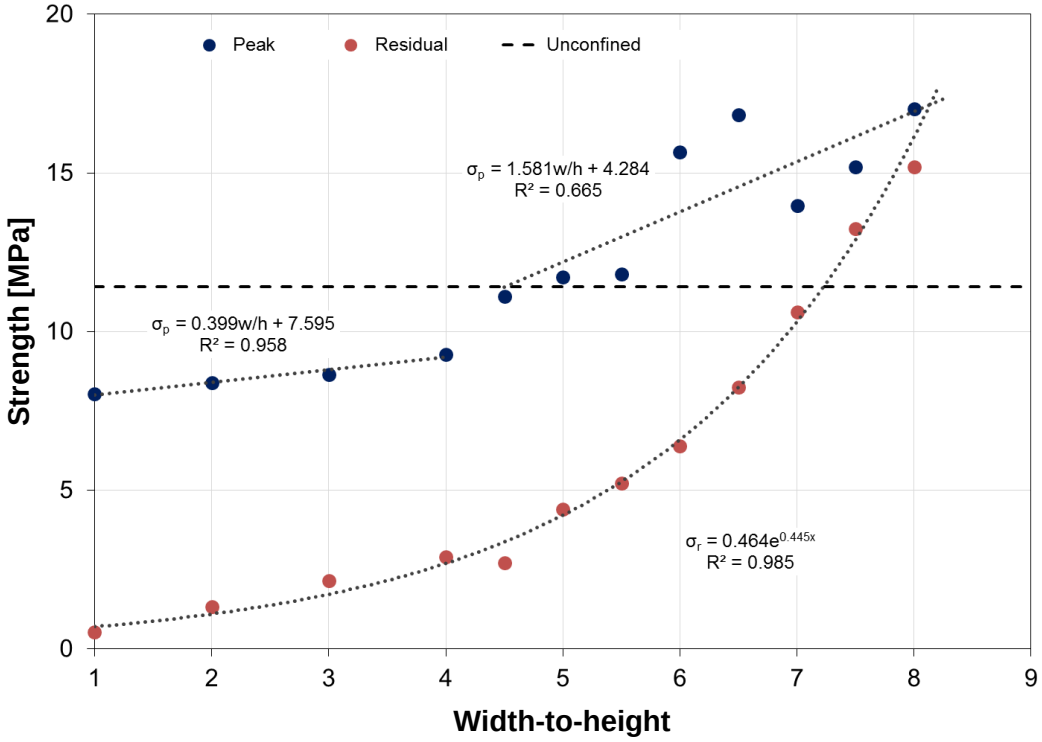


Figure 89. FLAC-computed peak and residual pillar strength versus w/h-ratio for model pillars in scenario S3.

17.2.1 Residual pillar strength

As it can be seen from Figure 87 to Figure 89, the residual pillar strength increases exponentially in all three scenarios. This is in general agreement with limit equilibrium solutions for pillar strength (see Chapter 3.4.1).

For a pillar $w/h=$ 1 the difference in residual strength does not differ markedly between the three scenarios S1 – S3. However, the influence of the residual frictional strength of the material develops an increasingly significant influence as width-to-height ratios increase. Scenario S1 with the highest residual friction property of $\phi_r=$ 30˚, exhibits both the highest residual strength magnitudes and the steepest upward curvature across the various pillar width-to-height ratios. This eventually results in an early brittle-ductile transition of the pillars at just beyond $w/h=$ 4.5.

The scenarios S2 and S3, in which different intact material properties but the same residual friction properties of $\phi_r=$ 20˚ are assumed, show very similar residual strength trends and magnitudes. The slight differences in the regression parameters shown in Figure 88 and Figure 89 are likely to result from the fact that the model pillars are not fully plastic in every zone at the point when the residual strength is recorded, and hence the small dilution of the results with few remaining intact strength properties.

17.2.2 Peak pillar strength

There are two features immediately noticeable about the development of peak strength over the range of width-to-height ratios in the three scenarios:

The first feature is that not a single, continuous trend exists in the relationship between peak pillar strength and width-to-height ratio, but that at least two different types of behaviour prevail. The first trend in the lower width-to-height range is approximately linear, the second one in the higher width-to-height range is markedly more scattered. This is similar in appearance to the described squat effect on specimens in the laboratory.

The second immediate observation is that up until the point in the width-to-height ratio curve where the second strength trend occurs, the pillar's load bearing capacity remains at levels lower than the unconfined strength of the material. This observation is certainly unexpected and will be discussed first.

The evolution of failure in the model pillars is showcased in Figure 90, for a pillar of $w/h=$ 3 in scenario S2. For demonstration purposes, the quarter-symmetric model pillar is mirrored over its symmetry lines to show the full cross-sectional view. The corresponding pillar stress-strain curve for this pillar was shown in Figure 86.

While the pillar is loaded at a constant rate of vertical compression, the first stage of failure occurs at the point where vertical stress concentrations at the pillar corners between the free sidewall and the rigid interface approach a level of 14.4 MPa (Figure 90, image 1). This failure is slightly above the unconfined compressive strength of 13.85 MPa of the material, given the fact that the element is partially constrained along its upper side. The average pillar stress at this point of failure initiation is about 7.1 MPa, or just about 50 % of the unconfined compressive strength of the material. It is apparent from this that the fully rigid interface causes excessive stresses to build up, so that the corner elements fail in shear.

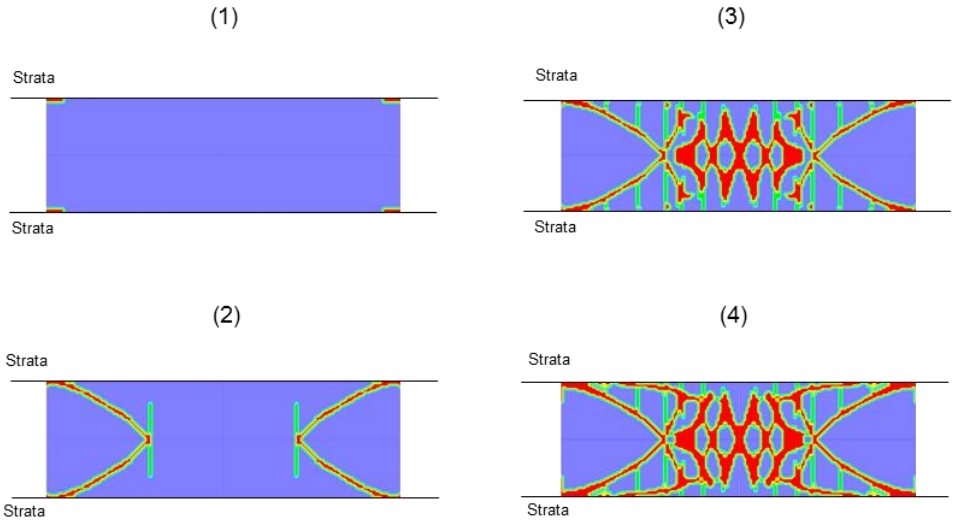


Figure 90. Evolution of failure in a pillar of $w/h=$ 3 with perfectly stiff and rigid interfaces with the surrounding strata, demonstrated as stepwise loss of cohesion (red zones) during pillar loading.

At the same instant, a larger number of zones below the failed corner elements fail in tension. At mid-height of the pillar sidewall, the tensile failure stress is approximately 0.58 MPa, which is about the tensile strength of 0.5 MPa of the material. The difference arises again from the fact that the zone in question receives some small confinement from its neighbouring zones.

The failed pillar sidewalls are consequently de-stressed, and the further displacements forced upon the pillar causes further stresses to be pushed into the remaining intact pillar core.

Next (Figure 90, image 2), a shear band develops from the pillar-strata-interface towards the pillar centre, originating at about $APS=$ 10.0 MPa. This is also the peak load bearing capacity of the pillar in the given scenario, since it will not be able to recover from the development of the shear band with further compression. In scenario S2, only pillars of width-to-height ratios greater than 4 demonstrate the capacity to recover from this early failure and to increase its load-bearing capacity with further deformation.

It should be noted that at the stage of peak strength failure, the pillar consists of both a failed zone, and an inner, intact core. The failed zone, in which the shear band has developed carries practically no vertical stress (as it will later be shown in Figure 91).

This remaining intact core however, is not able to sustain a further increase in vertical strain forced upon it. Gradually, failure penetrates further into the core while the stress-strain reaction curve is on its descending branch, until the onset of the residual strength phase (Figure 90, image 3). At this point, the pillar is not entirely crushed, as can be seen from the cohesion plot in Figure 90. However, further deformation upon the pillar is only partially converted into a crushing of the residual intact fragments, since only smaller changes occur in the distribution of cohesion within the pillar between 5 – 20 mStr average vertical strain (Figure 90, image 4). For the other part, the deformation of the pillar boundaries is compensated for by relative sliding of the remaining intact wedges.

In summary, one must conclude that a pillar-strata-interface, which is too rigid and does not allow for relaxation movements to occur along its boundaries, causes undue stress-concentration and therefore initiates premature failure of the pillar. This premature failure, i.e. failure at average stress levels below the unconfined compressive strength, is seen to be overcome only by pillars with larger width-to-height ratios.

The critical width-to-height ratio, at which the pillar strength exceeds the unconfined compressive strength of the material, is $w/h=$ 3.5 for the scenario S1 (Figure 87) with competent intact and residual friction angles of 30°. For scenarios S2 (Figure 88) and S3 (Figure 89), where lower residual friction angle of 20° is used, the critical width-to-height ratio is about $w/h=$ 5.

These critical width-to-height ratios coincide with the point at which a markedly increased strength in the strength versus width-to-height relationship appears. This brings the discussion back to the observations that at least two trends prevail in the peak strength versus width-to-height relationship.

Regressing the peak strength points in Figure 87 to Figure 89 from $w/h=$ 1 forward to the critical width-to-height ratios, shows that the first trend is linear, in all three scenarios. Magnitude of peak strength and the strength gradient (i.e. the rate of increase in strength over width-to-height) ranks in the three scenarios from highest to lowest in the order of S1 – S2 – S3.

It is therefore shown that both the intact and the residual properties influence the shape effect in pillars, which can further be understood from the context that at peak strength failure, the pillar is only partially destroyed and partially intact. This aspect will be dealt with in more detail at a later stage.

By the end of the linear strength trend, i.e. from the critical width-to-height ratio of $w/h=$ 3.5 in S1 and $w/h=$ 5 in S2 and S3 onwards, a rapid increase in the strength versus width-to-height ratio relationship follows. The peak strength of pillars that follows is now more scattered and does not exhibit a clear trend. However, a linear relationship is approximated here for simplicity of analysis.

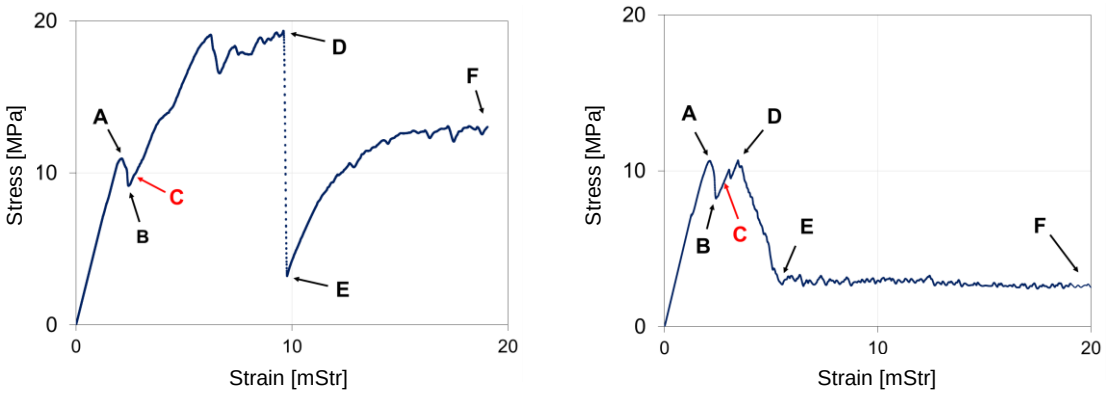
The question arises as to the mechanism behind the kink in the strength versus width-to-height ratio relationship. The following two statements can be derived from the modelled scenarios S1 – S3 so far:

- The kink occurs in all three scenarios, regardless of the magnitude of intact or residual properties, and at different width-to-height ratios. It occurs at the same critical width-to-height ratios for scenarios S2 and S3, where different intact material friction but the same residual material friction was selected. This suggests that the critical width-to-height ratio for the occurrence of the kink is related to the residual friction properties.
- If the magnitude of the kink is quantified as the ratio κ of the assumed two linear strength gradients m_1 and m_2, with $\kappa= m_2/m_1$ and $m_2>m_1$, then it ranks from S1 ($\kappa=$ 6.90) over S3 ($\kappa=$ 3.76) to S2 ($\kappa=$ 2.21). The kink is larger the higher the intact material properties and the lower the drop to the residual properties is.

Further studies will have to be conducted to confirm the observed trends. The influence of residual strength properties on the occurrence of the kink at a given width-to-height ratio is demonstrated in Figure 91, where the example of a pillar of $w/h=$ 4 in S1 and S2 is taken up. In S1 the pillar has already experienced a squat effect, while in S2 this is not the case. The investigation is carried out to identify the relationship between residual friction and the squat effect. The complete stress-strain behaviour of pillars with $w/h=$ 4 in the two scenarios S1 and S2 is showcased in Figure 91.

Scenario S1: $\phi_p = \phi_r = 30^\circ$
w/h= 4
Analysis at Point C: 85000 steps,
APS= 10.2 MPa , Strain= 2.8 mStr

Scenario S2: $\phi_p = 30^\circ, \phi_r = 20^\circ$
w/h= 4
Analysis at Point C: 85000 steps,
APS= 9.4 MPa , Strain= 2.8 mStr



Plots of cohesion (1), vertical stress distribution YY-stress (2) and horizontal stress distribution XX-stress (3) in pillars in scenarios S1 (left) and S2 (right) modelled in quarter-symmetry.

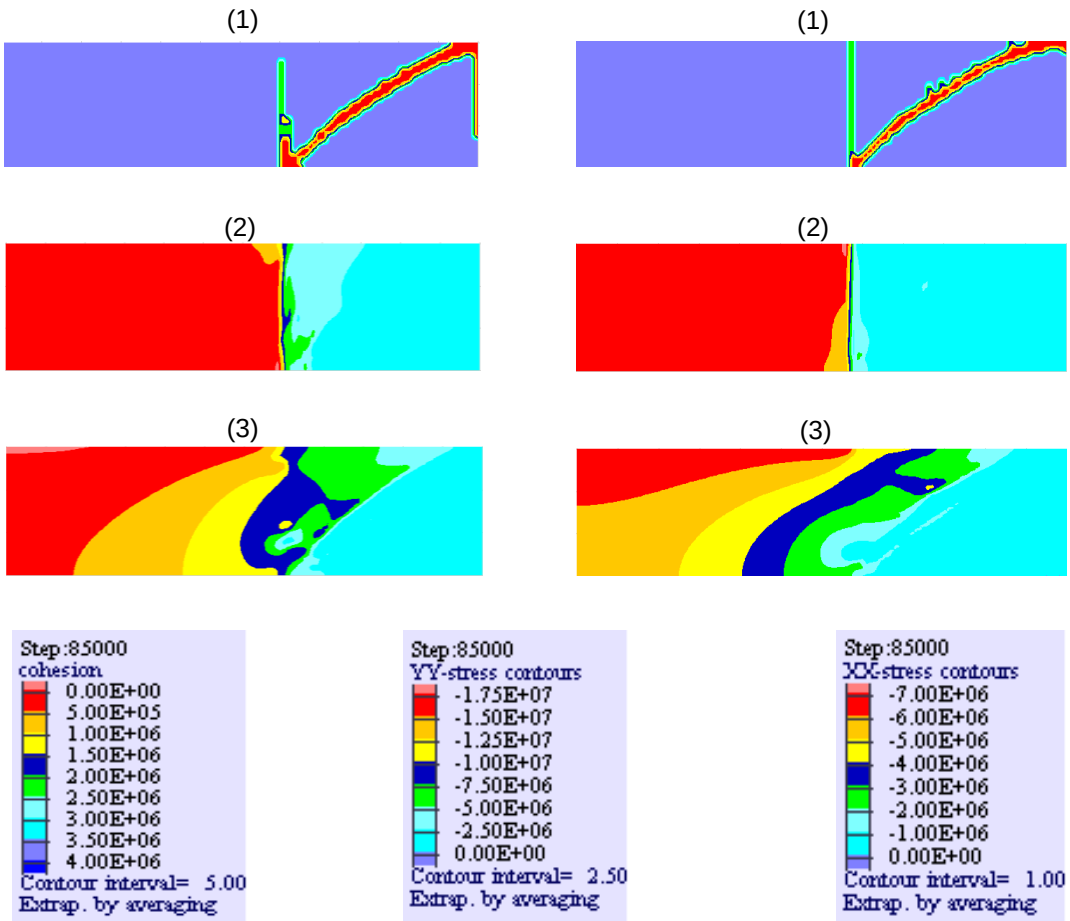


Figure 91. The effect of residual friction on the squat effect in FLAC model pillars.

The characteristic features of the two curves are outlined in the following:

- **Origin – A:** Initial elastic response of the pillars to vertical compression. At stress levels of approximately 70 % of point A, the corner elements along the upper pillar boundary, i.e. the fictional interface with the strata, fail.

- **A – B:** Development of a shear band in both pillars, which can be observed in the cohesion plots in Figure 91**.** The shear band starts from the upper right edge at APS= 10.9 MPa in S1 and APS= 10.4 in S2 and propagates towards the specimen centre. The shear band development causes a temporary drop in the average pillar stress.

- **B – D, C:** The average pillar stress recovers from its drop after the shear band development and increases towards the peak pillar strength. In this phase, the failed pillar sidewalls are essentially de-stressed and the increasing average vertical pillar stress is carried by the remaining intact pillar core.

  Point C is an arbitrarily selected point after the shear band has fully developed. In both scenarios, it gives the state of the pillar at 85000 calculation steps in FLAC and therefore the same vertical strain of 2.8 mStr. Subsequent to this point, the pillar in scenario S1 with residual friction ϕ_r= 30˚ can increase its APS significantly beyond the stress level where the first shear band developed. The pillar in scenario S2 with residual friction ϕ_r= 20˚, however, reaches its peak load bearing capacity soon after point C is crossed.

- **D – E:** Failure of the remaining pillar core. In scenario S1 this failure causes instabilities in the FLAC model, which in return cause a large drop in average pillar stress. This drop can be partially recovered up to the level of residual pillar stress. In scenario S2, the failure of the core is less abrupt and the average pillar stress reduces gradually to the residual strength level.

- **E – F:** The pillar stress approaches its residual stress level.

Point C has been selected in order to demonstrate how the fate of the pillar depends on its residual strength properties after some initial failure has taken place. At point C, both pillars in scenarios S1 and S2 are subjected to the same level of vertical strain and show the same pattern of failure. However, the pillar in S1 will be able to increase its strength markedly (i.e. it will show a squat effect), while the pillar in S2 will fail prematurely at a significantly lower stress level.

The plots of the vertical stress distribution (2) indicate that the outer zone of the pillar, from the sidewall towards the depth of the shear band penetration within the pillar, carries very little or no vertical stress. Therefore, all remaining and further induced vertical stresses will be imposed on the pillar centre. At point C, the average vertical pillar stresses in both scenarios are similar, APS= 10.2 MPa in S1 and APS= 9.4 MPa in S2.

The horizontal stress distribution (3), however, follows a different pattern: only the wedges enclosed by the pillar sidewall and the shear bands are de-stressed. The immediately adjacent, intact material, is laterally confined by the failed wedges and therefore carries some amount of horizontal stress.

The stress-contour plots (3) reveal that the generated horizontal confinement in the remaining intact core is much more competently developed in scenario S1 compared to S2, i.e. it increases more rapidly towards the pillar core. The higher horizontal confinement allows the pillar to carry greater vertical stresses and hence the superiority in strength of the pillar in S1 compared to S2. In this context, it should be noted again that the only difference between S1 and S2 is the assigned value for residual friction. It was thus demonstrated how sensitive pillar strength and possible squat effect are t the residual material strength properties.

17.3 Correlations between material properties and shape effects

The parametric study on the influence of residual material strength on the overall pillar performance is expanded to incorporate a wider range of residual friction properties. The intact material strength is again defined by c_i= 4 MPa and ϕ_i= 30˚ and the residual strength by the previously chosen c_r= 0.1 MPa and, in 6 different scenarios, ϕ_r= 30˚, 27˚, 25˚, 23˚, 20˚, 15˚ and 10˚. The drop from intact to residual values occurs again instantaneously over a plastic strain of 0.1 mStr. Both the development of residual strength and peak strength is studied until brittle-ductile transition occurs, or up to a width-to-height ratio of 12.

It has been shown previously in Chapter 17.2 that the predicted **residual pillar strength** over width-to-height follows an exponential trend. It was observed that the higher the residual material friction angle in the models, the steeper the curvature of the residual strength trend.

The generic expression for the residual strength trend is:

$$\sigma_r = a \exp(b\frac{w}{h}) \tag{31}$$

where parameter a is responsible for shifting the residual strength proportionally over the range of width-to-height and parameter b influences the curvature, i.e. the rate of exponential strength increase.

Both parameters have been found to be a function of the residual friction angle, which is the only parameter varied in this study. Figure 92 shows the correlation plots between a, b and ϕ_r.

Parameter a appears to be practically unaffected by residual friction angles less than 20˚ and a strong correlation only develops for friction angles above that value. In the interval of 20˚$\leq \phi_r \leq$ 30˚, parameter a is seen to decrease approximately linearly despite the fact

that the residual strength increases at a given width-to-height ratio the higher the residual angle of friction is. This is because the parameters a and b are not independent in the regression analysis.

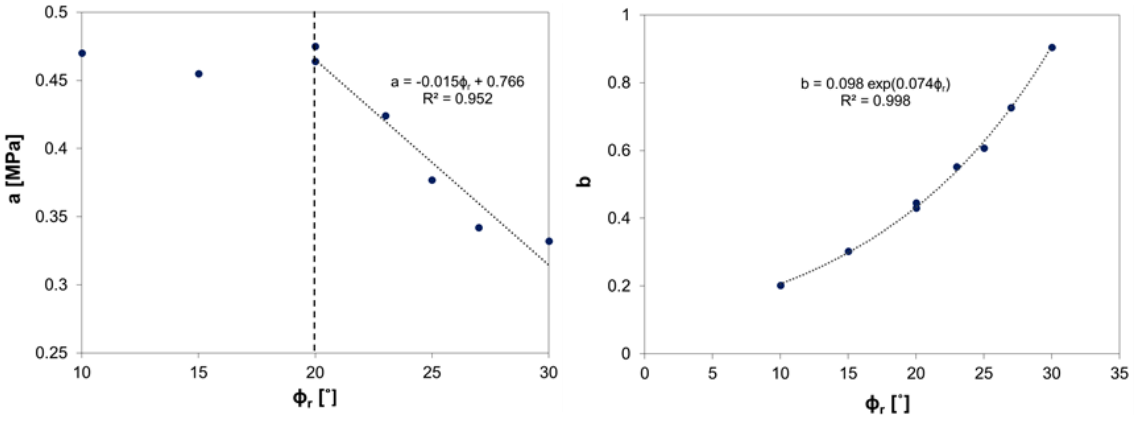


Figure 92. Relationship of the exponential strength parameters a and b with ϕ_r in the FLAC models.

Parameter b is observed to increase drastically over the entire range of residual friction angles used in this study. Since parameter b controls the rate of residual strength increase, it follows that the most rapid exponential strength trend is observed for a friction angle of 30˚, while the trend for a low friction angle of 10˚ is only gently sloping.

Given the exponential nature of the residual strength increase, the critical pillar width-to-height ratio at which **brittle-ductile transition** is supposed to occur should be the lowest for ϕ_r= 30˚ and the highest for ϕ_r= 10˚. In fact, brittle-ductile transition was observed in the models at w/h= 5 for ϕ_r= 27 – 30˚; at w/h= 7 for ϕ_r= 23 – 25˚; at w/h= 9 for ϕ_r= 20˚ and no brittle-ductile transition was observed for the very low residual friction angles of ϕ_r= 10 – 15˚ up to w/h= 12.

The **pillar peak strength** has proven in all scenarios to develop as an approximately bi-linear function of the width-to-height ratio up until the occurrence of brittle-ductile transition. In all modelled scenarios in this study, the first linear trend starting at w/h= 1, is at some critical width-to-height ratio interrupted by a kink. The kink is followed by a second and more rapid increase in strength over width-to-height ratio (compare with Figure 87 to Figure 89). This kink is interpreted as the squat effect in pillars.

The critical width-to-height ratio at which the **squat effect** occurs is again found to be dependent on the residual friction angle of the failed material in the pillar. For high residual friction angles of ϕ_r= 25 – 30° the squat effect occurs at w/h= 3.5, for ϕ_r= 23˚ at w/h= 4, for ϕ_r= 15 – 20 ˚ at w/h= 4.5 and for ϕ_r= 10˚ at w/h= 6.

The rate of peak pillar strength increase before and after the width-to-height ratio at which the squat effect occurs is quantified by the linear slopes m_1 and m_2 respectively. The relationships between these slopes and the residual angle of friction in the different models are plotted in Figure 93.

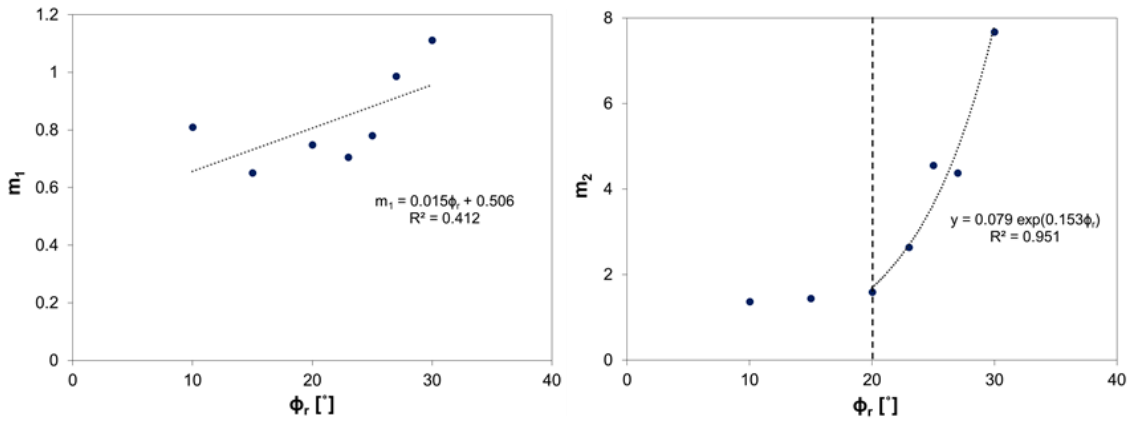


Figure 93. Rates of pillar strength increase m_1 and m_2 prior and subsequent to the squat effect as a function of the assigned residual friction in failed zones of the FLAC models.

The indicated trends are conclusive for the rate of strength increase m_2, after the occurrence of the squat effect: for residual friction levels less than 20°, the rate of strength increase remains practically unaltered at values between m_2= 1.3 – 1.5. With increasing residual friction angles between 20 – 30° however, m_2 increases rapidly and consistently by nearly five-fold over the entire range. This is yet more evidence for how closely the squat effect in pillars is linked to the residual material properties of failed pillar zones.

Prior to the occurrence of the squat effect, a correlation between the strength gradient m_1 and the residual friction angle is less discernible. An incremental analysis of the results indicates that m_1 scatters within a wider band for friction angles of ϕ_r= 10 – 25° without showing any sign of increase and improvement for pillar strength. A relevant increase in m_1 is only evident for friction angles of ϕ_r= 27 – 30°.

This may show that for slender pillars prior to the squat effect, the residual friction angles must be higher, i.e. in the range of ϕ_r> 25°, than those relevant for squat pillars (ϕ_r> 20°) in order to contribute to the overall pillar strength. Also, it is apparent that alterations in ϕ_r have a significantly stronger impact on the strength gradient m_2 than on m_1.

It has been suggested in Chapter 17.2 that the squat effect may be quantified by the parameter $\kappa = m_2/m_1$. In the given scenarios, κ remains at a low value of approximately κ= 2 for friction angles of 10° ≤ ϕ_r ≤ 20°, i.e. a squat effect is also predicted for very low residual friction properties. The ratio then increases very rapidly and approximately linearly in the interval of 20° ≤ ϕ_r ≤ 30° up to a value of just below κ= 7.

It should be noted that all the presented values are only valid for the boundary conditions, mesh sizes, and material properties selected in the current study. Nevertheless, the trends are clear as to the dominating importance of residual material properties on the occurrence of a squat effect, the rate of squat pillar strength increase m_2 thereafter, and the eventual brittle-ductile transition in pillars.

17.4 Accounting for in-situ boundary conditions

The boundary conditions used so far in the conceptual study were drastically simplified: either fully lubricated – allowing for equal lateral displacements across the entire pillar height, or perfectly stiff and rigid – zero lateral displacements at upper and lower boundary, and maximum lateral displacement in the pillar centre.

It was found that model pillars with fully lubricated interfaces experienced an instantaneous strength loss, which always occurred at the uniaxial compressive strength of the material, irrespective of the pillar width-to-height ratio.

On the contrary, model pillars with perfectly rigid and stiff upper and lower boundaries exhibited a shape effect, i.e. the strength increase with increasing width-to-height ratio. However, it was also found that under those rigid boundary conditions undue stress concentrations occurred in the pillar corners which, after propagation, caused premature pillar failure below the uniaxial compressive strength of the material.

Both scenarios exemplify extreme cases and oversimplify the boundary conditions experienced by laboratory specimens and in-situ pillars. Some attempt will be made in the following paragraphs to reproduce the more complete boundary conditions encountered in those environments.

In general these boundary conditions should encompass that (a) forces are transferred onto specimen/pillar through loading platens or rock strata in the roof and floor, which has superior stiffness to the coal specimen/pillar and some geometrical overlap over the specimen/pillar and (b) the specimen/pillar is separated from its loading environment through a mechanical interface, controlled by cohesion and friction.

In the following modelling exercise condition (a) will be realized by modelling a 2D strip pillar with a sandstone-type hanging wall and footwall in quarter symmetry. The overlap of the hanging and footwall over the pillar will be kept very small as compared to in-situ conditions and will be just enough to produce the common stress concentrations at the pillar edges. Also, the lateral boundaries of the rock strata surrounding the pillar will be restricted in its lateral expansion, as would be the case in-situ. The mechanical interface between the pillar and the rock strata, condition (b), is either rigidly attached or modelled with a low cohesion and moderate angle of friction. The model geometry and material properties are shown in Figure 94.

Initial models were also run with the same brittle constitutive law for coal, i.e. instantaneous cohesion and/or friction drop at the onset of plasticity. However, it was observed that these models did not provide meaningful results, in that all pillars of different width-to-height ratios failed at the same stress level, and immediately after fracturing initiated in the pillar corners.

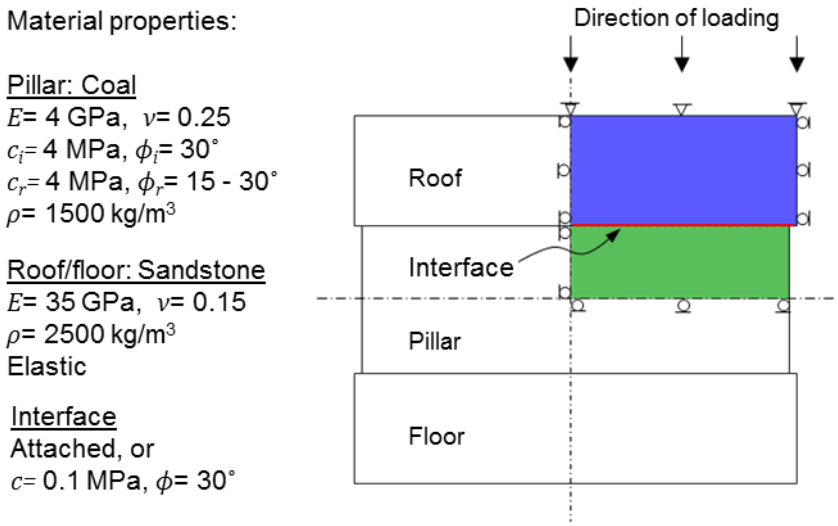


Figure 94. Conceptual FLAC pillar model with in-situ boundary conditions.

This behaviour was found to be similar to that of a soft compression loading system in the laboratory: upon initiation of failure in the test specimens, the stored energy in the loading system is released onto the brittle specimens which results in immediate failure of the specimens.

The solution was then to adjust the model so as to increase its overall stiffness. A first approach was to reduce the loading rate drastically and eventually to use a FISH-function for servo-controlled loading (Anon, 2011) in order to keep the unbalanced forces in the models to less than 400 N. The running time of these models were consequently impractically high and the problem of immediate destruction of the pillar at onset of failure still prevailed.

The next attempt was then to enhance the post-peak stiffness of the coal pillar by means of (a) keeping a fine pillar mesh but reducing the brittleness of the coal by allowing cohesion and friction to reduce over a longer interval of plastic strain $d\varepsilon_p$ or (b) by keeping the brittle constitutive law but reducing the number of zones used in the model to a coarse grid, so as to prevent discrete strain localization.

Both attempts were successful in that meaningful shape effects were encountered in the model pillars. The results of the two different modelling approaches are presented in the following.

17.4.1 Fine grid with reduced pillar brittleness

The characteristics and trends encountered for the pillar models with a fine resolution grid and non-brittle behaviour are summarized in Figure 95. It was found that the brittleness of the coal pillar had to be reduced significantly in order to achieve meaningful shape effects, and after several iterations a suitable plastic strain interval for the drop from peak to residual properties was determined to be $d\varepsilon_p = 0.1$.

The model shown in Figure 94 was run with varying width-to-height ratios, with either attached strata (Figure 95, left column) or a mechanical interface between strata and pillar (Figure 95, right column). In both cases, the coal pillar itself is attributed with the same mechanical properties and constitutive law. All pillars were loaded until core failure occurred.

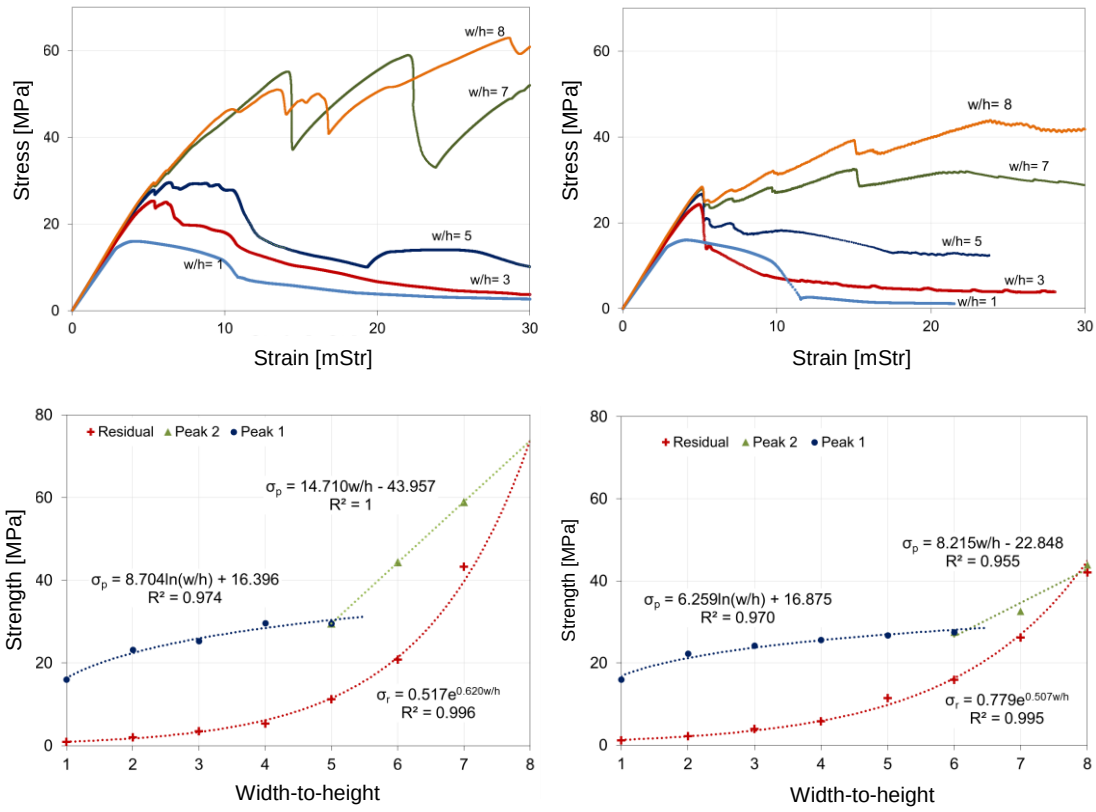
In both scenarios, the shape effect is such that the peak strength increases lognormally, i.e. in a regressive manner, between $w/h=$ 1 and $w/h=$ 5 (attached strata) or $w/h=$ 6 (interface). In this range, the rate of strength increase is only slightly larger for the pillars that are rigidly attached to the strata. Failure always originates at the pillar corner, where the first shear band that will penetrate into the pillar is produced. All pillars fail as soon as yielding is initiated. The same mechanism has been described for the simplified models in the previous study.

A second peak strength trend is observed for pillars with greater width-to-height ratio: the rate of strength increase becomes linear and steeper up to $w/h=$ 8, where brittle-ductile transition occurs in both pillar scenarios. It is important to note that for the second ascending branch of the strength versus width-to-height relationship, the boundary conditions between pillar and strata have a significant impact on the general model performance. A rigidly attached strata produces the greatest rate of strength increase as compared to the mechanically inferior interface.

The corresponding stress-strain curves, however, demonstrate that the peak strength of pillars with $w/h>$ 5 or 6 in the two scenarios is only reached at significantly higher strain values than encountered for the more slender pillars. This gives rise to the question of whether the performance of these pillars should rather be interpreted as strain-hardening for practical mine design purposes, where such large strains might be unlikely to occur. A suitable answer to this question can only be found from calibrated numerical models.

"Fine" pillar mesh, 30 zones vertically
Roof "attached"
Coal pillar strain-softening:
Cohesion drop 4 – 0.1 MPa over $d\varepsilon_p$= 0.1
Friction drop 30 – 20˚ over $d\varepsilon_p$= 0.1

"Fine" pillar mesh, 30 zones vertically
Interface: c= 0.1 MPa , φ= 20˚
Coal pillar strain-softening:
Cohesion drop 4 – 0.1 MPa over $d\varepsilon_p$= 0.1
Friction drop 30 – 20˚ over $d\varepsilon_p$= 0.1



Below: Zones of intact cohesion (blue) and bands of cohesion loss (green, yellow, red) in quarter-symmetric coal pillars after core failure. Left: Pillar model with "attached" elastic sandstone roof (not plotted). Right: Pillar model with elastic sandstone roof separated by mechanical interface.

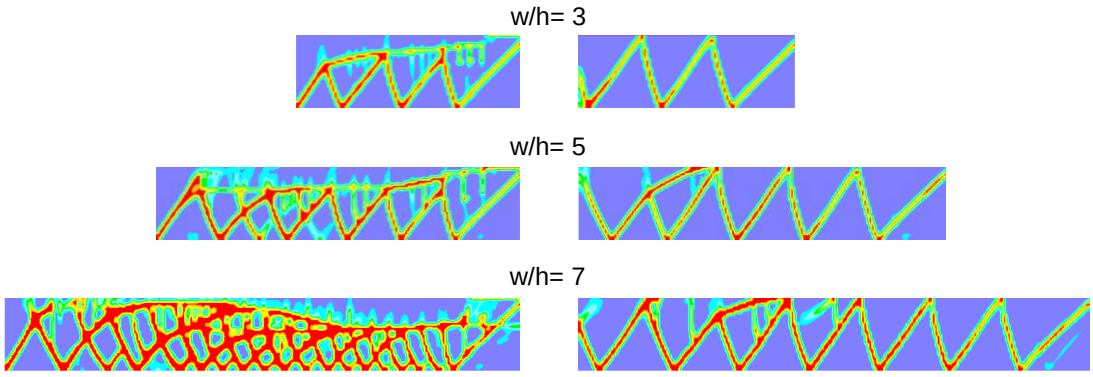


Figure 95. Stress-strain behaviour, strength trends and failure pattern in FLAC model pillars with "fine" mesh, non-brittle constitutive law, in-situ boundary conditions and different w/h-ratios.

An explanation for the relatively poor performance of models with a weak mechanical interface between the strata and the pillar can be found in the failure patterns (Figure 95) produced in the coal pillars. In the scenario where the strata is rigidly attached to the coal pillar, the shear failure occurs just off the pillar-strata boundary within the coal itself, as the coal is the weakest element in the pillar-strata system. The resistance to shear failure of the coal, with c_p= 4 MPa and ϕ_p= 30° is greater than that of the mechanical interface in the other scenario, with c= 0.1 MPa and φ= 20°. Therefore, one function of the attached pillar-strata system is to provide greater resistance to shear failure. The other contribution is that the intact coal immediately adjacent to the strata does not slip laterally and therefore contributes to the overall confinement generated in the pillar. Due to this enhanced confinement, the resistance of the coal pillar against failure is additionally improved. The overall consequence is that the squat effect in these model pillars occurs at an earlier width-to-height ratio, with a more rapid second strength increase.

In return, the failure patterns observed in pillars with a relatively weak mechanical interface are such that shear bands can easily develop between the interface and the pillar centre, producing a uniform zig-zag pattern. Since the interface slips after failure, the residual confinement generated in the pillar is lower. In fact, it is observed in the stress-strain graphs in Figure 95 that pillars up to w/h= 6 and with the weak interface cannot regain strength after the first shear band has developed from the pillar corner. The partial regain of strength, however, can be observed for the rigidly attached pillars.

The residual strength of pillars after failure is again observed to increase exponentially in both scenarios over the full range of investigated width-to-height ratios. However, the interface conditions retain their impact on the pillar performance, even in the final residual strength state, in that the rate of exponential strength increase is markedly more rapid for the attached coal-strata system as compared to the interface boundary condition.

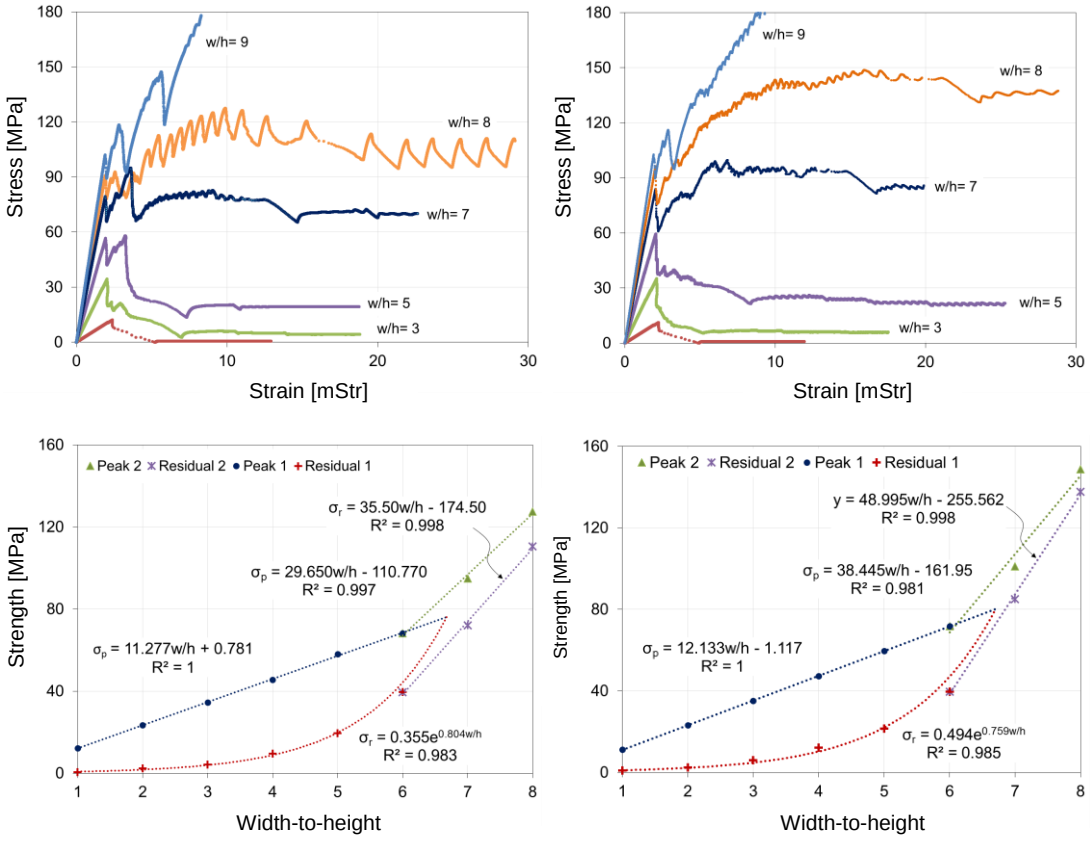
17.4.2 Coarse grid with high pillar brittleness

The performance of model pillars with a coarse grid, i.e. only 10 square zones in vertical direction, and the brittle constitutive law (dε_p= 0.001 as used in the previous, simplified models) is summarized in Figure 96.

The shape effects produced by these models are principally similar to those described for the “fine” mesh and non-brittle models described above, in that two branches of strength increase prevail and that brittle-ductile transition is encountered at an elevated width-to-height ratio. However, the role of the pillar-strata boundary condition is now reversed in these brittle models: the first rate of strength increase in intervals of w/h= 1 – 6 is now slightly higher for the models with a mechanically inferior interface as compared to the fully attached strata. After the squat effect, the superiority of the weaker interface becomes even more pronounced, allowing the pillars to become stronger than their counterparts with attached strata.

"Coarse" pillar mesh, 10 zones vertically
Roof "attached"
Coal pillar strain-softening:
Cohesion drop 4 – 0.1 MPa over $d\varepsilon_p$= 0.001
Friction drop 30 – 20˚ over $d\varepsilon_p$= 0.001

"Coarse" pillar mesh, 10 zones vertically
Interface: c= 0.1 MPa , φ= 20˚
Coal pillar strain-softening:
Cohesion drop 4 – 0.1 MPa over $d\varepsilon_p$= 0.001
Friction drop 30 – 20˚ over $d\varepsilon_p$= 0.001



Below: Zones of intact cohesion (blue) and zones of cohesion loss (green, yellow, red) in quarter-symmetric coal pillars after core failure. Left: Pillar model with "attached" elastic sandstone roof (not plotted). Right: Pillar model with elastic sandstone roof separated by mechanical interface.

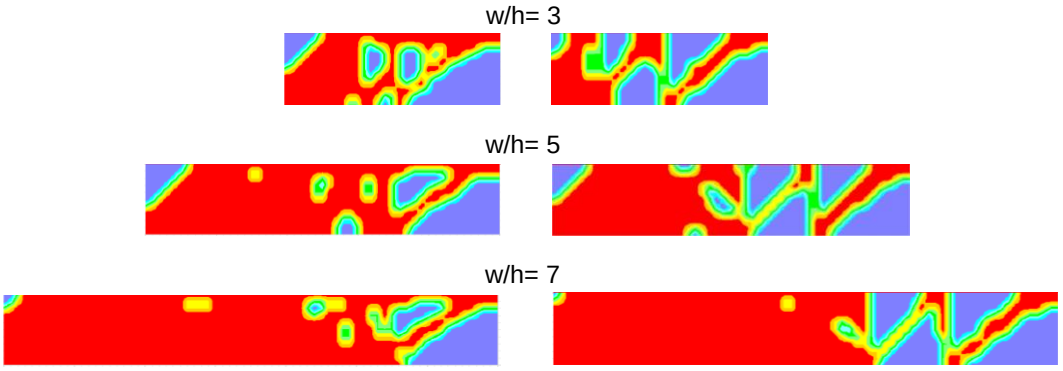


Figure 96. Stress-strain behaviour, strength trends and failure pattern in FLAC model pillars with "coarse" mesh, brittle constitutive law, in-situ boundary conditions and different w/h-ratios.

This observation was certainly unexpected, and some attention was given to the question of whether this effect was caused by the brittle constitutive law or by the coarse pillar mesh and the avoidance of strain localization (the failure patterns in pillars with a coarse mesh are “smeared”). A practical answer was found by running the “coarse” mesh models with the same non-brittle law as for the previous “fine” mesh models. Here it was observed again that the rate of strength increase in pillars was higher for the attached boundary conditions. This suggests that it is the brittleness of the pillar, and not its mesh density, which determines whether a weak interface will work to the advantage or disadvantage of the structure.

Besides the discrepancies produced by the different boundary conditions for the peak pillar strength behaviour, the residual pillar strengths in both scenarios are very similar, which suggests once more that the sensitivity of pillars in different boundary conditions is also dependent on the brittleness of the structure.

An interesting observation is that the exponential trend for the residual strength appears to be terminated as soon as the squat effect occurs in pillars: for pillars with larger width-to-height ratio, the rate of residual strength increase appears to be only linear.

In this context, the question must be raised once more whether pillars beyond the squat effect were not more suitably addressed as being strain-hardening, given the following facts: For one, the strain at which the peak strength of these pillars is encountered is disproportionally large as compared to the more slender pillars. This can be observed in particular for the pillars of $w/h = 8$ in Figure 96. The second reason is that the first trends of linear peak strength and exponential residual strength do predict brittle-ductile transition in pillars of $w/h \geq 7$.

It has been experienced in FLAC modelling that every strain-softening pillar eventually suffers a breakdown in strength, provided that sufficient compression is applied to its boundaries. Therefore, the distinction between brittle pillars (i.e. those which exhibit a strength drop) beyond the squat effect, and strain-hardening pillars, is only a conceptual one. This is also true for the specimens tested in the laboratory, since every intact core of seemingly strain-hardening pillars would eventually crush, if sufficient load can be provided to the specimen.

17.5 Comparison with shape effects in physical specimens

The numerical simulation of pillar strength under various boundary conditions has confirmed all three main characteristics of the shape effect in rocks encountered in the laboratory study. These are: (1) a progressive increase in residual strength over width-to-height ratio; (2) approximate bi-linearity in the peak strength trend; (3) brittle-ductile transition in specimens and pillars. A detailed discussion follows:

1) Progressive increase in residual pillar strength with increasing width-to-height ratio up to the brittle-ductile transition

Numerical pillar models compute an exponentially increasing residual strength for increasing width-to-height ratios, which is in general agreement with analytical models that have been developed by different authors (see Chapter 3.4.1).

Similarly, the residual strength of the rock, coal and coal-crete specimens tested in the laboratory increase particularly, even though an exponential trend is less discernible for most rocks. The trends are generally less well developed, presumably because of the loss of fractured material from the specimen during the post-peak compression, which almost invariably occurs for rocks and coal if no artificial constraint is provided. In the ideal continuum computations of the numerical and analytical models, this loss of material or modification in shape is not considered and hence the improved results for residual strength.

The best trend has indeed been observed for coal specimens. Figure 97 plots the residual strength in coal specimens of different width-to-height ratio as obtained in the laboratory study (Chapters 12 – 14). The best-fitting regression to the data yields a polynomial curve, even though an exponential trend may still represent the development appropriately, in particular for width-to-height ratios up to w/h= 9.

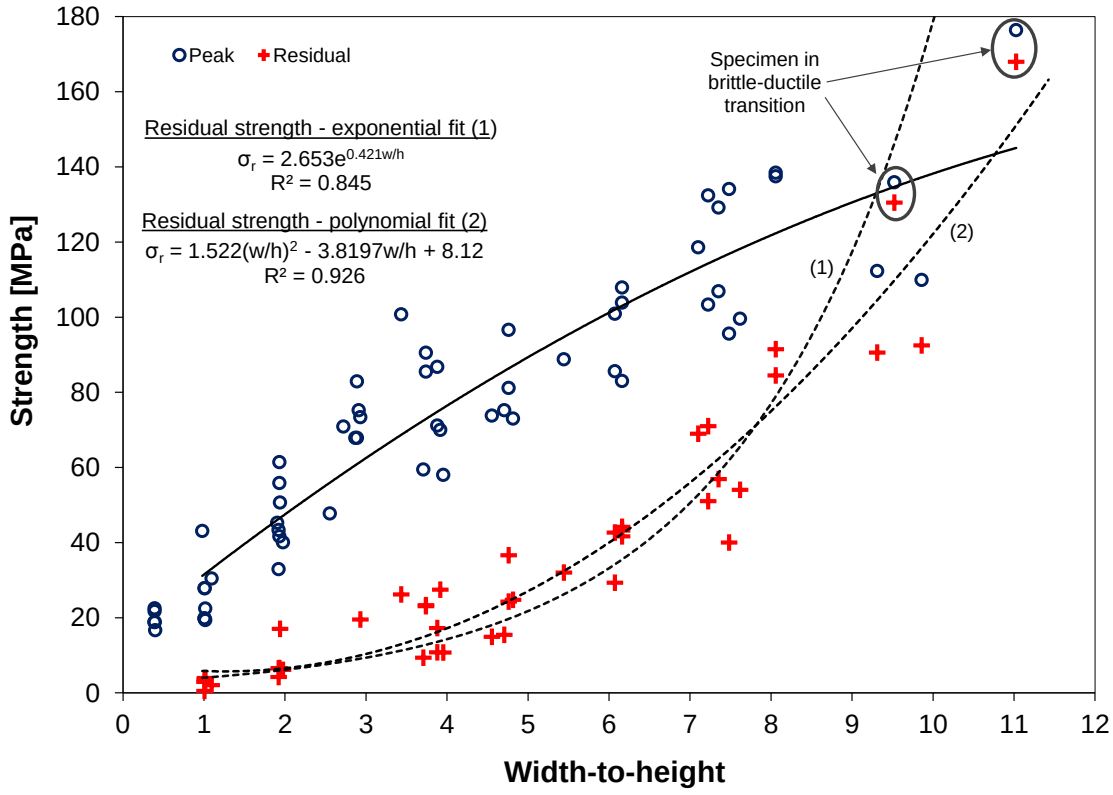


Figure 97. Trends in the residual strength of coal specimens of different w/h-ratio.

2) Approximate bi-linearity of peak pillar strength in its relationship to the width-to-height ratio, caused by a squat effect

Bi-linearity in the peak strength trend has been observed most precisely on the granite specimens tested in the laboratory. It was also indicated by the coal-crete and sandstone specimens. The numerical models do generally confirm this bi-linearity, including two minor phenomena which occurred in the laboratory, namely the small offset in between the first and the second trend branch in the strength versus width-to-height relationship and the relatively larger scatter of results in the second branch.

The critical width-to-height ratio for the occurrence of the second branch of strength increase and the related gradient of strength increase has been shown to depend significantly, though not entirely, on the residual material strength properties. The great sensitivity towards the residual strength properties is because a pillar is always partially failed and intact just before its maximum load bearing capacity is reached and hence the contribution of the failed material to the confinement and load bearing capacity of the remaining intact core. Other contributing factors are the material intact properties and the boundary conditions at the pillar-strata-interface, as shown in Figure 95.

The occurrence of bi-linearity in pillar strength is called the squat effect. The squat effect starts in pillars and specimens when a critical combination of residual strength properties and width-to-height ratio is reached. The lower the residual material strength, the greater the required width-to-height ratio for the occurrence of the squat effect, and vice versa.

In numerical models it was demonstrated that pillars in the first branch of the bi-linear peak strength trend, i.e. before the squat effect, reach their maximum load-bearing capacity when the first shear failure is produced in the structure. They are not able to exceed the stress level at which this first failure is encountered, even if the first shear fracture does not penetrate through the pillar core.

However, specimens and pillars in the second branch, i.e. after the squat effect, can recover from the first shear failure development in its sidewalls, since sufficient confinement is provided to the remaining intact core. The points of first yielding and peak strength loss are therefore clearly distinguished.

This behaviour can also be observed precisely on the granite test specimens. It had already been noted in Chapter 13.1.1 that some stress-strain curves for granite display distinct kinks, related to fracturing of the specimen, before the peak strength is reached.

The stress-strain graphs of granite specimens were re-analysed for the specimen yielding behaviour and the results are plotted in Figure 98 (left). Before the occurrence of the squat effect, the moment of yielding and peak strength loss are practically indistinguishable (yield= peak). When the strength of the specimens increases more rapidly at greater width-to-height ratios, the pre-peak yielding becomes more evident. Interestingly, the level at which yielding first occurs in the specimens appears to be a continuation of the

trend where peak strength loss was encountered in the more slender specimens. This Yield 1 sometimes manifests in the stress-strain graphs as a very small and temporary drop in strength, sometimes only as a deviation of the curve from linearity. Yield 2 however, which occurs subsequent to Yield 1, is always a short breakdown in strength. For comparative purposes, the behaviour of numerical models (the pillar model with attached roof presented in Figure 95 is taken as an example) is plotted in Figure 98 (right) as well.

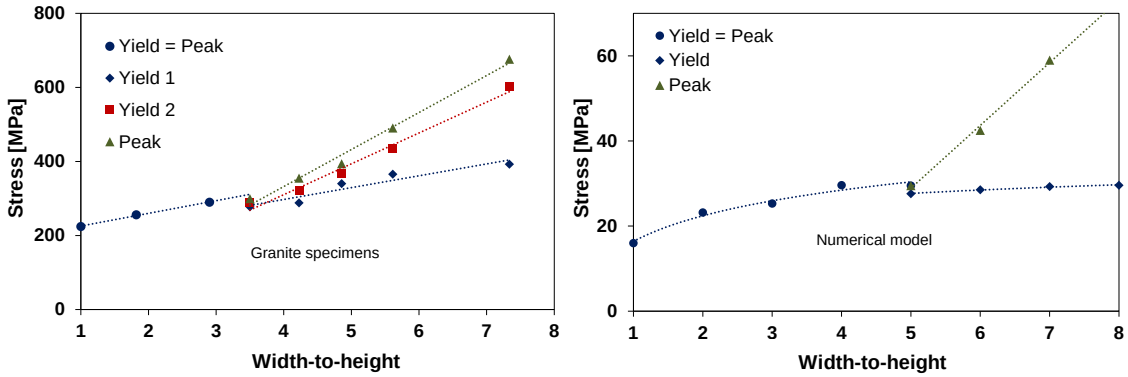


Figure 98. Yield and peak stresses observed in granite specimens (left) and numerical models (right).

Unfortunately, the numerical models have not been able to explain why the squat effect did not occur in coal specimens. The coal specimens tested in the laboratory had shown only a regressively increasing strength trend for the entire range of $1 \leq w/h \leq 10$, without showing any bi-linearity. This was found to be in line with tests on coal specimens published by international authors.

The experience with numerical modelling of shape effects in specimens and pillars would suggest that, in order for bi-linearity to be absent, two conditions must apply: for one, a very low residual strength of coal, which does not allow for early-brittle-ductile transition and for a meaningful squat effect. Secondly, very poor boundary conditions, i.e. a low frictional contact between the specimen and the loading platens, which additionally contributes to a low confining environment.

At this stage, however, this can only be hypothesized. It has been experienced that two-dimensional FLAC models always produce at least very small squat effects, even if comparatively low residual material cohesion (0.1 MPa) and friction (15˚) in combination with low interface friction (15˚) are used. This may indicate that the problem lies within the continuum assumptions made in FLAC, in that no spalling and reduction of core confinement can occur.

The shear strength of the coal-steel interface in the laboratory setup has also been shown to be relatively competent as compared to the other rock-steel interfaces in the tests, at least at the low normal stresses at which the shear box tests were conducted. This leaves only the possibility that the coal-steel-interface properties weaken at higher normal stresses and deteriorate very rapidly once the first failure starts in the coal specimens. It seems likely that the contact between the coal specimens and steel platen is

partially lost in the brittle failure process, with adverse consequences for the confinement generated in the remaining intact portions of the coal specimens.

3) Brittle-ductile transition

Laboratory specimens fail in a brittle manner at low width-to-height ratios, in that they encounter a sudden or gradual loss of load-bearing capacity at some level of compression, until they reach a more or less constant residual strength level at higher vertical deformation. The residual strength increases progressively, and the post-peak stress-strain slope flattens gradually with increasing width-to-height ratio. At some critical width-to-height ratio the post-peak slope is a horizontal line and the residual strength conceptually equals the peak strength of the specimen, i.e. no further drop in strength is encountered. This is the point at which brittle-ductile transition is encountered.

Specimens and pillars with width-to-height ratios beyond the critical range experience some amount of failure in their sidewall, but can increase their load bearing capacity far beyond the point of yielding. This behaviour has been termed ductile or strain-hardening.

It has been shown in the numerical models – and also in a few cases experienced in the laboratory – that even those strain-hardening pillars and specimens may eventually experience a temporary and relatively small, recoverable drop in load-bearing capacity, when shear cracks develop through the central core of the structure. These drops occur invariably at much larger stresses and strains as compared to the range where strength drops would occur in the more brittle specimens and one could argue that these strains are unlikely to occur in pillars in regular bord-and-pillar layouts. Nevertheless it must be noted that some amount of temporary load-shedding and energy dissipation may occur in strain-hardening pillars as well.

Numerical models have shown that an early brittle-ductile transition at a relatively low width-to-height ratio indicates a relatively competent residual material strength. In the laboratory, sandstone and coal-crete specimens experienced the brittle-ductile transition at very similar width-to-height ratios, which may indicate a comparable residual strength of the two materials. Coal, however, did not show any signs of brittle-ductile transition in the same range and it is therefore concluded that the residual strength of coal specimens in the laboratory environment is relatively poor (see discussion above). Granite specimens did not experience the brittle-ductile transition either because the specimens failed so violently that a further, stable loading through the testing machine could not be guaranteed or because they disintegrated so abruptly that a residual specimen strength practically did not exist.

18 On calibrated coal pillar models – in-situ compression tests revisited

A number of calibrated coal pillar models are published in literature, as reported in Chapter 16. The calibration procedures, however, can differ significantly and hence the predicted (extrapolated) behaviour of pillars with larger width-to-height ratio also differs.

The problem of extrapolating pillar behaviour in FLAC or any other numerical code beyond the calibration range lies in the fact that the required combination of model input parameters to represent one single pillar stress-strain curve or peak strength trend is not unique. Usually, a number of parameter combinations, together with a suitable mesh density and loading rate can give the desired output in the calibration range.

The particular problem with extrapolating squat pillar behaviour lies with the correct estimation of residual strength properties. In calibrated models published so far, the residual parameters were estimated based on laboratory experience or arbitrarily selected. However, it has been shown in the previous chapters that the squat effect and the brittle-ductile transition are very sensitive to the correct choice of residual material properties.

Unfortunately, the residual strength properties of large-scale coal pillars are unknown and unlike the elastic properties, are difficult to obtain from physical testing. They will depend on the fragmentation pattern in coal pillars subsequent to failure, i.e. the number, orientation and shear strength of discontinuities produced. Furthermore, the pillar may lose its residual strength characteristics further in the process of spalling.

In absence of feasible direct testing techniques for residual pillar strength properties, these parameters will have to be inferred from observations such as the full stress-strain behaviour of pillars in compression. The most accurate and complete information in this regard is available from compression tests reported by Van Heerden in 1974.

Van Heerden tested 10 pillars of 1.4 m square width, of which two pillars each had about the same height of 1.2 m, 1 m, 0.7 m, 0.5 m, 0.4 m to account for varying width-to-height ratios between w/h= 1 – 3.4. The test pillars were cut out from the corners of real mine pillars and maintained their natural attachment to the mine floor, while hydraulic jacks were placed tightly in the gap between the top of the test pillars and the mine roof. The pillars were then loaded through the hydraulic jacks in displacement control, i.e. equal displacement across the entire pillar base area, until the residual strength state was reached. The vertical deformation of the test pillars during compression was recorded through LVDTs attached to the pillar sidewalls and, after failure, calculated from the displacement of the hydraulic pistons.

The original CSIR report (Van Heerden, 1974) on Van Heerden's investigation was obtained, in which stress-strain graphs for all ten pillars tested were provided. The graphics were reproduced digitally and checked for accuracy by comparing the peak pillar strength provided by Van Heerden in his report with the result obtained from the digitized graphics. The average deviation between the two sets of measurements was found to

be only 0.112 %. The reproduced stress-strain behaviour of coal pillars in Van Heerden's test are plotted in Figure 99. The characteristic features, i.e. average stresses and strains for the pillar width-to-height pairs at the point of yield (here interpreted as the point of deviation from linear elasticity), peak and residual strength (the point upon which the flat portion of the post-peak curve is reached) are analysed in Figure 100.

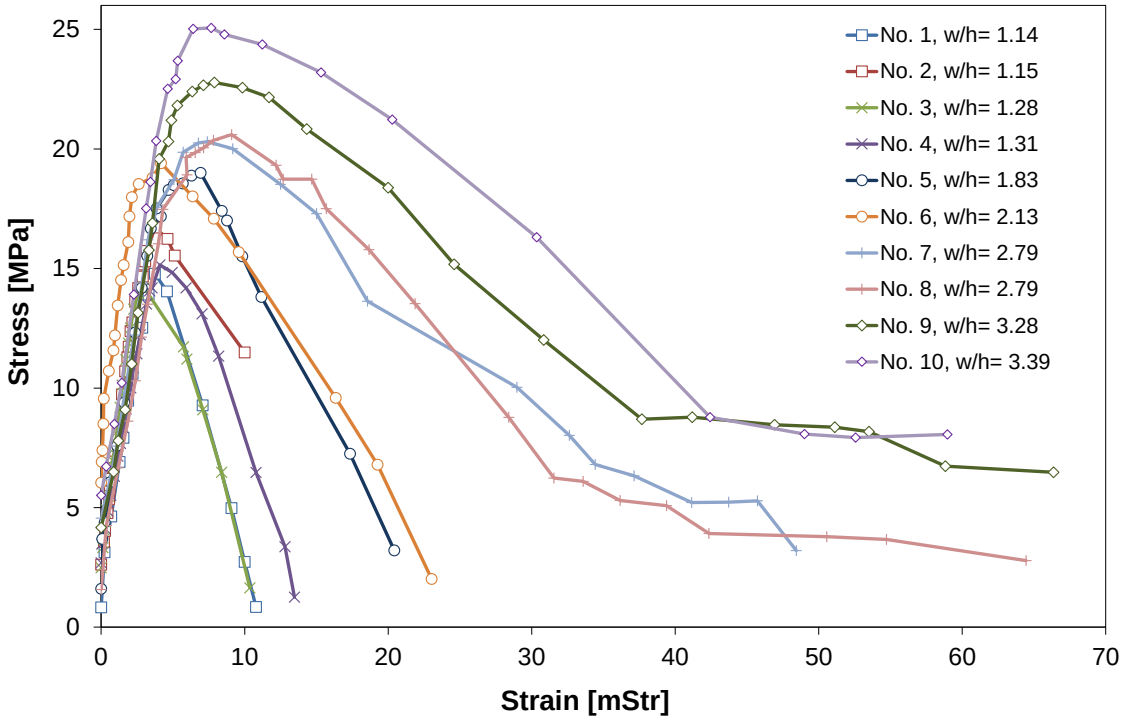


Figure 99. Stress-strain behaviour of coal pillars in Van Heerden's large-scale in-situ tests, reproduced from Van Heerden (1974).

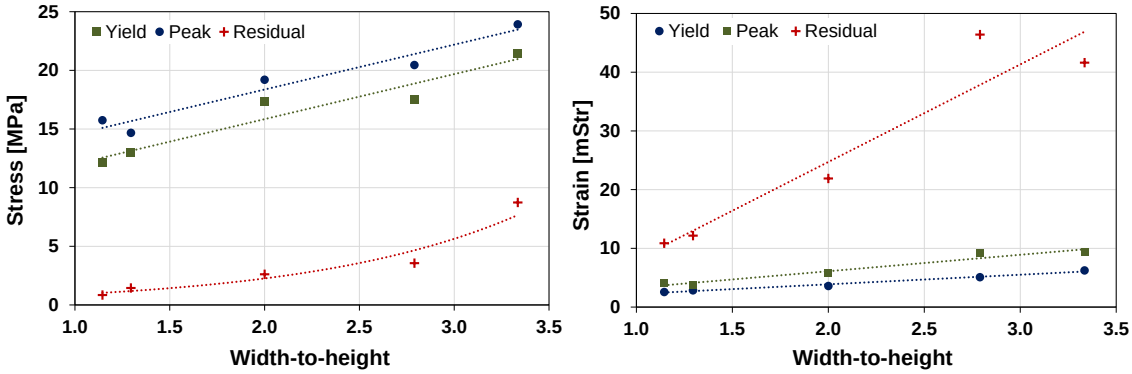


Figure 100. Average yield, peak and residual stress and strains in coal pillars of different w/h-ratios tested by Van Heerden.

It is observed that yielding was initiated in these pillars at about 90 % of the ultimate load bearing capacity, a threshold that is somewhat higher than the 70 % level for yielding reported by Bieniawski (1968b) and Wagner (1974) for their in-situ experiments.

The trend of yield and peak stress levels is approximately linear over the investigated range of width-to-height ratios, seemingly without any divergence between the two trends. The residual strength is observed to increase progressively.

The related strains at yield, peak and residual strength develop linearly, with some small amount of divergence occurring between the strains at yield and peak with increasing width-to-height ratio. This indicates that the pre-peak yielding modulus reduces, i.e. the pillar becomes softer in the pre-peak yielding stage with increasing width-to-height ratio. The level of strain at which a pillar reaches its residual strength level increases most rapidly, causing the post-peak brittleness of the pillar to decrease.

A perfectly calibrated numerical model would be able to reproduce these trends in quality and magnitude. Important in this context is that one set of model input parameters must be found that matches the evolution of stress and strain trends over the entire empirical range of width-to-height ratios.

The trends for peak and residual strength in Van Heerden's experiments are extrapolated to greater width-to-height ratios in Figure 101. Both exponential and polynomial fits are presented, to cover different scenarios of progressive strength increase encountered in numerical models and in the laboratory. Also shown in Figure 101 are different trend lines fitted to the post-peak slopes observed in Van Heerden's tests.

Following the peak and residual strength trends, the prediction is such that brittle-ductile transition would occur between $w/h = 5 – 6$. This predicted interval is in the range where brittle-ductile transition is encountered for other rocks and rock-analogue materials in the laboratory, such as the sandstone and coal-crete specimens. The question however, is why the predicted results differ from the observations made on the coal specimens tested in the laboratory.

It has already been suggested in Chapter 17.5 that the relatively poor performance of coal specimens in the lab might be due to a partial loss of contact between the coal specimens and steel loading platens in the brittle failure process, with adverse consequences for the confining environment around the specimens. In Van Heerden's large-scale tests however, the coal specimens were rigidly attached to the mine floor and the top loading platen, which consisted of strong concrete, was cast onto the specimens. One can therefore safely assume that both the cohesive and frictional strength of these interfaces were far more competent compared to those in the laboratory, which made it more difficult for the failed coal material to lose contact and deteriorate the loading environment. This may explain why, in Van Heerden's tests, the overall residual specimen strength can increase at a faster rate.

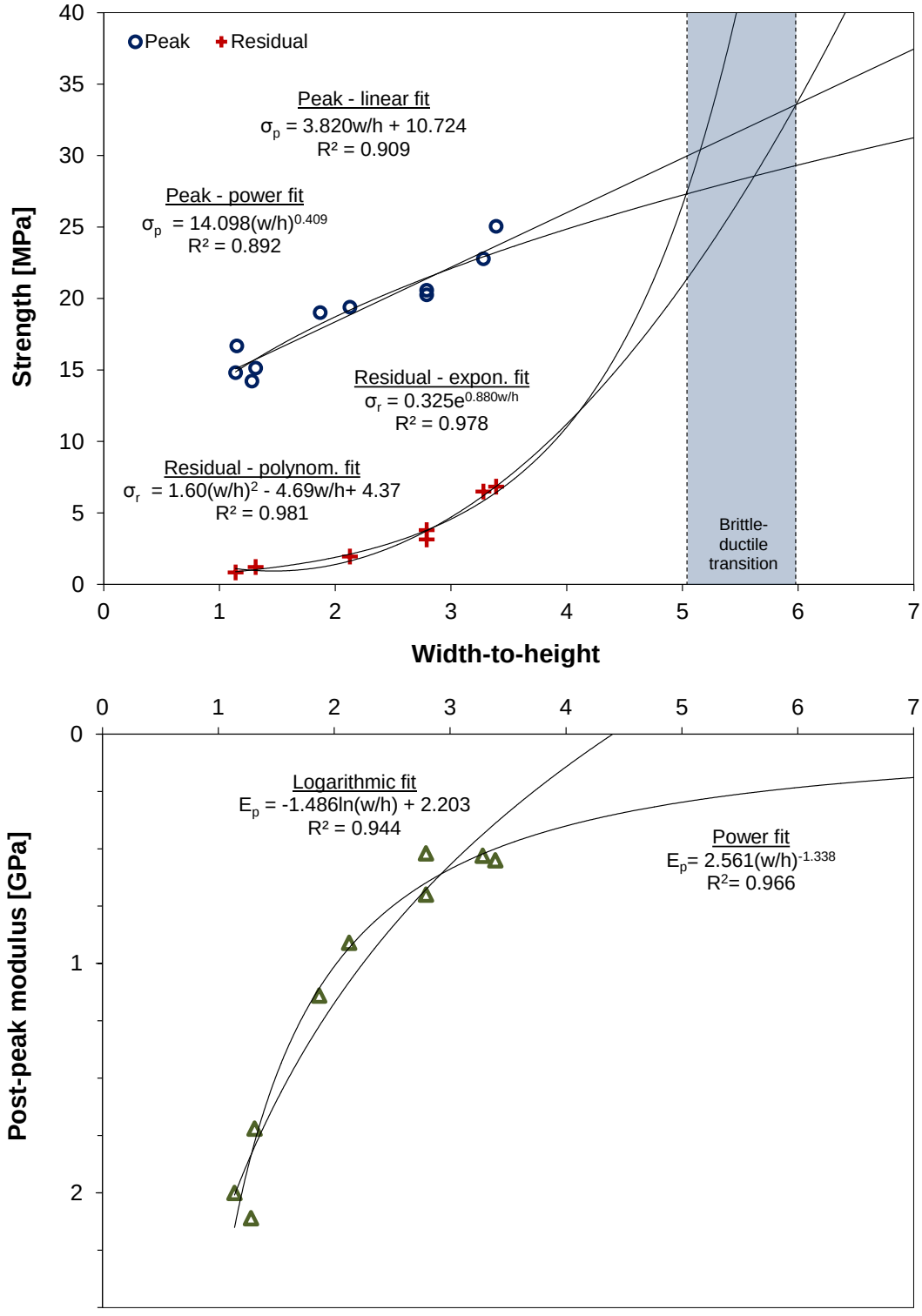


Figure 101. Extrapolated trends for peak and residual strength (top) and post-peak stiffness (below) in Van Heerden's large-scale in-situ tests.

It is important to note that a FLAC pillar model that is accurately calibrated against Van Heerden's peak and residual strength trends must *necessarily* predict the same range for brittle-ductile transition, in particular because FLAC always computes an exponential increase in residual strength. Only the linear or regressively curving peak strength trend

may be interrupted by a squat effect shortly before brittle-ductile transition occurs. This, however, may not be of great practical consequence for pillar design, since the latest update of empirical pillar strength equations (Van der Merwe and Mathey, 2013c) has shown that one single trend in strength can be safely assumed for coal pillars up to $w/h=$ 4.4.

The observation that the trend for post-peak slopes in pillars does not reach zero in the interval may compromise to some extent the reliability of the prediction of brittle-ductile transition at $w/h=$ 5 – 6. In fact, the best-fit power equation for post-peak slope trends even implies that a slope of zero will not be reached for any width-to-height ratio, which does not seem plausible.

The question is also how reliable post-peak trends are for the prediction of brittle-ductile transition in pillars. Even in the controlled environment of a laboratory it has not been possible to determine one continuous trend in post-peak slopes of the test specimens (see Chapter 13.1.3), at least not reliable enough to base accurate predictions on these trends. The fundamental trends in peak and residual strength of pillars and specimens of different width-to-height appear to be more conclusive for the prediction of brittle-ductile transition.

It has also been experienced that it is very difficult to mimic the decreasing brittleness of post-peak slopes of increasing pillar width-to-height ratios in FLAC models. Typically, the immediate post-peak behaviour of FLAC model pillars tend to become increasingly brittle (see Figure 86, Figure 91, Figure 95, Figure 96) with increasing width-to-height ratio, in particular when mechanical interfaces are used between pillar and strata. This has also been observed in full stress-strain curves provided by other authors (Salamon et al., 2003). Attempts have been made to control the post-peak brittleness of FLAC model pillars through variations in loading rates and the servo-controlled loading FISH function.

Some further caution must be exercised when interpreting FLAC or analytical predictions on pillar strength trends: the assumption that underlies both analytical models and numerical FLAC models is that the pillar remains a continuum in the pre-failure and post-failure state, in that failed portions of the pillar stay attached to the intact parts and therefore always provide some level of confinement.

This is rarely true for in-situ pillars, where invariably some kind of spalling of failed material occurs, if no additional constraint is provided to the pillar sidewalls. Consequently, the trends in the residual strength of specimens may differ to some extent from the ideal exponential curve predicted by FLAC models.

Principally, FLAC would allow users to set the mechanical and physical properties of failed zones along the pillar sidewalls to zero in an interactive process in order to simulate the loss of material and confinement. This modelling exercise is, however, complicated by the fact that a failure criterion for spalling is not available and that spalling is to a large extent influenced by the time-dependent weakening process of coal, which is not fully understood yet.

The importance of generated confinement in the pillar core from failed peripheral material has been clearly pointed out in the numerical modelling exercise, in particular in terms of possible squat effects, the second rate of strength increase thereafter, and the critical width-to-height ratio for brittle-ductile transition. It is therefore evident that spalling of pillar sidewalls over time work to the disadvantage of all the effects relevant for squat coal pillar behaviour.

PART V

Conclusions and outlook

19 Research conclusions

The strength and failure associated with squat coal pillars has piqued the interest of international researchers for many years. Despite the various efforts that were directed at observing in-situ pillar behaviour, or studying model pillars analytically, numerically or through physical modelling in the laboratory, a unified understanding of the mechanisms contributing to strength and failure of these structures could not be derived so far.

The problem manifests already in the squat pillar terminology adopted internationally: while in South Africa and Australia, squat pillars are said to have width-to-height ratios greater than 5 and follow an exponential rate of peak strength increase, the understanding in the United States is such that a squat pillar has a width-to-height ratio greater than 8 and is essentially characterized by a strain-hardening failure mechanism beyond the brittle-ductile transition.

Both explanations for strength and failure mechanisms have been observed by different researchers in physical laboratory tests on sandstone model pillars, and the question arises as to how the two opposing phenomena can be reconciled. There is however, a clear understanding in literature that compression tests on coal model pillars neither support an exponential strength trend for pillars with width-to-height ratios greater than 5, nor the occurrence of brittle-ductile transition at a shape ratio of 8 or lower. Strength trends for coal model pillars have always been observed to take a regressively increasing, or at best linearly increasing form, and brittle-ductile transition does not occur for width-to-height ratios smaller than 10. That is, if it occurs at all in the presented studies.

The discrepancy between test results for rocks and coals strongly suggests that intrinsic material properties can have a significant influence on the relationship between pillar shape and strength.

A clarification of the role of intrinsic material properties for shape effects in pillars also becomes important because a number of coalfield-, seam- and site-specific strength formulae for South Africa have already been suggested. Would this strength variation also have an impact on the evolution in strength of pillars with squat width-to-height ratios?

Ultimately this question gains momentum by the fact that the current South African squat pillar formula has been proposed based on the observation of sidewall failure patterns of squat pillars at three sites in the coalfields of KwaZulu-Natal. The argument has been that sidewall failure in these pillars was so limited that they would suggest a significantly higher strength of the structures as compared to the conservative estimation from the extrapolated Salamon and Munro (1967) equation, which was mainly derived from pillar failures in the Witbank coalfield. However, it can be hypothesized that this mismatch in observed and predicted strength could have simply arisen from variations in coalfield-, seam- or site-specific coal strength. Unfortunately, no attempts had been made to compare the fractures in squat pillars to those in slender pillars at the same site, which could have served as some kind of calibration to the observation.

Further evidence for the validity of the exponential form of the South African squat pillar formula was sought in laboratory tests on sandstone model pillars (Madden, 1990). The finding however, was such that no exponential peak strength trend occurred for specimen width-to-height ratios greater than 5, but instead brittle-ductile transition occurred. The validity of simulating coal pillar behaviour by using sandstone model pillars must further be questioned, as coal and sandstone evidently behave very differently in laboratory tests.

Since no further proof of the validity of the South African squat pillar formula is available from in-situ large-scale testing or failed pillar cases, the question as to the strength and failure mechanism of squat pillars is open to further investigation.

The research conducted within the frame of this thesis is structures into a statistical analysis of mechanical properties of South African coals; a comparative testing of coal and rock model pillars under the same boundary conditions in the laboratory; and a conceptual numerical evaluation of shape effects in model pillars.

The mechanical properties of South African coals

The statistical analysis of mechanical properties of South African coals is based on a comprehensive database compiled from tests conducted by the different local coal mining houses, and which sources to a smaller extent from tests conducted by the author. The mechanical properties of 13 seams in 5 coalfields are represented in this database.

The initial intention was to detect local variations in strength properties that would explain the differences in pillar strength encountered in South Africa. Interestingly, however, evidence for such variations could not be established:

For the uniaxial compressive strength of coal specimens, the South African average is around 22 MPa. The individual seam averages scatter only very little around this value; minimum and maximum seam averages of around 20 MPa (e.g. Witbank Nos. 1 and 4 seams, Vereeniging-Sasolburg Middle seam) to 26 MPa (e.g. Highveld No. 2 and Vereeniging-Sasolburg No. 2 B seams) are found. This highlights a remarkably small difference between the seams in South Africa, while published results for seams in the U.S. and India are significantly more diverse. Colliery-specific or site-specific uniaxial compressive strength of South African coals could not have been determined so far, because a greater amount of statistical evidence is required for this detailed level of analysis.

Greater seam-specific differences for South African coals can only be identified from triaxial tests. The available data suggests that seams No. 5 in the Witbank coalfield and No. 4 in Highveld exhibit a significantly more rapid increase in strength with confinement as compared to the relatively consistent group of Witbank Nos. 2 and 4, and the Vereeniging-Sasolburg Top and Middle seams. The Ermelo C Lower seam displayed the lowest rate of strength increase. It must, however, be admitted that perhaps too few statistical data are available on the triaxial strength of different seams to substantiate this conclusion.

Therefore, the review of mechanical coal properties in South Africa does not yield direct implications for pillar strength and design in the different mining environments. However, a number of findings of academic interest arose, which may stimulate further research. These findings are:

(1) The uniaxial and triaxial compressive strength and the indirect tensile strength of all South African or seam-individual coal tests can be represented satisfactorily by a single statistical distribution. This may further support the view that no site-specific pattern in basic coal strength can be detected from laboratory testing.

(2) Mechanical tests which apply a uniaxial stress field to the specimen tend to give a lognormal distribution of the results, (UCS, E, ITS), while triaxial compressive strength test results are normally distributed.

(3) It is suggested that the differences in the distributions arise from the influence of discontinuities in the coal specimens. While test reports indicated that around 90 % of strength failures on UCS specimens was influenced by natural discontinuities, only 27 % of all TCS specimens showed this pattern. It can also be demonstrated that very small confining pressures of 2 MPa are already sufficient to minimise the number of specimens whose failure is influenced by discontinuities. This bears the implication that the unconfined compressive strength of *intact* coal can be more suitably addressed from triaxial strength tests at low confining pressures than from direct unconfined testing.

(4) The analysis further suggests that for confining pressures of 20 MPa and higher the adverse influence of discontinuities on specimen strength vanishes. Practically, this means that pillars which can generate this confinement in their confined cores may not be adversely affected by the presence of discontinuities either.

It was shown that correlations between material properties, such as density and UCS, or UCS and elastic modulus, or other correlations between mechanical properties and the depth of sampling, are not discernible from the database.

Laboratory investigation into the shape effect in rocks and coal

The influence of intrinsic material properties on shape and possible squat effects was then further investigated in a laboratory testing programme on specimens with small and very large width-to-height ratios.

A coal sample was obtained from the No. 4 seam operations at South Witbank colliery. Two samples of sandstone and granite were chosen to represent soft and hard rock in the testing programme. Also, a composite material called coal-crete, consisting of coal fragments and a binder mixture was developed as a mechanical analogue to coal. The particular mixture used in the testing programme on shape effects in model pillars was weaker than the coal sample obtained from South Witbank colliery and therefore provided the lower limit of material properties investigated in the study.

Rock, coal and coal-crete specimens were prepared from 42 mm cores, which were truncated in height to represent different width-to-height ratios. Additional coal-crete specimens were obtained by casting the material into moulds of 100 mm and 150 mm square base width and various width-to-height, so as to create specimens of sufficient size to allow for accurate observations of fracture patterns in the model pillars.

The tests were carried out in an MTS testing machine, making use of hardened-steel loading platens to apply compressive forces to the specimens. During the tests, the force-displacement relationship of the machine's actuator was recorded and the stress-strain response of the specimens were inferred. The contact friction angle between the loading platens and specimens was determined through a number of shear box tests. The basic mechanical properties of the selected materials was determined from uniaxial compression tests with strain-gauges and triaxial compression tests.

The test results for coal-crete and sandstone show a gradual reduction of the post-peak slope of the stress-strain curve with increasing width-to-height ratio, while the residual strength increases. At a critical width-to-height ratio the post-peak slope becomes practically zero and the residual strength equals the peak strength. This phenomenon is termed the **brittle-ductile transition** in pillars or specimens. Specimens with width-to-height ratios greater than the critical point still undergo some yielding, but perform in a ductile or strain-hardening manner. They can increase their load-bearing capacity far beyond the expected range of failure with further deformation taking place.

The critical width-to-height ratio for brittle-ductile transition in coal-crete and sandstone specimens is between w/h= 5 – 7.5. Also, coal model pillars indicated this behaviour, but at higher width-to-height ratios of w/h= 9 – 11, consistent with the experience published by other researchers in literature. The gradual reduction of brittleness, however, only manifested in coal as a progressive increase in the residual strength of coal with increasing width-to-height ratio, but not conclusively as a flattening of the post-peak slope. The granite specimens failed in a very brittle, even violent manner at peak strength, so that a post-peak behaviour could not be determined for this material.

A second phenomenon observed in the testing programme is that of **bi-linearity** in the peak strength versus width-to-height relationship of the non-coal model pillars. This phenomenon is defined as the **squat effect**. Bi-linearity is strongly evident for the granite specimens, where the first, linear branch in the peak strength trend is succeeded by a second linear and more rapid rate of strength increase from a critical width-to-height ratio of about 4 onwards. Bi-linearity is also suggested by the test results for coal-crete and sandstone, with the squat effect occurring at between w/h= 4 – 5. In these two cases, however, the second branch of strength increase was soon interrupted by the occurrence of brittle-ductile transition so that the evidence is not as conclusive as for the granite.

Coal specimens, in contrast, are different in behaviour from the rock and composite materials in that they only showed a single, regressively increasing strength trend over the entire range of tested width-to-height ratios, up to the point where brittle-ductile transition is indicated (w/h= 9 – 11). A squat effect is therefore not evident for coal specimens.

Further investigation included the observed relationship between bi-linear strength trends and the intrinsic material properties. When the results from the laboratory programme are combined with data published by other researchers, it can be shown that the first linear rate of strength increase, up to about $w/h = 4$, is strongly correlated to the material's cohesion. The stronger the cohesion, the more rapid the rate of strength increase. Elastic modulus and UCS, which both correlate with cohesion in standard core testing, also correlated well with the rate of strength increase. Interestingly, the angle of internal friction, which quantifies a material's capacity to convert confinement into additional load-bearing capacity, does not show any correlation with the shape effect.

The relationship between the basic strength of a material and its potential strength increase with increasing width-to-height ratio is also evident for in-situ coal. The latest update of coal pillar failures, together with large-scale in-situ compression tests conducted in South Africa, was reviewed in this regard. The analysis confirms that Bieniawski's formula for the strength of coal pillars with different seam strength and $w/h \leq 4$, equation (14), is still the most versatile expression to address the correlation between strength and shape effects in relatively slender coal pillars in different environments.

A relationship between the intact material properties and the second, linear rate of strength increase for model pillars with $w/h > 4$ could not be established from laboratory data. However, an important clue can be derived from the observation that all peak strength trends would eventually lead to the occurrence of brittle-ductile transition at sufficiently large width-to-height ratios: the fracture patterns in specimens at the point of brittle-ductile transition show extensive fracturing and core failure. It is obvious that the high transitional stress levels were only sustained by the frictional resistance of the fracture network, assisted perhaps by a smaller contribution of residual cohesion.

It is thus hypothesised that the strength and failure mechanism in specimens transits from a predominantly cohesion-controlled strength to a predominantly (or at least significantly) friction-controlled strength with increasing width-to-height ratio. This logic would also suggest that the second linear branch of strength increase before the brittle-ductile transition, i.e. the squat effect, is caused by a substantial contribution of friction and in general by the residual material properties to the peak strength. The hypothesis has been further tested in the conceptual numerical study of shape effects in model pillars.

The absence of squat effects in the coal model pillars is remarkable and remains to some extent unexplained. This is because the intact material properties of coal, in terms of cohesion and friction, lie in between those of the rock and coal-crete materials, for which the squat effect was observed. Further, the shear box tests conducted on the loading platen-specimen interface indicated that the contact friction angles were the same for coal and the sandstone specimens and even more competent than those for granite specimens. This suggests that the reason for the outlying performance of coal in the tests cannot lie in different boundary conditions and that it cannot be found in the intact mechanical properties which are commonly used in rock engineering.

Instead, it is hypothesised that the difference between the coal and other materials could have resulted either from a difference in residual strength properties of fractured coal or from a change in coal-steel interface properties in the post-failure state, when the contact between the specimens and the loading environment is partially lost. In particular, the former argument could subsequently be substantiated in the numerical modelling study, where the influence of residual material properties on overall shape effects was explicitly investigated.

Numerical modelling of shape effects in pillars

The numerical investigation was hence designed as a conceptual assessment of the contribution of residual material properties, in particular friction, on shape and possible squat effects in coal pillars. The two-dimensional finite-difference code FLAC (Itasca Consulting Group, Minnesota, U.S.) for engineering computations in geomechanics was utilized for this exercise.

A literature review on calibrated coal pillar models preceded the work and assisted in limiting the range of possible input parameters to the relevant and most typical range of coal material properties and boundary conditions.

In general, all shape effects encountered on rock and coal-crete specimens in the laboratory study can be reproduced in numerical model pillars: a progressive increase in residual strength with increasing width-to-height ratio; bi-linearity in the peak strength trend and the brittle-ductile transition. Interestingly, however, none of the simulations yielded results comparable to the tests on coal model pillars in the laboratory.

The trend for **residual strength** of pillars in numerical models is always observed to take an exponential form, which principally agrees with analytical solutions. The higher the residual material properties, the faster the exponential rate of residual strength increase, and consequently, the lower the critical width-to-height ratio for brittle-ductile transition in pillars.

In the context of **bi-linearity in peak strength** behaviour of pillars, it became evident through the numerical models that pillars in the first branch reach their maximum load-bearing capacity at the point where the first shear band develops in the pillar. This is irrespective of whether this first shear band penetrates through the pillar core or is restricted to the pillar sidewalls, because in any case, the remaining confinement is insufficient to allow the structure to regain strength. If the first shear band had not penetrated the core yet, further shear failure would soon follow with further loading in the descending branch of the stress-strain curve and cause ultimate core failure. It is further observed that in this first branch of the bi-linearity, the rate of strength increase is practically independent of the residual strength properties – a general correlation is not clearly discernible.

It is suggested that if the first trend in the strength versus width-to-height relationship is extrapolated to greater aspect ratios, it continues to indicate the level where major yielding develops in pillars. Observations on the progressive development of failure in granite specimens do validate this conclusion.

Pillars with sufficiently large width-to-height ratios, whose strength lie in the second branch of the bi-linear trend, do recover from the first occurrence of shear failure and continue to increase their load-bearing capacity with further compression, until core failure is finally reached. For these squat pillars, the residual friction acting in the failed part of the pillar now plays a very sensitive role: even small changes in the residual friction can cause drastic reduction or increase in the strength gradient. The relationship is such that the higher the residual friction, the more rapidly the pillar strength can increase for increasing width-to-height ratios, and vice versa.

The critical width-to-height ratio at which the squat effect occurs in pillars is identified to be dependent on the residual material properties: if the residual friction generated in the failed pillar sidewalls is relatively large, then the squat effect will occur at earlier width-to-height ratios, and vice versa.

Unfortunately, the residual strength properties of in-situ coal or of any rock material are unknown, so that the question of squat pillar performance in terms of bi-linearity and brittle-ductile transition as ascribed above can only be answered in this conceptual form with numerical models.

The strength of squat coal pillars

Despite the apparent difficulty in determining a most- probable squat coal pillar behaviour in numerical models, there is sufficient evidence delivered in this thesis to reformulate the state-of-the art of squat coal pillar strength and behaviour for South Africa.

The study concludes that an exponential strength increase in coal pillars at w/h-ratios greater than 5, as assumed in the past, based on work by Salamon (1982; Salamon and Wagner, 1985) and Madden (1990, 1991), is not supported by experimental studies on model coal pillars in the laboratory. All published tests on model coal pillars in the United States, India and South Africa, including those conducted within this thesis, unambiguously agree that the strength versus width-to-height ratio relationship follows a single, continuous and most-probably regressively increasing trend up to width-to-height ratios of 9 or 11. It is further indicated that model coal pillars with greater width-to-height ratios transit directly from brittle to ductile behaviour, without showing a squat effect in terms of bi-linearity.

The laboratory experience suggests that the empirical coal pillar strength equations, derived from direct testing or observed pillar failures in the range of w/h=1 – 4, can be extrapolated to width-to-height ratios of at least 10. Three observations validate the qualitative transference of laboratory trends into the underground mining environment:

For one, an influence of specimen size on the effect of shape in terms of the gradient of strength increase is not discernible in the tests on coal model pillars of 25- 300 mm size and w/h= 1 – 8 conducted in the SIMRAC COL021a project (Madden et al., 1993).

Secondly, the effect of the external angle of friction along the interface between the model pillar and the loading platens at specimen w/h-ratios of 4 – 8 has been tested by Meikle and Holland (1965) and Khair (1994). All tests under various competent and weak frictional conditions did result in continuous trends in the strength versus width-to-height relationship, without evidence of a squat effect.

Thirdly, and most importantly, the experience with squat coal pillars in U.S. mines has shown that the empirical coal pillar strength equations, originally derived for slender pillars, can estimate squat pillar strength for w/h-ratios up to 8 (Mark, 2000) or 12 (Bieniawski, 1992) reasonably well. This upper limit for a single, continuous trend in pillar strength agrees favourably with the laboratory findings.

The majority of evidence therefore corroborates to the verdict that an extrapolation of established pillar strength equations up to width-to-height ratios of 10 is currently the most appropriate way to address squat coal pillar strength.

Nevertheless it is acknowledged that the presented evidence is only circumstantial, as no direct measurement or determination of squat coal pillar strength, either through compressive strength testing of the structures or through observations on failed and stable cases, is currently available or feasible in South Africa.

This implies that some uncertainty remains and final clarity on the matter can only be found in detailed in-situ studies on squat pillar strength in the country. It has been argued in this thesis that the available observations on sidewall fracturing in squat coal pillars in the coalfield of KwaZulu-Natal are inconclusive. However, the extrapolated peak and residual strength trends found in Van Heerden's large-scale in-situ compression tests have been shown to favour an early brittle-ductile transition in coal pillars at around w/h= 5 – 6. This discrepancy to the evidence listed above opens up room for future research on squat coal pillars.

20 Implications for squat coal pillar design

The study has concluded that, at the current state of knowledge, the strength of squat coal pillars in South Africa is most suitably addressed by extrapolating the empirical strength equations derived from pillars with w/h= 5 into the squat range, i.e. up to w/h= 10.

A number of empirical strength equations exist in South Africa, which are summarized and extrapolated already in Figure 1, Chapter 3.1.1 of this thesis. Commonly, the original Salamon and Munro (1967) equation or the formula developed by Van der Merwe (2003b) is used in the current production areas in the country. Updates are available for both approaches (Van der Merwe and Mathey, 2013c) and will be utilized in the following considerations.

The updated overlap reduction strength formula (Equation 7) based on Van der Merwe's approach, is evidently more advantageous for squat coal pillar design, as it predicts a significantly higher strength than the updated maximum likelihood strength formula (Equation 6) based on Salamon and Munro's approach, and still a higher strength than the previously proposed South African squat pillar formula (Equation 8).

The question is how the extrapolated strength equations will perform in terms of economic efficiency of underground deposit extraction when applied to squat pillar design. In general, the concern is that squat pillars will lock up too great a portion of a coal deposit, and this was also the motivation behind the development of the South African squat pillar formula in the late 1980s.

The following statistics on underground bord-and-pillar extraction are available:

The average extraction ratio achieved in bord-and-pillar mining layouts using slender pillars of w/h< 5 is approximately 66.6 %, according to 253 cases recorded in the South African database of stable pillar layouts, Figure 102 (left). This extraction ratio is used as the industry benchmark for an economically efficient extraction of a deposit.

The extraction ratio in squat pillar layouts recorded in the databases (w/h≥ 5; 84 cases; the average, minimum and maximum depth below surface is 130 m, 50 m, and 255 m respectively), is somewhat lower, at an average of 48.5 %, and may be judged to be inefficient in terms of economy. The following consideration, however, reveals that squat pillar design to extrapolated pillar strength equations must not necessarily result in an economic disadvantage:

For the plot in Figure 102 (right), the pillar strength has been calculated by extrapolating the latest updated maximum-likelihood pillar strength equation, which has been argued to be the most conservative estimate for squat pillar strength. Evidently, the great majority of the recorded squat pillar layouts still exhibit safety factors greater than 1.6, the industry standard, and about two-thirds of all cases lie even above 2.0.

If the required pillar and bord widths in these cases are recalculated at an unaltered pillar centre distance to arrive at the industry standard safety factor of 1.6 according to the

conservative maximum-likelihood pillar strength equation, then the achievable average extraction ratio was increased to 62.3 %. This is just below the industry benchmark for slender pillar layouts of 66.6 %.

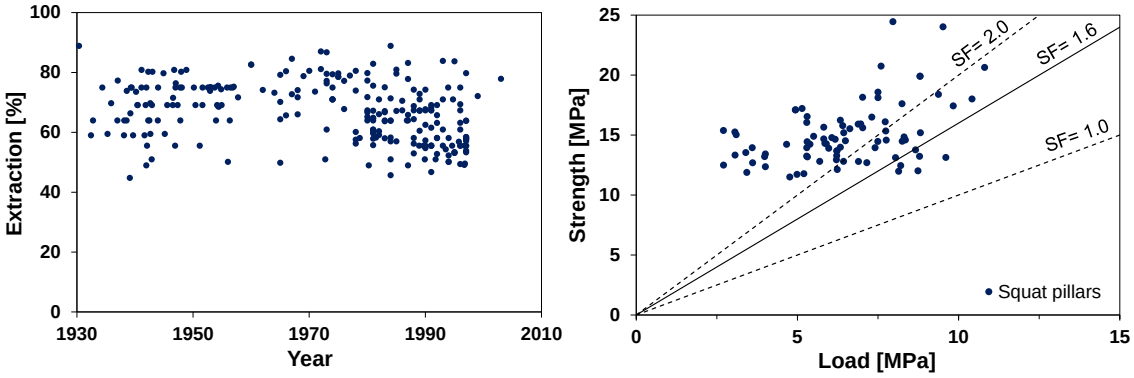


Figure 102. Extraction ratio in slender pillar layouts (w/h< 5) over time (left) and safety factors used in squat pillar layouts calculated after the latest maximum-likelihood updated pillar strength equation (right).

Nevertheless, the influence of mining depth on pillar design and extraction ratio deserves some further attention. The average depth below surface of the above considered squat pillar cases was said to be only 130 m. The future of underground coal mining in South Africa may lie in much greater depth below 400 m, for instance in the Waterberg coalfields.

Figure 103 plots the expected theoretical extraction ratios in bord-and-pillar mining layouts, when the updated maximum-likelihood or the overlap-reduction pillar strength equation is used. The following typical mining scenario is considered: H= 50 – 600 m; h= 3 m; B= 6 m; SF= 1.6.

In this scenario, squat pillars with $w/h \geq 5$ will only be required from approximately 150 m depth onwards. This is also the approximate depth where theoretical extraction ratios would reduce to 50 % or less. It is observed that systematic bord-and-pillar mining may very rapidly become uneconomic in terms of deposit extraction with increasing depth, and that high-extraction techniques such as longwall mining or stooping will have to be considered. Alternatively the possibility of developing yield or crush pillar layouts should be considered. This again requires further knowledge about the residual strength properties of large-scale coal.

The extraction ratios that could be achieved in the chosen scenario with the current South African squat pillar strength formula are not explicitly plotted, but would range in between the two curves shown in Figure 103 and therefore yield no improvement.

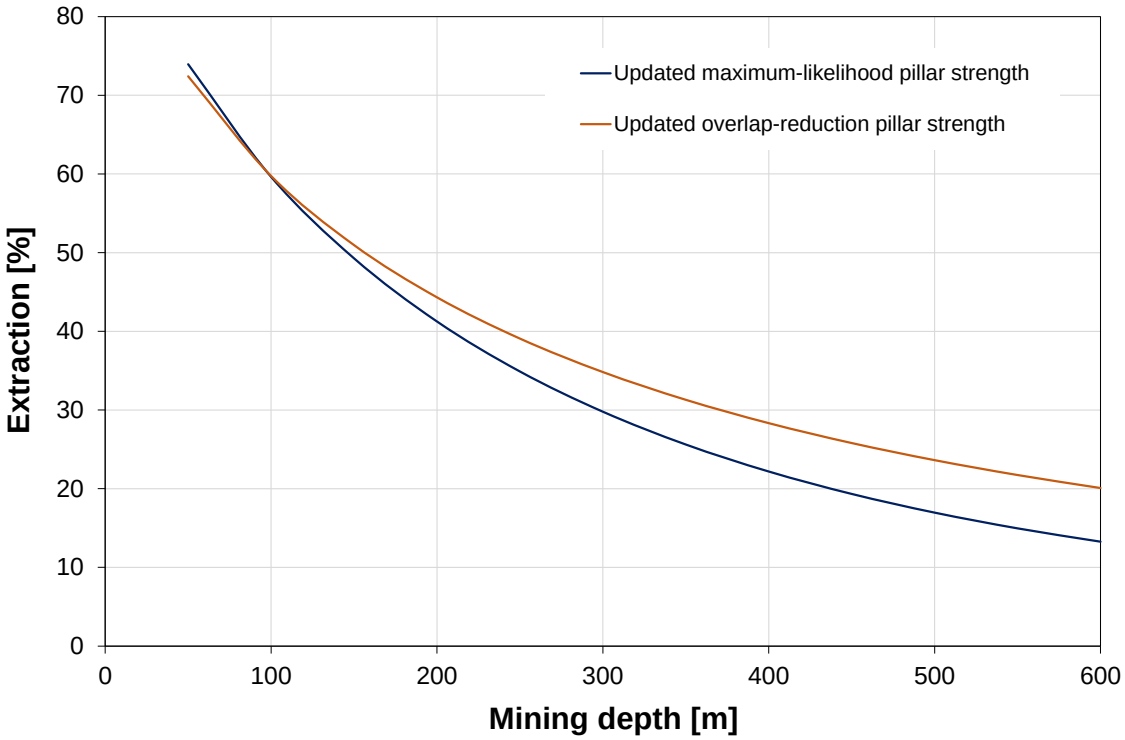


Figure 103. Extraction ratio versus mining depth for pillar design based on the updated empirical pillar strength equations.

21 Indications for further research

Further research and experience is required before squat coal pillars can be designed for optimal safety and economic benefit. The current experience with squat pillars is still largely based on laboratory and numerical modelling studies, and extends only very little into the real underground mining environment. Ideally, in-situ large-scale compression tests on squat model pillars and long-term deformation monitoring on real pillars, in bord-and-pillar layouts and stooping environments, should be conducted to ascertain squat pillar performance in a more holistic way. Such studies will require long-term planning.

Other studies can, however, yield short- and mid-term progress. In the following sections two laboratory studies are proposed, which aim at understanding the fracture mechanism of coal in brittle-ductile transition and the impact of sidewall scaling on the loss of core confinement and strength. Two further in-situ studies are suggested, with the intent to quantify pillar integrity and the extent of yielding in different ground conditions.

21.1 Laboratory investigation into the brittle-ductile transition in coal

One of the central themes of this thesis is the brittle-ductile transition in coal pillars. This has been understood as both a geometrical and physical phenomenon. A critical combination of width-to-height ratio and material strength properties, in particular the residual parameters, is required in order to generate sufficient confinement in the pillar for brittle-ductile transition to occur.

It is suggested that further laboratory studies are conducted to investigate the brittle-ductile transition in coal. A simple and typical test design is to measure the full stress-strain response of cylindrical coal specimens at various triaxial confining pressures and to observe the arising fracture patterns.

The brittle-ductile transition has been studied comprehensively for rocks by Mogi (1966). The so-called ‘Mogi criterion’ for brittle-ductile transition in silicate rocks,

$$\sigma_1 = 3.4\ \sigma_3 \tag{32}$$

relates the vertical stress at which brittle-ductile transition occurs in specimens to the required confining pressure through a simple empirical equation. The criterion is also used to approximate the stresses involved in brittle-ductile transition in carbonate rocks, although to a lesser accuracy. Barron and Pen (1992) also applied Mogi’s equation to predict brittle-ductile transition in their analytical coal pillar models.

Very few experimental evidences are available as to the brittle-ductile transition in coal. Most triaxial tests conducted on South African coals do not exceed confining pressures of 20 MPa. Hobbs (1964) presented a comprehensive study on the triaxial strength of different coals, using confining pressures of up to 35 MPa, without observing brittle-ductile transition. Kripakov (1981) presented full stress-strain curves of triaxially confined

coal specimens, also without experiencing brittle-ductile transition in the empirical range. However, the peak and residual strength indicated by the stress-strain curves may suggest that brittle-ductile transition would occur in coal at confining pressures of around 50 MPa (Figure 104, right). Mogi's criterion, applied to the average Hoek-Brown peak strength trends for South African coal seams (see Chapter 8.3), suggests a range of possible stresses at the brittle-ductile transition. The majority of data, however, lies at confining pressures of around 50 – 60 MPa.

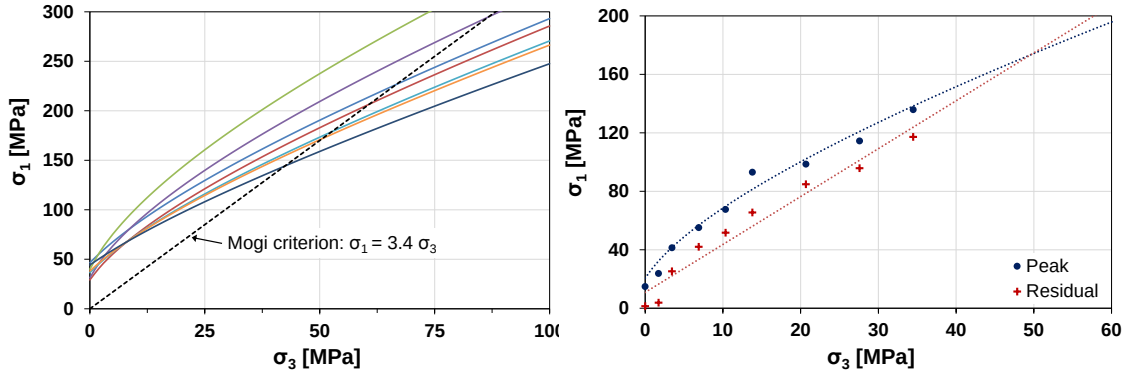


Figure 104. Estimation of brittle-ductile transition in coal specimens through Mogi's criterion in conjunction with extrapolated peak strength trends for South African coals (left) and from triaxial tests conducted by Kripakov (1981) (right).

21.2 The strength of coal pillars after spalling

It has been said that, for brittle-ductile transition to occur in pillars, sufficient confinement must be generated within the pillar core. Coal pillars, however, have been found to experience some amount of sidewall spalling in the course of time (Van der Merwe, 2003c, 2004) and therefore lose core confinement partially.

Typically, the effect of sidewall spalling or scaling is such that the rectangular shape of pillars is gradually lost and an 'hourglass' shape is assumed over time. The strength of these structures has so far not been investigated in detail, and it is suggested that a laboratory or numerical study is conducted in this regard.

Some indications on the expected compressive strength behaviour of 'hourglass' shaped specimens can be found from the following study conducted by the author (Mathey, 2012):

A laboratory investigation was carried out to investigate the strength and deformation behaviour of 'hourglass'-shaped strike-stabilizing pillars for a massive mining layout in a deep level mine. The idea was to compare the performance of the 'hourglass' geometry to the rectangular pillars of different cross-sectional area and length.

The geometrical characteristics of the 'hourglass' specimens is shown in Figure 105. Two groups of rectangular specimens were designed for comparison. In both designs, the cross-sectional width of the rectangular specimens was altered in three steps in order to represent the maximum, minimum and average width of the 'hourglass' specimens.

The difference between the test series was that for specimens in test series 1, the length of the specimen was adjusted and the width was reduced, so as to maintain the same specimen volume as compared to the 'hourglass' geometry. In test series 2, the length of the rectangular test specimens remained unaltered and equal to the length of the hourglass specimens.

During the compressive loading of the specimens, the strains occurring in the specimens' cross-sectional centre were monitored with strain-gauges.

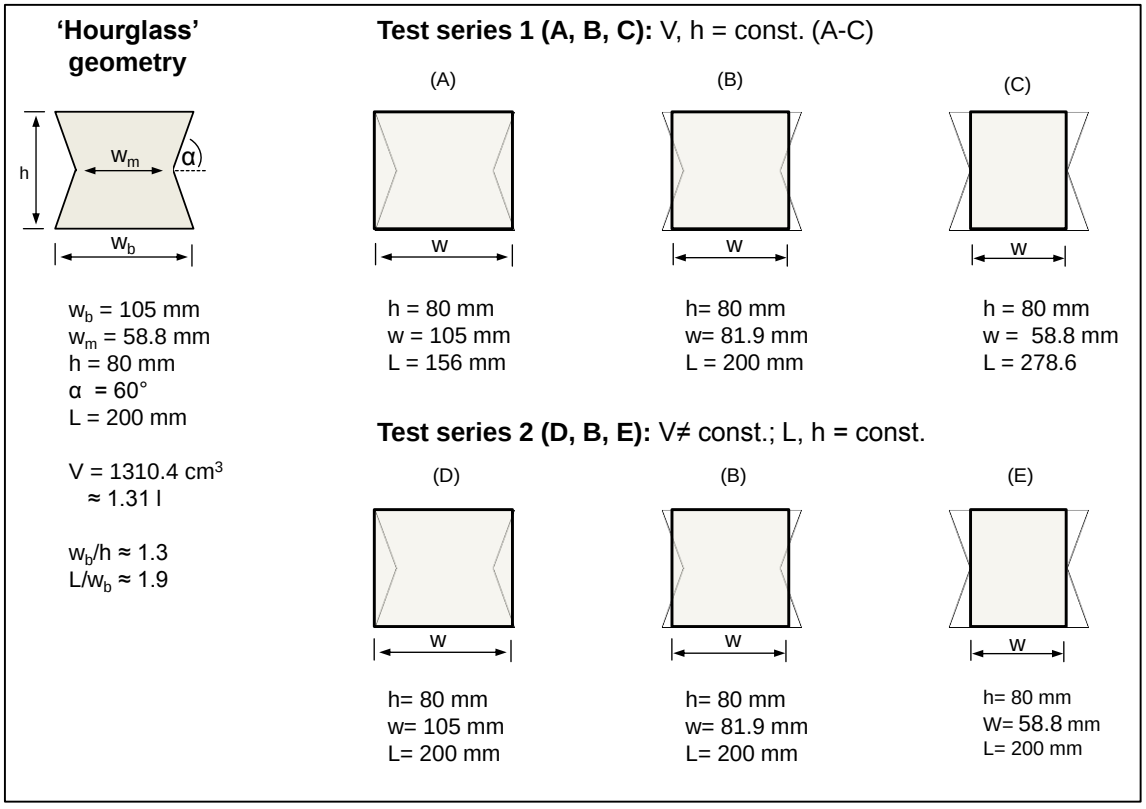


Figure 105. Test specimen design for laboratory investigation into the strength of 'hourglass' shaped pillars.

The results from the compressive strength tests which were performed on the rectangular geometries A – E were as follows:

- Within the group of specimens with equivalent volume (test series 1; types A, B and C), the compressive strength ranked according to A> B> C. In other words, a rectangular specimen with relatively larger w/h-ratio but a smaller length was stronger than a specimen with relatively smaller w/h-ratio and greater length.

- Within the group of specimens with unequal volume, but with equal length (test series 2; types D, B and C), the strength ranked D> B> E. In other words, a rectangular specimen was stronger the greater its w/h-ratio was.

- The difference in strength between the samples in test series 1 was apparently smaller than the difference in strength between samples in test series 2. This is

due to the fact that in series 1 the decrease in the specimen width is compensated by an increase in length of the sample, while this was not the case in test series 2.

What is unique about the compressive loading behaviour of the ‘hourglass’ shaped specimens is that both the axial and lateral strains measured in the specimen centre were compressive. Rectangular specimens had only exhibited extensive lateral strains in the specimen centre. The compressive strains in the ‘hourglass’ shaped specimens effectively provided a confined core. The ultimate load bearing capacity of these specimens was found to be about the same as the rectangular shaped specimen in case B, which had the same cross-sectional area.

21.3 Monitoring of failure patterns in coal pillar sidewalls

This is a relatively simple task that can be accomplished by drilling horizontal holes through the pillar and observing fracture patterns along the length of the borehole with a camera. Of particular interest are the following parameters: depth of fracture penetration into the pillar, frequency and inclination of fractures. The depth of fracturing should indicate the depth of yielding in the pillar and the width of the remaining, intact core. The merits of this exercise lies in the potential for a more reliable calibration of numerical models for coal pillar design.

Ideally, fracture monitoring should be conducted on a number of different pillars in different mining environments (depth, bord width, width-to-height ratios, contact conditions to surrounding strata), to account for different stress environments around the pillars. This may allow for the establishment of an empirical predictive model for pillar sidewall failure.

21.4 Probe-hole drilling in coal pillars

The ‘probe-hole’ or ‘drilling-yield’ experiment is a method for the qualitative assessment of stresses and stress changes in coal seams based on phenomenological criteria. It has been continuously developed and applied in Germany and elsewhere since the 1960s for the detection and relaxation of high-stress zones ahead of longwall faces in burst-prone coal seams (Jahns, 1965; Metcalf, 1967).

The method is simple to execute and relatively inexpensive. A horizontal borehole is drilled into the longwall face and the obtained amount and size of coal cuttings per advancing borehole meter is recorded. Borehole breakouts and dynamic events experienced by the drill operator, e.g. tensile forces on the drill rod or acoustic emissions from the seam, are taken as indicators of increased stress in the coal into which the borehole penetrates. While the method has proved its relevance for the detection of peak stress zones ahead of the longwall face, it has the disadvantage that it cannot provide the direct quantification of the magnitude of in-situ stresses.

In order to correlate the observed phenomena with stress magnitudes, comprehensive laboratory programmes have been conducted on small and large scale coal specimens

(Bräuner, 1969; Müller, 1990). Generally, all in-situ observations could be reproduced in the experiments. However, a direct translation from laboratory findings to the in-situ stress conditions proved to be difficult. This is in particular due to an apparent size effect in the relationship between the borehole diameter, sample size and the amount of recoverable coal cuttings. Further influencing factors, such as differences in the applied drilling techniques and time complicate matters further.

Nevertheless a wealth of information is available from these laboratory investigations. The influence of coal rank, petrography, micro tectonics, uniaxial compressive strength, drilling speed and diameter on the observed drilling phenomena has been assessed with insightful results. Detailed descriptions on the experiment set up and procedures are published (Bräuner, 1969; Müller, 1990).

In addition to physical testing, analytical models have been developed to describe the mechanical behaviour of coal during the drilling of a borehole, in particular to determine the extent of failure in the vicinity of a hole on a theoretical basis (Lippmann, 1979).

The probe-hole method can yield great benefits if applicable to coal pillars: for one, it will assist in quantifying the depth of failure in pillars. Secondly, this method may help to estimate stress profiles across the pillar width, in particular when observed breakout phenomena can be calibrated through laboratory tests.

Some limitations of this method are perceivable. The available experience suggests that a 42 mm diameter borehole in coal will only breakout at stress levels of around 20 MPa. This threshold may be reduced if larger drill diameters can be used. In any case, it seems likely that breakouts will only be detected in coal pillars in deep, high stress mining situations. The potential of this method to analyse the performance of coal pillars should therefore first be investigated in laboratory and numerical studies.

22 References

Anon (2011) 'FISH in FLAC', in *FLAC 7.0 User's Manual*. Itasca Consulting Group.

Babcock, C. O. (1969) 'Effect of end constraint on the compressive strength of model rock pillars', *Transactions - Society for Mining, Metallurgy and Exploration Inc.*, 344, pp. 357–363.

Baker-Duly, C. G. (1995) *The effect of width to height ratio and size on the strength of hard rock test specimens under uniaxial compression*. Master Thesis. University of the Witwatersrand.

Barron, K. and Pen, Y. (1992) 'A revised model for coal pillar strength', in *Proceedings of the Workshop on Coal Pillar Mechanics and Design. Pittsburgh, PA: US Department of the Interior, Bureau of Mines, IC*, pp. 144–157.

Bieniawski, Z. T. (1968a) 'In situ strength and deformation characteristics of coal', *Engineering Geology*, 2(5), pp. 325–340.

Bieniawski, Z. T. (1968b) 'Propagation of brittle fracture in rock', in *The 10th US Symposium on Rock Mechanics (USRMS)*. American Rock Mechanics Association. Available at: https://www.onepetro.org/conference-paper/ARMA-68-0409 (Accessed: 23 July 2014).

Bieniawski, Z. T. (1986) 'The compressive strength of hard rock', *Tydskrif vir Natuurwetenskappe*, 8, pp. 163–182.

Bieniawski, Z. T. (1992) 'A method revisited: coal pillar strength formula based on field investigations', in *Proceedings of the workshop on coal pillar mechanics and design. Pittsburgh, PA: US Department of the Interior, Bureau of Mines, IC*, pp. 158–165.

Bräuner, G. (1969) 'The evaluation of rock stresses from in-seam boreholes (German)', *Glückauf*, pp. 1057–1062.

Briggs, D. J. (1988) 'The load-bearing properties of fill materials (uncemented fills)', in *Proceedings of the Backfill in South African Mines Symposium, South African Institute of Mining and Metallurgy, Johannesburg, South Africa*, pp. 35–60.

Cruise, J. A. (1969) *The determination of the strength characteristics of wide pillars*. Master Thesis. University of the Witwatersrand.

Das, M. N. (1986) 'Influence of width/height ratio on post-failure behaviour of coal', *International Journal of Mining and Geological Engineering*, 4(1), pp. 79–87.

Deere, D. U. and Miller, R. P. (1966) *Engineering classification and index properties for intact rock*. Technical report AFWL-TR-66-116. Urbana, Illinois: University of Illinois.

Dolinar, D. R. (1993) 'Techniques to increase yield pillar residual strength', in *12th International Conference on Ground Control in Mining. Morgantown, WV: West Virginia University*, pp. 284–291.

Duncan Fama, M. E., Trueman, R. and Craig, M. S. (1995) 'Two-and three-dimensional elasto-plastic analysis for coal pillar design and its application to highwall mining', *International Journal of Rock Mechanics and Mining Sciences & Geomechanics Abstracts*, 32, pp. 215–225.

Esterhuizen, E., Mark, C. and Murphy, M. M. (2010) 'Numerical model calibration for simulating coal pillars, gob and overburden response', in *Proceeding of the 29th international conference on ground control in mining, Morgantown, WV*, pp. 46–57.

Esterhuizen, G. S. (1998) *The effect of structural discontinuities on coal pillar strength as a basis for improving safety in the design of coal pillar systems*. SIMRAC COL 005a final research report.

Esterhuizen, G. S. (2000) 'Jointing effects on pillar strength', in *Proceeding of the 19th international conference on ground control in mining, Morgantown, WV*.

Gadde, M. M. (2009) 'Numerical model evalutation of floor-bearing capacity in coal mines', in *Proceedings of the International Workshop on Numerical Modelling for Underground Mine Excavation Design*. NIOSH.

Gaddy, F. L. (1956) *A study of the ultimate strength of coal as related to the absolute size of the cubical specimens tested*. Virginia Polytechnic Institute (112).

Gale, W. J. (1999) 'Experience of field measurement and computer simulation methods of pillar design', in *Proceedings of the Second International Workshop on Coal Pillar Mechanics and Design, National Institute for Occupational Safety and Health, IC*, pp. 49–61.

Galvin, J. M. and Hebblewhite, B. K. (1995) 'UNSW pillar design methodology', *Sydney, Australia: University of New South Wales, Department of Mining Engineering, Research Release*, (1).

Galvin, J. M., Hebblewhite, B. K. and Salamon, M. D. G. (1999) 'University of New South Wales coal pillar strength determinations for Australian and South African mining conditions', in *Proceedings of the second international workshop on coal pillar mechanics and design, National Institute for Occupational Safety and Health, Report IC*, pp. 63–71.

Ghose, A. K. and Chakraborti, S. (1986) 'Empirical strength indices of Indian coals - an investigation', in *Proceedings of the 27th US Symposium on Rock Mechanics (USRMS)*. American Rock Mechanics Association.

Greenwald, H. P., Howarth, H. C. and Hartmann, I. (1939) *Experiments on strength of small pillars of coal in the Pittsburgh bed*. Bureau of Mines, Washington, DC (USA).

Van Heerden, W. L. (1974) *In situ determination of complete stress-strain characteristics fro 1.4 m square coal specimens with width to height ratios up to 3.4*. ME 1265. Pretoria: CSIR.

Van Heerden, W. L. (1975) 'In situ complete stress–strain characteristics of large coal specimens', *Journal of the South African Institute of Mining and Metallurgy*, 75, pp. 207–217.

Hobbs, D. W. (1964) 'The strength and the stress-strain characteristics of coal in triaxial compression', *The Journal of Geology*, pp. 214–231.

Holland, C. T. and Gaddy, F. L. (1957) 'Some aspects of permanent support of overburden of coal beds', in *Proceedings of the West Virginia Coal Mining Institute*.

Iannacchione, A. T. (1990) 'The effects of roof and floor interface slip on coal pillar behavior', in *Proceedings of the 31st US Symposium on Rock Mechanics*, pp. 156–160.

Jahns, H. (1965) ‘Detection and removal of dangerous stresses in burst-prone seam Sonnenschein (German)’, *Glückauf*, 101(3), pp. 184–191.

Jaiswal, A. and Shrivastva, B. K. (2009) ‘Numerical simulation of coal pillar strength’, *International Journal of Rock Mechanics and Mining Sciences*, 46(4), pp. 779–788.

Khair, A. W. (1994) ‘Integrated Coal Pillar Strength Formula’, *Preprints - Society of Mining Engineers of AIME*, 155.

Kripakov, N. P. (1981) *Analysis of pillar stability on steeply pitching seam using the finite element method*. 8579. US Bureau of Mines, Department of Interior.

Kroeger, E. B., Roethe, E. and Li, X. (2004) ‘Laboratory Strength Testing of Coal from Selected Illinois Seams’, in *Proceedings of the 23rd International Conference on Ground Control in Mining*. Department of Mining Engineering, College of Mineral and Energy Resources, West Virginia University, p. 77.

Lippmann, H. (1979) ‘Mechanics of drilling in pre-stressed brittle or granular material, in particular in coal seams (German)’, *Ingenieur-Archiv*, 48, pp. 347–361.

Lu, J., Ray, A., Morsy, K. and Peng, S. (2008) ‘Effects of rock/coal interface property in coal pillar strength’, in *Proceedings of the 27th International Conference on Ground Cpontrol in Mining, Morgantown: West Virginia*, pp. 262–267.

Madden, B. J. (1990) *An investigation into the factors affecting the strength of pillars in South African coal mines*. PhD Thesis. University of the Witwatersrand.

Madden, B. J. (1991) ‘A re-assessment of coal-pillar design’, *Journal of the South African Institute of Mining and Metallurgy*, 91(1), pp. 27–37.

Madden, B. J. and Canbulat, I. (1995) *A re-assessment of coal pillar design procedures*. COL 021.

Madden, B. J., Canbulat, I., Jack, B. W. and Prohaska, G. D. (1993) *A reassessment of coal pillar design procedures*. SIMRAC interim project report, COL 021A.

Maleki, H. (1992) ‘In situ pillar strength and failure mechanisms for US coal seams’, in *Proceedings of the Workshop on Coal Pillar Mechanics and Design. Pittsburgh, PA: US Department of the Interior, Bureau of Mines, IC*, pp. 73–77.

Mark, C. (2000) ‘State-of-the-art in coal pillar design’, *Transactions - Society for Mining, Metallurgy and Exploration Inc.*, 308, pp. 123–128.

Mark, C. and Barton, T. M. (1996) ‘The uniaxial compressive strength of coal: should it be used to design pillars’, in *Proceedings of the 15th International Conference on Ground Control in Mining. Golden, CO: Colorado School of Mines*, pp. 61–78.

Mark, C. and Chase, F. E. (1997) ‘Analysis of retreat mining pillar stability (ARMPS)’, in *Proceedings - New Technology for Ground Control in Retreat Mining. Pittsburgh, PA: US Department of Health and Human Services, Public Health Service, Centers for Disease Control and Prevention, National Institute for Occupational Safety and Health, DHHS (NIOSH) Publication*, pp. 17–34.

Mathey, M. (2011) *Towards the failure probability of coal pillars: A review of intact and failed cases in South Africa*. Master Thesis. RWTH University.

Mathey, M. (2012) *Comparative investigation into the deformation behaviour and peak strength of 'hourglass' shaped specimens in uniaxial compression*. Unpublished report to South Deep gold mine.

Medhurst, T. P. and Brown, E. T. (1998) 'A study of the mechanical behaviour of coal for pillar design', *International Journal of Rock Mechanics and Mining Sciences*, 35(8), pp. 1087–1105.

Meikle, P. and Holland, C. T. (1965) 'The effect of friction on the strength of model coal pillars', *Transactions - Society for Mining, Metallurgy and Exploration Inc.*, 232(2), pp. 322–327.

Van der Merwe, J. N. (2003a) 'A laboratory investigation into the effect of specimen size on the strength of coal samples from different areas', *Journal of the South African Institute of Mining and Metallurgy*, 103(5), pp. 273–280.

Van der Merwe, J. N. (2003b) 'New pillar strength formula for South African coal', *Journal of the South African Institute of Mining and Metallurgy*, 103(5), pp. 281–292.

Van der Merwe, J. N. (2003c) 'Predicting coal pillar life in South Africa', *Journal of the South African Institute of Mining and Metallurgy*, 103(5), pp. 293–301.

Van der Merwe, J. N. (2004) 'Verification of pillar life prediction method', *The Journal of the South African Institute of Mining and Metallurgy*.

Van der Merwe, J. N. and Mathey, M. (2013a) 'Probability of failure of South African coal pillars', *Journal of the Southern African Institute of Mining and Metallurgy*, 113(11), pp. 849–857.

Van der Merwe, J. N. and Mathey, M. (2013b) 'Update of coal pillar database for South African coal mining', *Journal of the Southern African Institute of Mining and Metallurgy*, 113(11), pp. 825–840.

Van der Merwe, J. N. and Mathey, M. (2013c) 'Update of coal pillar strength formulae for South African coal using two methods of analysis', *Journal of the Southern African Institute of Mining and Metallurgy*, 113(11), pp. 841–847.

Metcalf, J. R. (1967) 'The front abutment of a longwall face', *International Journal of Rock Mechanics and Mining Sciences*, 4, pp. 195–207.

Mogi, K. (1966) 'Pressure dependence of rock strength and transition from brittle fracture to ductile flow.', *Bulletin of the Eartquake Research Institute*, 44, pp. 215–232.

Mohan, M. G., Sheorey, P. R. and Kushwaha, A. (2001) 'Numerical estimation of pillar strength in coal mines', *International Journal of Rock Mechanics and Mining Sciences*, 38(8), pp. 1185–1192.

Müller, W. (1990) 'Relaxation behaviour of triaxially confined coal specimens during drilling (German)', *Glückauf-Forschungshefte*, 51(2), pp. 76–84.

Müller, W. (1991) 'Numerical simulation of rock bursts', *Mining science and technology*, 12(1), pp. 27–42.

Napier, J. A. L. and Malan, D. F. (2007) 'The computational analysis of shallow depth tabular mining problems', *Journal of the South African Institute of Mining and Metallurgy*, 107(11), pp. 725–742.

Oraee, K., Hosseini, N. and Gholinejad, M. (2009) 'Estimation of coal pillar strength by finite difference model', in *Proceedings of the Coal 2009: Coal Operators' Conference, University of Wollongong & the Australasian Institute of Mining and Metallurgy, Wollongong: University of Wollongong / The Australasian Institute of Mining and Metallurgy*, pp. 54–61.

Oravecz, K. I. (1973) *Loading of coal pillars in bord and pillar workings*. PhD Thesis. University of the Witwatersrand.

Ozbay, M. U. (1987) *Design considerations for mining of hardrock tabular deposits situated at moderate depths*. PhD Thesis. University of the Witwatersrand.

Ozbay, M. U. and Rozgonyi, T. (2003) 'Numerical modelling of stress and deformations encountered in deep longwall coal mines using strain softening failure criterion', in *Proceedings of the International Conference on Safety and Environmental Aspects in Mining*.

Du Plessis, M., Malan, D. F. and Napier, J. A. L. (2011) 'Evaluation of a limit equilibrium model to simulate crush pillar behaviour', *Journal of the Southern African Institute of Mining and Metallurgy*, 111(12), pp. 875–885.

Roberts, D. P., Ryder, J. A. and Van der Merwe, J. N. (2005) *Development of design procedures for long slender pillars*. Coaltech 2020 research report, Task 2.14.

Rose, J. C. and Howell, R. C. (1979) 'Proposed coal pillaring procedure using concrete containing coal refuse (coal-crete)', *Preprints - Society of Mining Engineers of AIME*, (77-B-102).

Salamon, M. D. G. (1982) *Report to Wankie Colliery*. Unpublished Unpublished.

Salamon, M. D. G. (1992) 'Strength and stability of coal pillars', in *Proceedings of the Workshop on Coal Pillar Mechanics and Design. Pittsburgh, PA: US Department of the Interior, Bureau of Mines, IC*, pp. 94–121.

Salamon, M. D. G., Badr, S., Mendoza, R. and Ozbay, M. U. (2003) 'Pillar failure in deep coal seams: numerical simulation', in *10th ISRM Congress*. International Society for Rock Mechanics.

Salamon, M. D. G., Canbulat, I. and Ryder, J. A. (2006) *Development of seam-specific strength formulae for South African collieries.* Coaltech 2020 final research report, Task 2.16.

Salamon, M. D. G. and Munro, A. H. (1967) 'A study of strength of coal pillars', *Journal of the South African Institute of Mining and Metallurgy*, 68(2), p. 55.

Salamon, M. D. G. and Wagner, H. (1985) 'Practical experiences in the design of coal pillars', in *Proceedings of the 21st International Conference of Safety in Mines Research Institutes (Sydney, Australia). Balkema*, pp. 3–9.

Schümann, E. H. R. and Cook, N. G. W. (1967) *The load-deformation characteristics of broken rock ribs*. Project no. 105/66 Report no. 13/67. Johannesburg: Chamber of Mines Research Organization.

Shen, B., Alehossein, H., Poulsen, B., Huddlestone-Jolmes, C. and Zhou, B. (2010) *Collingwood park mine remediation - subsidence control using fly ash backfilling*. Report EP 105068. CSIRO Eart Science and Resource Engineering.

Sheorey, P. R. (1992) ‘Pillar strength considering in situ stresses’, in *Proceedings of the workshop on coal pillar mechanics and design. Pittsburgh, PA: US Department of the Interior, Bureau of Mines, IC*.

Sheorey, P. R., Das, M. N., Barat, D., Prasad, R. K. and Singh, B. (1987) ‘Coal pillar strength estimation from failed and stable cases’, in *International Journal of Rock Mechanics and Mining Sciences & Geomechanics Abstracts*. Elsevier, pp. 347–355.

Sheorey, P. R. and Singh, B. (1974) ‘Strength of rectangular pillars in partial extraction’, *International Journal of Rock Mechanics and Mining Sciences & Geomechanics Abstracts*, 11, pp. 41–44.

Stavropoulou, V. (1982) *Constitutive laws for brittle rocks*. PhD Thesis. University of the Witwatersrand.

Su, D. W. H. and Hasenfus, G. J. (1999) ‘Coal pillar strength and practical coal pillar design considerations’, in *Proceedings of the second international workshop on coal pillar mechanics and design, National Institute for Occupational Safety and Health, Report IC*, pp. 155–162.

Tesarik, D. R., Whyatt, J. K. and Larson, M. K. (2013) ‘Inferring Mine Floor Properties from Pillar Size and Floor Heave’, in *47th US Rock Mechanics/Geomechanics Symposium*. American Rock Mechanics Association.

Ulusay, R. and Hudson, J. A. (eds) (2007) *The complete ISRM suggested methods for rock characterization, testing and monitoring: 1974-2006*.

Vervoort, A. (1992) ‘Monitoring and simulation of sidewall fracturing in coal mines’, in *Proceedings of the ISRM conference Eurock ’92*.

Wagner, H. (1974) ‘Determination of the complete load-deformation characteristics of coal pillars’, in *Proceedings of the Third International Congress on Rock Mechanics. National Academy of Sciences*, pp. 1076–1081.

Wang, H., Poulsen, B. A., Shen, B., Xue, S. and Jiang, Y. (2011) ‘The influence of roadway backfill on the coal pillar strength by numericalinvestigation’, *International Journal of Rock Mechanics and Mining Sciences*, 48(3), pp. 443–450.

Watson, B. P. (2010) *Rock behaviour of the Bushveld Merensky Reef and the design of crush pillars*. PhD Thesis. University of the Witwatersrand.

Wilson, A. H. (1981) ‘Stress and stability in coal ribsides and pillars’, in *Proceedings of the First International Conference on Ground Control in Mining. Morgantown, WV: West Virginia University*, pp. 1–12.

Yavuz, H. and Fowell, R. J. (2001) ‘Softening effects of coal on the design of yield pillars’, in *FLAC and numerical modelling in geomechanics*.

York, G. and Canbulat, I. (1998) ‘The scale effect, critical rock mass strength and pillar system design’, *Journal of the South African Institute of Mining and Metallurgy*, 98(1), pp. 23–37.

York, G., Canbulat, I. and Jack, B. W. (2000) *Coal pillar design procedures*. SIMRAC final project report.

York, G., Canbulat, I., Kabeya, K. K., Le Bron, K., Watson, B. P. and Williams, S. B. (1998) *Develop guidelines for the design of pillar systems for shallow and intermediate depth, tabular, hard rock mines and provide a methodology for assessing hangingwall stability and support requirements for the panels between pillars*. SIMRAC final project report GAP 334.